Monitoring of Micro RNA Maturation and Its Inhibition in Living Cells

Dissertation
zur Erlangung des akademischen Grades
Doctor rerum naturalium
(Dr. rer. nat.)

Eingereicht an der
Mathematisch-Naturwissenschaftlichen Fakultät
der Humboldt-Universität zu Berlin

von
M. Sc. Natalia Loibl (geb. Ogorodnikova)

Präsidentin der Humboldt-Universität zu Berlin
Prof. Dr.-Ing. habil. Dr. Sabine Kunst

Dekan der Mathematisch-Naturwissenschaftlichen Fakultät
Prof. Dr. Elmar Kulke

Gutachter:
1. Prof. Dr. Christoph Arenz
2. Prof. Dr. Oliver Seitz
3. Prof. Dr. Sabine Müller

Mündliche Prüfung am 26.10.2021

The experimental work was conducted from April, 2013 till July, 2017 in the laboratories of Prof. Christoph Arenz and Prof. Oliver Seitz (Institute of Chemistry, Humboldt University of Berlin).

Abstract

MicroRNAs (miRNAs) represent small non-coding RNA molecules that function in the posttranscriptional regulation of the gene expression. During biogenesis, primary miRNA precursors go through two consequent RNAse cleavages by two type III ribonucleases, namely Drosha and Dicer, to yield the ~22-nt long mature miRNAs. The liberated miRNAs target mRNAs, which leads to mRNA degradation or translation repression. Since altered miRNA expression has been associated with a variety of diseases, miRNAs are important diagnostic markers and potential therapeutic targets. This work describes the development of tools for inhibition und monitoring the dicer-mediated miRNA processing.

Here, peptide nucleic acid (PNA) based probes, targeting the precursor miR-21 (pre-miR21), were designed with the expectation that they would inhibit the dicer-mediated miR-21 maturation. In contrast to the expectation, no change in miR-21 level was observed after cell treatment with the pre-miR21 specific PNA probes. To detect the probe/target hybridization state, the fluorogenic forced intercalation (FIT) PNA probes were developed. The intercalator dye thiazole orange (TO) served as a reporter and signalled target hybridization by an increase of its fluorescence. The pre-miR21 specific TO PNA-CPP probes were evaluated in high miR-21 abundant Hela cell, low abundant A549 cells and control HEK293 cells (with the lowest miR-21 level). As preliminary results show, the TO PNA probe might be useful for discrimination of high miR-21 abundant cells, but further probe improvement is still required. Next, the FIT probes were applied for monitoring the dicer-mediated miR-21 maturation.

To monitor the pre-miR21 cleavage, the combination of the two spectrally distinguishable FIT PNA probes, bearing quinoline blue (QB) and TO fluorophore, was developed to allow the rapid and simultaneous detection of pre-miR21 and antisense mature miR-21 (as-miR21). The pre-miR21 specific QB PNA probe signalled the presence of pre-miR21 by an 14-fold enhancement of fluorescence intensity and showed no enhancement in presence of the mature form. The 11nt-long TO probe discriminated between pre-miR21 and the miR-21: as-miR21 duplex by the three-fold higher emission of the latter. The probe set was successfully used for detection of the modelled dicer reaction. However, the monitoring of rhDicer reaction have revealed that rhDicer cleaves the *in vitro* transcribed pre-miR21 nonspecifically, since the loss of both QB and TO signals was observed. Additionally, the shorter as-miR21 specific TO PNA probe (7nt) was responsive to the presence of Ago-2 protein, which loads the miR-21 strand and releases the as-miR21 strand, thus making it accessible for probe hybridization. In future, the developed probes can be applied for the fast *in vitro* screening of new Dicer and Ago-2 inhibitors.

In the second part of this work, an alternative approach for the inhibition of miRNA maturation, small molecular inhibitors (SMIs) was tested. This strategy is based on the recognition of specific RNA secondary structures by SMIs. A set of 80 SMIs was previously designed, synthesized and screened in the cell-free dicer-mediated branched rolling circular amplification (BRCA) assay by the Arenz group to test their ability to inhibit the dicer-mediated processing of four pre-miRNAs[1]. In the work presented here, the action of the most promising pre-miR122 and pre-miR21-targeting SMIs from the BRCA assay was assayed in Huh7 cancer cells. Two potential inhibitors of miR-122 maturation were identified in a luciferase reporter assay and RT-qPCR assay, although they were not as efficient as a commercially available antimiR-122. Unexpectedly, the identified SMIs did not cause an increase of the *Adam10* protein expression level, which is a direct target of miR-122. Conclusively, the two identified SMIs might be used for inhibition of the miR-122 maturation, although, a specificity of these SMIs remains questionable and possible off target effects can not be excluded.

Zusammenfassung

MicroRNAs (miRNAs) sind nicht-kodierende Ribonukleinsäuren (RNA) und übernehmen eine wichtige Funktion in der posttranskriptionelen Regulation der Genexpression. Im Zuge der Biogenese wird das Primärtranskript (*primary microRNA)* durch zwei RNAse-katalysierte Spaltreaktionen in die ~22 Nukleotid-lange (22nt) miRNA prozessiert. An diesem Schritt sind die zwei Ribonukleasen III Drosha und Dicer beteiligt. Durch Bindung der produzierten miRNAs an die mRNA der jeweiligen Zielgene wird der mRNA-Abbau oder die Hemmung der Translation induziert. Da die verändernde miRNA Expression mit einer Vielzahl von Krankheiten in Verbindung steht, sind miRNAs wichtige diagnostische Marker und potenzielle therapeutische Targets. Die vorliegende Arbeit beschreibt die Entwicklung von Methoden zur Analyse und Inhibierung der Dicer-vermittelnden miRNA-Reifung.

Im ersten Teil der Arbeit wurde die Verwendung von Präkursor miR-21(*pre-miR21*)-spezifischen Peptidnukleinsäure(PNA)-Sonden zur Inhibierung der Dicer-vermittelnden miRNA-Reifung untersucht. Im Gegensatz zur Arbeitshypothese wurde bei der Behandlung von Zellen mit den pre-miR21-spezifischen PNA-Sonden jedoch keine Änderung des miR-21 Niveau beobachtet. Um die Hybridisierung der Sonde an die Zielsequenz zu nachzuweisen, wurden fluorogene Hybridisierungssonden zur erzwungenen Interkalation (FIT-Sonden) entwickelt. Der Interkalationsfarbstoff Thiazolorange (TO) dient als Reporter und signalisiert die erfolgreiche Hybridisierung durch den Anstieg der Fluoreszenz. Die pre-miR21 spezifischen FIT-Sonden wurde in miR-21-reichen *Hela*-Zellen, miR-21-armen *A549*-Zellen und Kontrollzellen (*HEK293*-Zellen mit niedrigsten miR-21-Level) evaluiert. Wie vorläufige Ergebnisse zeigen, könnte die TO-PNA Sonde für die Unterscheidung von Zellen mit hohem miR-21-Gehalt nützlich sein, aber eine weitere Verbesserung der Sonde ist noch erforderlich. Im nächsten Teil der Arbeit wurden neuartige FIT-Sonden für die Analyse der Dicer-vermittelnden miR-21-Reifung entwickelt. Um die gleichzeitige Detektion der entstehenden pre-miR21 und der antisense miR-21 (as-miR21) in Echtzeit zu ermöglichen, wurden die Verwendung von spektral unterscheidbaren FIT-Sonden auf Quinolinblau(QB)-und TO-Basis getestet. Die leistungsfähigste pre-miR21-spezifische QB-Sonde zeigte eine 14-fache Erhöhung der Fluoreszenzintensität nach erfolgter Hybridisierung mit pre-miR21 und keine Erhöhung der Fluoreszenz in Gegenwart der miR-21. Die Diskriminierung zwischen pre-miR21 und dem miR-21:as-miR21-Duplex konnte durch die Verwendung einer optimierten 11 Nukleotid-langen (11nt) TO-Sonde erreicht werden. Das entwickelte Sonden-Paar ermöglichte die Analyse der rhDicer-Reaktion. Dabei wurde entdeckt, dass die rhDicer-Reaktion an der *in vitro* transkribierten pre-miR21 unspezifisch spaltet, was anhand der Abnahme des QB- und TO-Signales angezeigt wurde. Zusätzlich wies die kürzere as-miR21 spezifische TO-Sonde (7nt) eine Sensitivität gegenüber der Anwesenheit des Ago-2 Proteins auf, welches den miR-21-Strang auflädt und dabei den as-miR21-Strang freisetzt. Letzter ist dadurch für die Hybridisierung mit der Sonde verfügbar. In der Zukunft könnten die entwickelten Sonden für schnelle *in vitro* Screenings neuer Dicer-und Ago-2-Inhibitoren angewendet werden. Im zweiten Teil der Dissertation wurde die Verwendung von niedermolekularen Inhibitoren (*small molecular inhibitors,* SMIs) für die Inhibierung der miRNA-Reifung getestet. Die Strategie basiert auf der Erkennung spezifischer RNA-Sekundärstrukturen durch SMIs. Die verwendeten 80 SMIs wurden zuvor in der Arbeitsgruppe von Prof. Arenz entwickelt[1]. In dieser Arbeit wurde die Aktivität von vielversprechenden pre-miR122- und pre-miR21-spezifischen SMIs in Huh7 Krebszellen untersucht. Dabei wurden zwei potentielle Inhibitoren für die miR-122-Reifen mittels *Luciferase Reporter Assay* and Reverse-Transkriptase-PCR (RT-qPCR) identifiziert, obwohl nicht sehr effizient wie kommerziell erhältlich AntimiR-122. Überraschenderweise, verursachten die identifizierte SMIs keinen Anstieg des *Adam10*-Proteinlevels, welches das direkte Ziel der miR-122 ist. Zusammenfassend könnten die zwei identifizierten SMIs für die Inhibierung der miR-122-Reifung genutzt werden, allerdings bleibt die Spezifität der SMIs fraglich und mögliche *off-target*-Effekte können nicht ausgeschlossen werden.

Contents

Abbreviations

RNA and DNA are listed in the common format from 5‘-terminus to 3‘-terminus (PNA- from N-terminus to C-terminus). Nucleobases are abbreviated using the common one-letter codes for RNA (G, A, C, U) or DNA/PNA (G, A, C, T).

ACN	Acetonitrile
Ahex	6-Aminohexanoic acid
as-miRNA	antisense miRNA strand (passenger strand)
ASO	Antisense Oligonucleotide
Boc	Tert. Butyloxycarbonyl
bp	Base pair(s)
BRCA	Branched Rolling Circle Amplification
CPP	cell-penetrating protein
DCM	Dichloromethane
DGCR8	DiGeorge syndrome critical region gene 8
D-MEM	Dulbecco's modified essential medium
DMSO	Dimethylsulfoxide
DNA	Deoxyribonucleic acid
ds	Double-stranded
ds-RBD	ds-RNA-binding domain
DTT	Dithiothreitol
EDTA	Ethylenediamine-N, N, N’, N’-tetraacetic acid
em	Emission
EtOH	Ethanol
ex	Excitation
EXP5	exportin 5 protein
FACS	Fluorescence-activated cell sorting
FAM	Fluorescein
FCS	fetal calf serum
FIT probes	forced intercalation probes
Fmoc	9-Fluorenylmethoxycarbonyl
FRET	Fluorescence Resonance Energy Transfer
HBV	Human Hepatitis B virus

HCTU	2-(6-Chlor-1*H*-benzotriazol-1-yl)-1,1,3,3-tetramethylaminium-hexafluorophosphat
HCV	Human Hepatitis C virus
HPLC	High Performance Liquid Chromatography
HTS	High throughput screening
LNA	Locked-nucleic acid
MeOH	Methanol
min.	Minute
miRNA	Micro RNA
mRNA	Messenger RNA
NMM	N-Methylmorpholin
NMP	N-Methylpyrrolidon
NMR	Nuclear magnetic resonance (spectroscopy)
nt	Nucleotide(s)
PACT	Protein Kinase R-activating protein
PAGE	Polyacrylamide gel electrophoresis
PAZ	Piwi/Argonaute/Zwille domain
PCI	Phenol /chloroform / isoamyl alcohol
PFA	Paraformaldehyde
PNA	Peptide Nucleic Acid
PPTS	Pyridinium-p-toluolsulfonic acid
Pre-miRNA	Precursor miRNA
Pri-miRNA	Primary miRNA PS
PyBOP	Benzotriazol-1-yloxy-tris-pyrrolodinophosphonium
QB	quinoline blue
rhDicer	Recombinant Human Dicer
RISC	RNA-induced silencing complex
RNA	Ribonucleic acid
RNAi	RNA interference
RRE	Rev response element
RT	Reverse Transcription
rt	Room temperature

RT-PCR	Reverse transcription polymerase chain reaction
RT-qPCR	Reverse Transcription quantitative Polymerase Chain Reaction
SDS	Sodium dodecyl sulfate
siRNA	Short interfering RNA
SMI	Small Molecular Inhibitor
SNP	single nucleotide polymorphism
SPPS	solid-phase peptide synthesis
SPS	solid-phase synthesis
ss	Single-stranded
SYBR Gold	Cyanine-based nucleic acid stains
TBE	Tris/ borate/ EDTA
TO	thiazole orange
TRBP	TAR RNA binding protein TRBP
UPLC	Ultra Performance Liquid Chromatography

1. Introduction

1.1 MiRNA Biogenesis

MiRNAs are small, non-coding RNA molecules, which regulate gene expression in essential cell processes (proliferation, differentiation, apoptosis and others). They target mRNA and negatively regulate gene expression by translation repression or mRNA degradation. As estimated in the Rajewsky group, about 30% of protein-coding genes in eukaryotes are regulated by miRNAs[2]. According to the another prediction of Friedman *et al.*, more than 60% of human-protein genes contain at least one conserved miRNA-binding site and might be regulated by miRNAs in human[3]. Dysregulation of miRNA expression has been shown in many pathologies, such as cancer, cardiovascular diseases, myopathies, inflammation and others [4-6]. One example of oncogenic miRNAs is miRNA-21 (miR-21), which is known to down-regulate tumor suppressor genes and is found to be overexpressed in various malignancies. Thereby, miR-21 is considered as a promising target for diagnostics and cancer drug development [7].

The canonical miRNA biogenesis (Fig. 1a) starts from transcription of miRNA genes mainly by polymerase II or in some cases by polymerase III and results in a long primary miRNA transcript (pri-miRNA), usually with the length over 1kb. The pri-miRNA contains a local stem-loop hairpin structure, containing the mature miRNA sequence. Then miRNA processing goes through two consequent RNAse cleavages by Type III ribonucleases, namely Drosha and Dicer, to yield the ~22-nt long mature miRNAs. Beyond the canonical miRNA biogenesis, non-canonical miRNA biogenesis can bypass Drosha or Dicer cleavage[3].

After transcription the pri-miRNA structure is recognised and cleaved by the microprocessor complex, containing Drosha, DiGeorge syndrome critical region gene 8 (DGCR8) and other proteins to form a 60-70nt long stem-loop hairpin-shaped RNA (precursor miRNA, pre-miRNA).[8-9] As a hallmark of the RNAse II products, the product of Drosha has a 2 nucleotides (nt) long 3' overhang at the cleavage site. Drosha is a 160kDa nuclear protein, consisting of the tandem RNAse III domains (RIIIDs) and ds-RNA-binding domain (dsRBD). Pri-miRNA is recognized by DGCR8 in a complex with Drosha and is cleaved by Drosha RIIDs 11nt away from the junction on the stem (ssRNA-dsRNA junction). Drosha and DGCR8 are conserved in animals, proving their vital role in a cell life. Drosha deficiency causes lethality in embryonic mice and depletion of *Dgcr8* gene leads to the genetic disorder, called DiGeorge syndrome. [10-15]

Afterwards, the exportin 5 protein (EXP5) in a transport complex with RanGTP recruits the Drosha processed pre-miRNA and exports it from the nucleus to the cytoplasm through a nuclear pore complex. During the export to the cytoplasm, the transport complex protects pre-miRNA also from the RNAse cleavage [16-20].

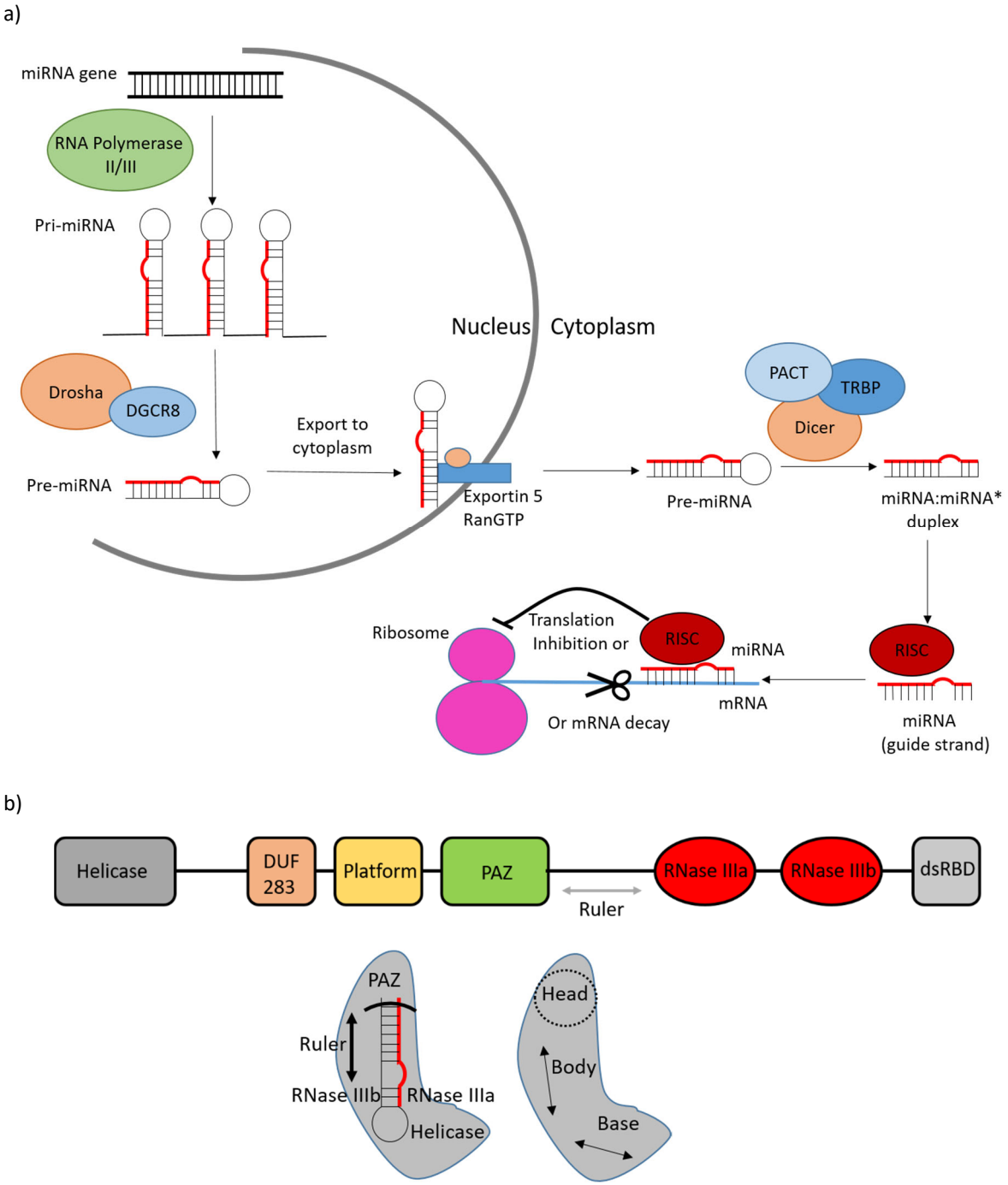

Figure 1. a) MiRNA biogenesis: the miRNA gene is transcribed by RNA Polymerase II/III to form the pri-miRNA transcript that is sequentially cleaved by RNases Drosha and Dicer to generate miRNA duplex (miRNA: miRNA*, where miRNA* is a passenger strand). After unwinding of the miRNA duplex, the mature miRNA is loaded into RISC, which is guided by miRNA to the target mRNA. Once miRNA binds to mRNA, RISC performs their function either by inhibition of translation or mRNA cleavage. b) The schematic human Dicer domain structure and molecular architecture were generated based on previously published data[21-22].

In the cytoplasm Dicer recognises the Drosha-processed pre-miRNA, containing a 2-nt 3' overhang, and cleaves it, generating a double stranded miRNA duplex (miRNA: miRNA*) with 3' overhanging ends, consisting of the mature miRNA (guide strand) and the antisense miRNA* (as-miR, passenger strand) [23-24]. Dicer acts in the complex with the TAR RNA binding protein (TRBP) and the Protein Kinase R-activating protein (PACT), which have multiple dsRNA-binding domains[25]. *In vitro* TRBP stabilizes the Dicer-pre-miRNA complex and enhances the dicer-mediated cleavage of pre-miRNA [26], whereas PACT inhibits the dicer-mediated cleavage of pre-siRNA by forming a Dicer-PACT complex[27]. Hence, TRBP

and PACT effect the Dicer activity differently, they can be regulatory factors of the miRNA and siRNA biogenesis. However, the detailed role of PACT in the miRNA pathway should be still clarified[9]. Dicer is a ~200kDa member of the RNAse III family which is found in all eukaryotes (except budding yeast) [28] and well conserved[29]. Human Dicer is presented by one isoform, which is responsible for both miRNA and small interfering RNA (siRNA) biogenesis.[23, 30-33] Conversely, *Drosophila* has two separate Dicer isoforms for miRNA and siRNA biogenesis. [34-35] Dicer is a multi-domain protein that is composed of an N-terminal ATPase/Helicase domain, a domain of so far unknown function namely, DUF283, a structure known as 'platform', a Piwi/ Argonaute/ Zwille (PAZ) domain, RNase IIIa and RNase IIIb nuclease domains, and a C-terminal dsRNA-binding domain (dsRBD) (Fig. 1b). The N-terminal Helicase domain recognises pre-miRNA by binding to its terminal loop. Simultaneously, the PAZ domain binds to the terminus of pre-miRNA [36-38]. Although, the whole crystal structure of human Dicer is not determined yet, the individual domains of human Dicer and the apo-Dicer form of *Giardia intestinalis* have been crystalized and studied by X-ray crystallography [38-40]. The crystal structure of Dicer form of *Giardia intestinalis* showed that two RNAse nuclease domains (RNAse IIIa and RNAseIIIb) dimerize to create a catalytic centre, being positioned in a specific distance from the PAZ domain. The PAZ domain is separated from the nuclease catalytic centre by the positively charged helix domain. This distance between the PAZ and the RNAse III domains act as a "molecular ruler" during the dicer-mediated cleavage of pre-miRNA. This "molecular ruler" model would explain, why the small RNAs produced by Dicer are equal in size. [38, 41]

In the final stage of the miRNA biogenesis, miRNA (guide strand) is loaded into the RNA-induced silencing complex (RISC), the main components of which are Dicer, Ago-2, PACT and TRBP. In this complex miRNA binds to its target to accomplish their regulation mission either through translation suppression or mRNA deadenylation, resulting in mRNA decay [4]. For recognition of mRNA by the miRISC complex (the RISC with loaded miRNA), a perfect complementarity in the "seed" region (2-8 nt of the miRNA) is sufficient. The choice of posttranscriptional mechanism (mRNA cleavage or translation repression) depends on the degree of complementarity and the miRNA sequence-composition [12, 33, 42-43]. The cleavage of mRNA by the Ago-2 protein within RISC occurs if miRNA is complementary to mRNA in its seed region and, additionally, in the 10-11th bases. Whereas, the multiple imperfect complementary sites between miRNA and mRNA cause bulges in RNA duplex and repress translation. It is important to note that the mRNA cleavage is irreversible and translation repression is reversible, therefore, target mRNA can be translated after cancellation of translation repression[4]. After mRNA cleavage miRNA can mediate the recognition and destruction of additional targets[43]. The most of mature miRNAs are considered to be highly stable, although, the exact half-life time of the individual miRNAs is not known [44-45].

It is not clear what happens with the remaining passenger miRNA* strand. In some reviews about miRNA biogenesis, it is reported that after loading of the guide miRNA intro RICS, the passenger miRNA* strand is released and degraded [46-49]. However, there is increasing evidence of regulatory function of passenger strand [50-54]. One of these examples is the passenger miRNA-21* strand, which stimulates cardiac hypertrophy, being exported from the fibroblasts to cardiomyocytes [55].

1.2 MiRNAs and Diseases (miRNA-21 and miRNA-122)

MiRNAs play a vital role in maintaining cell homeostasis and in organism development. It is not surprising that deregulation of miRNAs is associated with a range of diseases such as many types of cancer, cardiovascular diseases, immune diseases, neurodegenerative disorders and other disorders.

In cancer pathogenesis miRNAs can be qualified (within the specific tissue) as oncogenes or tumour-suppressor miRNAs[56]. Malignant cells have an altered pattern of miRNA expression comparing to the healthy tissue, usually, with the prevalence of downregulated miRNAs, and just a few oncogenic miRNAs are found to be upregulated. The altered miRNA expression is not only a consequence of tumorigenesis, a cancer causative role of individual miRNAs has also been proved. The first miRNAs associated with cancer were the tumour suppressors, miR-15 and miR-16, which down regulate the anti-apoptotic B-cell lymphoma factor 2 (Bcl-2) [57]. The deletion of miR-15a/16-1 was sufficient for generation of lymphomagenesis in mice. The human let-7 tumour suppressor miRNA was decreased in lung cancer comparing to the normal tissue, leading to RAS overexpression [58]. Another study has reported that lymphoma can be also initiated by induced oncogenic miR-21 overexpression in mice model, demonstrating the cancerogenic role of a single miRNA[59].

Oncogenic miR-21 is miRNA of particular interest for researchers, since it is found to be overexpressed in most tumour types and cardiovascular diseases. Knockdown of miR-21 let to reduced proliferation and tumour growth in breast cancer MCF-7 cells and reduced invasion and metastasis in MDA-MB-231 cells.[60-61] Validation of miR-21 targets showed that most of them are tumour suppressors, i. e. Phosphatase and Tensin Homolog (PTEN), Programmed Cell Death 4 (PDCD4), tropomyosin I (TPMI), transforming growth factor–b (TGF-β), Epidermal growth factor receprot (EGFR), Reversion-inducing cysteine-rich protein with Kazal motifs (RECK)[62]. The increased expression of PTEN in response to miR-21 inhibition caused decreased tumour cell proliferation, migration and invasion in hepatocellular carcinoma cells [63]. PDCD4 is shown to inhibit invasion and extravasation in colorectal cancer cells and negatively regulated by miR-21 [64]. Furthermore, miRNA-21 serves as a biomarker: Circulating miR-21 is a diagnostic marker for colorectal cancer, whereas tissue miR-21 could predict survival of patients with colorectal cancer. Regarding the cardiovascular diseases, the miR-21 expression is also found to be deregulated in heart ischemia, cardiac hypertrophy, arrhythmias and cardiac fibrosis, but the role of miR-21 in cardiac tissue is more complex and not fully understood[65].

Another promising target miR-122 is highly expressed in liver and most abundant liver human miRNA (52% of whole liver miRNA profile) [66-67]. MiR-122 is involved in the regulation of liver development, differentiation and homeostasis, as well as in cholesterol and fatty acid metabolism. It was reported that the reduced expression of miR-122 causes liver disease [68-70]. Moreover, the miR-122 knock-out mice developed liver tumours and abnormal expression of genes of cell growth and apoptosis. Delivery of miR-122 in these mice leads to the tumour regression proving an anti-tumour role of miR-122 [68-70]. MiR-122 mimics have been successfully used for treatment of hepatocellular carcinoma in mice and for increasing the tumour cells sensitivity for chemotherapy [71-73]. Furthermore, miR-122 is an important miRNA for virus life cycles, such as hepatitis B virus (HBV) and hepatitis C virus (HCV). HCV binds to miR-122 and uses it for viral translation and replication. Inhibition of miR-122 led to reduced HCV abundance, presenting miR-122 as a promising antiviral target.[74] Conversely, miR-122 negatively regulates the HBV virus production by inhibition of the HBV polymerase production and core proteins[75]. Moreover, miR-122 reduces cyclin G1 expression, which inhibits the HBV transcription[76]. Summarizing the role of miR-122 in liver and infectious disorders, miR-122 serves as an important drug target to modulate hepatocellular carcinoma and fibrosis by miR-122 mimics and to reduce HCV replication and plasma cholesterol by anti-miR-122 agents [67].

1.3 MiRNA mimics and inhibitors and their application

1.3.1 MiRNA mimics and inhibitors

As mentioned above, the various gain- and loss-of function studies of specific miRNAs showed increasing evidence of miRNA involvement in diseases, which makes miRNA an appealing target for research, diagnostics and therapeutics. To modulate the function of single miRNAs and elucidate their

potential for therapeutics, two main strategies are applied. The first strategy, restoring of miRNA function, can be achieved either by introduction of the synthetically modified miRNA mimics or by viral vector-based miRNA overexpression [77] [78]. The second strategy, inhibition of miRNA, uses the chemically modified antimiR oligonucleotides [79]. In this section, only the chemically modified miRNA mimics and inhibitors will be described.

The restoring of miRNA activity is achieved by substituting the miRNA mimics with the chemical modifications to improve their stability and cellular uptake (Fig. 2a). Unmodified single-stranded mature miRNA mimics are easily accessible to RNases and unstable in cells. In contrast to unmodified miRNA mimics, the single-stranded miRNA mimics with 5'-phosphorylated end and 2'-fluoro ribose modifications were reported to show substantial miRNA seed-based activity in cells[80]. Despite this fact, the double-stranded miRNA mimics are used preferentially [81]. The double-stranded miRNA mimics are designed as a duplex, where the miRNA of interest is a guide strand and the passenger strand is complementary to the guide strand. The passenger strand can be chemically modified to avoid its loading into RISC and to increase cellular uptake. The guide strand can also contain some chemical modifications that do not disturb its recognition by the RISC , such as the 2'-fluoro modification. Additionally, the double-stranded miRNA mimics should have features of the dicer product (2 nucleotides 3'-overhang and 5'-phosphate group) for efficient recognition and loading into RISC.[79, 82] One example of therapeutic miRNA mimics is the synthetic miR-34 mimic MRX34, which is a double-stranded RNA containing one strand of mature miR-34[83-84]. MiR-34 is a tumour suppressor miRNA, which is found to be downregulated in different cancer types. It was shown in an animal model that systemic delivery of miR-34 mimic, led to a 60% reduction of tumour area in non-small cell lung cancer mouse model in comparison to the control group[85]. Several strategies for improved miR-34 mimic delivery have been developed, such as coating of miR-34 mimics to nanoparticles with tumour-specific antibodies (i.e. anti-disialoganglioside GD_2), administration with atelocollagen or even neutral lipid emulsions[85-87]. In 2020, the results of phase 1 clinical study for MRX34, a liposomal formulation of miR-34a mimic, were published, in which MRX34 was administrated to patients with advanced solid tumours. Unfortunately, the study revealed an immune-related toxicity of MRX34 and an inefficient delivery to the tumour. Consequently, the clinical trial was closed. [88]

The second strategy of miRNA modulation is the miRNA inhibition by chemically modified antisense oligonucleotides (ASOs), also called anti-miR or antagomirs. ASOs specifically hybridise to the target miRNA to form a duplex and, thereby, inhibit their function by sequestering miRNAs and, in some cases, by RNAse H degradation of miRNA[81]. For effective miRNA inhibition, ASOs can contain a variety of the chemical modifications (Fig. 2a) to improve their resistance to nucleases, cellular delivery, binding affinity and selectivity. Several modifications of the sugar moiety, the nucleobase or the linkage between nucleotides were developed to chemically modify ASOs with improved affinity and nuclease stability, such as phosphorothioates, locked nucleic acids (LNA), 2'-modified oligonucleotides (2'-O-methyl (2'-O-Me) and 2'-O-methoxyethyl (2'-O-MOE)), morpholino oligonucleotides. The affinity of chemically modified nucleotides complementary to miRNA decreases in the following order LNA > 2'-O-MOE > 2'-O-Me > morpholino. The nuclease resistance of LNA and 2'-O-MOE is much higher than 2'-O-Me. Morpholinos are uncharged and resistant to nucleases.[89-90] One of the promising therapeutic miRNA inhibitors is a miR-122 antisense targeting drug, named Miravirsen, which contains locked nucleic acid-modified nucleotides. Miravirsen was developed for hepatitis C treatment and is currently being evaluated in the Phase II clinical trials.[91]

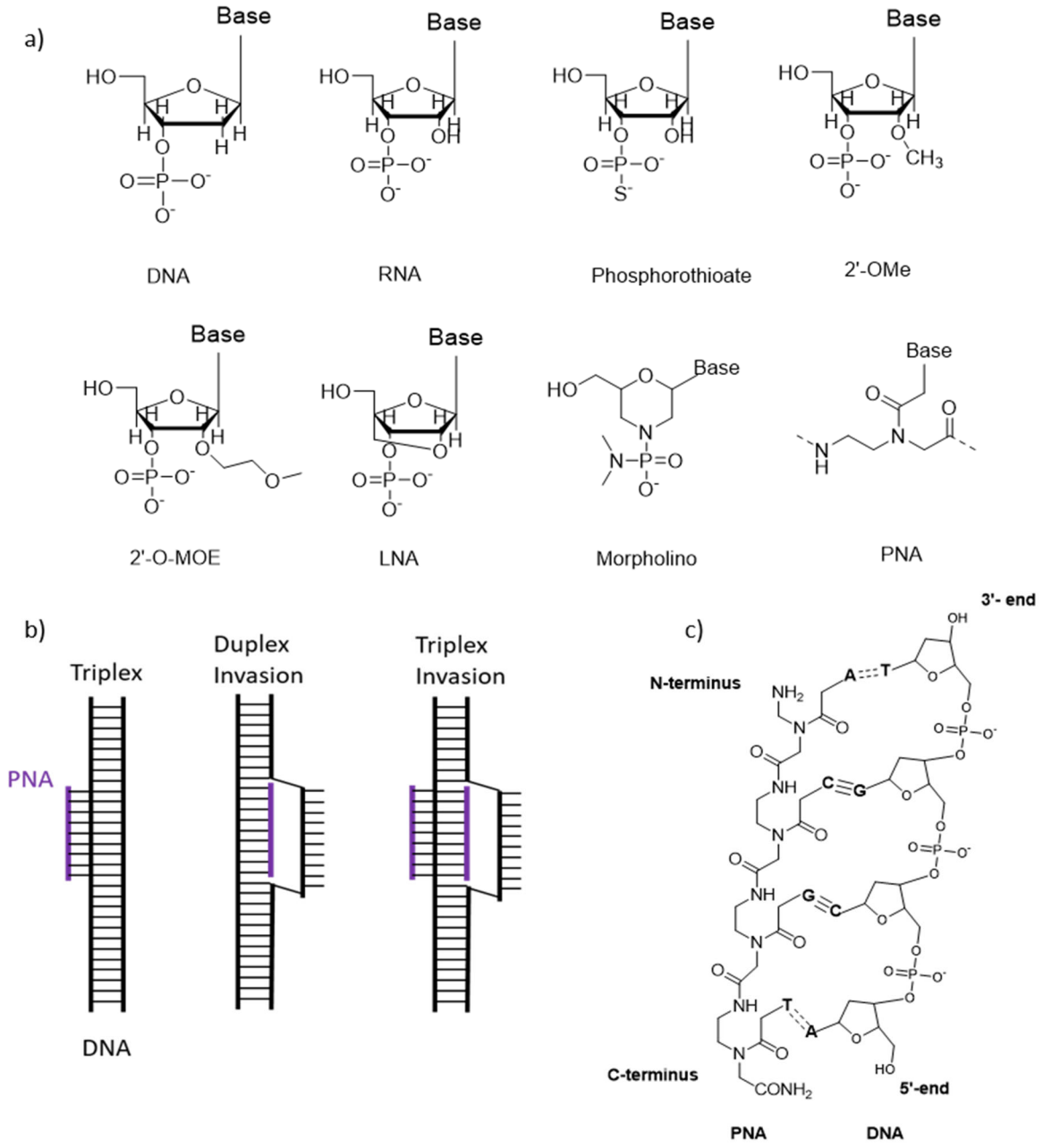

Figure 2. a) Chemically modified nucleotides used for the synthesis of miRNA mimics and inhibitors. b) DNA-PNA binding modes (triplex formation - for pyrimidine-containing PNAs and duplex invasion - for purines/pyrimidine-containing PNAs). c) PNA-DNA duplex (antiparallel orientation). The figures are generated based on previously published data[81, 92].

1.3.2 Peptide Nucleic Acid (PNA)

Peptide nucleic acid (PNA) is a DNA/RNA mimic, which is composed of an uncharged pseudopeptide backbone, consisting of repeating N-(2-aminoethyl)-glycine units linked by amide bonds (Fig. 2a). The nucleobases are connected to the backbone via methylene carbonyl linkages. Since PNAs are uncharged, they do not have an electrostatic repulsion upon DNA/RNA binding and, therefore, have exceptionally high affinity and specificity to complementary DNA and RNA. Thermal stability of PNA-DNA (PNA-RNA) predominates over thermal stability in DNA-DNA or RNA-RNA duplexes [93-95]. In the study of M. Egholm *et al.,* a variety of mismatches was introduced in a DNA target sequence and a single mismatch in the 13-nucleotides DNA target could cause a decrease in T_m (melting temperature) by 8-20°C (depending on the mismatch), which was greater than for DNA-DNA duplexes [93, 96]. PNA-DNA

(PNA-RNA) duplexes are much more sensitive for mismatches, than DNA:DNAduplexes making PNAs suitable for diagnostics, i.e. single-base mutation detection[97].

PNAs can bind in both orientations, parallel (PNA N-terminus to DNA/RNA 5'-end) and antiparallel (PNA N-terminus to DNA/RNA 3'-end). However, antiparallel orientation is much more stable[92, 98]. Depending on sequence composition, PNAs can bind to target DNA/RNA mainly in two modes, such as duplex and triplex (Fig. 2 b, c). The duplex, ruled on Watson–Crick hydrogen bonding, is formed, when PNA is composed of mix nucleobases (purines/pyrimidines), whereas triplex, i.e. PNA_2-DNA, can only be formed with pyrimidine-containing PNAs (the first PNA strand binds to DNA through Watson–Crick bonding, whereas the second PNA shapes Hoogsteen hydrogen bonds).[93, 99-102]

PNAs are not recognised by nucleases and proteases[92] and show high stability in biological fluids. Furthermore, PNA-miRNA duplexes are also resistant towards RNAse H degradation and, for this reason, miRNA inhibition by PNAs should be based on the stability of PNA-miRNA duplex or can be caused by unknown catabolic pathway [98, 103].

In spite of nuclease resistance, high affinity and specificity of PNAs, PNAs have some drawbacks for application in therapeutics, such as poor water solubility and cellular uptake. Since PNAs are not charged, they have a poor water solubility compared to DNA and tendency to aggregate, especially for longer PNAs (>12 mers) and G-rich (>60%). However, modified PNA or chemical incorporations, such as addition of lysine residues, could improve solubility[92, 104-105].

PNA Synthesis

Since PNAs have a peptide backbone, the procedure of solid phase peptide synthesis (SPPS) can be applied for the synthesis of PNA oligonucleotides. The standard SPPS protocol for PNA synthesis gives relatively large quantities, and high yield and purity of PNA[106]. As for SPPS, PNA monomers should also have the amino-protecting groups. The most common among them are tert-butyloxycarbonyl (Boc) and 9-flurorenylmethoxycarbonyl (Fmoc) protecting groups. These PNA monomers are commercially available.

Principally, PNA synthesis consists of repetitive PNA monomer coupling cycles, each of which includes deprotection (removal of protective group) of N-terminus of PNA monomer, coupling of the next N-terminus protected PNA monomer and capping of truncated uncoupled sequences (Fig. 3). PNA synthesis starts from the loading of the first N-protected PNA monomer on polymer support (resin). The first step, deprotection of the N-protecting group, is performed by base (Fmoc-strategy) or by acid (Boc-strategy). Secondly, the next N-protected PNA monomer is coupled to the free amine group of the first PNA monomer by using coupling reagents, typically, of phosphonium or uronium classes. And in the third step, the uncoupled PNA monomers and truncated PNA sequences are capped by acetylation . From that point the steps are repeated until the desired PNA sequence is assembled on the resin. Synthesized PNA sequence is cleaved from the solid support by using TFA-scavenger mixture and purified by preparative HPLC.[107]

In the process of SPPS, PNA sequences can be combined with specific amino acids or peptides to improve solubility and cell penetration. Other chemical modifications, such as labels, dyes and special linkers can be also introduced into PNA sequence.

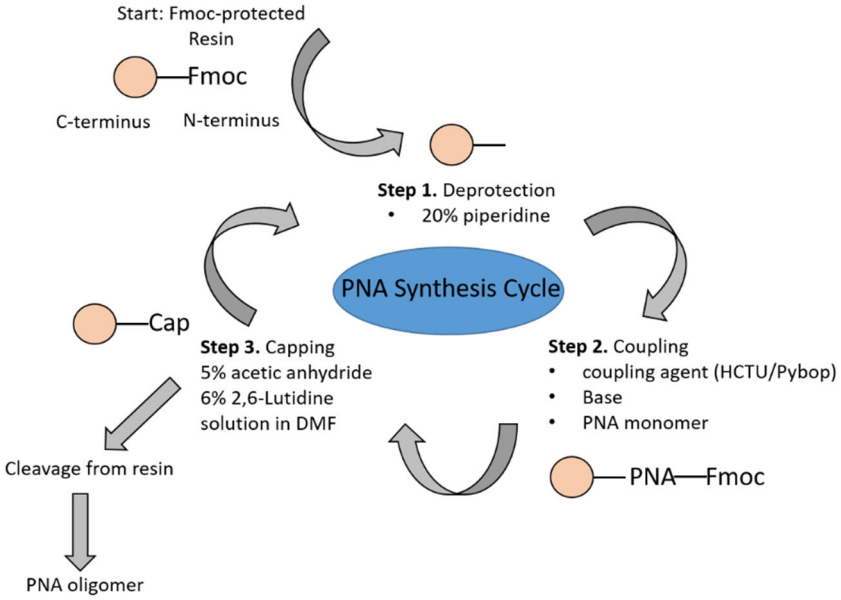

Figure 3. PNA synthesis. The synthesis of PNA oligomer consists of repeated cycles of the deprotection, coupling and capping steps.

PNA Delivery

The main obstacle for the application of PNAs in therapeutics remains the challenge of effectively delivering PNAs into cells. As it was already mentioned, due to the neutral charge the cellular uptake of naked PNAs is really poor.[108] Therefore, the different strategies of PNA transfection have been developed for delivery of modified and unmodified PNAs, including PNA conjugation with cell-penetrating peptides (CPP), microinjection, electroporation, co-transfection with DNA, use of cationic lipids, conjugation with nanoparticles[108-109]. The strategy of CPP conjugation to PNA is widely used for PNA cellular delivery for miRNA inhibition[110].

The principal of CPP was accidently discovered by virologists (A. Frankel *et al.*, 1988) on HIV-1 Tat trans-activating factor and by neurobiologists (A. Joliot *et al.*, 1991) on the *Antennapedia* Drosophila transcription factor, which were able to enter cells and perform their functions [111-112]. The short amino-acids sequences of the TAT (48-60 amino-acids) and Penetratin, derived from these proteins, behave the same way as original proteins. TAT and Penetratin were successfully used for conjugation to oligonucleotides as a cellular delivery tool.[113-114] After elucidation of the penetration ability of TAT 48-60, the polyarginins were also proposed for cellular uptake[115]. Moreover, coupling of PNA sequence to positively charges polypeptides, such as polyarginins and polylysines, has been reported to significantly enhance cellular delivery of PNAs[110]. The next generation polyarginin peptide $(R\text{-}Ahx\text{-}R)_4$ consists of arginines linked with the spacer, aminohexanoic acid, which results in enhanced CPP flexibility and enables superior cellular internalization over regular polyarginin [116]. Later, chimeric CPP, such as MPG and Transportan were developed, which contains conjugated domains from the different protein sources [117-118].

Initially, a receptor-free and non-endocytotic mechanism of cellular internalization has been proposed by many groups. However, it was carefully evaluated and revealed to be based on method artefacts, caused by fixed cells in fluorescence microscopy and FACS. [119-121] Use of live cells microscopy without fixation and modified FACS protocol, including trypsin treatment, helped to conclude active process of cellular internalization involving endocytosis.[119, 122] Richard J. *et al*. have revealed a clathrin-dependent endocytosis as a high priority pathway for TAT and TAT-PNA cellular internalization.[122] Nevertheless, for high CPP concentrations the energy-independent non-endocytotic mechanism could be preferential, whereas for low CPP concentrations the endocytosis is a predominant mechanism.[115]

PNA Application

PNAs have already found their application in diagnostics and in development of gene therapy. However, low solubility in water and poor cellular delivery of PNAs are still the main obstacles on the way to transferring research progress to therapeutics.[108]

In the field of diagnostic, PNA are used for fluorescence *in situ* hybridization (PNA-FISH), polymerase chain reaction (PCR) and microarray. The method FISH is often used in clinical studies for the pathogen identification. The PNA-FISH method is reported for detection of catheter-related bloodstream infections (i.e. *Staphylococcal* bacteraemia, *E. coli* serotype O157), *Stenotrophomonas maltophilia* from common bacterial species in the respiratory tract, *candida sp*. from blood and peritoneal fluid specimens, *proteus spp*., which causes urinary infectious and many other pathogens. [108, 123] QuickFISH is an improved PNA-FISH method with reduced diagnostic time from AdvanDx inc. The additional PNA-involved method is a variation of PCR, PNA-mediated PCR clamping. For example, PNA-mediated PCR clamping technique is applied for detection and quantification of the Multiple Sclerosis-Associated Retrovirus (MSRV), where PNA blocks amplification of MSRV's close relative ERVWE1[124]. The second example of application of PNA in PCR clamping is a detection of single point KRAS mutations in colorectal cancer patients, where PNA probes discriminate alleles differing by one single nucleotide[125]. Besides PCR clamping, PNA probes are used in PCR as a sensor probe for the detection of low copies of drug-resistant influenza viral gene[108]. In microarray technique the PNA probes are immobilised on solid surface and enable the detection of DNA/RNA in a high-throughput panel. PNA-microarray has found its application in the detection of single-nucleotide polymorphism (SNP), monitoring of disease-related miRNA expression and pathogen detection[126].

1.3.3 Small Molecular Inhibitors (SMI)

ASOs for miRNA inhibition are currently being developed for therapeutic use, although, there are still some remaining challenges, such as insufficient delivery, poor pharmacodynamics and pharmacokinetic properties[127-129]. As an alternative, small molecules can be used for inhibition of miRNA expression, which have the advantage of higher uptake than ASOs and lower cost. The Small Molecular Inhibitor (SMI) approach is based on the recognition of special characteristics of secondary RNA structure, which determine "drugability" of a particular RNA[130]. The special characteristics of secondary RNA structure, which can be recognized by SMI, are perturbations in RNA helix, which are formed by un- or mispaired bases, such as hairpin loops, internal loops and bulges regions. Targeting the major and minor grooves of RNA (deep and shallow grooves) by SMI is usually not possible. Although, only the major groove contains discrimination edges of all base pairs, it is too narrow for SMI binding [130-132]. The three major RNA classes, which became SMI targets, were antibacterial, antiviral RNA and mRNA. Binding to the specific RNA/mRNA, the SMIs can inhibit RNA-protein interactions or protein production. However, most of SMIs, which bound to their RNA target *in vitro*, were rarely tested in cell culture or *in vivo*[130]. Beginning from the discovery of antibacterial RNA targets, the primary data from the crystal structure of the bacterial ribosome complex showed that antibiotics prefer to bind to the ribosomal RNA (rRNA), rather than to ribosomal proteins. Looking for treatment of infectious diseases, researchers found several antibiotics of the aminoglycoside family, which interact with the bacterial rRNA. Antibiotics can bind to different structures of rRNA, such as shallow groove (spectinomycin), deep groove (hygromycin) or at a three adenine bulge (aminoglycosides) [133-134]. In relation to viral RNA targets, the investigations have revealed an important HIV-1 Rev response RNA element (RRE), to which the REV protein binds in order to transport viral RNA from host nucleus into cytoplasm. The inhibition of REV-RRE protein-RNA interaction disturbs viral replication and its maturation. [130, 135] Green *et. al.* have shown that aminoglycosides, including neomycin, can specifically inhibit REV-RRE interaction by binding to the RRE RNA. [136] However, it should be taken into

consideration that the RNA self-assembly and recognition motifs are modular (block-structured) and repetitive, which can be a main obstacle for the specificity in the SMI drug development[134]

MiRNAs and their precursors also offer suitable secondary structures for SMI targeting: bulges and internal loops in mature miRNAs and hairpin loop structures of pre-miRNAs. Theoretically, miRNA maturation can be modulated on all stages: pre-transcriptional, transcriptional and post-transcriptional. The pre-transcriptional stage includes modulation of miRNA expression through control over promotor regions, the transcriptional stage by targeting of transcriptional factors and the post-transcriptional stage by inhibiting of Drosha and Dicer activity. However, it is hard to achieve modulation of the specific miRNA expression on the pre- and transcriptional stages, since alteration of the promotor state and transcriptional factors can affect numerous genes[137]. The high-throughput screening of SMI libraries helps to identify the SMIs with the highest selectivity, which can block the biogenesis of the specific miRNAs[127, 138]. Gumireddy *et.al.* was the first to publish a study about specific miRNA inhibition by SMIs. They have screened more than 1000 SMIs for their ability to selectively inhibit miR-21 expression and discovered the specific miR-21 inhibitor azobenzene 2. The cells treated by azobenzene 2 have decreased expression of not only mature miR-21, but also pri-miR-21, showing inhibition of miR-21 gene transcription. [139] Young *et. al.* has performed a high-throughput screen of 1364 compounds on their ability to modulate miR-122 expression and discovered small molecular inhibitors and small molecular activator of miR-122 expression, which affect transcription of the miR-122 gene. The small molecular miR-122 inhibitor also demonstrated inhibition of HCV replication in liver cells. [140] Costales *et al.* reported a small molecule bis-benzimidazole, Targepremir-210 (discovered by Inforna approach[141]) that specifically binds to the dicer site of the miR-210 precursor (pre-miR210) and, thus, blocks the dicer-mediated production of miR-210[142]. MiR-210 is an oncogenic miRNA and a promising diagnostic/drug target, which is overexpressed in breast cancer tissues and associated with a poor prognosis, cancer progression and resistance to chemotherapy[143]. Targepremir-210 treatment caused a significant decrease in tumour growth *in vivo* by using mouse xenograft model of hypoxic triple negative breast cancer (negative for estrogen and progesterone receptors, and HER2 protein)[142]. It is worth to mention, Targeprimir-210 downregulated only miR-210 and none of 28 other hypoxia-related miRNAs. Moreover, the selectivity of the compound was also validated by using a microarray of 2500 miRNAs[142].

The same group identified a small molecular inhibitor, namely Targaprimir-515/885, which targets Drosha-processing sites of primary miR-885 and miR-515, which have structural similarities. An advanced inhibitor Targaprimir-515, which is a dimer of Targaprimir-515/885 exhibited a selectivity only against pri-miR155.[144] MiR-515 is also oncogenic miRNA, which downregulates sphingosine kinase 1 (SK1). The cellular role of SK1 is to promote the synthesis of the sphingosine 1 phosphate (S1P) and, therefore, cell proliferation, by activating the growth-associated proteins (e.g. human epidermal growth factor receptor 2 ERBB2/ HER2). The authors showed that specific inhibition of miR-515 by Targaprimir-515 in MCF-7 breast cancer cells led to the HER2 upregulation, thus making MCF-7 cells sensitive for Herceptin, HER2-targeted anticancer therapy. The selectivity of compound was also investigated by using RNA sequencing and proteome screening methods, demonstrating minor changes in a whole transcriptome (99.7% were not affected) and expected changes in protein and RNA level of SK1 and HER2 expression, as well as in the mediators of cellular proliferation pathways.[144]

Although, several SMIs were reported as specific miRNA inhibitors, which affect the mature miRNA level and target the transcription of specific miRNA-coding genes, a careful evaluation of their selectivity should be conducted in *in vitro* and *in vivo* assays for revealing their off-targets. Moreover, current computational tools (e.g. Inforna) for SMI design allow to identify SMI's potential off-targets and, thus, assess the selectivity of candidates already on the SMI design step.

1.3.4 Techniques for SMI high-throughput screening (HTS)

The high-throughput screening (HTS) of SMIs can be conducted *in vitro* or *in silico.* The most popular methods for HTS *in vitro* include fluorescence assays (fluorescent beacon approach, polarization assay) and assays with luciferase reporter constructs. In addition, the dicer-mediated branched rolling-circular- amplification (BRCA) has been reported as a convenient and rapid method for the assessment of miRNA maturation and evaluation of SMI (Fig. 4) [137, 145].

The Fluorescence beacon approach is based on a hairpin shaped fluorescent probe, containing a 5'-fluorophore and 3'-fluorescence quencher (Fig. 4a). This technique was applied for SMI screening on the ability to inhibit the dicer-mediated miRNA-maturation, where the labelled pre-miRNA hairpin structures are used as fluorescence beacon probes. In the intact pre-miRNA fluorescent beacon, the fluorophore and the quencher are positioned in the close proximity, whereas dicer-mediated cleavage of pre-miRNA beacon lead to the dissociation of the fluorophore and the quencher and, therefore, to an increase in fluorescence. The SMI binds to pre-miRNA and inhibits the interaction of Dicer, which results in reduced fluorescence or lack of fluorescence[146-147]. However, it has recently been reported that both the 5'- and 3'- ends are important for Dicer recognition of pre-miRNA and its proper cleavage [37-39]. That is why the modifications of the 5'- and 3'-ends of pre-miRNA might inhibit the binding and activity of Dicer themselves. Thus, Bose *et. al*. has modified this technique by using the DNA molecular beacon (with a 5' fluorophore and 3' quencher), which is independent from pre-miRNA structure and complementary to the mature miRNA produced in the Dicer cleavage reaction. In this assay, the fluorescence raises as a result of successful dicer-mediated cleavage due to hybridization of the DNA molecular beacon to mature miRNA. In the case of inhibition of dicer-mediated pre-miRNA cleavage, there is no mature miRNA and the fluorescence is not observed[148].

The Polarization assay. The method of fluorescence polarization (FP) is developed for the analysis of diverse molecular interactions. The theory of FP has been first described in 1926 by Perrin [149], and its principle is based on the fact that the degree of polarization is inversely proportional to its molecular rotation[150]. A fluorescent molecule is excited with plane polarized light through excitation polarizing filter. If a molecule is very large and remains stationary during excitation, then the emitted light is highly polarized. The small molecules rotate and tumble fast and the emitted light is depolarized relative to the excitation plane.[151] The FP technique was applied for HTS of modulators of RISC components. Tan *et al.* have used the fluorescence polarization assay to identify SMI for RISC-loading inhibition, based on fluorescence polarization of TAMRA-labelled miRNA - Ago2 complex. In this FP assay, the labelled miRNA alone is free to rotate in the absence of Ago2 and its fluorescence polarization is low. In contrast, the labelled miRNA in the complex with Ago-2 rotates slowly and, therefore, emitted light is highly polarized. The FP assay can be also applied for the validation of small inhibitory compounds in other steps of miRNA biogenesis. [137, 152]

In 2010*, The Luciferase reporter assay* was established by Young *et. al.* for the SMI HTS for detection of specific miRNA expression in cells based on psiCHECK-2 vector (Promega) (Fig. 4b)[140]. The psiCHECK-2 vector is one of the numerous commercially available vectors, in which a specific miRNA target sequence can be inserted downstream of a luciferase reporter gene. The plasmid containing the miRNA target sequence is transfected into cells for the detection of miRNA expression level via the luciferase luminescence. In the psiCHECK-2 vector (Promega) a miRNA target sequence is cloned downstream of a *Renilla* luciferase gene. After plasmid transfection into cell, the cellular specific miRNA binds to the transcribed miRNA target conjugated with *Renilla* luciferase, causing its cleavage by RNA interference mechanism (RNAi). As a result, the *Renilla* luminescence is low for highly

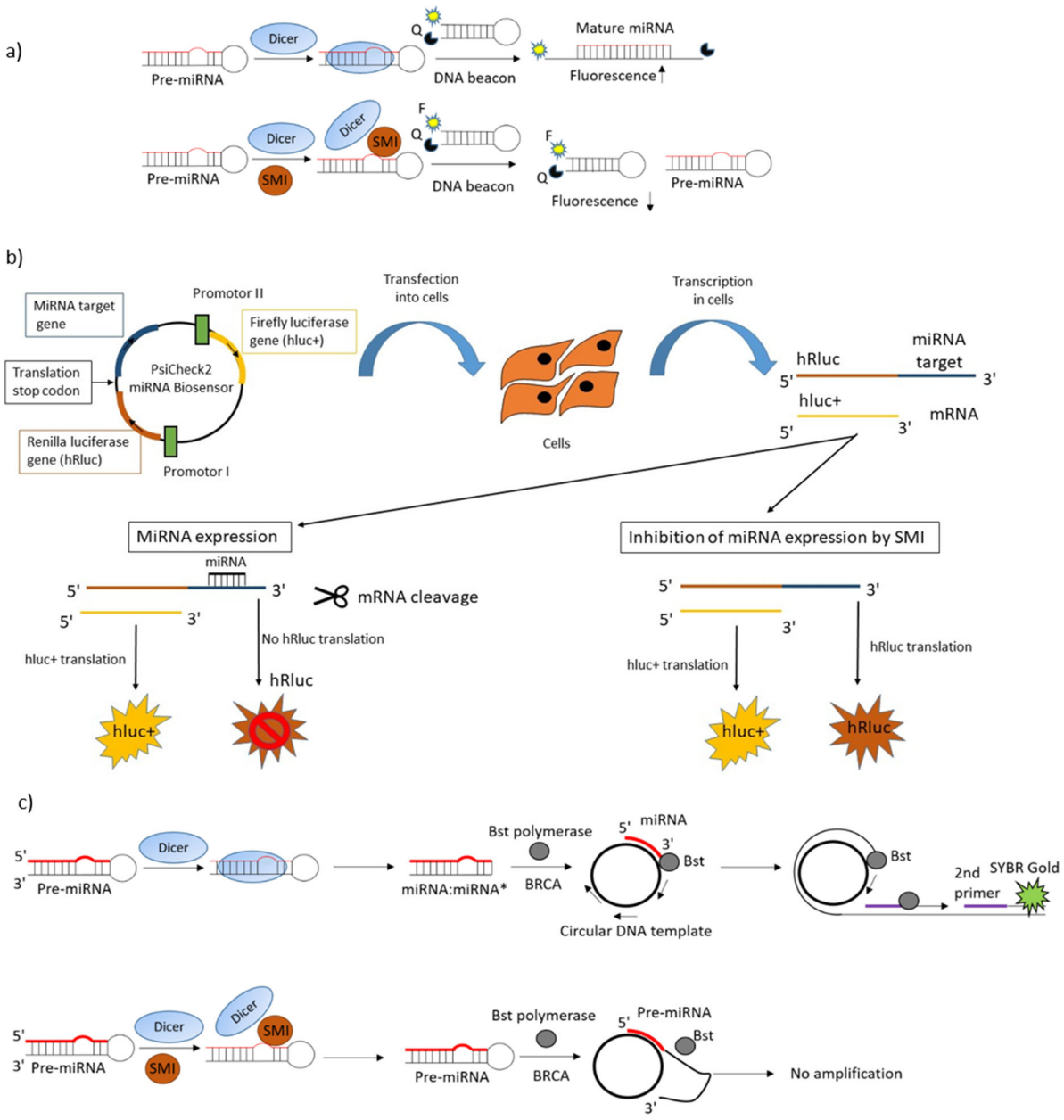

Figure 4. High-throughput techniques for SMI screening in vitro. a) *Fluorescent DNA molecular beacon.* Fluorescent DNA molecular beacon hybridizes to the specific mature miRNA. Inhibition of dicer-mediated miRNA maturation leads to the decreased level of fluorescence. b) *Luciferase reporter psiCHECK-2 (Promega)* with introduced specific miRNA target gene. The psiCHECK-2 miRNA biosensor is transfected into cells, where the *Renilla* luciferase (hRluc) mRNA fused with the miRNA target and *Firefly* luciferase (hluc+) mRNA are transcribed. The hRluc luminescence exhibits the presence or absence of specific miRNA, whereas hluc+ luminescence serves as a transfection control. Increase in hRluc luminescence shows inhibition of miRNA expression by small molecular inhibitors. c) *Dicer-mediated Branched Rolling Circular Amplification (BRCA)*. BRCA is capable to monitor the production of the specific mature miRNA in the dicer cleavage reaction. In case of successful pre-miRNA cleavage, mature miRNA serves as a primer for the Bst DNA polymerase in the BRCA reaction from a circular DNA template. The additional amplification will occur from the secondary primer from the linear ssDNA product. In contrast, the amplification will not be initiated from unprocessed pre-miRNA. SYBR Gold is used for detection of the BRCA reaction.

expressed miRNAs. In case of a decreased miRNA level, i.e. in the presence of miRNA inhibitors, such as SMI, the *Renilla* luminescence increases. The psiCHECK-2 vector contains also a control *Firefly* luciferase gene, which is not fused to the miRNA target sequence, and, consequently, is independent

of the miRNA level. The *Firefly* luciferase luminescence serves as a transfection control. The *Renilla* luciferase reporters provide high sensitivity, convenient and rapid detection of miRNA level in cells. Using the psiCHECK-2 reporter plasmid, Young *et al.* have screened the panel of SMIs, targeting miR-122 maturation. The huh7 cells were treated with 1364 SMIs, and the *Renilla* luciferase signal was assessed after 48h. Two compounds were identified to increase the relative luciferase signal and showed inhibition of HCV replication in liver cells[140]. In a similar approach, Bose *et. al.* used the luciferase-based pEZX-MT01 reporter for screening of 15 SMIs (aminoglycosides) in MCF7 cells on the ability to inhibit the miR-21 maturation. Among them, streptomycin was discovered to inhibit the miR-21 maturation. However, analysis of its selectivity on ten additional miRNAs showed that besides miR-21, miR-27a expression was also downregulated after treatment by streptomycin[153].

Dicer-mediated branched rolling circular amplification (BRCA) method enables the detection of mature miRNA formation in the dicer-mediated pre-miRNA cleavage reaction (Fig. 4c). Therefore, this method can be used for the assessment of novel specific inhibitors of miRNA maturation. The principle of BRCA lies on an isothermal and linear DNA amplification by DNA polymerase (i.e. Bst), using mature miRNA as a primer, which is complementary to the circular DNA template. Additionally, a primary DNA product serves as a template for the amplification from the secondary primer. SYBR Gold, a double-stranded DNA specific fluorescent dye, is used for the detection reaction, which can be monitored on a regular real-time polymerase chain reaction (PCR) machine. The more miRNAs form in dicer cleavage reaction, the more fluorescence raises. In case of dicer inhibition, unprocessed pre-miRNA can not initiate amplification, and fluorescence does not increase. [145 154-156].

HTS techniques in silico are computational strategies for predictive SMI modelling, which include structure-based or receptor-based approaches and ligand-based approaches. The first approach (structure-based or receptor-based) is directed on the identification of miRNA-binding molecules, which energetically match the pocket of the predicted or existing miRNA structure. The second approach (ligand-based) models structure-activity relationships (QSAR) or pharmacophore, which means using chemical databases to identify potential inhibitors of specific miRNA[137, 157-158].

Recently, Shi *et al*. have identified AC1MMYR2, a SMI for inhibition of miRNA-21 maturation, by using *in silico* 3D structure prediction. AC1MMYR2 blocks the dicer processing of pre-miRNA-21, which was validated *in vitro* on epithelial tumour cells and *in vivo* on orthotopic nude mouse models. Moreover, AC1MMYR2 was determined to suppress tumour growth and invasion through upregulation of miR-21 targets (PTEN, PDCD4 and RECK) and provided reversal of epithelial-mesenchymal transition (EMT) *in vitro* and *in vivo* models. Furthermore, the selectivity and specificity of AC1MMYR2 was investigated by RT-qPCR, measuring the expression of additional eleven miRNAs. It was shown that five miRNAs were downregulated in response to AC1MMYR2 treatment[137, 159]. Despite the AC1MMYR2 inhibitory activity of miR-21 maturation and its robust antitumor efficiency, the specificity issue makes its further therapeutic potential study doubtful.

1.4 Forced intercalation (FIT) probes

1.4.1 Introduction into Forced Intercalation (FIT) probes

The concept of forced intercalation (FIT) PNA-based probes was introduced by Seitz *et al.,* in which an intercalator cyanine dye, thiazole orange (TO), replaces a canonical nucleobase, thereby, serving as a nucleobase surrogate (Fig. 5) [160-163]. Upon hybridization with target DNA/RNA, the dye is forced to intercalate at a desired position in the probe-target complex, which results in an increase of fluorescence. The cyanine dyes are environmentally sensitive fluorophores and intercalation restricts torsions around the central methine bridge and increase the lifetime of the excited state[164]. The fluorescence of FIT probes is strongly dependent on their hybridization state: the unbound FIT-probes

have a low fluorescence (F_0), whereas the hybridized probes have an enhanced fluorescence (F). The ratio F/F_0 describes the responsiveness of the FIT probes.

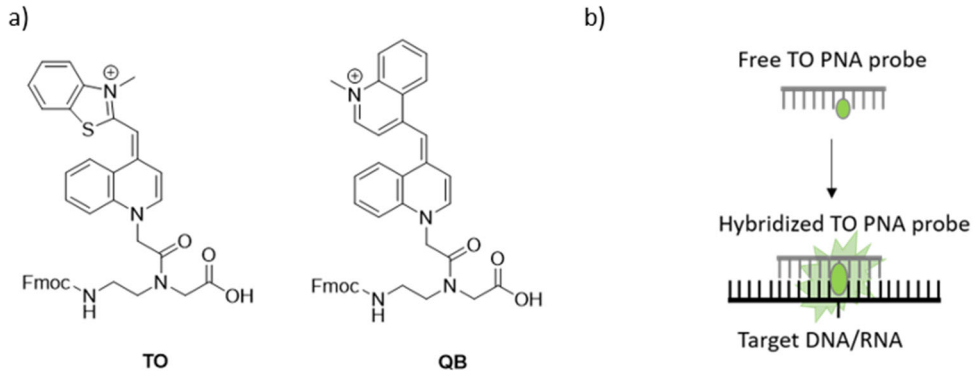

Figure. 5. Chemical structures of TO- and red-shifted QB-labeled PNA monomers (a). The principle of nucleic acid detection by FIT probe (b).

For simultaneous multiple target detection in homogeneous solution, besides TO (λ_{em} =535 nm), additional dyes of the cyanine family were investigated and applied, such as BO (λ_{em} =485 nm), high emissive oxazole yellow YO (λ_{em} =498 nm), quinoline blue QB (λ_{em} =610 nm), etc. [165-166]

1.4.2 Application of FIT probes

The FIT-PNA probes enable sequence-specific detection of DNA and RNA, what makes them suitable for many applications in research and diagnostics, such as detection of single-nucleotide polymorphisms (SNP) and point mutations and visualisation of particular RNAs in live cell imaging. For cancer diagnostics, FIT-PNA probes were utilised for single nucleotide mutation detection in the KRAS oncogene, of which transition G to A in the 12th codon is the most frequent mutation in pancreatic cancer[165, 167-169]. FIT-PNA probes have been also applied for the analysis of two important single nucleotide polymorphisms (SNPs) in the CFTR gene by quantitative PCR[170]. Regarding the visualization of RNA in cells, it was shown by Seitz *et. al.* that single-chromophore FIT PNA probes enabled the detection of influenza H1N1 mRNA in infected living cells[171]. In another study, benzothiazole orange (BO) labelled and TO-labelled PNA probes were successfully used for the simultaneous imaging of two viral mRNAs, coding neuraminidase and matrix protein 1, in influenza H1N1 infected live cells[162]. To decrease the background fluorescence of the unbound probes, Seitz and co-workers developed dual labelled PNA probes that contained two dyes for the energy transfer, such as donor TO dye, which is sensitive to the target hybridization, and acceptor dye attached to the probe terminus. By this means, the probe provided high responsiveness, up to 450-fold fluorescence enhancements upon target hybridization[161]. In a recent study, FIT PNA probes were designed for detection of RNA editing, a mechanism of post-transcriptional regulation of gene expression, which results in sequence variation (conversion of specific cytosine to uracil or adenosine to inosine) in the RNA molecule. In this case, the three dyes have been used in a binary probe system, which contains dual labelled TO/JO (oxazolopyridine) hybridization probe 1 (donor for FRET) and NIR664-labeled sequence specific probe 2 (acceptor for FRET) (Fig. 6a). The probe system is capable of distinguishing between three states: absence of RNA target, presence of C→U edited RNA target or unedited RNA target[172].

The FIT approach was also transferred to DNA probes. DNA oligonucleotides have a good water solubility in comparison to PNA. Moreover, the transfection of DNA oligos into cells is well established and does not require additional sequence modifications of DNA probes. However, it was shown that unbound TO-labelled DNA probes have a higher background fluorescence than PNA probes, since cationic TO is attracted to DNA electrostatically and interact with

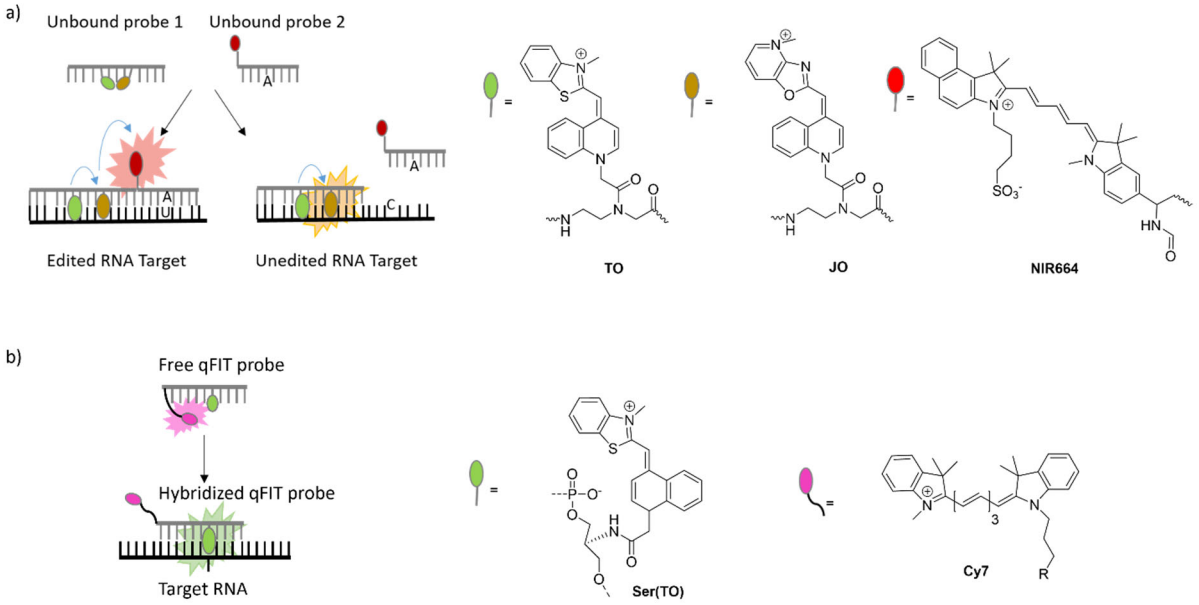

Figure 6. The strategies for nucleic acid detection using thiazole orange: a) Binary probe system, TO: λ_{ex} =515 nm, λ_{em} =530 nm , JO: λ_{ex} =530 nm, λ_{em} =545 nm, NIR664: λ_{ex} =667 nm, λ_{em} =690 nm. b) DNA qFIT probes. The figures are generated based on previously published data[172-175].

DNA nucleobases within probe[173, 176]. The different modifications were applied to DNA FIT probes to improve their brightness and responsiveness. The strategy of multi-TO-labeled probes helped to increase responsiveness but did not enhance the brightness due to self-quenching of two TO dyes. Seitz *et. al.* offered to use the combination of the TO and oxazolopyridine analogue JO dye, which was effective in the improving of both brightness and responsiveness. The unbound TO/JO DNA FIT probe had a contact-quenching and was non-fluorescent in the absence of target. After probe-target hybridization, the TO/JO pair serves as a highly responsive donor and a highly bright acceptor, respectively, for efficient FRET. The TO/JO probe enabled the visualization of oskar mRNA in *Drosophila* oocytes by fluorescence microscopy.[177]

As an alternative strategy to enhance the probe brightness, LNA-enhanced DNA FIT probes were developed by Seitz *et.al.* TO-containing DNA FIT-probes were improved by introduction of a local constraint (LNA modification) in a close proximity to the TO dye, which brings increased viscosity in the TO vicinity and, therefore, improved brightness upon probe-target binding. LNA-enhanced FIT DNA probes were capable to track of oskar mRNPs in wild-type living *Drosophila melanogaster* oocytes by using confocal microscopy method.[177] To further develop this strategy for multicolour RNA imaging, the red-shifted QB dye (λ_{em} =610 nm) was used in FIT DNA probes by Seitz *et. al.*, which is capable to overcome cell autofluorescence and, thus, is convenient for application in cell imaging. Moreover, QB showed a high responsiveness and increased their fluorescence up to 195-fold upon target hybridization. For simultaneous detection of three RNA targets in homogenous solution, the set of three BO-, TO- and QB-labeled FIT probes has been used. In *Drosophila melanogaster* oocytes, LNA-enhanced TO- and QB-containing DNA FIT-probes enabled to localize oskar mRNA and other polyadenilated mRNA molecule by using of wash-free fluorescent *in situ* hybridization and super resolution microscopy.[166]

Although, the DNA FIT-probes were successfully applied for visualization of RNA in cells, the quantitative RNA imaging remained to be challenging, because a fluorescence of high concentration of unbound probes masks a fluorescence of low concentration of target-bound probes. To address this issue, DNA qFIT (quantitative forced intercalation) probes were designed by Seitz and co-workers,

which contained the combination of TO and near-infrared (IR) Cy7 dye (Fig. 6b). The TO dye served as a reporter of the hybridization state and its fluorescence increased upon target hybridization, while Cy7 fluorescence, which was recorded on the second channel, is a measure of probe concentration. The DNA qFIT probes were utilized for localization and quantification of *oskar* mRNA in specific compartments of *Drosophila melanogaster* oocytes by wash-free fluorescence in situ hybridization[175].

1.4.3 Alternative strategies for nucleic acid detection using thiazole orange

The Light-Up probes, discovered by Svanvik et al. (Fig. 7a), have a TO chromophore bound to the N-terminus of PNA through a long flexible linker. This flexible and long linker has the advantage to decrease background fluorescence of the unbound TO PNA probe, whereas hybridization with the DNA target results in up to 50-fold fluorescence enhancement. The Light-Up probes were successfully tested for the post detection of PCR products and for hybridization assays in homogeneous solutions[173].

In contrast to abovementioned FIT probes and Light-UP probes, where a single TO chromophore was used, the double-labeled TO strategy was introduced by Okamoto et al, named them exciton-controlled hybridization oligonucleotides (ECHO) probes (Fig. 7b)[178]. ECHO probes contain two thiazole orange dyes, which are conjugated via long, flexible linkers to a pyrimidine base. The emission of free ECHO probe is suppressed by the formation of H-aggregate between two TO dyes. As soon as the ECHO probe hybridizes to its DNA/RNA target, the H-aggregate is destroyed and the TO chromophores intercalate in the probe/duplex, which leads to an increase of fluorescence. The Okamoto group has synthesized multicolour ECHO DNA-based probes for multiple target detection. ECHO probes were effectively used for intracellular RNA imaging as well as for live-cell RNA-imaging, including simultaneous detection of three miRNAs in Hela cells[174, 178-180].

Another approach for nucleic acid detection by TO relies on the structure of a molecular beacon, which was presented by Wagenknecht *et. al.* (Fig. 7c) [181-182]. The authors used a combination of TO and thiazole red (TR) in a molecular beacon-like structure, named in-stem labelled beacon, which served as a chromophore pair for FRET. Excitation by TO-selective wavelength (490 nm) leads to red colour fluorescence emission (670 nm) for the intact non-hybridized in-stem labelled beacon, while the hybridized probe changes its emission colour for green (530 nm)[181]. This double-labelled FRET principal was also applied for so-called “RNA traffic lights” by Holzhauser *et. al.*, to monitor siRNA integrity in live cells (Fig. 7d). [183]

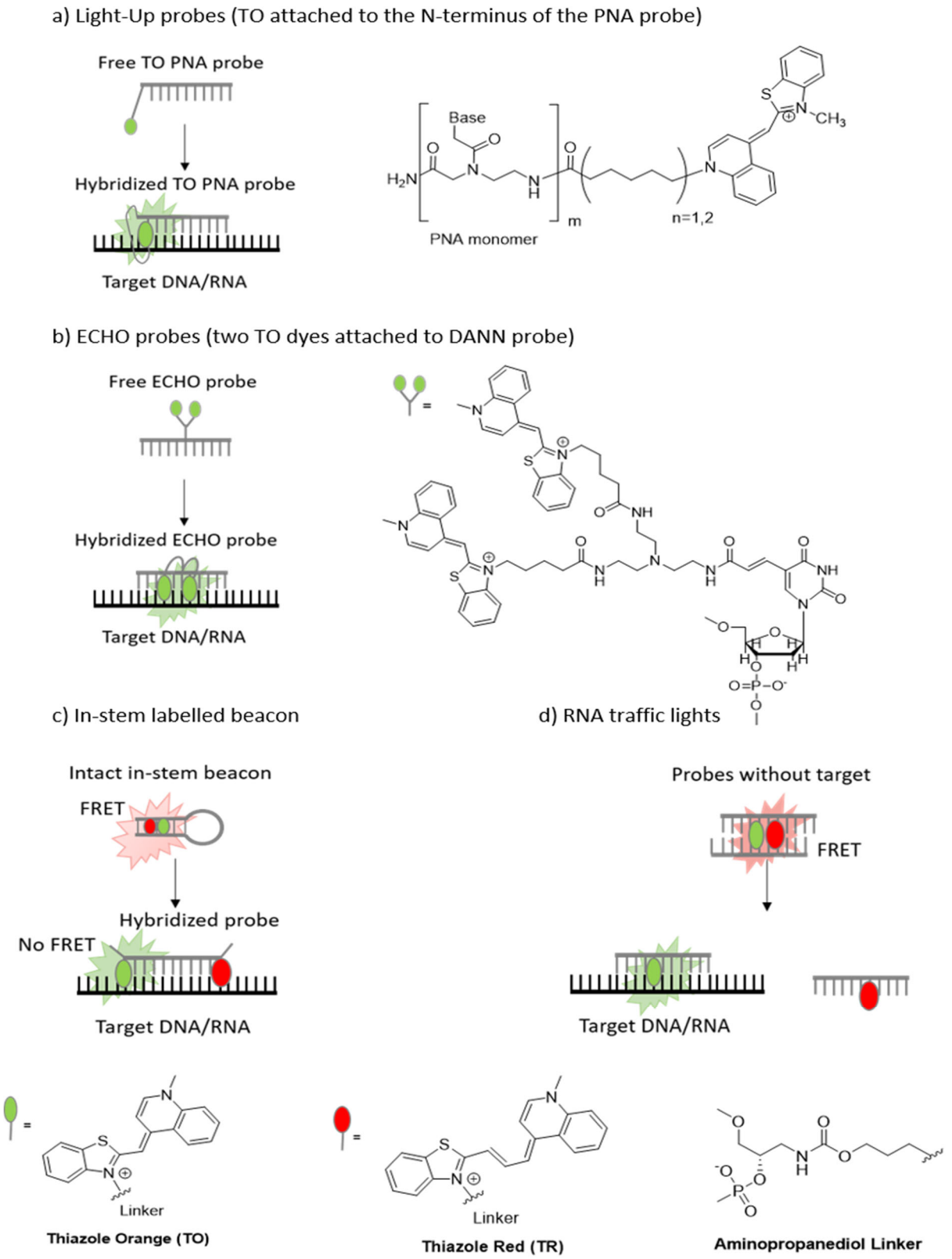

Figure 7. Alternative strategies for nucleic acid detection using thiazole orange – a) Light-Up probes, b) ECHO probes, c) In-stem labelled beacon (molecular beacon structure, where the two dyes TO and TR are in the close proximity to each other, therefore, potentially ready for FRET) and d). RNA traffic lights. The figures are generated based on previously published data[172-175].

1.5 Quantitative Reverse Transcription Polymerase Chain Reaction (RT-qPCR) as a gold standard method for miRNA detection

Since miRNAs are promising biomarkers in clinical diagnostics and potential drug targets, miRNA detection methods are rapidly developing to achieve high sensitivity, multiplexity, practicability and advantage of low cost. The Quantitative reverse transcription polymerase chain reaction (RT-qPCR) is very sensitive and widely-used method for miRNA detection (even for low abundant miRNAs). The RT-qPCR method is actively applied for the research purpose, including the validation of next-generation sequencing and microarray results, as well as for the examination of the miRNA expression in a clinical diagnostics. This method contains two steps, such as reverse transcription (RT), where target miRNA converts into cDNA, and followed by quantitative polymerase chain reaction (qPCR), where the resulted cDNA is amplified and quantified. Although, RT-qPCR method is well established for quantification of mRNA, the great efforts were directed for the method optimization specifically for miRNA quantification due to their short size. Moreover, the particular attention should be paid to miRNA sample preparation and miRNA extraction, since robust RT-qPCR results relies on the quality of input miRNA[184-185].

The first step, reverse transcription, could be done by using either miRNA-specific RT primer or a common RT primer. Chen *at el.* introduced the miRNA specific stem-loop primer for reverse transcription, followed by TaqMan PCR analysis (Fig. 8a). In the first step, the stem-loop RT primer, specific for particular miRNA, hybridizes to mature miRNA and is served for the initiation of reverse transcription by MultiScribe reverse transcriptase to produce cDNA. In the second step, the produced cDNA is used as a template for TaqMan PCR assay with the miRNA-specific forward primer, universal reverse primer and the miRNA-specific TaqMan probe. The intact TaqMan probe contains the fluorophore and the quencher, which are in a close proximity to each other, and, therefore, the probe is non-fluorescent. After TaqMan probe hybridization to cDNA template, the probe is cleaved by DNA polymerase during DNA polymerization process, and the non-quenched fluorophore emits light[186]. In contrast to Chen group, Raymond *et al.* have designed a linear tailed miRNA-specific RT primer for cDNA synthesis in order to introduce a universal PCR binding site in cDNA and to extend the cDNA length. The primer-extended cDNA was amplified and quantified in the following real-time PCR by using universal forward primer, LNA-containing short miRNA-specific reverse primer and SYBR Green intercalating dye for the reaction detection[187]. However, the design of linear RT primers is easier, the stem-loop RT primer enables more specific and sensitive reverse transcription of mature miRNAs comparing to linear RT primers, excluding unspecific amplification of pri-/pre miRNA. Commercially available miRNA-specific sets of primers (including the miRNA-specific stem-loop RT primer and TaqMan probe) and reagents are offered by Applied Biosystems/ Thermo Fisher for quantification of a variety of miRNAs[184]. In spite of the advantage of the high sensitivity of the miRNA-specific stem-loop RT method, the usage of the miRNA- specific RT primer means that it is impossible to simultaneously quantify multiple miRNAs from a single cDNA sample.

As opposed to the miRNA-specific RT primer, the universal RT primer can be also applied for cDNA synthesis, which allows multiple target quantification from one cDNA synthesis. Before using the universal RT primer, the miRNA sequence should be elongated by enzymatic methods, using poly(A) polymerase to add poly(A) tails to the target miRNAs or T4 ligase to ligate a common adapter sequence to miRNAs[184-185]. The polyadenylation of miRNAs is considered to be more convenient, since poly(A) polymerase has a stable activity independently of sequence, whereas T4 ligase can change its effectivity in a preference to sequence[185]. The group of Shi R. *et al.* has applied polyadenelate polymerase (PAP) for the polyadenylation of miRNAs before reverse transcriprion. After

polyadenylation of miRNAs, the reverse transcription has been performed with universal RT primer, which hybridizes only to miRNAs, elongated with poly(A) tails (Fig. 8b). The universal RT primer contains the poly(T) sequence conjugated with the adapter sequence.

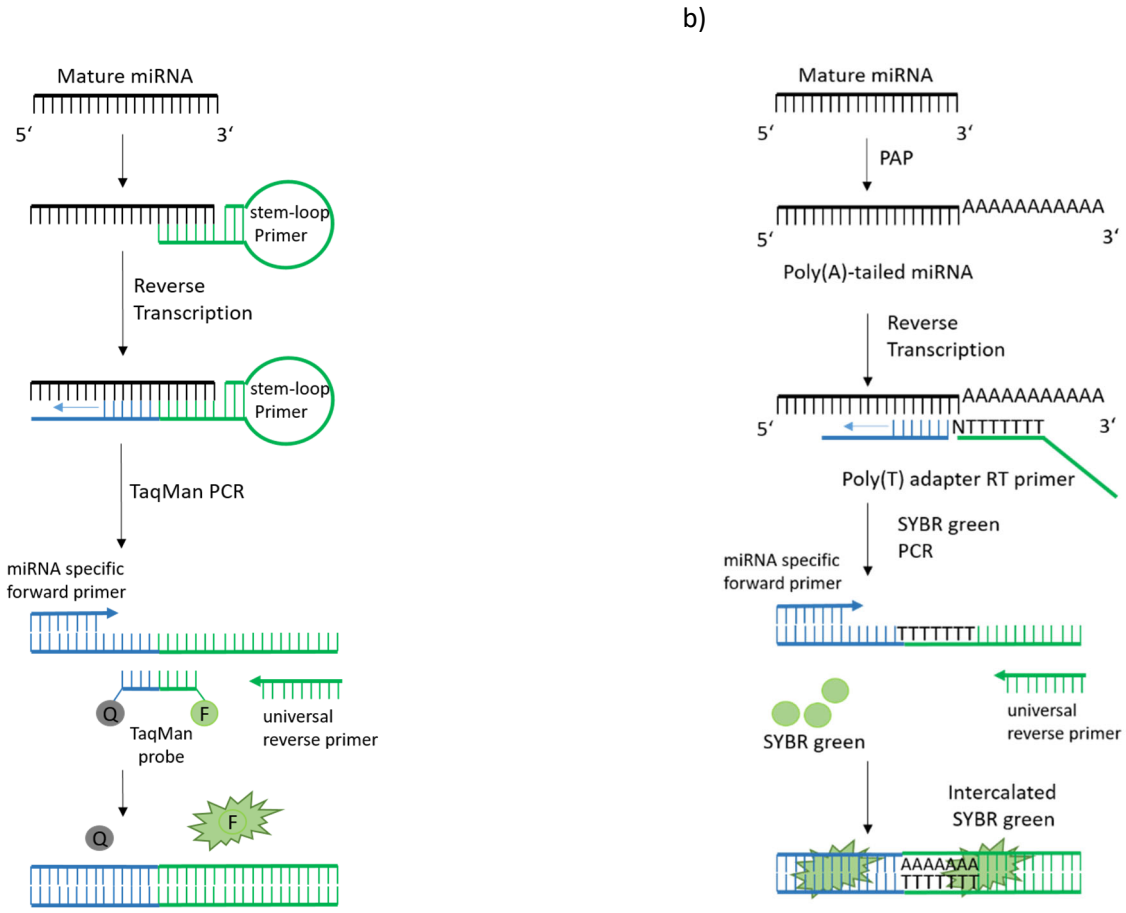

Figure 8. RT-qPCR methods, using a) the stem-loop miRNA-specific primer for reverse transcription, followed by TaqMan PCR assay, and b) the universal RT primer for miRNAs, extended with poly(A) tails, followed by qPCR quantification based on SYBR green detection. The figures are generated based on previously published data[186, 188]

In the real-time PCR, the cDNA is amplified by using the miRNA-specific forward primer and the sequence complementary to the poly(T) adapter as the reverse primer. The reaction is monitored by SYBR green fluorescence[188]. By this strategy not only mature miRNAs but also unprocessed forms of miRNA are polyadenilated and amplified during PCR step, which can cause an inaccuracy in the mature miRNA quantification. The sensitivity and selectivity of this technology was improved by Exiqon, using the two LNA-containing miRNA-specific primers for PCR[189].

Li J. *et. al.* have presented an alternative real-time PCR miRNA detection method, which does not required enzymatic elongation of miRNAs and is based on the enzymatic ligation of two DNA stem-loop probes. Each of the two DNA stem-loop probes contains one-half of the miRNA-complementary sequence, which is set into hairpin structure of the stem loop. T4 DNA ligase catalyses the ligation of these two DNA stem-loop probes only in the presence of miRNA template. In its turn, the resulting ligated DNA strand is used as a template for real-time PCR amplification by applying standard SYBR Green detection. This method has an increased specificity and allows to avoid the amplification of precursor miRNAs[190].

For the processing of qPCR data analysis, either absolute or relative quantification method could be applied. In the absolute quantification, the copy number of gene of interest is determined related to a

standard curve. Relative quantification is performed by the comparative C_T method (the alternative name is the $2^{-\Delta\Delta Ct}$ $_{method}$), where the specific miRNA expression is calculated as a relative to the expression of a housekeeping or reference gene (i.e. small nuclear RNA (snRNA) U6) according to formula:

$2^{-\Delta\Delta Ct}$= [($C_{T\ gene\ of\ interest}$ - $C_{T\ reference\ gene}$)] sample A - [($C_{T\ gene\ of\ interest}$ - $C_{T\ reference\ gene}$)] sample B,

where Ct (cycle threshold) is defined as the number of cycles required for the fluorescent signal to cross the threshold, $\Delta Ct = C_{T\ gene\ of\ interest} - C_{T\ reference\ gene}$, the $2^{-\Delta\Delta Ct}$ is a fold change in expression of specific miRNA between sample A and sample B[191].

2. Objectives

The aim in this PhD project was to develop the tools for inhibition and monitoring of the dicer-mediated miRNA maturation in cells. As a target, a well-known oncogenic miR-21 has been chosen, which is overexpressed in numerous cancer types. In the first part, it was intended to design the antisense peptide nucleic acid (PNA) probes, being specific to precursor miR21 (pre-miR21), for inhibition of the dicer-mediated pre-miR21 cleavage. Since these PNA probes did not inhibit the pre-miR21 cleavage by dicer in cells, the fluorogenic forced intercalation (FIT) PNA probes were developed for pre-miR21 detection in cells; and the set of two spectrally distinguishable FIT PNA probes was developed for sustainable monitoring of the dicer-mediated miR-21 maturation. The second part of the thesis is devoted to an alternative approach of inhibition of miRNA maturation by so-called small molecular inhibitors (SMIs). The objectives of this work included:

1). To design and synthesise pre-miR21 specific PNA probes for inhibition of the dicer-mediated miR-21 maturation; and to assay inhibition by means of the cell-free dicer-mediated BRCA assay and RT-qPCR in cells.

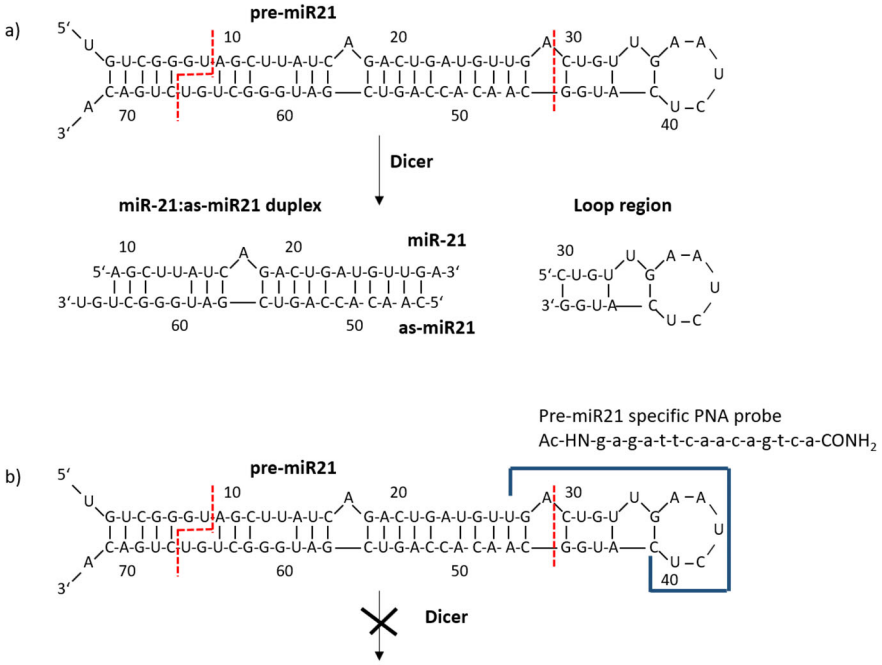

Scheme 2. Dicer-mediated cleavage of pre-miR-21 (a) and hybridization site (blue) for the pre-miR21 specific PNA probe (b), which is supposed to block the Dicer cleavage.

2). To develop fluorogenic FIT PNA probes for pre-miR21 detection in cells.

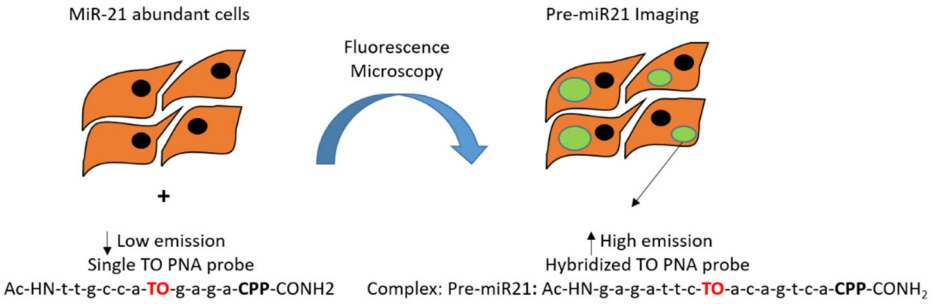

Scheme 3. The pre-miR21 detection in cells by the thiazol orange-labeled (TO) PNA probe, conjugated with cell-penetrating peptide (CPP).

3). To develop a set of two spectrally distinguishable FIT PNA probes for monitoring the dicer-mediated pre-miR21 cleavage, which enable to detect the unprocessed pre-miR21 and the reaction product (miR-21: as-miR21) simultaneously.

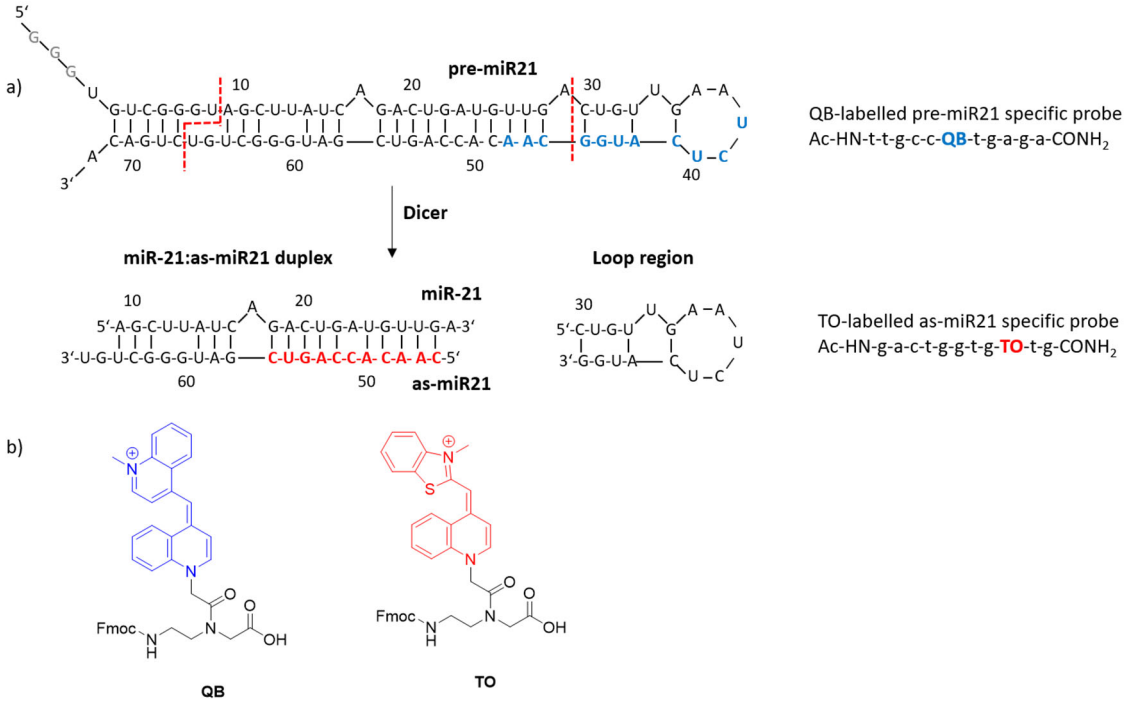

Scheme 4. Monitoring of miR-21 maturation by spectrally distinct FIT PNA probes (a), bearing quinoline blue (QB) and thiazol orange (TO) fluorophores. Structures of the Fmoc-protected TO- and QB-labeled PNA monomers (b). (The three 5'-terminal G residues of pre-miR21 are originated from the T7 RNA polymerase promoter in *in vitro* transcription reaction)

4). To select highly potential SMIs for inhibition of miR-122 and miR-21 maturation, which were developed by Dr. Claudine Dojahn (Arenz group); and to evaluate their inhibitory effects in cells.

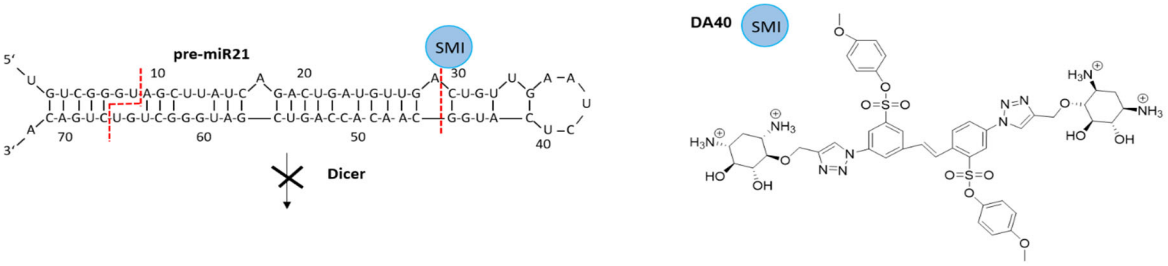

Scheme 5. Inhibition of miR-21 maturation by SMI.

3. Results and Discussion

3.1 Design and Synthesis of PNA Probes Targeting Pre-miR21 and Evaluation of their Inhibition of MiR-21 Maturation in Cells

The first goal of this work was to design PNA probes, which enable selective inhibition of miRNA maturation at the stage of the dicer-mediated pre-miRNA cleavage. There are many examples of effective miRNA inhibition on the mature miRNA level[192-194]. However, efficient specific inhibition on the pre-miRNA level by antisense oligonucleotides (ASO) has not been reported yet. Cells have an abundant amount of mature miRNAs due to their relatively long lifetime, whereas the short-living pre-miRNAs are fast processed by Dicer into their mature form. Consequently, pre-miRNAs have a lower expression level than their corresponding miRNAs[195]. Thus, it can be challenging to inhibit miRNA maturation on the pre-miRNA level in cells. Avitabile *et. al.* reported the application of pre-miRNA targeting PNA probes for effective inhibition of miRNA-210 maturation, but these probes were designed to be complementary to the region present in both forms, pre-miR-210 and miR-210[196]. This work is focused on the specific targeting of pre-miRNA to hinder the dicer binding and therefore, interfere with miRNA maturation. The precursor form of miR-21, pre-miR21, was selected as a target, since miR-21 is a well-known oncogenic miRNA and found to be overexpressed in the most of cancer types. Moreover, inactivation of miR-21 leads to repression of tumour growth and metastasis, opening a new avenue for cancer drug discovery[59].

3.1.1 Design and Synthesis of the PNA Probes Complementary to Pre-miR21

During the dicer-mediated miRNA-21 maturation, the Dicer RNAse cleaves the 72-nt long precursor miRNA-21 (pre-miR21) and liberates the 22-nt long duplex, consisting of the mature miRNA-21 strand (miR-21 from 5' arm) and the antisense mature miRNA-21 strand (as-miR21 from 3' arm) along with the terminal stem loop (C30-G45, Scheme. 6). The pre-miR21 structure is characterized by a stem-loop hairpin RNA with a small 5-nt loop as predicted by the *mfold* web server for nucleic acid folding (http://unafold.rna.albany.edu/). The loop region is highly conserved and, therefore, important for RNA-binding proteins, such as Dicer and Drosha. According to the SHAPE data from G. Varani et al., the loop region of pre-miR21 is highly dynamic and favorable for binding. In contrast to the loop, the stem region of pre-miR21, which contains the duplex miR-21: as-miR21, is rather stable even including the non-perfect complementarity[197]. However, the pre-miR21 structure, predicted with an alternative programmes, can look differently[198].

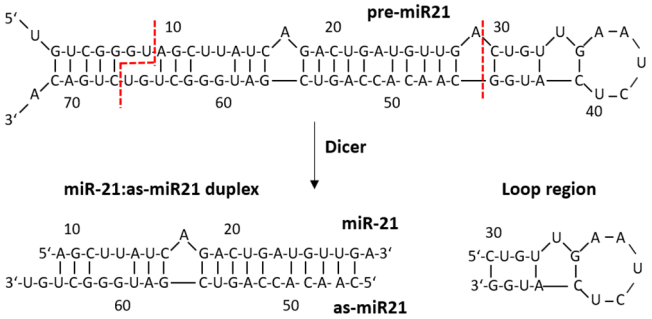

Scheme 6. Dicer-mediated pre-miR21 cleavage

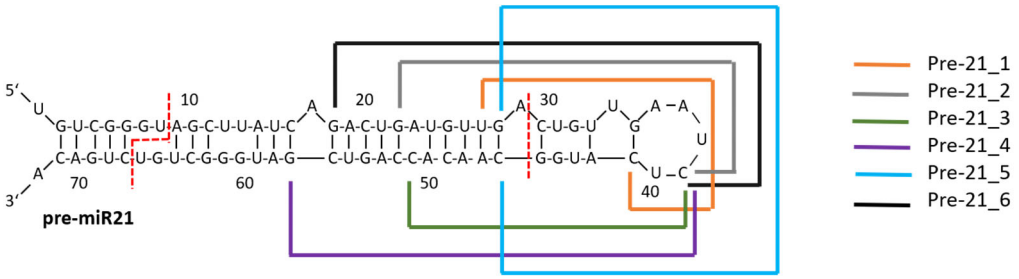

Name of PNA Probe	PNA sequence from N to C terminus	Length, nt
Pre-21_1	gagattcaacagtca	15
Pre-21_2	gattcaacagtcaacatc	18
Pre-21_3	gtgttgccatgag	13
Pre-21_4	cgactggtgttgccatgag	19
Pre-21_5	gccatgagattcaacagtc	19
Pre-21_6	gattcaacagtcaacatcagtc	22

Figure 9. Design of the pre-miR21 specific PNA probes.

The six PNA probes, **Pre-21_1** – **Pre-21_6**, ranging from a length of 13nt to 22nt, were designed to be complementary to pre-miR21 in the antiparallel orientation (PNA N-terminus to the pre-miRNA 3'-end, Fig. 9). The antiparallel orientation was preferable according to the protocols reported by Nielsen *et al*.[92]

The two probes, **Pre-21_1** and **Pre-21_5,** cover the loop region and are consequently specific for the unprocessed primary and precursor miR-21 forms. The other four probes (**Pre-21_2, Pre-21_3, Pre-21_4** and **Pre-21_6**) target not only the pre-miR21 specific loop region, but also a part of the pre-miR21 sequence, corresponding to either mature miR-21 or as-miR21. It was set as a goal to find an optimal probe length for opening the pre-miR21 structure to promote effective probe hybridization. At the same time, the probe should be long enough to provide high specificity. However, it can be hypothesized that the flexible structure of the pre-miR21 loop makes it favourable for hybridization of even short sized PNA probes. The PNA probes were synthesized by Solid Phase Synthesis (SPS), using a Fmoc-strategy (Experimental Section 5.1). Next, the synthesized PNA probes were purified by RP-HPLC and evaluated in the Branched-Rolling Circular Amplification assay (BRCA) by their ability to inhibit the dicer-mediated pre-miR21 cleavage.

3.1.2 Inhibition of Dicer-mediated MiRNA-21 Maturation by PNA Probes in the Branched Rolling Circular Amplification (BRCA) Assay

The PNA probes were designed to hybridize to pre-miR21, which should hinder the dicer binding to pre-miR21 and inhibit its cleavage. The BRCA method allows the detection of the formation of mature miRNA in the dicer-mediated pre-miRNA cleavage reaction and has been used for assessing the inhibitory activity of PNA probes[145, 156]. In this assay, after the successful cleavage of pre-miRNA, the mature miRNA (miR-21) serves as a primer for a circular DNA template (DNA template contains the sequence, complementary to miR-21), to initiate the DNA amplification by DNA polymerase. The DNA amplification is detected by fluorescence of intercalated SYBR Gold. Conversely, in case of dicer inhibition, the unprocessed pre-miRNA is not able to start the DNA amplification and the fluorescence signal is reduced or not detected (Scheme 7, more detailed in Introduction 1.3.4.). However, it should be taken into account that the **Pre-21_2** and **Pre-21_6** probes themselves could inhibit the BRCA reaction rather than the dicer-mediated cleavage, since they are partly complementary to miR-21. The

Pre-21_3 and **Pre-21_4** probes, partly complementary to as-miR21, could also change the BRCA efficiency. To note, the **Pre-21_1** and **Pre-21_5** probes, original for pre-miR21, should lack this behavior.

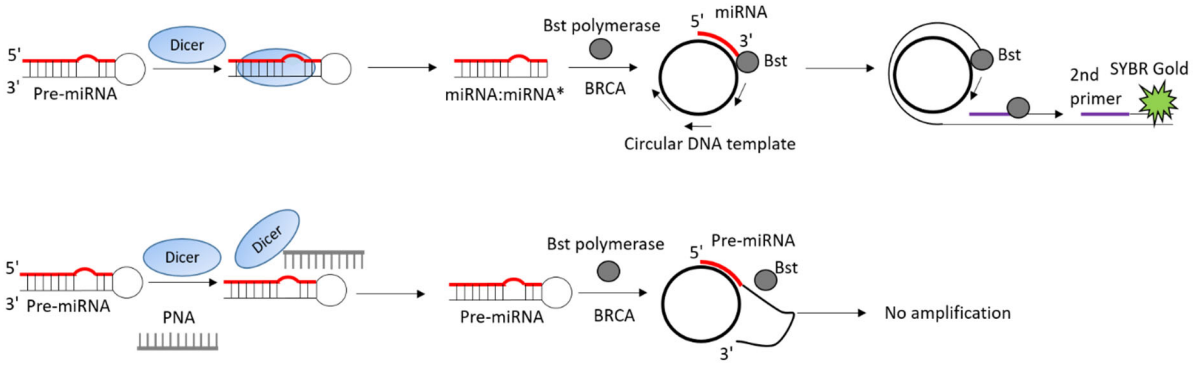

Scheme 7. Dicer-mediated Branched Rolling Circular Amplification (BRCA)

At the start, pre-miR21 was synthesized by *in vitro* transcription reaction. Prior to the BRCA, pre-miR21 (50 nM) was incubated for two hours with the dicer enzyme in presence or absence (positive control) of the PNA probes. Pre-miR21 incubated without Dicer served as a negative control. The effect of each PNA probe was investigated in the concentration range of 1-1000 nM. After the dicer cleavage reaction, the product was evaluated in the BRCA assay and the linear DNA amplification in BRCA was monitored by using the SYBR Gold fluorescent dye for real-time PCR readout. The time-course of fluorescence signals of BRCA assay is shown in the supporting information (figure S2). As expected, the positive control (absence of PNA probes) displayed a significant fluorescence increase during the BRCA assay, whereas the fluorescence of the negative control was extremely low. In this BRCA assay, the control with non-specific PNA was not evaluated since it was reported that the presence of PNAs did not affect the efficiency of BRCA reaction[199]. The presence of all PNA probes resulted in a decreased fluorescence signal in a similar way (Fig. 10a). The inhibitory activities of the PNA probes were compared by using the slope of the linear range of the fluorescence curve between 20th and 40th time points (Fig. S2). The IC50 values were calculated based on the slope values (Fig. 10b, the dose-response curves for PNA probes are presented in the supporting information, Fig. S1). At first glance the results might show that all six PNA probes, independent from their length, interfere with dicer-mediated pre-miR21 cleavage. However, presumably the probes inhibited the BRCA reaction by binding either to mature miRNA or to the circular DNA template. Therefore, it is difficult to determine the inhibitory effect, which is only caused by the dicer-mediated step. To draw a conclusion, a control experiment is still required, in which the isothermal BRCA reaction is carried out in presence of PNA probes, but in absence of the Dicer. Since pre-miR21 target was added in a concentration of 50 nM, the inhibition of dicer-mediated cleavage of pre-miR21 was incomplete in the presence of 20 nM of PNA, whereas in presence of the high excess of PNA probes (>100 nM) the fluorescence rate was close to the fluorescence of the negative control. The IC50 values were below 50 nM (Fig. 10). It is supposed that the PNA probes would bind the pre-miR21 target with a single binding site, thereby the dose-response curves would be generated as a standard S-shaped curve with the Hill coefficient of 1, showing the non-cooperative effect. Some dose-response curves (for **Pre-21_3**, **Pre-21_4** and **Pre21_5**), however, showed a high steepness, close to vertical line, which is typical for behavior of molecules with the cooperative effect[200] (Fig. S1 a). In this case the fit of the dose-response curves can be improved by taking more concentration points <100 nM.

a)

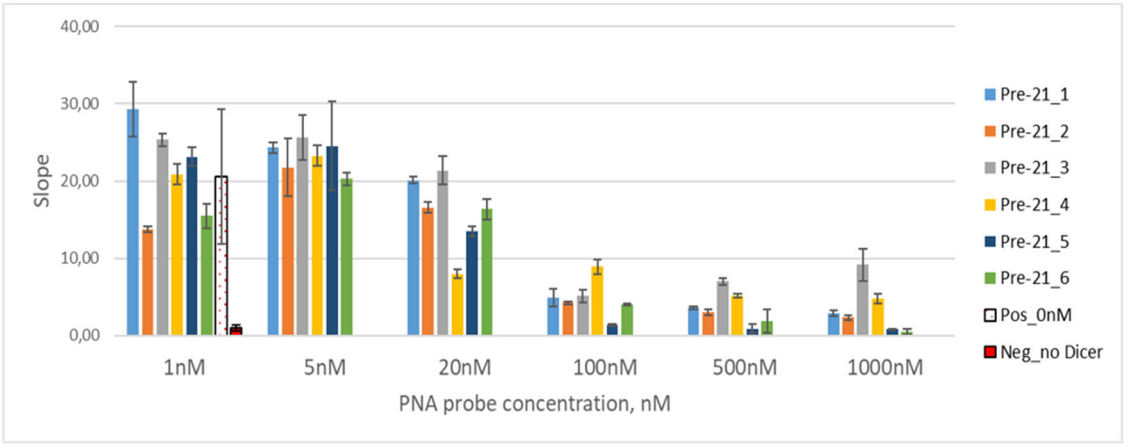

b)

IC50 determination by Graphpad Prism				
PNA probe	logIC50	St Deviation of LogIC50	IC50, nM	St Deviation of IC50
Pre-21_1	1,48	0,06	30	1
Pre-21_2	1,69	0,20	49	6
Pre-21_3	1,35	~ 660,7	23	undefined
Pre-21_4	1,22	~ 963,7	17	undefined
Pre-21_5	1,30	~ 6,783e+013	20	0
Pre-21_6	1,72	0,10	53	3

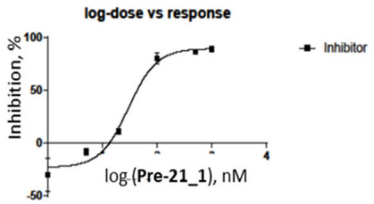

c)

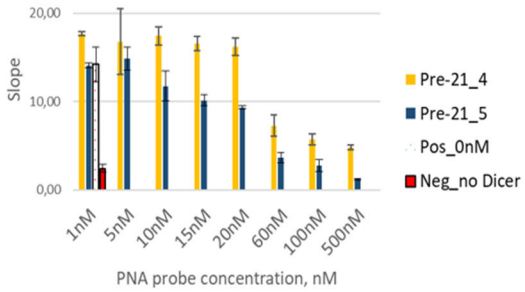

d)

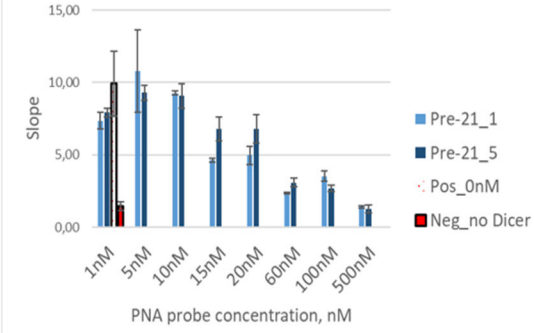

IC50 determination by Graphpad Prism				
PNA probe	logIC50	St Deviation of LogIC50	IC50	St Deviation of IC50
Pre-21_4	1,59	0,06	39	2
Pre-21_5	1,38	0,04	24	1

IC50 determination by Graphpad Prism				
PNA probe	logIC50	St Deviation of LogIC50	IC50	St Deviation of IC50
Pre-21_1	1,17	0,05	15	1
Pre-21_5	1,49	0,08	31	1,7

Figure 10. Effect of the inhibitory PNA probes (**Pre-21_1** – **Pre-21_6**) on Dicer cleavage assessed by BRCA assay. a) BRCA assay of the six PNA probes in the concentration range 1-1000 nM, including the positive control (the reaction in the absence of PNA (0 nM), no inhibition) and the negative control (the reaction without Dicer, full possible inhibition). The BRCA for probes is shown in supporting information, Fig. S2. The inhibitory activity of the PNA probes were compared based on the slope of the linear range of fluorescence in time course of reaction (between 20 and 40 time points, every time point is 2 min). Bars represent the mean of slopes of triplicate independent BRCA experiments +/- SD. b) The IC50 values for the PNA probes were calculated by Graphpad Prism software (nonlinear regression curve fit, dose-response stimulation (four parameters)) based on the slope values (supporting information, Fig. S1). As an example, the dose-response curve for **Pre-21_1** probe is shown. c) BRCA assay for the **Pre-21_4** and **Pre-21_5** probes within the concentration range 1-500 nM and their IC50 values, d) BRCA assay for the **Pre-21_1** and **Pre-21_5** in the concentration range 1-500 nM and their IC50 values.

The BRCA assay with more focus on the concentration range <100 nM was performed for the pre-miR21 original probes (**Pre-21_1, Pre-21_5**) and the **Pre-21_4** probe, partially complementary to as-miR21 (Fig. 10 c, d). The fluorescence decreased in a concentration-dependent manner with IC50 values < 40 nM. Predictably, the significant fluorescence decrease was detected at 60 nM, in which the

saturation of PNA concentration was reached. In the experiments with more concentration points <100 nM, the dose-response curves showed a sigmoidal form close to the standard curve (Fig S1 b, c).

Recalling to the PNA probe design, only the **Pre-21_1** and **Pre-21_5** probes are specific to pre-miR21, therefore, **Pre-21_1** and **Pre-21_5**, were selected for the further investigation of dicer-mediated inhibition of the miR-21 maturation in cells.

3.1.3 Cellular Uptake of FAM-labeled PNA Probes Conjugated with Cell-Penetrating Peptides (CPP)

In order to facilitate efficient inhibition of the dicer-mediated miR-21 maturation in cells, the PNA probes have to be effectively delivered into cells. PNAs have a neutral charge and, as a consequence, the delivery of "naked" PNA sequences into cells is extremely challenging. The conjugation of PNAs to different cell-penetrating peptides (CPPs) has been explored over the last decades to achieve intracellular delivery[110].

To deliver the **Pre-21_1** and **Pre-21-5** PNA probes into cells, three CPPs were selected: TAT (derived from viral HIV-1 Tat trans-activating factor)[114], octaarginine of new generation - $(RAhexR)_4$ [116], and polylysine (K3, three lysines)[110]. The CPPs were synthesized using automated SPPS and the resin with the attached CPP was used for the further PNA synthesis. To monitor the delivery efficiency a N^{ε}-(5/6-carboxy-fluorescein) modified lysine residue was introduced by using Mmt-protected Fmoc-lysine building block. After SPPS, the side-chain protecting group was selectively removed with 2% TFA in DCM and 5/6-carboxy- fluorescein (FAM) was coupled to the N^{ε}- amino group in presence of PyBOP and NMM. Additionally, a cysteine residue was attached to the N-terminus of the PNA sequence to improve cellular uptake. [192] The sequences of the CPPs, as well as the final sequences of the FAM-labeled CPP-PNA probes, are shown in Figure 11. The breast cancer miR-21 expressing cells, BT 474, were transfected with 0.5, 1 or 2 µM of the CPP-PNA probe for 24 h. After incubation the cells were detached by trypsinization and fixed by exposing to paraformaldehyde (PFA) solution. Trypsinization should remove the fluorogenic CPP-PNA-probes, attached on the cell surface[119]. The fluorescence of the fixed cells was analyzed by flow cytometry (Fig. 11).

The new generation octaarginine ($(RAhexR)_4$) provided the highest cellular uptake level, while the polylysine (K3) afforded the lowest cellular uptake (see Fig. 11). The fluorescence of the cells, treated with the $(RAhexR)_4$ –modified PNA probe, was 18-fold higher than for the K3-modified PNA probe and 1.8-fold higher than for the TAT-modified PNA probe (at 0.5 µM). Cellular entry of the compounds increased by the elevation of their concentration. Two arginine-rich CPPs, the $(RAhexR)_4$ and TAT, showed the similarities in the elevation of entry level depending from concentration. In contrast, polylysine K3 compound had a significant rise in cellular uptake at higher concentration of 2 µM, thus the difference between $(RAhexR)_4$ and K3 was significantly reduced: the $(RAhexR)_4$/ K3 fluorescence ratio was only 4.8-fold.

It was already reported earlier that CPPs, including TAT and oligoarginine, cross the cellular membrane through endocytosis. Although, the contradictory results were obtained about the involvement of specific endocytic pathway (macropinocytosis, clathrin-mediated endocytosis and caveolae/ lipid-raft-mediated endocytosis)[119, 201-203], Duchardt *et al*. observed that CPPs can use all three endocytic pathways simultaneously. Moreover, it was shown that at higher concentrations the peptides rapidly penetrate the cellular membrane by endocytosis-independent mechanism.[204] This could explain the reduction of difference between CPPs ($(RAhexR)_4$/ K3) in the cell uptake at higher concentration of 2 µM. The octaarginine of new generation, $(RAhexR)_4$, was chosen for the delivery of the **Pre-21_1** and **Pre-21-5** PNA probes for the evaluation of their inhibitory activity in cells.

Probe Name	Sequence of CPP	Final Probe Sequence (N' → C')
K3	K K K	C-K(FAM)-(Pre-21_1)-K3
$(RAhexR)_4$	R Ahex R R Ahex R R Ahex R R Ahex R Ahex β	C-K(FAM)- (Pre-21_1)-GG-$(RAhexR)_4$ Ahex β
TAT	R R R Q R R K K R	C-K(FAM)- (Pre-21_1)-GG-RRRQRRKKR

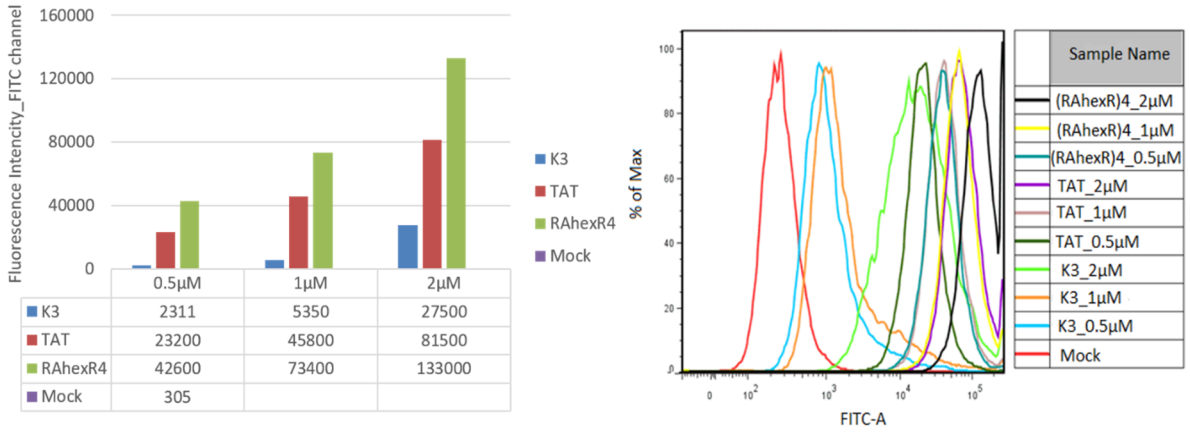

	0.5μM	1μM	2μM
K3	2311	5350	27500
TAT	23200	45800	81500
RAhexR4	42600	73400	133000
Mock	305		

Ratio	0.5μM	1μM	2μM
RAhexR4/K3	18,43	13,72	4,84
RAhexR4/TAT	1,84	1,60	1,63

Figure 11. Analysis of the cellular uptake of the FAM-labeled CPP-**Pre-21_1** PNA probes by flow cytometry. The sequences of FAM-labeled CPP-**Pre-21_1** probes are shown in the table. *Ahex: 6 -aminohexanoic acid; β: β-alanin; **Pre-21_1** PNA sequence: gagattcaacagtca. On the diagram and histogram the fluorescence intensity is graphed for the BT 474 cells, transfected with CPP-conjugated **Pre-21_1** probes ; Mock is the non-transfected BT 474 cells.

3.1.4 Analysis of the Inhibition of the Dicer-mediated MiR-21 Maturation by Pre-miR21 Specific PNA Probes in Cells

For the delivery into cells, the $(RAhexR)_4$-conjugated **Pre-21_1** and **Pre-21_5** PNA probes were synthesized as described in the previous chapter with one difference: the probes were not labeled with fluorescent dye. The PNA sequence being fully complementary to mature miR-21 was used as a positive control of inhibition and was also conjugated to $(RAhexR)_4$ (Fig. 12). In order to test the **Pre-21_1** and **Pre-21_5** PNA probes ability to inhibit the dicer-mediated miR-21 maturation, Huh7 hepatocarcinoma cells (expressing miR-21) were transfected with the $(RAhexR)_4$-conjugated PNA probes. After 48 h of incubation, the Huh7 cells were collected and the total RNA (including miRNAs) was extracted by using the miRNAeasy kit (Qiagen). For the following determination of the miR-21 expression by reverse transcription qPCR (RT-qPCR), the TaqMan MicroRNA assays and reagents from Applied Biosystems were used according to the manufacture's protocol. The miR-21 expression qPCR data was normalized to the expression of small nuclear RNA U6 as an internal control and analysed by comparative C_T method (see introduction 1.5). Thus, the data is presented as $2^{-\Delta Ct}$, where $\Delta Ct = Ct_{miR21} - Ct_{U6}$ (Ct-threshold cycle). The fold change in miR-21 expression between treated and untreated samples is the value $2^{-\Delta\Delta Ct}$, $2^{-\Delta\Delta Ct} = [(C_{T\ miR21} - C_{T\ U6})]_{\text{treated sample}} - [(C_{T\ miR\text{-}21} - C_{T\ U6})]_{\text{untreated sample}}$ (Fig. 12, Supplementary Information Fig. S3). The experiment was performed using the PNA probes at a concentration of 2 μM for transfection.

In comparison to the untreated control (Mock), the **Pre-21_1_CPP** and **Pre-21_5_CPP** probe treatment did not cause any significant changes in the miR-21 expression. The miR-21 level in the cells, treated with the positive control (**PNAmat21_CPP**), dropped in 59-times in reference to control. It appears that the treatment with the pre-miR21 specific probes did not have any impact on the mature miR-21 level. Judging on the positive control (**PNAmat21_CPP**) the probes were delivered into cells, however, its

accessibility for hybridization is still not confirmed. The possible endosome entrapment can sequester the probes from its target. Unfortunately, this fact would not influence the qPCR results[205]. It is also likely that the cellular dicer enzyme in the complex with its partners (TRBP and PACT proteins) provides higher affinity to the pre-miR21 than the pre-miR21 specific PNA probes and thereby blocks the probe hybridization. Another explanation can be that the pre-miR21/ PNA probe binding do not have an impact on Dicer processing. To investigate more carefully the binding event and affinity of the probes towards the target pre-miR21 inside the cells, the application of forced-intercalating (FIT) probes appeared promising, as these probes can detect the probe-target hybridization state by enhancement of their fluorescence (see introduction 1.4).

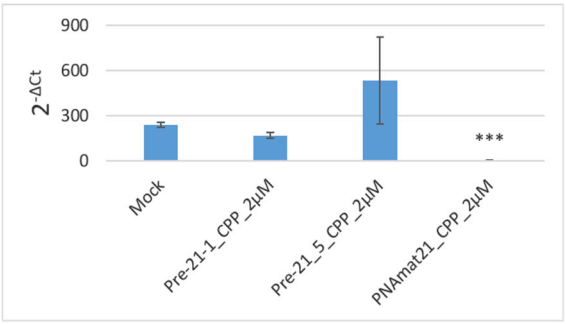

PNA probe	Sequence (N' → C')
Pre-21_1_CPP	C-K- gagattcaacagtca - GG-$(RAhexR)_4$ Ahex β
Pre-21_5_CPP	C-K- gccatgagattcaacagtc -GG-$(RAhexR)_4$ Ahex β
PNAmat21_CPP	C-K- tcaacatcagtctgataagcta- GG-$(RAhexR)_4$ Ahex β

Samples	$2^{-\Delta Ct}$	Fold Change due to treatment
Mock	239	1,00
Pre-21_1_CPP_2µM	169	-1,42
Pre-21_5_CPP_2µM	533	-0,45
PNAmat21_CPP_2µM	4	-58,76

Figure 12. Assessment of the dicer-mediated miR-21 maturation inhibition by pre-miR21 specific PNA probes in Huh7 cells using RT-qPCR. Sequences of the transfected PNA probes are shown in the table. The diagrams display the relative expression of miR-21 in the untreated cells (Mock) and cells treated with PNA probes. The data is analyzed by Ct comparative method ($2^{-\Delta Ct}$, where $\Delta Ct=Ct_{miR21}-Ct_{U6}$, Ct-threshold cycle; fold change due to treatment = $2^{-\Delta\Delta Ct}$, $2^{-\Delta\Delta Ct}= [(C_{T\ miR21} - C_{T\ U6})]_{\text{treated sample}} - [(C_{T\ miR\text{-}21} - C_{T\ U6})]_{\text{untreated sample}}$). Data are mean (+SD) of 2-3 replicates (T test significance: p-value, *p<0.05; **p<0,01; ***p<0,005)

3.2 Design and Synthesis of Thiazole Orange (TO) Labeled Pre-miR21 Specific PNA Probes and Evaluation of their Binding to Pre-miR-21 in the Cells

3.2.1 Design and Synthesis of Pre-miR21 Specific TO-Labeled PNA Probes

The TO-labeled PNA probes were designed on the basis of the **Pre-21_1** and **Pre-21_5** probe's sequences by incorporation of a single TO-modified PNA monomer at different internal positions. For every PNA sequence three TO positions were tested (see Fig. 13) to find a favorable TO position and to get highly responsive probes. Additionally, for evaluation of the probes in cells, the PNA sequences were equipped with $(RAhexR)_4$ as a CPP (final probe sequence: *C – K - PNA sequence – GG - $(RAhexR)_4$ Ahex* β). The TO-labeled PNA probes were synthesized by Fmoc-strategy SPS, using canonical PNA monomers (Link Technologies) and TO-modified monomers as described previously [206]. The TO-modified PNA monomer was available in the Seitz group from previous studies[161, 170]. The non-modified PNA monomers were coupled using during automated SPS, whereas the TO-PNA monomer was incorporated by manual synthesis using longer coupling time, PyBOP as an activator and PPTS to increase the low solubility of the TO-PNA monomer (details in the experimental part 5.1.). The final **Pre-21_1*_3** and **Pre-21_5*_2** probes with the same TO position were challenging to purify from the truncated sequences and were not used for further analysis. Next, the fluorescence responsiveness of the four TO-labeled PNA probes was analysed by fluorescence spectroscopy.

Name of PNA Probe	Sequence (N' → C')
Pre-21_1	C-K-gagattcaacagtca-CPP
Pre-21_1*_1	C-K-gagattcaa(TO)agtca-CPP
Pre-21_1*_2	C-K-gagattc(TO)acagtca-CPP
Pre-21_1*_3	C-K-gaga(TO)tcaacagtca-CPP
Pre-21_5	C-K-gccatgagattcaacagtc-CPP
Pre-21_5*_1	C-K-gccatga(TO)attcaacagtc-CPP
Pre-21_5*_2	C-K-gccatgaga(TO)tcaacagtc-CPP
Pre-21_5*_3	C-K-gccatgagattc(TO)acagtc-CPP

Figure 13. Sequences of the TO-labeled PNA probes for the evaluation of their miR-21 maturation inhibition in cells. CPP: *C-K-PNA sequence-GG-(RAhexR)$_4$ Ahex* β, where β is β-alanin, Ahex- 6-aminohexanoic acid linker.

3.2.2 Evaluation of the TO-labeled Pre-miR21 Specific PNA Probes *In Vitro* by Fluorescence Spectroscopy

The TO-labeled PNA probe fluorescence increases upon hybridization with the specific target[170]. To check the responsiveness of the synthesized probes (**Pre-21_1*_1**, **Pre-21_1*_2**, **Pre-21_5*_1**, **Pre-21_5*_3**), the fluorescence spectra were recorded before (I_0) and after (I) addition of the pre-miR21 target (Fig. 14). The fluorescence enhancement (I/ I_0) reflects the probe responsiveness. The **Pre-21_1*_2** PNA probe displayed the highest responsiveness (3.9-fold and 7.3-fold at 25°C and 37°C, respectively). **Pre-21_5*_3** PNA probe also provided a comparable fluorescence enhancement (3.1-fold and 4.6-fold at 25°C and 37°C, respectively). Remarkable, these two probes are carrying the TO fluorophore at the same position and differ only by their length (**Pre-21_1*_2**: 15 nt and **Pre-21_5*_3**: 19 nt). The **Pre-21_1*_1** and **Pre-21_5*_1** probes bear the TO fluorophore positioned two nucleotides further towards N-terminus and they were less responsive: only 1.9- and 0.9-fold at 25°C; 2.5 and 1.4-fold at 37°C, respectively. Accordingly, the probes **Pre-21_1*_2** and **Pre-21_5*_3** were chosen for the further evaluation of their hybridization with pre-miR21 in cells.

25°C

Name	Sequence (N' → C')	I_0	I	I/I_0
Pre-21_1*_1	C-K-gagattcaa(TO)agtca-CPP	11,2	21,7	1,9
Pre-21_1*_2	C-K-gagattc(TO)acagtca-CPP	4,9	19,2	3,9
Pre-21_5*_1	C-K-gccatga(TO)attcaacagtc-CPP	16,7	14,3	0,9
Pre-21_5*_3	C-K-gccatgagattc(TO)acagtc-CPP	8,8	27,0	3,1

37°C

Name	Sequence (N' → C')	I_0	I	I/I_0
Pre-21_1*_1	C-K-gagattcaa(TO)agtca-CPP	5,8	14,5	2,5
Pre-21_1*_2	C-K-gagattc(TO)acagtca-CPP	1,8	13,1	7,3
Pre-21_5*_1	C-K-gccatga(TO)attcaacagtc-CPP	7,0	10,0	1,4
Pre-21_5*_3	C-K-gccatgagattc(TO)acagtc-CPP	4,3	19,7	4,6

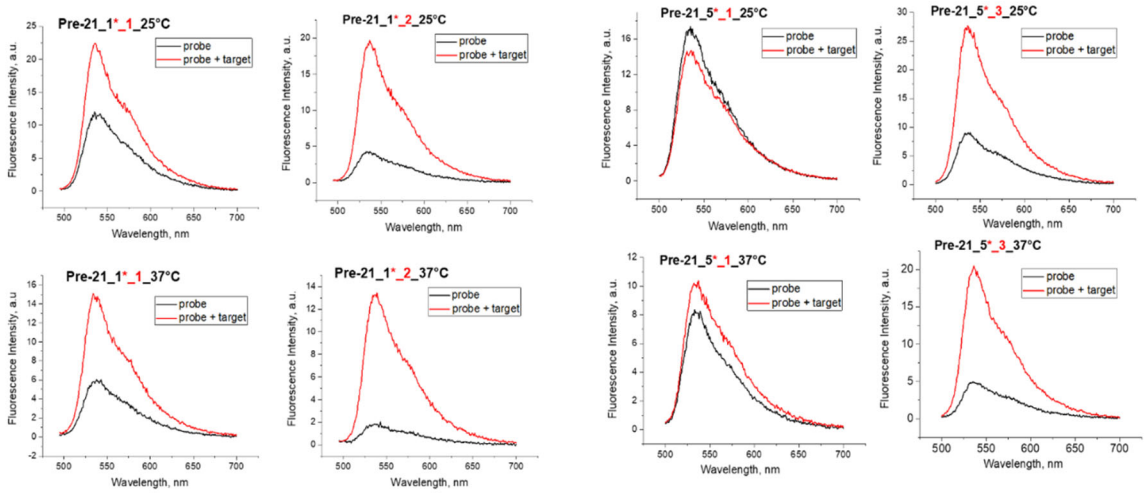

Figure 14. Comparison of fluorescence enhancement of the TO-labeled pre-21 specific PNA probes upon hybridization with pre-miR21. Conditions: in 150 µl of 1 x PBS, 0.5 µM of the TO PNA probe and 5 eq. of target, TO: λ_{ex} = 485 nm, λ_{em}= 495-700 nm, emission maximum is detected at 538 nm, $slit_{ex}$= 5 nm, $slit_{em}$= 5 nm, at 25°C and 37°C. Before measurement at 25°C and 37°C, the mixture of the PNA probe and the pre-miR21 target was heated till 95°C and cooled down till 25°C or 37°C.

Control TO-labeled PNA probes

In order to evaluate the specificity of **Pre-21_1*_2** and **Pre-21_5*_3**, the following four control PNA probes were synthesized (see Fig. 15): two mismatched probes for **Pre-21_1*_2** (**Pre-21_1*_2_mm1** and **mm2**), one mismatched probe for **Pre-21_5*_3** (**Pre-21_5*_3_mm**) and one unspecific TO-labeled PNA probe (**Viral mm**), being complementary to the influenza viral mRNA. The sequence of the **Viral mm** probe was derived from a publication [171]. The mismatched probes were designed as follows: two mismatched nucleotides were introduced in every probe, while the position of TO remained unchanged. These two mismatched nucleotides were either in close proximity to TO (for **Pre-21_1*_2_mm1** and **Pre-21_5*_3_mm**) or three nucleotides apart of TO position (**Pre-21_1*_2_mm2**). All four control probes were equipped with the CPP (final sequence: *C – K - PNA sequence – GG - $(RAhexR)_4$ Ahex* β). The mismatched **Pre-21_1*_2_mm1** and **mm2** probes displayed a half of the fluorescence enhancement in comparison to the perfect matched **Pre-21_1*_2** upon hybridization with pre-miR21. The fluorescence enhancement of the **Pre-21_5*_3_mm** PNA probe was 1.3 times lower in comparison to the fully complementary **Pre-21_5*_3** probe upon pre-miR21 target hybridization. The control **Viral mm** PNA probe showed the high fluorescence intensity of single strand (21.3 and 8.7 a.u. at 25°C and 37°C, respectively), which was about the same as the fluorescence of pre-miR21 specific probes in the presence of target (supporting information, Fig. S4). Due to this reason, the **Viral mm** probe was discarded from the analysis.

25°C				
Name	Sequence (N' → C')	I_0	I	I/I_0
Pre-21_1*_2	C-K-gagattc(TO)acagtca-CPP	4,9	19,2	3,9
Pre-21_1*_2_mm1	C-K-gagatta(TO)ccagtca-CPP	7,5	13,6	1,8
Pre-21_1*_2_mm2	C-K-gaggttc(TO)acaatca-CPP	6,3	8,7	1,4
Pre-21_5*_3	C-K-gccatgagattc(TO)acagtc-CPP	8,8	27,0	3,1
Pre-21_5*_3_mm	C-K-gccatgagatta(TO)ccagtc-CPP	9,0	19,9	2,2

37°C				
Name	Sequence (N' → C')	I_0	I	I/I_0
Pre-21_1*_2	C-K-gagattc(TO)acagtca-CPP	1,8	13,1	7,3
Pre-21_1*_2_mm1	C-K-gagatta(TO)ccagtca-CPP	2,4	8,6	3,5
Pre-21_1*_2_mm2	C-K-gaggttc(TO)acaatca-CPP	2,0	6,3	3,2
Pre-21_5*_3	C-K-gccatgagattc(TO)acagtc-CPP	4,3	19,7	4,6
Pre-21_5*_3_mm	C-K-gccatgagatta(TO)ccagtc-CPP	4,0	14,6	3,6

Figure 15. Evaluation of the control TO-labeled PNA probes in presence of pre-miR21 by fluorescence spectroscopy. Sequences of PNA probes and the corresponding control probes were equipped with $(RAhexR)_4$ as a CPP (the final probe sequence: *C – K - PNA sequence – GG - $(RAhexR)_4$ Ahex* β). Fluorescence spectra of the indicated probes are presented in Supporting information (Fig. S4). The mismatched nucleotides are marked in red. Conditions: in 150 µl of 1xPBS, 0.5 µM of the TO PNA probe and 3 eq. of target, TO: λ_{ex} = 485 nm, λ_{em}= 495-700 nm, emission maximum is detected at 536 nm, $slit_{ex}$= 5 nm, $slit_{em}$= 5 nm, at 25°C and 37°C. Before measurement at 25°C and 37°C, the mixture of the PNA probe and the pre-miR21 target was heated till 95°C and cooled down till 25°C or 37°C, respectively.

Concluding the results of comparison of the pre-miR21 specific probes and their mismatched probes, the **Pre-21_1*_2** and **Pre-21_5*_3** probes demonstrated the high specificity towards the pre-miR21 target. As expected, an introduction of the mismatched nucleotides in the probes led to the significant decrease of fluorescent enhancement.

3.2.3 Evaluation of the TO-labeled Pre-miR21 Specific PNA Probes in Cells by Flow Cytometry Analysis and Fluorescence Microscopy

After demonstrating the specificity of the TO-labeled pre-miR21 PNA probes by fluorescence spectroscopy, these probes **Pre-21_1*_2** and **Pre-21_5*_3** were further evaluated in cells. Prior to the cell experiments, a screening of the miR-21 expression was carried out on different cancer cell lines and control HEK293 cells with the goal to select cell lines with various levels of miR-21 expression. The cells were passaged into 24-well plates and after reaching full confluency, the cells were collected for the following analysis by RT-qPCR. The comparison of the miR-21 expression in a variety of cell lines is illustrated in Figure 16. As observed, the control HEK293 cells displayed the lowest level of miR-21 expression. Therefore, the miR-21 expression of all other cell lines is normalised to the miR-21 expression of the HEK293 cells in the table of fig. 16. While the two cell lines HEPG2 and Hela cells showed the highest level of miR-21 expression (273 and 264 times higher than HEK293), the cell lines A549, MCF7, MDA-MB and BTB-474 demonstrated rather lower, but approximately equal, levels of miR-21 expression (43-58-fold relative to the HEK293 miR-21 expression). The lowest miR-21 expression was registered in Huh7 and SKB3 cells (only 21 and 12-fold higher than in the HEK293 cells, respectively). Due to their significant different levels of miR-21 expression the three cell lines Hela, A549 and HEK293 have been selected for the following cellular investigations.

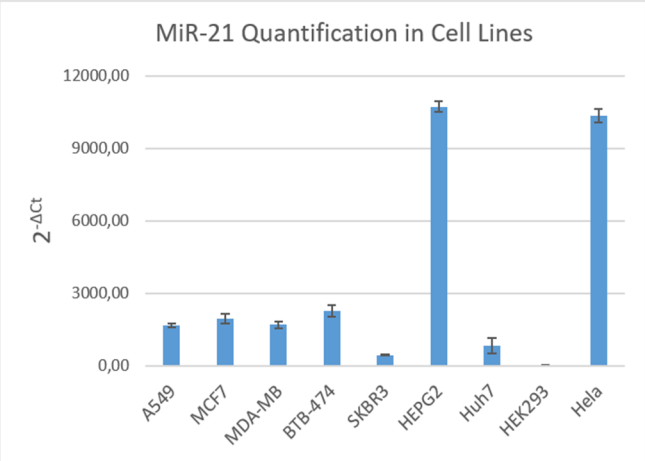

Cell line	$2^{-\Delta}$Ct	Standard Deviation	Fold increase over miR-21 expression in HeK293 cells
A549	1675,1	72,6	42,7
MCF7	1967,4	204,3	50,2
MDA-MB	1701,0	141,0	43,4
BTB-474	2272,1	235,4	57,9
SKBR3	453,2	1,8	11,6
HEPG2	10717,4	231,3	273,2
Huh7	835,2	316,7	21,3
HEK293	39,2	3,3	1,0
Hela	10355,0	278,3	264,0

Figure 16. Comparison of miR-21 expression in different cell lines by RT-qPCR using the comparative Ct method (Relative miR-21 expression = $2^{-\Delta Ct}$, where $\Delta Ct=Ct_{miR21}-Ct_{U6}$, Ct-threshold cycle). Data are mean (+SD) of 3 replicates.

Flow Cytometry

A flow cytometry experiment was planned to get an initial idea of how the probes would behave in cells. For the flow cytometry analysis, Hela, A549 and HEK293 cells were passaged into 24-well plates and after reaching 80-90% confluency, the cells were transfected with the TO-labeled PNA probes: **Pre-21_1*_2** and **Pre-21_5*_3**. The cells, transfected with the corresponding mismatched (**Pre-21_1*_2_mm1** and **mm2**, **Pre-21_5*_3_mm**) PNA probes served as control cells. After 24 h of incubation, the cells were detached from the surface by trypsinization and fixed with 4% paraformaldehyde. The collected fresh cells were analysed by fluorescence flow cytometry within 2 h. The results are displayed in Figure 17 (raw data is presented in the supplementary information, Fig. S5). The Hela cells were transfected with the indicated PNA probes in two different concentrations (0.5 µM and 0.25 µM), while the other cell lines were incubated at 0.5 µM of probes. The fluorescence of the pre-miR21 specific **Pre-21_1*_2** probe in miR-21 abundant Hela cells at a concentration of 0.5 µM was 1.52- and 1.27-times higher than the fluorescence of the two mismatched sequences **Pre-21_1*_2_mm1** and **mm2**, respectively. However, at 0.25 µM probe concentration the difference in fluorescence intensities was reduced (1.12- and 1.20-times). The **Pre-21_1*_2** probe treated A549 cells displayed 1.30- and 1.27-times higher fluorescence than the cells, incubated with the related mismatched sequences **Pre-21_1*_2_mm1** and **mm2**, respectively. Even less difference in fluorescence between specific and mismatched probes was observed in the low miR-21 level HEK293 cells (1.18 and 1.09-times). In the case of the **Pre-21_5*_3** probe, only the Hela cells demonstrated 1.6-times fluorescence increase relative to the control experiment with the **Pre-21_5*_3_mm** probe. The fluorescence of other cell lines and Hela cells at 0.25 µM probe concentration remained unchanged in comparison to the mismatched control. The preliminary flow cytometry results suggest that the **Pre-21_1*_2** and **Pre-21_5*_3** probes might target pre-mir21 in cells, and a ratio of fluorescences of specific probes to its mismatched control could probably give an indication of high and low miR-21 abundant cells using an optimal probe concentration. To verify the results of flow cytometry, the probes were analysed by fluorescence microscopy.

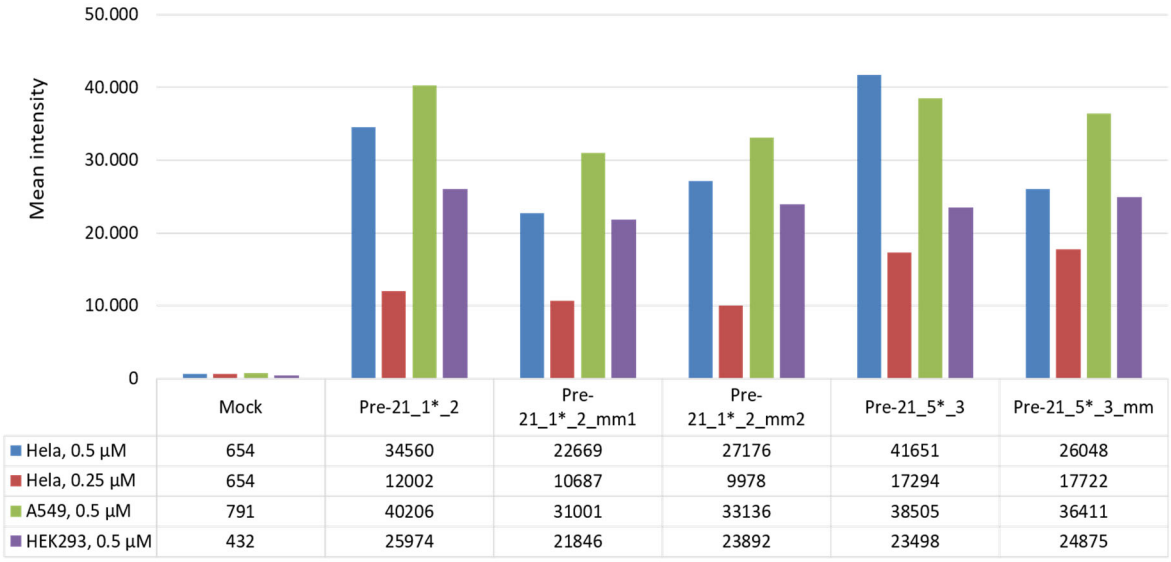

	Mock	Pre-21_1*_2	Pre-21_1*_2_mm1	Pre-21_1*_2_mm2	Pre-21_5*_3	Pre-21_5*_3_mm
Hela, 0.5 µM	654	34560	22669	27176	41651	26048
Hela, 0.25 µM	654	12002	10687	9978	17294	17722
A549, 0.5 µM	791	40206	31001	33136	38505	36411
HEK293, 0.5 µM	432	25974	21846	23892	23498	24875

	Comparison of Pre-21_1*_2 with its mismatched sequences		Comparison of Pre-21_5*_3 with its mismatched sequence
Cell samples	Mean Intensity Ratio Pre-21_1*_2/mm1	Mean Intensity Ratio Pre-21_1*_2/ mm2	Mean Intensity Ratio Pre-21_5*_3 /mm
Hela (0.5 µM)	1.52	1.27	1.60
Hela (0.25 µM)	1.12	1.20	0.98
A549 (0.5 µM)	1.30	1.21	0.94
HEK293 (0.5 µM)	1.18	1.09	1.06

Figure 17. Comparison of the TO fluorescence in cells treated with pre-miR21 specific (**Pre-21_1*_2** and **Pre-21_5*_3**) or control PNA probes (**Pre-21_1*_2_mm1** and **mm2, Pre-21_5*_3_mm**) by flow cytometry. The data is presented as a mean intensity of 10000 non-gated events per sample, one-repeat measure (SD of mean intensity is less than 1%).

Fluorescence Microscopy

Prior to the fluorescence microscopy experiment, Hela, A549 and HEK293 cells were incubated with **Pre-21_1*_2** and **Pre-21_5*_3** PNA probes and the corresponding control probes (**Pre-21_1*_2_mm1** and **mm2, Pre-21_5*_3_mm**). After 24 h, the cells were trypsinized and repassaged on glass coverslips. Another 24 h later, the cells were fixed with 4% paraformaldehyde and the glass coverslips were mounted on a clear glass slide. The cells were analysed the next day by fluorescence microscopy. Selected fluorescence microscopy pictures and the calculated mean fluorescence intensities are summarized in Figure 18 and 19.

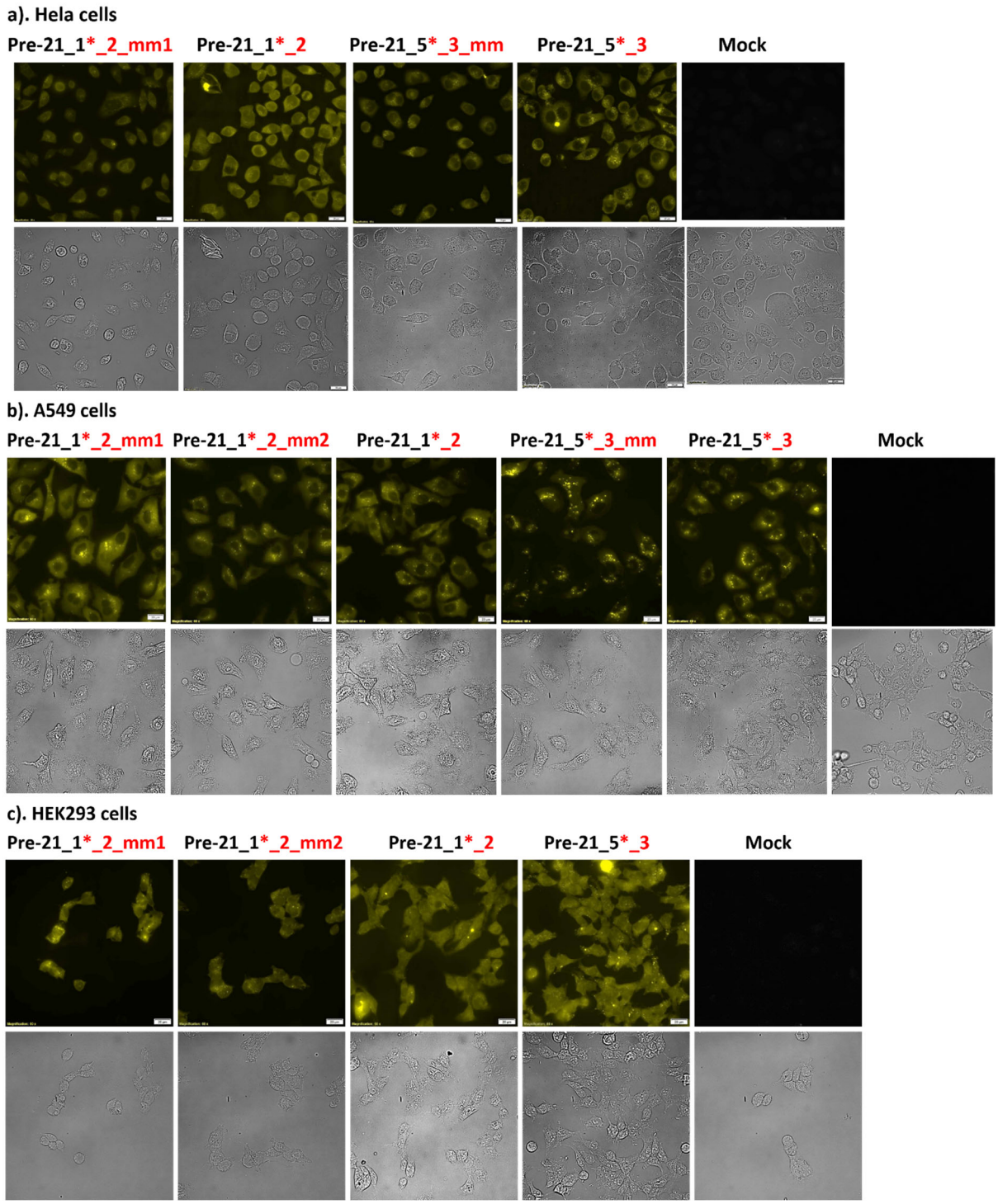

Figure 18. Fluorescence microscopy images of fixed Hela (a), A549 (b) and HEK293 (c) cells stained with the TO-labeled **Pre-21_1*_2, Pre-21_5*_3** PNA probes and their mismatched controls (**Pre-21_1*_2_mm1** and **mm2**, **Pre-21_5*_3_mm**). The fluorescence of the PNA probes was recorded on the YFP channel (λ_{ex} = 500 ± 24 nm, λ_{em} > 520 nm), using the same exposure time for measured samples within one cell line. Bright-field images are also shown for every sample.

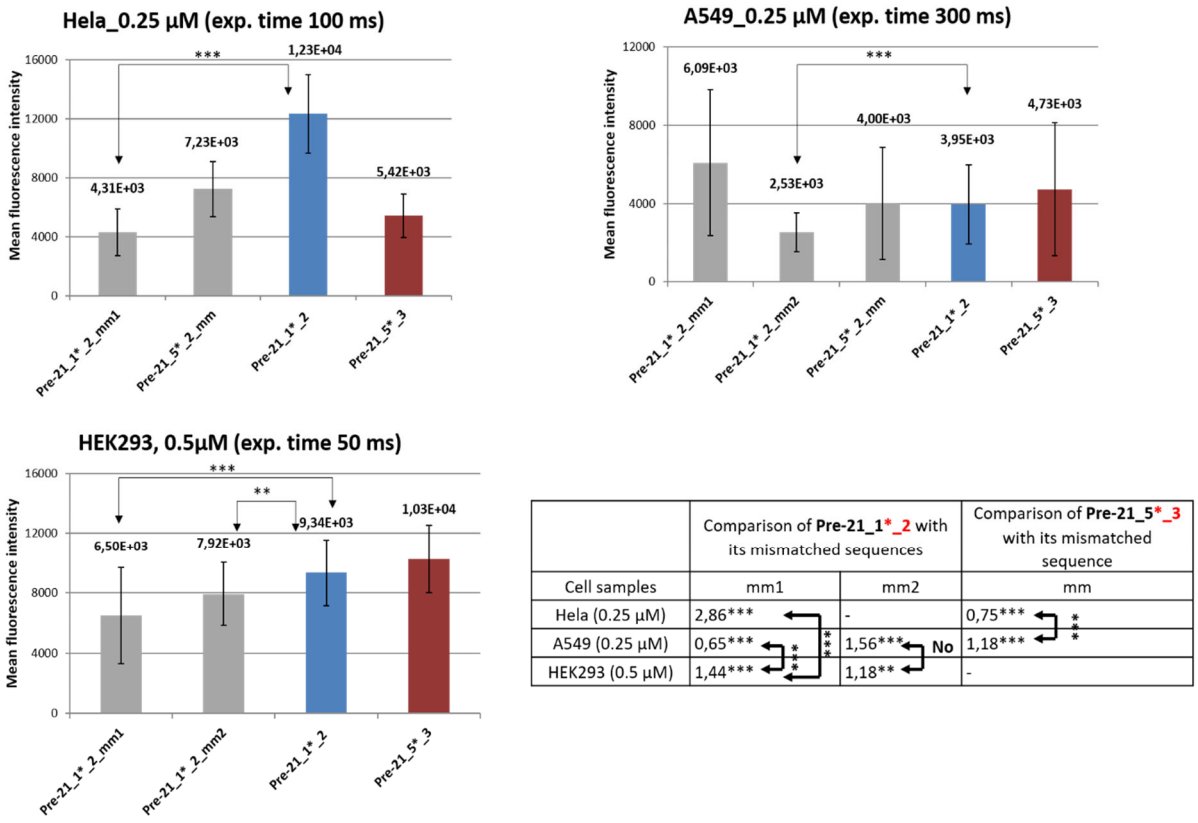

	Comparison of **Pre-21_1*_2** with its mismatched sequences		Comparison of **Pre-21_5*_3** with its mismatched sequence
Cell samples	mm1	mm2	mm
Hela (0.25 µM)	2,86***	-	0,75***
A549 (0.25 µM)	0,65***	1,56***	1,18***
HEK293 (0.5 µM)	1,44***	1,18**	-

Figure 19. Calculation of the mean fluorescence intensity in fixed Hela, A549 and HEK293 cells incubated with the TO-labeled pre-miR21 specific probes (**Pre-21_1*_2** and **Pre-21_5*_3**) and controls (**Pre-21_1*_2_mm1** and **mm2**, **Pre-21_5*_3_mm**). The images were processed by using the region of interest (ROI) tool to surround the whole cells. The fluorescence intensity was calculated as a mean fluorescence of 50 manually selected cells from 5 pictures. (Student's *t* test significance: p-value, *p<0.05; **p<0,01; ***p<0,005).

Since the cellular uptake of the CPP-PNA probe is highly varied among the cell lines, the comparison of the reporter matched probe with its mismatched control probe, which has the same CPP, should overcome this challenge when different cell lines are compared together. The **Pre-21_1*_2** probe demonstrated the highest ratio to its **mm1** control in the miR-21 abundant Hela cells (2.86-fold), whereas in the miR-21 low abundant A549 cells and the control HEK293 cells these ratios were only 0.65 and 1.44, respectively. Incorrectly, the probe indicated the lowest pre-miR21 level in A549 cells, which is not in agreement with the data of miR-21 expression obtained by RT-qPCR. Moreover, according to the RT-qPCR data, Hela cells have a 264-fold higher miR-21 expression than HEK293 cells. Here, the Hela cells only displayed a 2-fold higher fluorescence ratio compared to the HEK293 cells. Comparing to the second **mm2** control, the **Pre-21_1*_2** probe showed a 1.56-fold and 1.18-fold increase for the A549 and HEK293 cells, respectively. Nevertheless, the difference between A549 and HEK293 cells was not significant as shown by applying *t* test. The ratios of 0.75 and 1.18 were calculated for the **Pre-21_5*_3** relative to its mismatched control (**mm**) for the Hela and the A549 cells, accordingly. The discrimination of the **Pre-21_5*_3** treated cells and the cells, treated with its mismatched control, was failed even in the miR-21 highly expressing Hella cells. This data is based on the fluorescence measurements of 50 manually selected cells. It cannot be ruled out that the results may differ if a larger number of cells would be analyzed. For future experiments, a larger number of cells should be analyzed to avoid bias and to create more conclusive data. This data provides a first look on the pre-miR21 detection in cells by FIT probes and unveils some obstacles and limitations in a comparative analysis of pre-miR21 in different cell lines. The main obstacle that complicates an interpretation of fluorescence microscopy data is the high background fluorescence caused by

remaining unhybridized probes, which masks the specific fluorescence of hybridized probes. On one hand, for the detection of low abundant pre-miR21 target, the transfection concentration of the probe should be minimal to decrease the excess of the unhybridized probes. On the other hand, the fluorescence signal must be high enough to provide reliable detection. Therefore, a superior sensitivity of detection would require extremely bright and highly responsive probes. The brightness can be improved by using DNA-based probes instead of PNA-based probes[207]. Nonetheless, the PNA-based probes have a higher affinity than the DNA-based probes. This feature might be crucial for hybridization to the 72nt-long stem-loop structure of pre-miR21. Future probe improvement should include the screening of multiple TO positions to achieve the highest responsiveness. Sensitive discrimination among cell lines can be also reached by introduction of a second dye in order to detect the probe concentration inside the cell. These so-called qFIT (quantitative) probes were developed by Seitz *et.al.* and are using the combination of TO and the near-infrared (IR) Cy7 dye. In this case TO served as a reporter for target detection, while the Cy7 fluorescence determined the probe concentration inside cells. [175]

To sum up, the detection of pre-miR21 by FIT probes might be limited to miR-21 high abundant cell lines. Additionally, the specific probe fluorescence must be always compared to the fluorescence of an appropriate control (e.g., mismatched control probe). However, an additional optimization for the probe transfection concentration still might be required for different cell lines.

3.2.4 RT-qPCR-based Evaluation of the MiR-21 Maturation Inhibition by the TO-labeled Pre-miR21 Specific PNA probes in High MiR-21 Abundant Hela Cells

Next, the **Pre-21_1*_2** and **Pre-21_5*_3** probes were evaluated by RT-qPCR for their ability to inhibit miR-21 maturation in high miR-21 abundant Hela cells as mentioned in chapter 3.1.4. The inhibition of miR-21 maturation had failed using the non-labeled PNA probes in low miR-21 abundant Huh7 cells. In this experiment the highly miR-21 abundant Hela cells were transfected with the TO-labeled CPP-conjugated probes at 1 µM concentration and collected after 48 h. The commercially available miR-21 inhibitor from Qiagen (**antimiR-21**), was used as a positive control of inhibition. The **antimir-21** is a chemically synthesized, single-stranded modified RNA, complementary to miR-21, which was delivered into cells by using the Lipofectamine (Invitrogen) transfection agent. The total RNA, including miRNAs, was extracted by miRNeasy Kit (Qiagen) and was further used for the RT-qPCR analysis according to the manufacturer protocol (Applied Biosystems). The results of RT-qPCR are summarized in Figure 20. Only **antimiR-21** demonstrated significant inhibition of miR-21, whereas the reduced level of miR-21 was insignificant for the TO-PNA treated cells. Conclusively, the treatment with pre-miR21 specific PNA probes did not cause effective inhibition of the miR-21 maturation in cells.

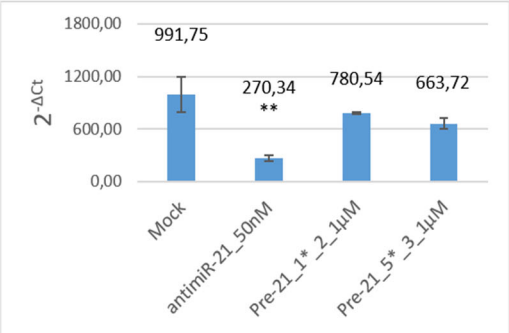

Samples	Fold change due to treatment
Mock	1,00
antimiR-21_50nM	-3,67**
Pre-21_1*_2_1µM	-1,27
Pre-21_5*_3_1µM	-1,49

Figure 20. RT-qPCR-based comparison of the miR-21 expression fold ($2^{-\Delta Ct}$, where $\Delta Ct=Ct_{miR21}-Ct_{U6}$, Ct-threshold cycle) of untreated (Mock) cells, cells treated with **antimiR-21** (Qiagen) and the PNA probes (**Pre-21_1*_2** or **Pre-21_5*_3**). Data are mean (+SD) of 3-4 replicates (Student's *t* test significance: p-value, *p<0.05; **p<0.01; ***p<0,005).

3.2.5 Summary and Conclusion

Considering miR-21 as a promising diagnostic and therapeutic target, it was set as a goal to develop pre-miR21 specific PNA probes, which can inhibit the miR-21 maturation on the precursor level. Six non-fluorogenic pre-miR21 specific PNA probes (**Pre-21_1** – **Pre-21_6**) were designed and synthesized. Although, in the BRCA assay all of them have demonstrated decreased fluorescence in a concentration-dependent way, it is much more likely that the probes inhibited the isothermal BRCA reaction rather than dicer-mediated cleavage. Consequently, the impact of inhibition of dicer-mediated cleavage is uncertain and can be determined by carrying out of a control BRCA reaction in presence of PNAs and in absence of the Dicer. The **Pre-21_1** and **Pre-21_5** PNA probes were chosen for the further evaluation in cells, since they were believed to be specific for pre-miR21 (with 3-nt overlap with the mature sequences). For the delivery of the indicated PNA probes into cell, three CPPs were investigated. Octaargenine of the second generation, $(RAhexR)_4$, provided the highest cellular uptake among them. The **Pre-21_1** and **Pre-21_5** sequences, conjugated with $(RAhexR)_4$, were delivered into the cells for assessment of their effect on the miR-21 expression by RT-qPCR. The **Pre-21_1_CPP** and **Pre-21_5_CPP** probes did not affect the mR-21 expression. In contrast to that, the treatment with the positive control **PNAmat21**, a fully complementary miR-21 PNA probe, showed a significant decrease in the miR-21 level identified by qPCR (59-fold decrease for 2 µM probe concentration). There are some possible scenarios why the probes did not inhibit the miR-21-maturation: 1) the probes were effectively delivered into cells, but were not accessible for hybridization, for example, because of endosomal entrapment. However, it was reported that the arginine of new generation $(RAhexR)_4$ was able to escape from endosome even without use of endosomolytic agent[208]; 2) the probes cannot hybridize to their pre-miR21 target, because the cellular Dicer, accompanied by its partner proteins, has a higher affinity to pre-miR21 than the PNA probes; 3) the probes hybridize with their pre-miR21 target, but this event does not affect the Dicer activity. In order to prove that the probe-target hybridization occurs, the use of so-called FIT probes appeared promising. These probes enable the detection of the target-probe hybridization state by an increase of fluorescence. According to the FIT concept, the pre-miR21 specific TO-labeled PNA probes were designed, synthesized and evaluated by fluorescence spectroscopy. The TO-labeled **Pre-21_1*_2** and **Pre-21_5*_3** probes demonstrated 3.9-/7.3-fold and 3.1-/4.6-fold fluorescence enhancement upon pre-miR21 hybridization at 25°/ 37°C, respectively. Based on the results obtained by fluorescence spectroscopy, the TO-labeled **Pre-21_1*_2** probe and **Pre-21_5*_3** probes were selected for the further analysis in cells. Additionally, the mismatched sequences for **Pre-21_1*_2** and **Pre-21_5*_3** were synthesized as controls for comparison with perfect complementary probes in cells. As before, all PNA sequences contained the conjugated $(RAhexR)_4$ CPP to enable cellular delivery. Based on RT-qPCR data, three cell lines with different miR-21 expression rates were selected for studies in cells: the high miR-21 abundant Hela cells, low miR-21 abundant A549 cells and control HEK293 cells (with the lowest miR21 level). These cells were transfected with the indicated probes and controls and analysed by means of flow cytometry and fluorescence microscopy. To draw a conclusion, additional experiments are mandatory to confirm a statistical significance of the observed effects. The preliminary data suggest that it might be possible to define a highly abundant miR-21 cells by comparing the fluorescence of specific probes with its mismatched control. However, for reliable and sensitive detection further probe improvements are still required, such as advanced probe responsiveness and brightness.

Nevertheless, the level of the miR-21 expression has not significantly changed after incubation with the TO-labeled PNA probes. Since the pre-miR21 specific TO-labeled PNA probes did not efficiently inhibit miR-21 maturation, it appeared promising to apply the FIT PNA probes as an analytical tool for monitoring the dicer-mediated miR-21 maturation.

3.3 Monitoring of MiR-21 Maturation by Forced Intercalation (FIT) PNA Probes

Concept of monitoring the miR-21 maturation by the FIT PNA probes

In order to monitor the dicer-mediated miR-21 maturation, it was envisioned to design two orthogonal fluorogenic FIT PNA probes, the one being specific for unprocessed pre-miR21 and the second targeting the mature form (as-miR21). To enable a simultaneous detection, two different reporter dyes should be used, namely thiazole orange (TO) and quinoline blue (QB), emitting light at 536 nm and 606 nm, respectively (Fig. 21). TO- and QB-containing FIT probes have been successfully applied for the multicolour detection of RNA targets in homogeneous solutions by Seitz *et.al.*[166] Here, the novel application of the FIT probes was focused on monitoring the time of course of an enzymatic reaction (dicer-mediated pre-miR21 cleavage) by performing a simultaneous readout of the starting material (pre-miR21) and the product (as-miR21) on the multichannel fluorescence spectrophotometer in the homogeneous mixture.

In the case of the pre-miR21 target, the probe targets a part of the pre-miR21 loop side (Fig. 21), which is only present in the precursor form. On the contrary, the antisense mature sequence is fully present in the pre-miR21 structure and, therefore, the design of an as-miR21 specific probe appeared challenging. It was decided to exploit the different probe affinities targeting the 72nt-long pre-miR21 and 22nt-long as-miR21. Probe hybridization with pre-miR21 would require unwinding of the stem region and opening of the pre-miR21 structure. Probe hybridization to the as-miR21 would lead to the destruction of the miR-21: as-miR21 duplex. The stability of pre-miR21 (ΔG = -35.8 kcal/mol) is higher than the stability of the miR-21: as-miR21 duplex (ΔG = -21.6 kcal/mol, ΔG calculations have been done by DINAMelt and mfold web servers, http://unafold.rna.albany.edu). Due to the fact that the affinity of the as-miR21 specific probe to 72nt-long pre-miR21 would be lower than to the shorter 22nt-long as-miR21, the as-miR21 specific probe would rather detect presence of as-miR21 by higher fluorescence enhancement.

Of note, it was also decided to design probe to be specific to the antisense mature form (as-miR21) instead of the mature form (miR-21). The downstream targets of the mature miR-21 guide strand have been extensively investigated, while the functions of the passenger strand (as-miR21) are still in investigation[51, 55]. In the beginning of the probe development, it was not excluded that the as-miR21 probe could be used for the cellular as-miR21 imaging.

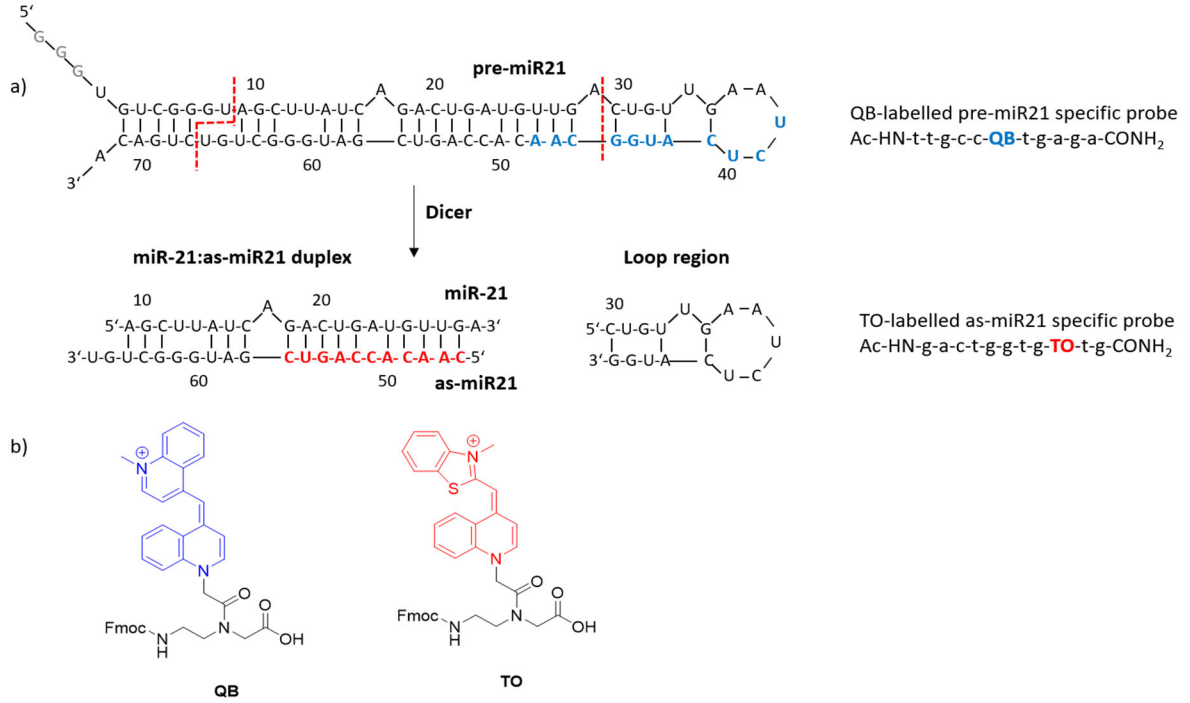

Figure 21. Concept of monitoring the miR-21 maturation by the FIT PNA probes (a). Structures of the Fmoc-protected TO- and QB-labeled PNA monomers (b). (The three 5'-terminal G residues of pre-miR21 are originated from the T7 RNA polymerase promoter in *in vitro* transcription reaction)

3.3.1 Design and Synthesis of Pre-miR-21 Specific FIT PNA Probes and their Validation by Fluorescence Spectroscopy

The precursor specific PNA probe was designed to be mainly complementary to the loop region, which is unique for pre-miR21, with an overhang of 3nt to the adjacent as-miR21 area (Fig. 22e). Next, each fluorophore (TO or QB) was incorporated at different positions within the 10-nt pre-miR21 specific PNA sequence. This so-called "TO-walk" /"QB-walk" method is used to find the best fluorophore position in the PNA probe sequence by means of providing the highest fluorescence enhancement upon target hybridization. The TO- and QB-containing PNA monomers were available in the Seitz group from the previous studies. [165, 170, 206] The fourteen PNAs (**TO1 - 7** and **QB1 - 7**) were synthesized by Fmoc-SPS to screen 7 different positions of fluorophores. Twelve of the desired PNAs were isolated in high purity and were used for evaluation by fluorescence spectroscopy. However, intense efforts to purify the **TO5** and **QB5** probes failed due to coelution of the desired probe with truncated sequences. For this reason, the **TO5** and **QB5** could not be used for further analysis. The fluorescence enhancements of the probes in presence of pre-miR21 target are shown in Figure 22: The term fluorescence enhancement (I/I_o) is defined as the ratio of fluorescence emissions after target hybridization (I) and before hybridization (I_o). Depending on the TO position within the PNA sequence, the fluorescence enhancement ranged from 1.2 to 6.6-fold upon pre-miR21 hybridization (Fig. 22a). The **TO2** PNA probe displayed the highest responsiveness upon hybridization (6.6.-fold). The QB-labelled PNA probes showed 2-14-fold enhancements of fluorescence upon hybridization with pre-miR21. The **QB3** PNA probe provided the highest responsiveness. A similar observation was already reported by Seitz *et. al.* and Yavin *et. al.*, describing the QB chromophore as a superior responsive reporter in FIT probes[165-166, 209]. The TO and QB positions in the **TO2** and **QB3** PNA probes are represented in Figure 22 c, d. Of note, none of FIT PNA probes exhibited an increase of fluorescence upon addition of the unspecific mature miR-21 (Fig. 22).

a)

Name	Sequence	I_o Pre-21/miR21	I Pre-21/miR21	I/I_o Pre-21/miR21
TO1	ttg(TO)catgaga	42,0/44,1	132,4/48,1	3,2/1,1
TO2	ttgc(TO)atgaga	21,/17,8	142,6/19,0	6,6/1,1
TO3	ttgcc(TO)tgaga	111,9/112,9	163,8/106,9	1,5/0,9
TO4	ttgcca(TO)gaga	41,4/35,4	103,0/36,7	2,5/1,0
TO5	ttgccat(TO)aga	-	-	-
TO6	ttgccatg(TO)ga	147,8/140,5	180,3/127,7	1,2/0,9
TO7	ttgccatga(TO)a	12,3/12,0	51,2/12,4	4,2/1,0

b)

Name	Sequence	I_o Pre-21/miR21	I Pre-21/miR21	I/I_o Pre-21/miR21
QB1	ttg(QB)catgaga	18,5/ 18,7	36,9/22,2	2,0/1,2
QB2	ttgc(QB)atgaga	10,1/10,6	49,3/11,3	4,9/1,0
QB3	ttgcc(QB)tgaga	9,9/10,5	135,4/10,6	13,7/1,0
QB4	ttgcca(QB)gaga	21,8/21,9	68,5/20,9	3,1/0,9
QB5	ttgccat(QB)aga	-	-	-
QB6	ttgccatg(QB)ga	24,5/ 23,1	65,6/20,8	2,7/0,9
QB7	ttgccatga(QB)a	6,5/6,6	22,4/6,3	3,5/0,9

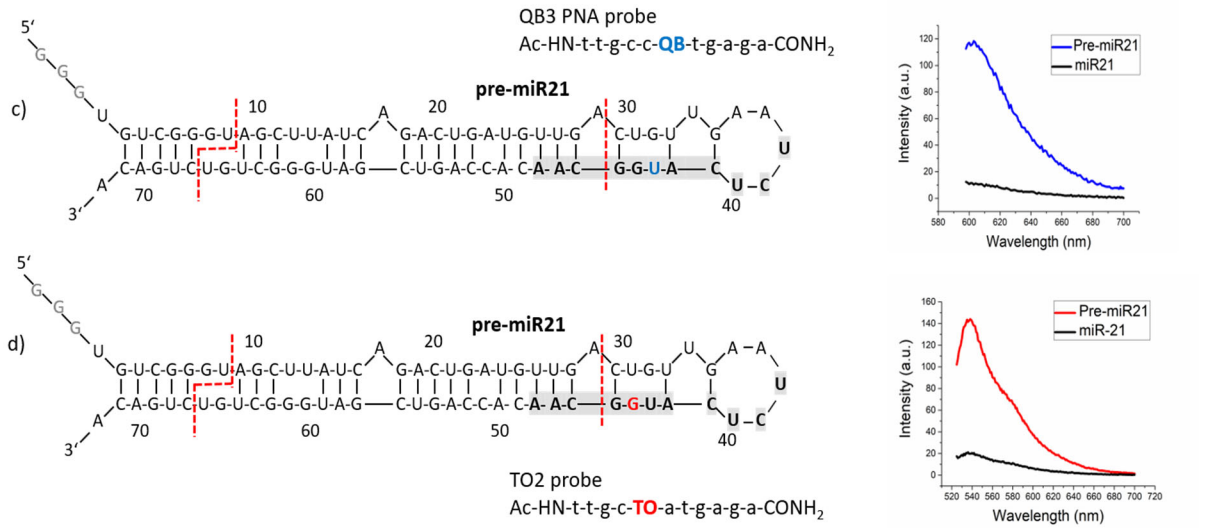

Figure 22. Evaluation of the pre-miR21 specific FIT PNA probes by fluorescence spectroscopy: a) Fluorescence emission of the TO probes before (Io) and after (I) hybridization with pre-miR21 or miR-21. Conditions: in 150 µl of 1 x PBS, c(TO probe) = c(target) = 0.5 µM; TO: λ_{ex} = 516 nm, λ_{em}= 525-700 nm; $slit_{ex}$= 5 nm, $slit_{em}$= 10 nm, 37°C. Underlined values display the fluorescence intensity upon hybridization with pre-miR21, non-underlined values with mature miR-21. b) Fluorescence emission of QB probes before (I_o) and after (I) hybridization with pre-miR21 or miR-21. Conditions: in 150 µl of 1 x PBS, c(QB probe) = c(target) = 0.5 µM, QB: λ_{ex} = 588 nm, λ_{em} = 595 - 700 nm , $slit_{ex}$ = 5 nm, $slit_{em}$ = 10 nm, 37°C. Fluorescence spectra of the pre-miR21 specific **TO2** (c) and **QB3** (d) PNA probes in the presence of pre-miR21 (red/blue) and miR-21 (black). The sequences of the **TO2** and **QB3** PNA probes are identified by bold type. The intercalation sites for the QB and TO fluorophores are highlighted by colour.

Next, the study was continued with the promising candidates: **TO2** and **QB3** probes. In this context it is important to note that the loop region is cleaved during the miR-21 processing by Dicer and further degraded by RNAses in cells. However, since the pre-miR21 specific PNA probes were designed to target the loop and the adjacent area, it could not be ruled out that the fluorescence would increase in the presence of the cleaved loop region, which would disturb the monitoring of the pre-miR21 cleavage reaction. To examine this possibility, the fluorescence of the **TO2** or **QB3** probes was measured in the presence of a synthetic RNA molecule encompassing the C30-G45 sequence. The **TO2** and **QB3** PNA probes experienced in 5.2- and 3.8-fold increases of fluorescence, respectively (Fig. 23). The **QB3** PNA probe afforded a higher specificity for pre-miR21. For that reason, the pre-miR21 specific **QB3** PNA probe was chosen for the further evaluation in the dicer cleavage reaction.

a) **TO2** PNA probe

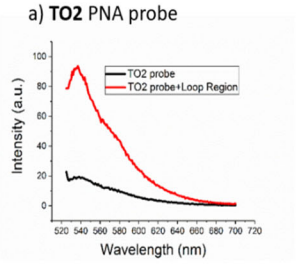

b) **QB3** PNA probe

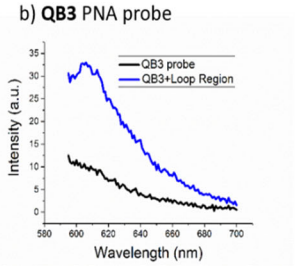

c)

Name	Sequence	I_o	I	I/ I_o
QB3	ttgcc(QB)tgaga	9,5	33,7	3,8
TO2	ttgc(TO)atgaga	19,4	93,0	5,2

Figure 23. Fluorescence spectra of the **TO2** (a) and **QB3** (b) PNA probes in absence of target (black) and in presence of the C30-G45 segment (red/ blue). c) Fluorescence emission of the **QB3** and **TO2** PNA probes before (I_o) and after (I) hybridization. Conditions: in 150 µl of 1 x PBS, the **TO2** or **QB3** PNA probe, c(probe) = c(target) = 0.5 µM (target is the loop region), TO: λ_{ex} = 516 nm, λ_{em} = 525 – 700 nm., $slit_{ex}$ = 5 nm, $slit_{em}$ = 10 nm, QB: λ_{ex} = 588 nm, λ_{em} = 598 – 700 nm., $slit_{ex}$ = 5 nm, $slit_{em}$ = 10 nm, 37°C.

3.3.2 Design and Synthesis of As-miR21 Specific TO PNA Probes and their Validation by Fluorescence Spectroscopy

It was assumed that a rather short PNA probe would preferably bind to the 22-nt long as-miR21 than to the 75-nt long pre-miR21 stem-loop hairpin, because probe hybridization in the stem region of pre-miR21 would require opening of the 75-nt hairpin or at least unwinding of the duplex in the stem region. Since the QB fluorophore was applied for the pre-miR21 targeting, the TO fluorophore was used for the as-miR21 detection. Four TO positions were examined within the 7-nt long PNA probe to find a favourable location for the fluorophore (Fig. 24). All four TO PNA probes signalled the presence of as-miR21 target by fluorescence enhancement ranging from 6.2 to 19.6-fold.

a)

Name	Sequence	I_o as-miR21/pre-miR21	I as-miR21/pre-miR21	I/ I_o as-miR21/pre-miR21
TO1*	ggtg(TO)tg	12,7/10,6	121,3/57,9	9,5/5,5
TO2*	ggt(TO)ttg	4,4/3,5	86,0/52,3	19,6/14,8
TO3*	gg(TO)gttg	9,0/9,6	108,2/127,4	12,0/13,2
TO4*	g(TO)tgttg	12,5/12,3	76,9/57,6	6,2/4,7

b) **TO1*** PNA probe

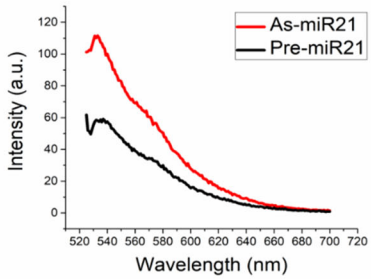

Figure 24. Sequences of TO PNA probes, designed to recognise as-miR21, and results of their evaluation by fluorescence spectroscopy: a) Fluorescence emission before (Io) and after (I) hybridization with either as-miR-21 or pre-miR21. Conditions: in 150 µl of 1 x PBS, c(TO* probe) = c(target) = 0.5 µM, TO: λ_{ex} = 516 nm, λ_{em} = 525 - 700 nm., $slit_{ex}$ = 5 nm, $slit_{em}$ = 10 nm, 37°C. b) Fluorescence spectra of the **TO1*** PNA probe in presence of as-miR21 (red) and pre-miR21 (black).

Unfortunately, also the presence of pre-miR21 resulted in an increased fluorescence (from 4.7 to 14.8-fold increase). However, the fluorescence enhancements of the three probes (**TO1*, TO2*, TO4***) were higher in presence of as-miR21 than in presence of pre-miR21. The **TO1*** PNA probe discriminated best between as-miR21 and pre-miR21 (9.5- and 5.5-fold fluorescence increase, respectively). This data might indicate that the pre-miR21 hairpin structure is flexible in the stem region probably due to the partial complementarity and, therefore, it is available for hybridization with even short 7-nt long PNA probe.

To increase the stability of the pre-miR21 structure with the objective to decrease the undesired binding of the **TO1*** PNA probe to pre-miR21, the addition of $MgCl_2$ to the assay buffer was tested. Initially, the concentrations of $MgCl_2$ ranging from 0 to 100 mM were examined (Fig. 25 a). Slight

improvement in as-miR21/ pre-miR21 discrimination was observed till 50 mM. Using a high concentration of 100 mM $MgCl_2$

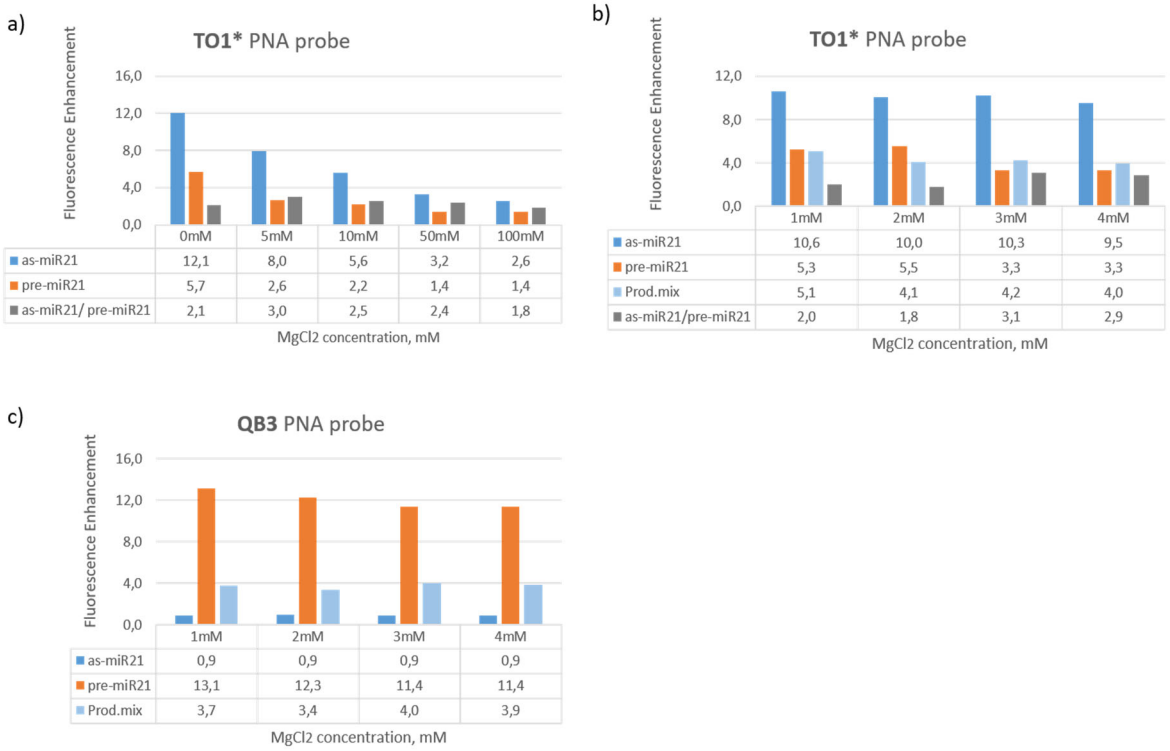

Figure 25. Optimization of the $MgCl_2$ concentration in the assay buffer: a) **TO1*** probe fluorescence enhancement in presence of either as-miR21 or pre-miR21 using an assay buffer with 0 – 100 mM $MgCl_2$. b) **TO1*** probe fluorescence enhancement in presence of as-miR21/ pre-miR21/ or product mix using an assay buffer with 1 – 4 mM $MgCl_2$. c) Fluorescence enhancement of the pre-miR21 specific **QB3** PNA probe in the presence of as-miR21/ pre-miR21/ or product mix using an assay buffer with 1 – 4 mM $MgCl_2$. Conditions: a) in 150 µl of 1 x PBS, 0 - 100 mM $MgCl_2$, c(**TO1***) = c(target) = 0.5 µM, TO: λ_{ex} = 516 nm, λ_{em} = 525-700 nm., $slit_{ex}$ = 5 nm, $slit_{em}$ = 10 nm, 37°C. Target: as-miR21/ pre-miR21; b) and c) in 150 µl of 1 x PBS, 1 - 4 mM $MgCl_2$, **TO1*** or **QB3** probe, c(probe) = c(target) = 0.5 µM, TO: λ_{ex} = 516 nm, λ_{em}= 536 nm., $slit_{ex}$ = 5 nm, $slit_{em}$ = 10 nm, QB: λ_{ex} = 588 nm, λ_{em} = 606 nm., $slit_{ex}$ = 5 nm, $slit_{em}$ = 10 nm, 37°C. Target: as-miR21/ pre-miR21/ or product mix (synthetic sequences of miR-21, as-miR21 and the C30-G45 segment).

the probe reduced its performance and showed even worse discrimination than in absence of $MgCl_2$.The presence of 5 mM $MgCl_2$ improved the discrimination between as-miR21 and pre-miR21 for the **TO1*** PNA probe by factor 1.5 in comparison to absence of $MgCl_2$. It is worth mentioning that the fluorescence enhancement dropped at both targets in presence of $MgCl_2$, but was still optimal at 5 mM. The second optimization of the $MgCl_2$ concentration involved testing smaller range from 1 mM to 4 mM in 1 mM steps. To simulate the dicer-mediated pre-miR21 cleavage reaction, the **TO1*** PNA probe fluorescence was also inspected in presence of a synthetic product mix, consisting of as-miR21, miR-21 and the C30-G45 segment in equimolar amounts (Fig. 25 b). In this concentration range the fluorescence enhancement in presence of as-miR21 was slightly affected (from 10.6-fold till 9.5-fold), whereas the fluorescence enhancement for the pre-miR21 was reduced by 1.6 times till 3.3-fold at 3 and 4 mM of $MgCl_2$. A concentration of 3 mM was identified as optimal for the discrimination between as-miR21 and pre-miR21. Remarkably, upon addition of the synthetic product mix, a reduced fluorescence intensity was observed for the **TO1*** PNA probe. This might indicate that the duplex formation (miR-21: as-miR21) hampers binding of the **TO1*** probe to as-miR21. In the presence of the product mix the **TO1*** fluorescence intensity dropped from a 5.1-fold enhancement to a 4.0-fold enhancement by raising the $MgCl_2$ concentration from 1 mM to 4 mM. However, as illustrated by figure

25 b, the 3 mM $MgCl_2$ concentration in the assay buffer was still optimal for the discrimination of pre-miR21 and the product mix by the **TO1*** probe (3.3-fold increase in presence of pre-miR21 against 4.2-fold increase in presence of product mix).

a)

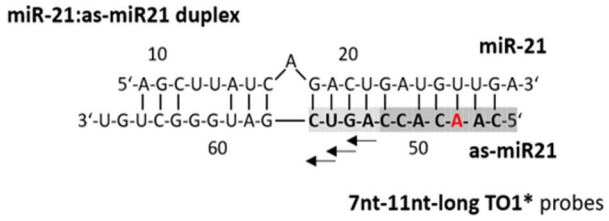

b) the **11nt_TO1*** PNA probe

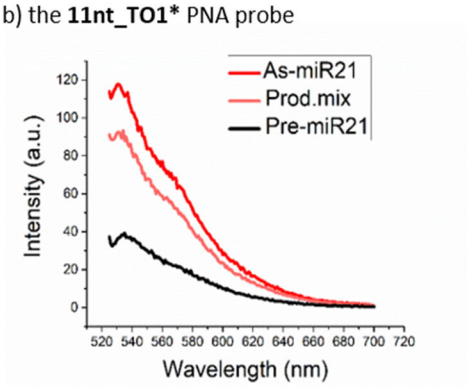

c)

Name	Length, nt	Sequence	I_o As-miR21/ pre-miR21/ product mix	I As-miR21/ pre-miR21/ product mix	I/I_o As-miR21/ pre-miR21/ product mix
7nt_TO1*	7nt	ggtg(TO)tg	10,0/11,7/7,8	102,3/39,1/33,4	10,3/3,3/4,2
8nt_TO1*	8nt	tggtg(TO)tg	11,4/10,5/10,2	51,2/25,7/27,0	4,5/2,4/2,7
9nt_TO1*	9nt	ctggtg(TO)tg	22,4/24,8/24,7	55,3/37,5/40,4	2,5/1,5/1,6
10nt_TO1*	10nt	actggtg(TO)tg	48,2/55,6/52,3	100,6/61,7/77,8	2,1/1,1/1,5
11nt_TO1*	11nt	gactggtg(TO)tg	26,4/22,5/26,2	111,6/38,6/90,3	4,4/1,7/3,4

d)

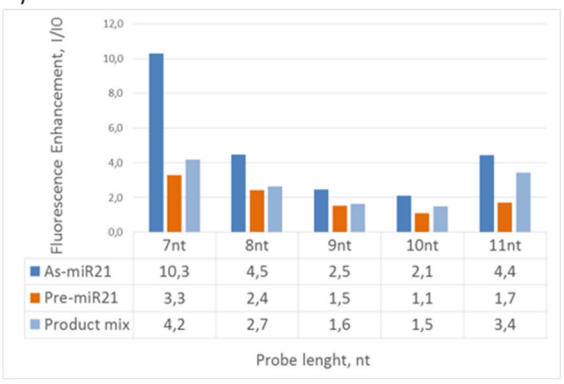

e)

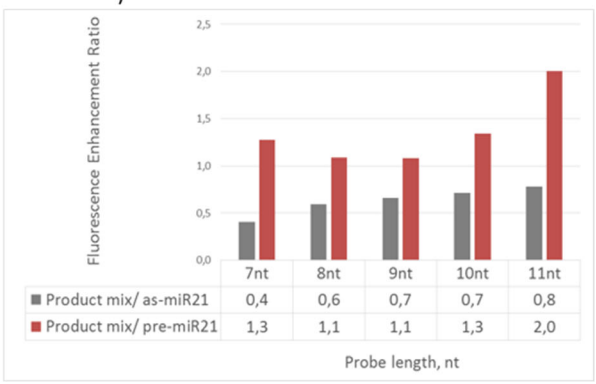

Figure 26. Evaluation of the 7nt-11nt-long as-miR21 specific TO PNA probes: a) Location of the **7-11nt-long TO1*** probes (identified by bold type). The intercalation site for the TO fluorophore is highlighted by red colour. b) Fluorescence spectra of the **11nt-long TO1*** PNA probe in the presence of as-miR21 (red)/ pre-miR21 (black)/ or the product mix (rose). c) Sequences of the **7-11nt-long TO1*** probes and their fluorescence emission before (Io) and after (I) hybridization with as-miR21, pre-miR21 or product mix. The underlined values display the fluorescence intensity upon hybridization with as-miR-21, non-underlined values with pre-miR21, dotted lined values with the product mix. d) Comparison of the fluorescence enhancements of the **7-11nt-long TO1*** probes in presence of as-miR21 (blue), pre-miR21 (orange) or the synthetic product mix (light blue). e) Graphic of the fluorescence enhancement ratios: $(I/I_0)_{\text{product mix}}/(I/I_0)_{\text{as-miR21}}$ and $(I/I_0)_{\text{product mix}}/(I/I_0)_{\text{pre-miR21}}$ for evaluated probes. Conditions: in 150 µl of 1 x PBS, 3 mM $MgCl_2$, c(probe) = c (target) = 0.5 µM, TO: λ_{ex} = 516 nm, λ_{em} = 525 -700 nm., (Kinetic mode: λ_{ex} = 516 nm, λ_{em} = 536 nm), $slit_{ex}$ = 5 nm, $slit_{em}$ = 10 nm, 37°C. Target: as-mir21/ pre-miR21/ or product mix (miR21, as-miR21 and the C30-G45 segment).

Nevertheless, this low discrimination rate (1.3 times) is not satisfactory. Further improvement of the affinity of the probe towards the antisense strand of the miR-21: as-miR21 duplex was required. Ideally, upon addition of the product mix the fluorescence enhancement should be as high as for presence of as-miR21 only.

The fluorescence enhancement of the pre-miR21 specific **QB3** PNA probe was also tested in the assay buffer with $MgCl_2$ addition (Fig. 25 c). Since $MgCl_2$ stabilizes the pre-miR21 structure, the **QB3** fluorescence enhancement was slightly decreasing in presence of 1-4 mM $MgCl_2$ (from 13.1 to 11.4-fold) upon pre-miR21 hybridization. Still no fluorescence enhancement was observed in presence of as-miR21.

To improve the **TO1** probe to invade the miR-21: as-miR21 duplex, the sequential elongation of the probe length was tested. Four novel TO PNA probes (**8nt_TO1*, 9nt_TO1*, 10nt_TO1*** and **11nt_TO1*,** Fig. 26) were synthesized ranging from 8 to 11 nt bearing the TO fluorophore at the same position. The probes were evaluated by fluorescence microscopy using buffer containing 3 mM $MgCl_2$ concentration optimized before. The single strand fluorescence increased with the probe elongation till 10 nt. The fluorescence enhancement in presence of as-miR21 decreased with increasing probe length from 10.3-fold (7nt) to 2.1-fold (10nt) enhancement. Exceptionally, the 11 nt-long probe had a higher fluorescence enhancement (4.4-fold increase) than the 9 nt- and 10 nt-long probes in presence of as-mir21. Of note, in presence of pre-miR21 target the fluorescence enhancement also dropped with increasing probe length. The decrease of fluorescence enhancement upon increased probe length was more pronounced when pre-miR21 was added than with miR21:as-miR21. The 10 nt-long probe fluorescence remained almost unchanged upon pre-miR21 addition.

To verify the affinity and selectivity improvement of the elongated probes, it is instructive to anlyze the ratios: $(I/I_0)_{\text{product mix}}/(I/I_0)_{\text{as-miR21}}$ and $(I/I_0)_{\text{product mix}}/(I/I_0)_{\text{pre-miR21}}$ (Fig. 26 e). The first ratio $(I/I_0)_{\text{product mix}}/(I/I_0)_{\text{as-miR21}}$ reflects an improvement of the ability to displace miR-21 in the miR-21:as-miR-21÷ ¡ïÕªº. The goal is to reach the ratio to be equal to 1.0. This means that the probe binding would not be affected by miR21. It was observed that this ratio increased from 0.4 to 0.8 with an increasing probe length (7 nt → 11 nt). The second ratio $(I/I_0)_{\text{product mix}}/(I/I_0)_{\text{pre-miR21}}$ demonstrates the selectivity of the probe. The rate of 1.0 means no selectivity, whereas higher rates display better selectivity. The 8 nt- and 9 nt- long probes could not discriminate between pre-miR21 and the product mix. The 7nt- and 10 nt- long probes showed poor discrimination, whereas the 11nt-long probe gave a useful discrimination (2-fold). In conclusion, the **11nt-long TO1*** PNA probe was selected for further evaluation.÷

3.3.3 Monitoring of Model Dicer Cleavage Reaction Using Synthetic RNA

The **QB3** PNA probe and the **11nt_TO1*** PNA probe were tested in a model of the dicer cleavage reaction. In this experiment, synthetic RNA sequences (pre-miR21, miR-21, as-miR21 and the C30-G45 segment) were mixed in different proportions in order to imitate selected stages of the dicer cleavage process (0%, 50%, 75% and 100% of conversion). The mixtures were added to the two FIT-PNA probes and the increase of fluorescence was monitored at the corresponding wavelengths of the reporters (λ_{em_TO} = 525 -700 nm, λ_{Max_TO} = 516 nm; λ_{em_QB} = 598 -700 nm, λ_{Max_QB} = 606 nm). As expected, the pre-miR21 specific **QB3** fluorescence was decreasing with the progress of the model dicer reaction, reflecting the reduced amount of pre-miR21 in the reaction mixture (Figure 27). The observed 4-fold enhancement of the QB-pre-miR21 signal in the 100% cleavage mix (no presence of pre-miR21) is explained by hybridization with the C30-G45 segment. In contrast to the QB signal, the **11nt_TO1*** fluorescence increases with the progress of the model reaction (from 1.2- to 3.9-fold), displaying the increased concentration of as-miR21. To summarize, the evaluated probe combination could successfully monitor the model dicer reaction on the pre-miR21- and the as-miR21-levels.

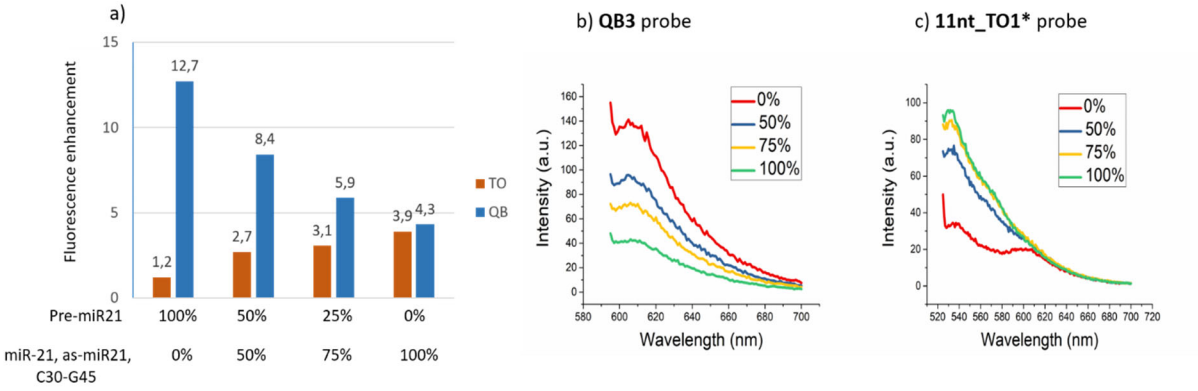

Figure 27. a) Fluorescence enhancements of the pre-miR21 specific **QB3** PNA probe and the as-miR21 specific **11nt_TO1*** PNA probe in presence of the synthetic product mixes corresponding to 0%, 50%, 75% and 100% of dicer cleavage. b) Fluorescence spectra of the **QB3** PNA probe and c) the **11nt_TO1*** PNA probe in presence of the different product mixes. Conditions: in 150 µl of 1 x PBS, 3 mM $MgCl_2$, c(**11nt_TO1***) = c(**QB3**) = c(reaction mix) = 0.5 µM, TO: λ_{ex} = 516 nm, λ_{em}= 525 -700 nm, $slit_{ex}$ = 5 nm, $slit_{em}$ = 10 nm, QB: λ_{ex} = 588 nm, λ_{em}= 598 -700 nm., $slit_{ex}$ = 5 nm, $slit_{em}$ = 10 nm, 37°C.

3.3.4 Application of the FIT PNA Probes in Enzymatic Reactions

The next step was to apply the FIT PNA probes in enzymatic reactions. In this context it was set as a goal to apply the two validated FIT probes **QB3** and **11nt_TO1*** for the detection of the dicer-mediated pre-miR21 cleavage. Additionally, it was supposed to use the **7nt_TO1*** probe for indirect monitoring the miR-21 loading into the Ago2 protein.

Monitoring of the dicer-mediated pre-miR21 cleavage using a recombinant Dicer

In order to monitor the dicer-mediated pre-miR21 cleavage, a recombinant dicer enzyme (rhDicer) from Genlantis (San Diego, USA) was used according to the manufacturer's protocol with the following modification: *in vitro* transcribed pre-miR21 was incubated with rhDicer in a buffer of 20 mM tris HCl, pH 7.74, 2.5 mM $MgCl_2$, 12 mM NaCl and 1 mM DTT, which has been optimized in the PhD work of Brian Patrick Davies.[210] The reaction was analysed after 6 h and 20 h by fluorescence spectroscopy using the probe set: **QB3** and **11nt_TO1***. After 20 h incubation with 1U rhDicer per 1 µg pre-miR21, the reaction reached only ~20% conversion, as judged by the 2-fold increase of the ratio TO/QB emission enhancements (10-fold is expected for the full conversion) (Fig. 28 a). Upon addition of 3U rhDicer per 1 µg pre-miR21, the comparison of the ratios TO/QB emission enhancements did not show the significant improvement of cleavage (Fig. 28 b, c). The pre-miR21 specific **QB3** probe reduced its fluorescence enhancement from 9.7-fold (0 h) only to 7.1-fold (18 h), whereas the as-miR21 specific **11nt_TO1*** fluorescence enhancement raised slightly from the 1.1-fold (0 h) to 1.5-fold (18 h). Unexpectedly, the results of the dicer cleavage analysis by the polyacrylamide gel (PAAG) did not confirm the results of the fluorescence spectroscopy (Fig. 29 a, b). Based on the PAAG analysis, rhDicer effectively cleaved pre-miR21 in the both reactions, since the corresponded to pre-miR21 bands disappeared after 18-20h of incubation. In the time course of the reaction, the products of variable length, detected by TO fluorescence were observed, whereas at the end point, the one product was predominant (especially for reaction with 3U of rhDicer), which run a little bit faster as compared with the synthetic as-miR21: **11nt-TO1*** duplex. The sequence of this product is unknown since its sequencing was not performed. This shows that rhDicer cleaved pre-miR21 in different positions as expected. Since dicer products are not visible on the UV-channel, either radioactive probes or radioactive labelling of pre-miR should be applied in future experiments. [211-212]

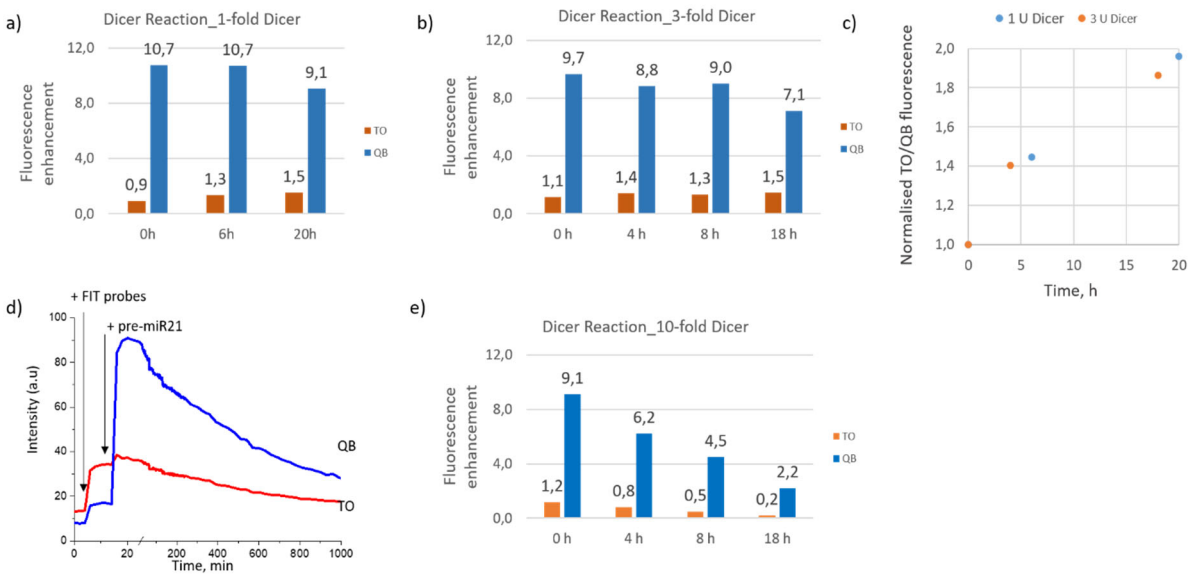

Figure 28. Monitoring of the pre-miR21 cleavage with FIT PNA probes (**QB3** and **11nt_TO1***) upon addition of a) 1 U, b) 3 U or d), e) 10 U rhDicer per 1 µg RNA. The TO/QB fluorescence ratios of reaction with 1 U and 3 U rhDicer are compared in c). The kinetic of reaction with 10 U rhDicer is performed in d). (reaction conditions are in the supporting information Fig. S6.)

Although the further increase of the Dicer load is not recommended, according to the manufacturer's protocol, the reaction with a 10-fold increased rhDicer concentration was performed (Fig. 28 d, e). Time course measurements revealed that under these forcing conditions, the reaction proceeded more rapidly and the QB signal dropped by 70% within 4 h. At the end of the reaction, the fluorescence enhancement for the **QB3** probe was only 2.2-fold, which is even less than in presence of the C30-G45 segment (4.3-fold in the model reaction). This might indicate unspecific rhDicer digestion of the loop segment. Surprisingly, the **11nt_TO1*** probe fluorescence also decreased. Upon addition of 10U rhDicer per 1 µg pre-miR21, the results of fluorescence spectroscopy were correlated with the data obtained by PAAG (Fig 29 c). The PAGE analysis of the dicer cleavage after 18h showed the absence of pre-miR21 and one band, detected by TO, corresponded to the same product, which was already observed in the previous reactions.

Here, the pre-miR21 has three additional guanine nucleotides (3G) at the 5'- terminus of pre-miR21, which originate from the T7 polymerase promotor in *in vitro* transcription reaction. By using the 3G 5'-overhang pre-miR21 and human rhDicer, possibly first-nick intermediate products as well as unspecific products, detected by TO probe, were observed after 4h and 8h in the experiment with 3U of rhDicer during the native PAGE-analysis. Of note, the abundance of these intermediates/side products decreased after 18h of reaction time. A similar behavior of intermediates has been reported in the literature [213]. Regarding to the final product, its amount is increasing during the course of reaction, as judged by the TO-fluorescence in the native PAGE-gel. It is important to note, the final product differs from native as-miR21 by a slightly higher electrophoretic mobility in the PAGE. Either the observed final product is homogeneous or heterogeneous, it can not be answered by the data of the PAGE analysis.

Besides the observed unspecific cleavage behavior of rhDicer, there is a probability of a shift in the dicer cleavage site, which would result in an alternative product formation. However, there is no sequencing data to confirm it. It has been demonstrated by Ando *et al.* that rhDicer can proceed the 3G 5'-overhang pre-miR21 into two-step cleavage, using the 3'-conting rule with a fixed distance of 23

nt[212]. The first cut is between U26-U27 and A48-C49. This would destroy the binding site for the **11nt-TO1*** probe and, consequently, lead to the loss of TO signal. Moreover, hybridization of the **QB3** probe with the released longer loop segment could give an elevated signal, which was already observed in the two first reactions.

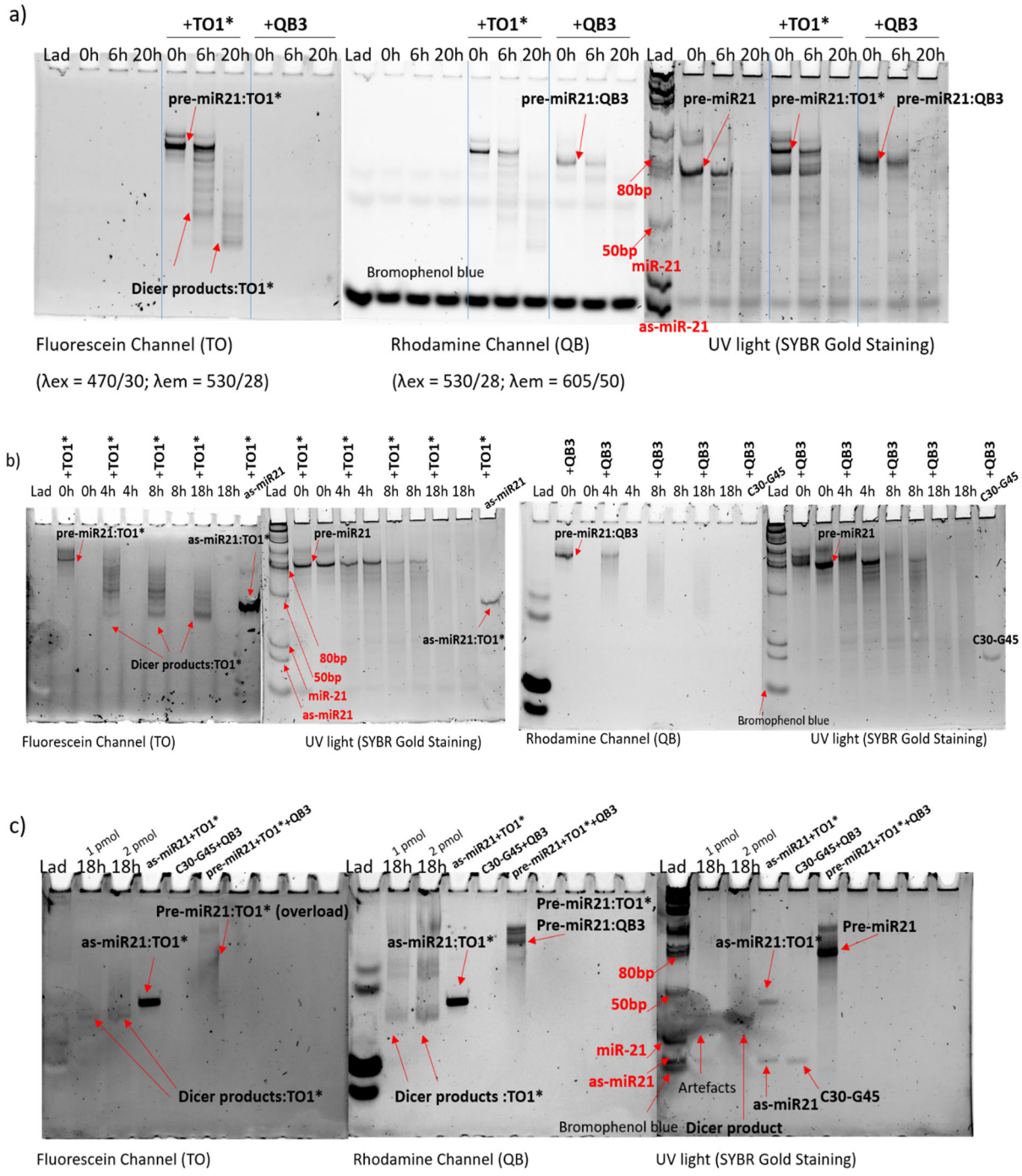

Figure 29. Polyacrylamide Gel Electrophoresis (PAGE) analysis of the pre-miR21 cleavage upon addition of 1U (a), 3U (b) and 10U (c) rhDicer per 1 µg RNA. Conditions: Native PAAG gel 15% (a), 20% (b,c); low molecular weight ssRNA ladder (NEB); used probes: the as-miR21 specific **11nt-TO1*** probe and the pre-miR21 specific **QB3** probe. The reaction mixture (c) contained already the two probes. The synthetic as-miR21, the C30-G45 segment and pre-miR21 were used as controls. TO fluorescence: Fluorescein channel (λex = 470/30; λem = 530/28), QB fluorescence: Rhodamine Channel (λex = 530/28; λem = 605/50), SYBR Gold staining: UV light.

This issue of variability in dicer cleavage positions was already actively discussed in the literature[37, 39, 211, 214-215] and can be matter of the substrate recognition by dicer. As determined, Dicer functions as a molecular ruler and select the cleavage site by measuring a fixed distance from either 2nt-3'-overhang (3'-counting rule) or 5'- phosphorylated end (5'-counting rule). [37, 39] The 5'-counting rule is shown to be prevalent in mammalians, however, additional factors can influence the dicer recognition. For example, it depends on the thermostability of the 5'- stem termini and on the presence of the 5'-end phosphate group. For the substrates with the thermodynamically unstable 5' stem termini Dicer follows 5'-counting rule. However, upon substrate stabilization with $MgCl^{2+}$ (4mM), it was demonstrated that dicer changes its recognition on the 3'-counting rule. The substrates bearing a 5'-end phosphate group followed the 5'-counting rule, while the substrates lacking 5'-end phosphate group were determined by 3'-counting rule. Of important note, the Dicer binding to 5'-phosphate end, yields in more precise cleavage.[37]

Ando *et al.* showed that the native pre-miR21 is cleaved according to the 5'-counting rule with a fixed distance of 23 nt[212]. However, this sequence is lacking the U1-G7 and C67-A72 segments of the predicted stem-loop obtained from miRNA registry (www.mirbase.org). Further optimization of the rhDicer reaction could be done in the direction of improvement of rhDicer recognition of the 5'-end. In this consideration, the use of the not full pre-miR21 sequence (lacking U1-G7 and C67-A72) can be advantageous in combination with the decreased $MgCl^{2+}$ concentration.

Detection of the miR-21 loading into Ago2 using the as-miR21 specific TO PNA probe

Ago2 is a crucial component of the RISC machinery and is responsible for loading the guide miRNA strand into the RISC complex. As soon as the guide miRNA strand is loaded onto Ago2, the passenger strand is released. After Ago2-loading, the guide miRNA directs the RISC complex to the complementary mRNA target for the gene-silencing. Since it was shown that the as-miR21 specific short **7nt_TO1*** probe has a poor affinity to as-miR21 in a form of the miR21: as-miR21 duplex and strongly binds to the single stranded as-miR21 (4.2-fold enhancement against 10.2-fold enhancement, respectively, chapter 3.3.3), it was intended to use the **7nt_TO1*** probe for the indirect analysis of the miR-21 loading into Ago2 by detecting the released as-miR21. The **7nt_TO1*** probe should signal the released as-miR21 by an increase of fluorescence (Fig. 30 a).

To test this hypothesis, the dicer product mixture (prod. mix) comprised of the synthetic RNA sequences (miR21: as-miR21 duplex and the C30-G45 segment) was added to the two PNA probes (as-miR21 specific **7nt_TO1*** and pre-miR21 specific **QB3** as an internal control) (Fig. 30 b). As it was observed earlier, the **7nt_TO1*** probe promoted the miR21: as-miR21 dissociation and signalled the released as-miR-21 by 4.3-fold fluorescence increase. On a side note, the TO fluorescence was slightly decreasing after the sharp fluorescence increase, which can be caused by further miR-21: as-miR21 association. The **QB3** probe increased its fluorescence in four times upon recognition the loop region. Nextly, the Ago2 protein was added to the product mix and probes (Fig 30 a). It is assumed that the Ago-2-mediated loading of miR-21 would release the as-miR21 and contribute to the **7nt_TO1***: as-miR21 complex formation. Therefore, it would lead to the TO fluorescence increase, whereas the **QB3** fluorescence should stayed unchanged. To control the specific change in the TO fluorescence, the experiments with a heat-inactivated Ago2 and in absence of Ago2 were also conducted (Fig. 30 c, d). As expected, the fluorescence of the **7nt_TO1*** PNA probe rapidly increased after addition of the Ago2 functional protein, whereas the addition of the inactive Ago2 protein did not affect the TO fluorescence. (The later (after 200 min) slight increase of the TO fluorescence in the case of inactivated Ago-2 can be caused by evaporation, since the QB fluorescence also slightly increased). In case of the negative control (no Ago2 protein), the **7nt_TO1*** PNA probe fluorescence remained constant. As an

internal control, the fluorescence of the pre-miR21 specific **QB3** PNA probe was not affected by the Ago2 addition.

These results had proven that the **7nt_TO1*** probe can indirectly detect the presence of the functional Ago-2. This method might be helpful in estimation of the Ago2 functional activity (e. g., activity of recombinant proteins) and in the evaluation of the new Ago2 inhibitors.

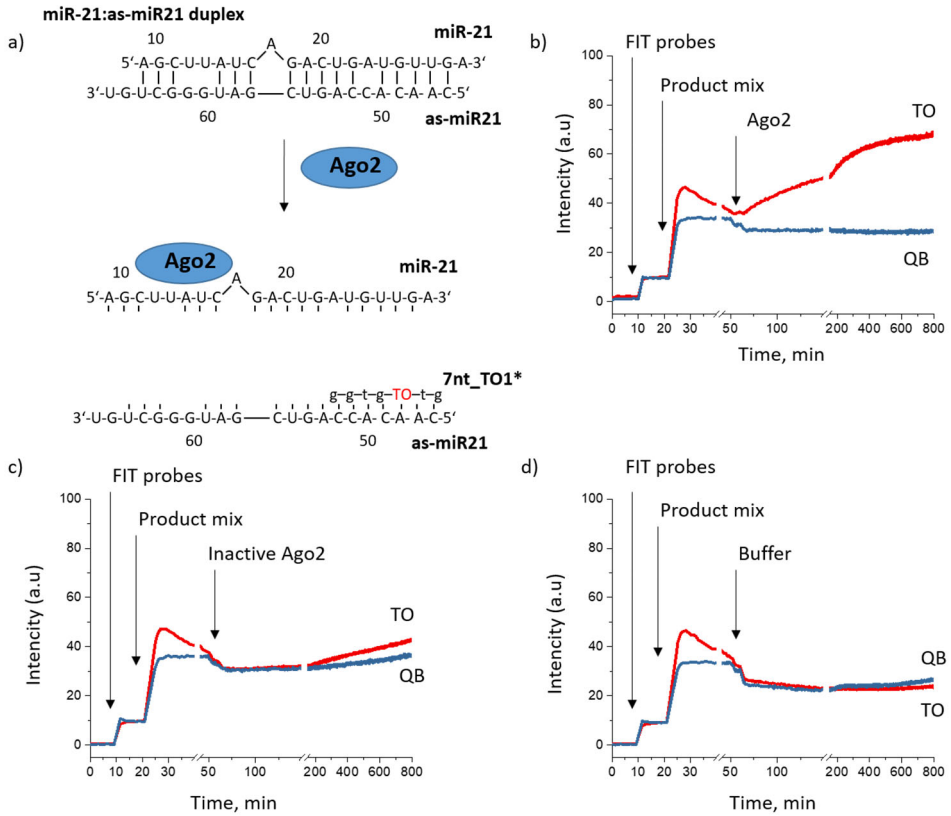

Figure 30. a) Concept of the detection of the miR-21 loading onto Ago2 by using the as-miR21 specific **7nt_TO1*** PNA probe. Fluorescence spectra of the **7nt_TO1*** PNA probe and the control **QB3** PNA probe in presence of the product mix and b) Ago2 protein, c) heat-inactivated Ago2 protein and d) no Ago2 protein (negative control). The drop of the TO and QB fluorescence directly after Ago2/ Ago2 inactivated/ Buffer addition is due to the dilution of the assay buffer. Conditions: in 150 µl of 1 x Ago2 buffer (30 mM Tris, pH = 7.25, 130 mM KCl, 1.1 mM $MgCl_2$, 1 mM DTT, 0.1 mM EDTA), c(**7nt_TO1***) = c(**QB3**) = c(product mix) = 0.5 µM, product mix (miR21, as-miR21 and the C30-G45 segment) and b) 0.4 eq Ago2 protein; c). 0.4 eq Ago2 heat-inactivated protein and d) no Ago2 protein (negative control), TO: λ_{ex} = 516 nm, λ_{em} = 536 nm., $slit_{ex}$ = 5 nm, $slit_{em}$ = 10 nm, QB: λ_{ex} = 588 nm, λ_{em} = 606 nm, $slit_{ex}$ = 5 nm, $slit_{em}$ = 10 nm, 37°C.

3.3.5 Summary and Concluding Remarks

Two orthogonal FIT PNA probes bearing the QB and the TO fluorophore have been developed for the rapid and simultaneous detection of pre-miR21 and as-miR21 in homogeneous solution. The pre-miR21 specific **QB3** PNA probe successfully differentiated between the precursor and the mature form of miR-21. The probe provided 13.7-fold fluorescence enhancement upon hybridization to the pre-miR21 and no enhancement in presence of the mature form. Comparably to the **QB3** PNA probe, the as-miR21 specific **7nt_TO1*** PNA probe enhanced its fluorescence up to 10.3-fold upon hybridization with as-miR21, whereas in presence of pre-miR21 the fluorescence raised only by a factor of 4.2 using

an optimized MgCl2-containing buffer. However, it was observed that the as-miR21 specific **TO1*** probe did not reach its maximal potential fluorescence enhancement in presence of the miR-21: as-miR21 duplex. A possible explanation for this might be that the formed duplex miR21: as-miR21 hinders the **TO1*** PNA probe hybridization to as-miR21. To improve the affinity of the probe for as-miR21, the probe length was elongated from 7 nt to 11 nt, which resulted in a 3-fold discrimination rate between pre-miR21 and the miR-21: as-miR21 duplex.

To evaluate the performance of the probe combination, **QB3** and **11nt_TO1***, the dicer cleavage reaction was modelled by mixing the synthetic RNA sequences of the corresponding pre-miR21, miR-21, as-miR21 and the C30-G45 segment in different proportions. As expected, with the processing of the model reaction, the fluorescence signal of pre-miR21 specific **QB3** probe dropped, while the as-miR21 **11nt_TO1*** probe fluorescence raised, reflecting the decreased amount of pre-miR21 and increased amount of as-miR21, respectively.

The two probes were tested for monitoring the enzymatic reactions. In the time course of reaction with 10U rhDicer per 1 µg pre-miR21, the loss of both TO and QB emission was observed, which shows the rapid pre-miR21 cleavage and the loss of the binding site for the TO probe. The gel electrophoresis data confirmed these results, after 18 h of incubation no band corresponded to pre-miR21 was observed and the cleavage product migrated faster as the control as-miR21. Unspecific cleavage behavior of rhDicer can be explained by using an *in vitro* transcribed pre-miR21 with three additional 5'-terminal guanine overhang. Taking it into account, the shortened synthetic sequence of pre-miR21 can be used, which lacks the U1-G7 and C67-A72 segments of the predicted stem-loop obtained from miRNA registry[212]. This method might be helpful for future screening of the new dicer inhibitors and pre-miR21 binders, as well as for the evaluation of new as-miR21 targets.

The short **7nt_TO1*** probe provided a tenfold enhancement of fluorescence upon recognition of as-miR21. Although, the probe was not successful to invade the miR21: as-miR21 duplex, and therefore, to monitor the dicer-mediated pre-miR21 cleavage, the **7nt_TO1*** probe was useful in the detection of the miR-21 loading by the Ago2 protein. Ago2 protein is a member of the RISC machinery, which loads miR21 and releases as-miR21, thereby, making it accessible for probe hybridization. The **7nt_TO1*** probe had a minimal 4-fold fluorescence response in the presence of the miR-21: as-miR21 duplex, whereas at a time, when Ago2 was added, the **7nt_TO1*** probe increased its fluorescence to 10-fold. These results indicate that this assay could be a valuable tool for the evaluation of the Ago2 functional activity and for the fast screening of new Ago2 inhibitors.

3.4 Evaluation of Small Molecular Inhibitors (SMI) of the MiRNA Maturation in Cells

In the previous chapters, the antisense oligonucleotide strategy was applied for the development of pre-miR21 specific inhibitory PNA probes and for monitoring the dicer-mediated miR-21 maturation by FIT PNA probes. However, it appeared that the pre-miR21 specific PNA probes did not inhibit the dicer-mediated miR-21 maturation effectively. An alternative approach for the inhibition of the miRNA maturation is the use of small molecular inhibitors (SMI), which are designed to target the specific secondary structures of pre-miRNAs. A set of the 80 SMI derivatives was designed and synthesized by Dr. Claudine Dojahn in the Arenz research group. [1] In this work, the SMI's potential inhibition effect on the dicer-mediated pre-miRNA cleavage was evaluated in the BRCA assay, using four pre-miRNAs (pre-Bantam, pre-let-7, pre-miR21 and pre-miR122). [1] Based on these results, the most promising

compounds for inhibition of miR-122 (**DA8, DA40, D*A20, DA18**) and miR-21 (**DA8, DA40, D*A20, DA18, NA17**) maturation were chosen for their evaluation in cells. The chemical structures of the studied compounds are shown in Fig. 31.

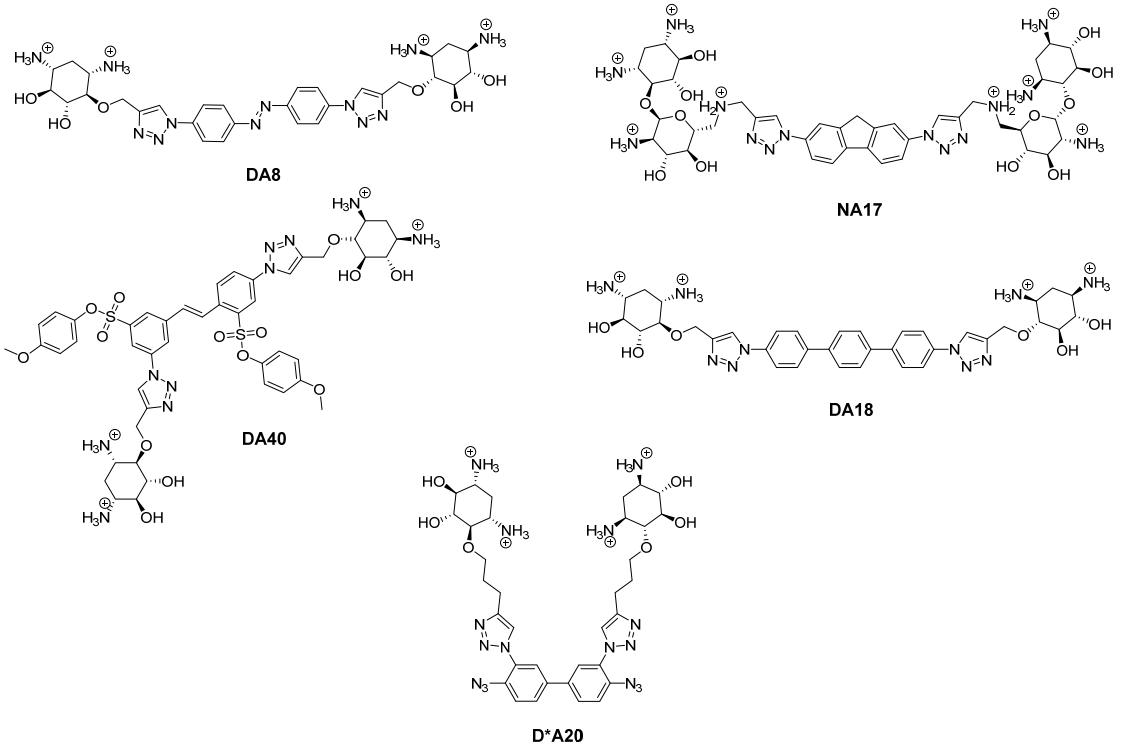

Figure 31. Chemical structures of the most promising SMI for inhibition of the miR-122 and miR-21 maturation.

3.4.1 Luciferase Assay

For the evaluation of the abovementioned SMIs in cells, the luciferase reporter assay has been chosen, using the psiCHECK-2 vector (Promega). The compounds **DA8, DA40, D*A20** and **DA18** were screened for their ability to modulate the miR-122 and miR-21 expression. The compound **NA17** was tested only for its potency to inhibit the miR-21 maturation according to the results of the BRCA assay.

The advantage of the psiCHECK-2 vector is that it contains a *Renilla* luciferase and an independently transcribed *Firefly* luciferase reporter gene, which is used as an internal control of the transfection efficiency for normalization of the *Renilla* signal. The fully complementary sequence of the target miRNA (miR-122 or miR-21) was placed downstream of the *Renilla* luciferase gene. Thereby, the *Renilla* luciferase signal should decrease in presence of miR-122 or miR-21, respectively. In case of successful inhibition of miR-122 or miR-21 maturation by SMIs, the *Renilla* luciferase signal should be restored. For conducting the screening of the abovementioned compounds, human hepatoma (Huh7) cells were transfected by the psiCHECK-2 plasmid, containing the target miRNA complementary sequence. Next, the cells were incubated with SMIs for 48 h. After incubation, the *Renilla* and *Firefly* signals were recorded accordingly to the manufacture's protocol. As shown in figure 32a, the miR-122-containing reporter psiCHECK-2 transfected without a SMI (negative control) displayed a low normalized *Renilla* signal (0.34) in comparison to the psiCHECK-2 reporter without miR-binding site (positive control, *Renilla* signal = 2.26). The low *Renilla* luciferase signal was caused by post-transcriptional inhibition of the *Renilla* luciferase by high miR-122 level. To analyse the impact of the SMIs, the values of *Renilla* signal were scaled so that the positive control is assigned the value of 1 and the negative control is assigned the value of 0. Additionally, a commercial miR-122 inhibitor from Qiagen (**antimiR-122**) was used, which has been proven to inhibit

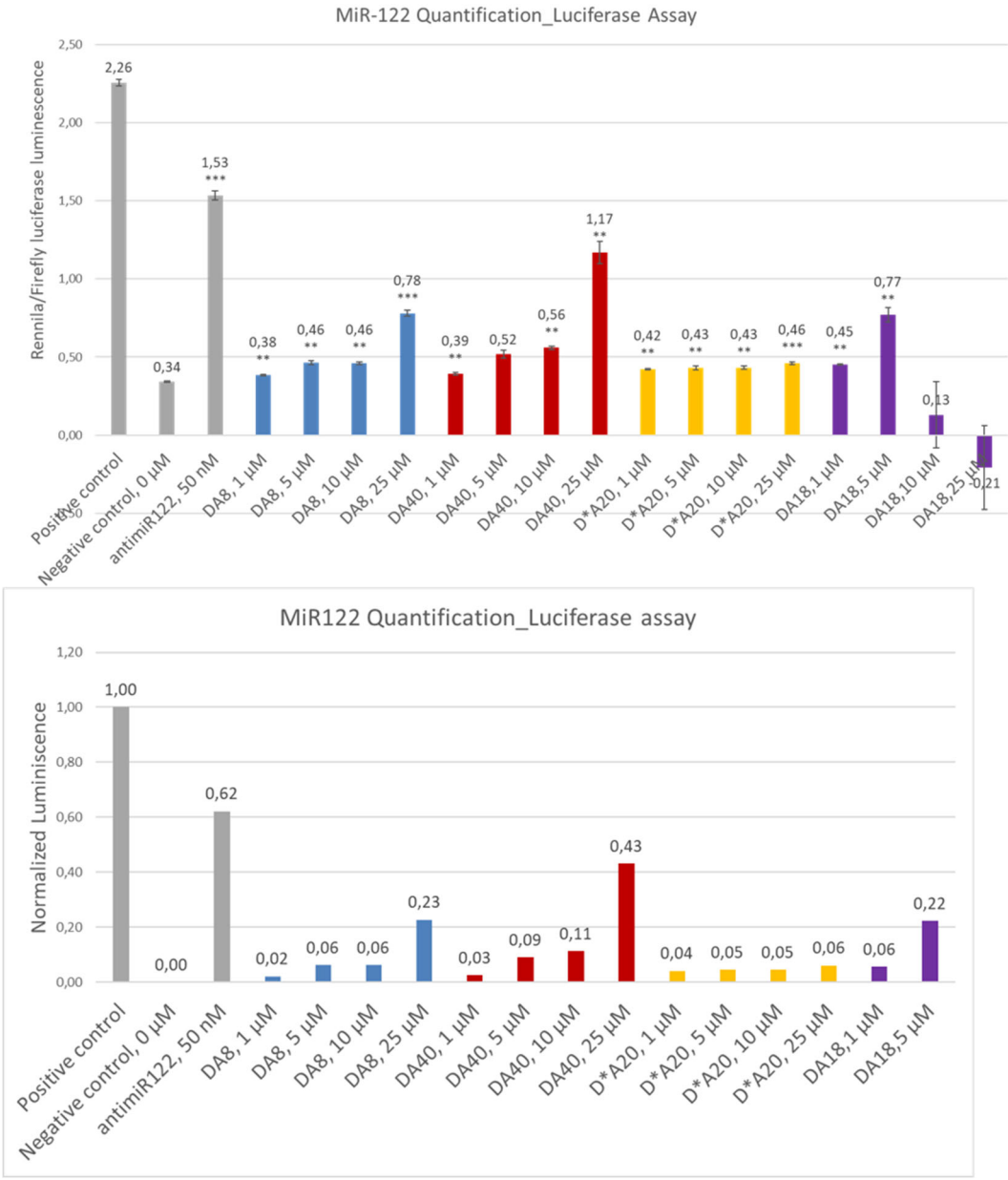

Figure 32. Relative normalized *Renilla* luciferase activity of the miR-122 reporter psiCHECK-2 transfected into Huh7 cells after treatment with **DA8, DA40, D*A20** or **DA18** at different concentrations. The normalized *Renilla* signal is represented as a relative luminescence, in which the signal from psiCHECK-2 reporter without miRNA-binding site (positive control) is assigned the value of 1 and the signal from psiCHECK-2 reporter with miR-122-binding site is set as the value of 0 (negative control). Bars represent the mean ± SD of normalized *Renilla* signal (3 measurements of one sample). *** $p < 0.001$, ** $p < 0.01$, * $p < 0.05$ (Student's t test). The raw data is represented in the supporting information (Fig. S8).

miR-122 in low concentration. The antisense oligonucleotide **antimiR-122** is a single-stranded complementary to miR-122 modified RNA, which hybridizes to mature miR-122 and inhibits its binding to mRNA target. Upon treatment by **antimiR-122**, the *Renilla* luciferase was restored for ~60%, showing the effective inhibition of miR-122. Next, the concentration range of 1-25 µM for every compound was evaluated. The compounds **DA8** and **DA40** displayed a restoration of the normalized *Renilla* luciferase activity, giving 6-23% (**DA8**) and 9-43% (**DA40**) of luminescence increase for 5-25 µM concentrations. However, a 3-4-fold decrease of the *Firefly* signal (internal control of transfection and

cell viability) at a concentration of 25 µM of **DA8** and **DA40** suggests a cytotoxicity of compounds (supporting information, Fig. S8), which will be discussed in detail in chapter 3.4.4. Of note, the **DA8** and **DA40** inhibited the miR-122 maturation in a concentration dependent manner. In contrast to that the compound **D*A20** demonstrated only a slight increase of normalized *Renilla* luminescence, corresponding to 4-6% of inhibition. This inhibition effect was constant and independent of concentration. A relatively high *Firefly* signal at concentrations of 1-25 µM of **D*A20** indicated satisfactory transfection efficiency and an absence of cytotoxicity. Although, **DA18** (5 µM) provided 22% of normalized *Renilla* signal increase, the compound was cytotoxic at this small concentration. It is clearly shown that treatment with increasing amounts of **DA18** above 5 µM decreased the *Firefly* luciferase signal in a dose dependent manner.

Remarkably, the SMIs **DA8**, **DA40**, **D*A20**, **DA18** and **NA17** did not show any inhibitory effect on the miR-21 expression (Fig. 33). The positive control (reporter without miR-binding site) displayed a high value of luminescence (2.8), whereas for the negative control (reporter with miR-21 binding site, no SMI) this value was only 0.03. Upon treatment with the miR-21 inhibitor from Qiagen (**antimiR-21**), the normalized *Renilla* luminescence elevated till 0.15, showing a 5-fold increase of luminescence in comparison to the negative control. Incubation of the cells with **DA8**, **DA40**, **D*A20** or **NA17** at a concentration of 10 µM did not lead

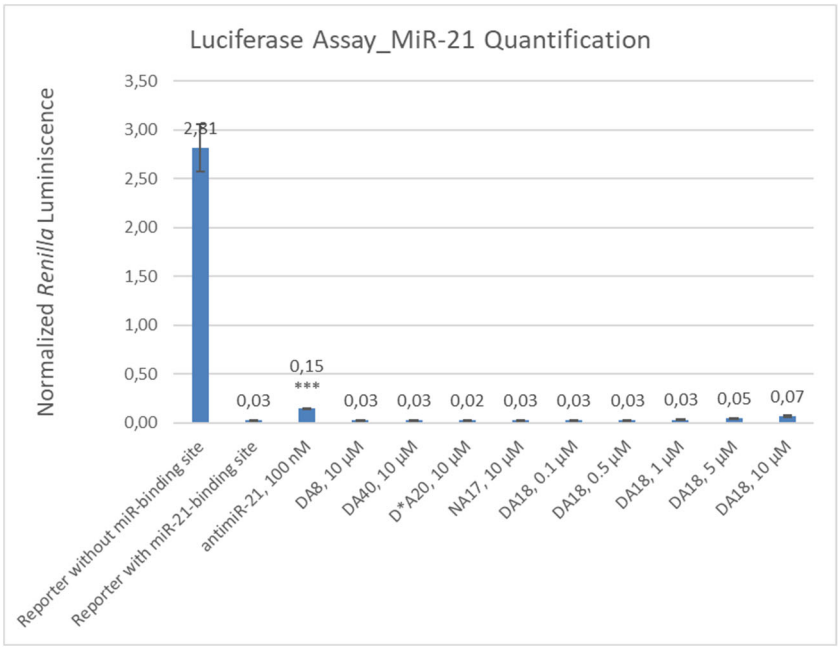

Figure 33. Normalized *Renilla* luciferase activity of the miR-21 reporter psiCHECK-2 transfected into Huh7 cells treated with **DA8, DA40, D*A20, DA18** or **NA17**. The *Renilla* luminescence is normalized to the *Firefly* luminescence. The positive control is a reporter without miR-binding site, the negative control is a reporter with miR-21-binding site. Bars represent the mean ± SD of normalized *Renilla* signal (3 measurements of one sample). *** $p < 0.001$, ** $p < 0.01$, * $p < 0.05$ (Student's t test). The raw data is represented in the supporting information (Fig. S9).

to the restoration of the luciferase activity. In all cases the normalized *Renilla* luminescence remained low (≤0.03). Also, **DA18** did not exhibit a restoration of the luciferase signal at low concentrations (0.1, 0.5 and 1 µM). However, at concentrations of 5 and 10 µM, **DA18** demonstrated already a cytotoxic effect as judged by the dramatically reduced *Firefly* luminescence (supporting information, Fig. S9).

3.4.2 RT-qPCR Quantification of MiR-122 in Huh7 Cells treated with **DA8** and **DA40**

Identified as potential miR-122 inhibitors in luciferase reporter assay, the SMIs **DA8** and **DA40** were additionally evaluated by RT-qPCR. Moreover, in order to verify the selectivity of **DA8** and **DA40** regarding their miR-122 inhibitory activity, the levels of two unspecific miRNAs (miR-16 and miR-22) were also quantified by RT-qPCR. Huh7 cells were incubated with **DA8**, **DA40** or **antimir-122** (at a concentration of 100 nM) for 48 h. Next, the cells were collected and the total RNA, including miRNAs, was extracted by using the miRNeasy Kit (Qiagen). Before RT-qPCR, the reverse transcription was performed by Taqman® MicroRNA Reverse Transcription Kit (Applied Biosystems) using a miRNA-specific RT primer. The samples were further proceeded for the RT-qPCR miRNA analysis using the TaqMan assay according to the manufacturer's protocol (Applied Biosystems).

As depicted in Figure 34a, the relative miR-122 expression in Huh7 cells was decreased after treatment with **DA8** and **DA40** at concentrations of 1, 5 and 10 µM. Also the normalized miR-122 expression dropped in a similar way for both compounds, which was 2-3-times lower using **DA8** and **DA40** at a concentration of 1-10 µM. However, the two compounds inhibited the formation of miR-122 in a concentration-independent manner and values of miR-122 decrease remained unchanged with increasing compound concentration. There was also no difference in the decrease of the relative miR-122 expression between treatments with **DA8** at a 10 and 20 µM concentration (see supporting information, Fig. S12). In contrast to **DA8**, **DA40** caused a dramatic drop (50-fold) of the relative miR-122 expression at 20 µM concentration (Fig. S12). Nevertheless, such a prominent effect might be also caused by cytotoxicity of **DA40** at a high 20 µM concentration (see chapter 3.4.4.). Moreover, it can not be excluded that **DA8** and **DA40** treatment might have an impact on the expression of endogenous control U6, which was used for miR-122 expression normalization. In this case, the calculated effect of the miR-122 decrease would be caused by changes in U6 expression. As expected, treatment with a specific miR-122 inhibitor from Qiagen (**antimiR-122**, 100nM) led to a 4-fold decrease in miR-122 expression.

In contrast to the miR-122 expression and as desired, the expression of miR-16 and miR-22 was not significantly changed in Huh7 cells incubated with **DA8** or **DA40** (10 µM each) (Fig. 34 b). Therefore, the selectivity of the compounds **DA8** and **DA40** was proven against two unspecific miRNAs. Certainly, the selectivity of compound can not be fully confirmed based just on unchanged expression of two control miRNAs. More careful evaluation of the compound selectivity might be required, for example, by using the microarray technology, which can detect changes in the expression of thousands of miRNAs in a single experiment.

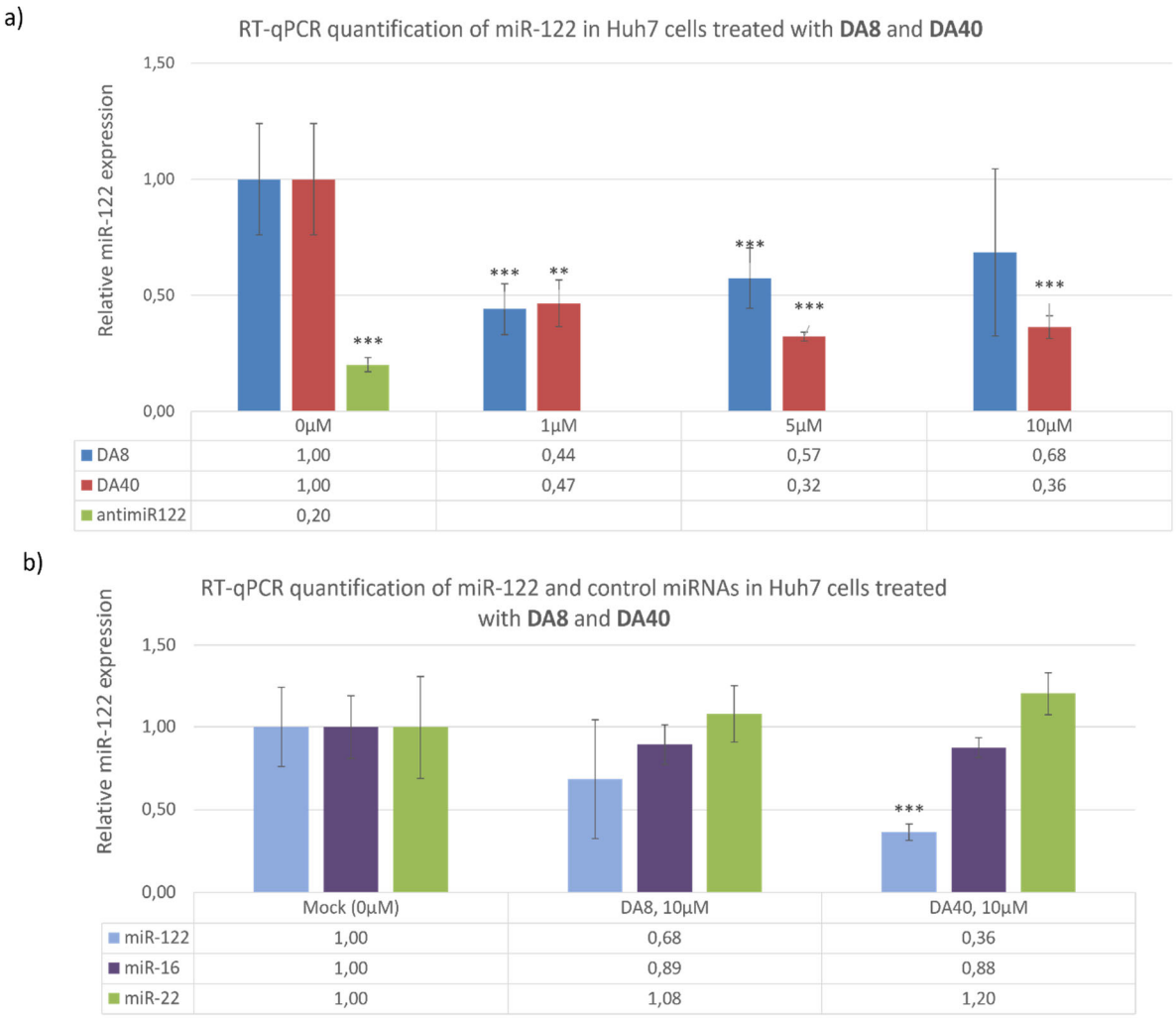

Figure 34. RT-qPCR quantification of miR-122 (a) and control miRNAs (miR-16 and miR-22) (b) in Huh7 cells after a 48-h treatment with **DA8**, **DA40** or **antimir-122** (at a concentration of 100 nM). Bars represent the mean ± SD of miRNA expression normalized to the small nuclear RNA U6 and compared to untreated cells (n = 4). *p<0.05; **p<0.01; ***p<0.005 (Student's *t* test). Raw data and an additional experiment are presented in the supporting information (Fig. S10, S11, S12).

3.4.3 Quantification of MiR-122 targets by RT-qPCR and Western Blot

To further assay the specific miR-122 inhibition of **DA40**, it was set as a goal to evaluate how the expression of the miR-122 targets is affected by the **DA40** treatment. Logically, a specific miR-122 inhibition should result in an increased expression of the miR-122 targets. Therefore, the three validated direct targets of miR-122 (ADAM10, IGf1R and AldoA) were chosen for the analysis by RT-qPCR [71, 216]. For this experiment, Huh7 cells were incubated with **DA40** in a concentration range of 5-20 µM for 48 h. Next, the cells were collected, and the total RNA was extracted by miRNeasy Kit (Qiagen). The total RNA was converted into cDNA by using the SuperScript™ III First-Strand Synthesis System (Thermo Fisher Scientific). The Fast SYBR Green Master Mix (Thermo Fisher Scientific) was applied for the real-time PCR according to manufacturer's protocols. As summarized in figure 35, only the ADAM10 expression increased by 2 times after treatment with **DA40** at a concentration of 20 µM, whereas the incubation at lower concentration (5 and 10 µM) did not cause a significant change of the ADAM10 expression. Unexpectedly, the expression of the other two targets, AldoA and IGf1R, decreased after the **DA40** treatment. Surprisingly, the expression of all three miR-122 targets remained constant after incubation with the control miR-122 inhibitor, **antimiR-122** (Qiagen; see supporting information, Fig. S14). As an additional control, the expression of the non-miR-122 target, Lin28B, has

been also quantified (supporting information, Fig. S14). The Lin28B exhibited a 5-fold drop of expression in the **DA40** (20 µM) treated cells. It can be supposed that **DA40** in a concentration of 20 µM induces the cytotoxic effect.

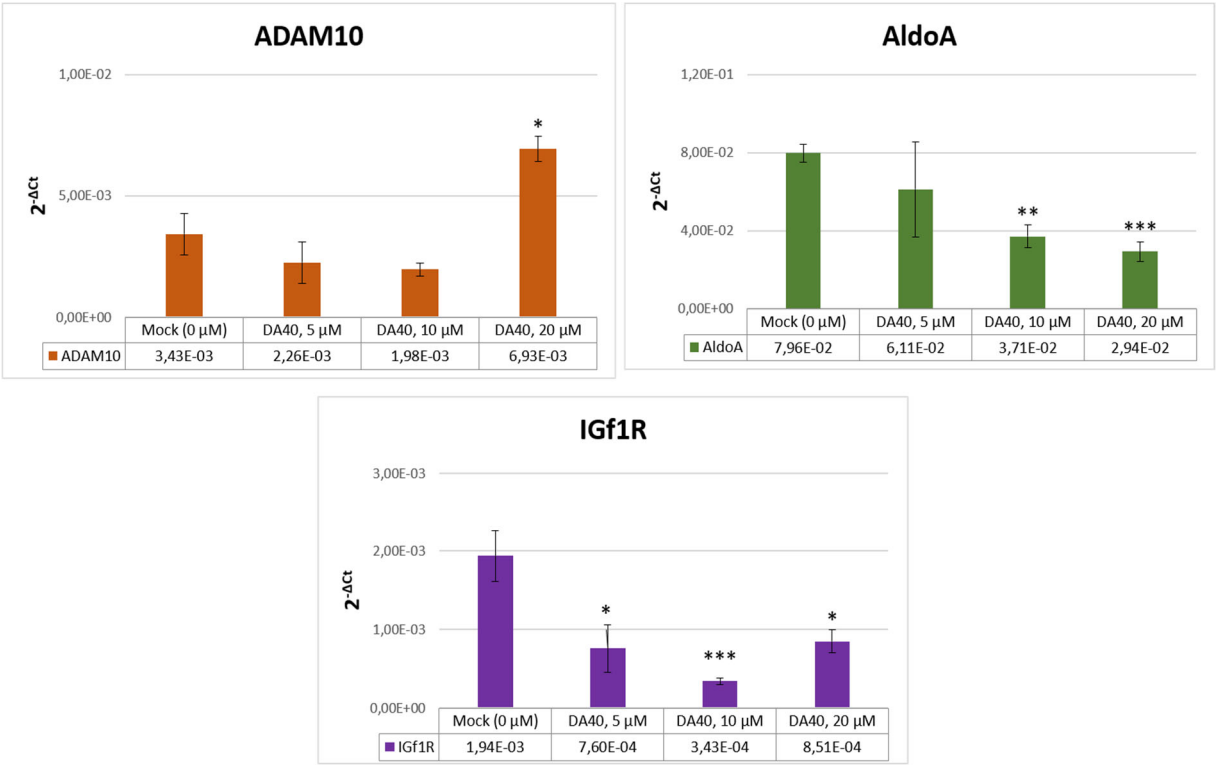

Figure 35. Quantification of the miR-122 targets (ADAM10, IGf1R and AldoA) in Huh7 cells treated with **DA40** by RT-qPCR. Comparison of the miR-122 target expression fold ($2^{-\Delta Ct}$, where $\Delta Ct=Ct_{target\ gene} - Ct_{reference\ gene\ GAPDH}$, Ct-threshold cycle) in the untreated cells (Mock) and treated with **DA40** cells. Data are mean (+SD) of 3 replicates (T test significance: p-value, *p<0.05; **p<0.01; ***p<0,005). Raw data is presented in supporting information (Fig. S13).

As stated in the review from Vogel and Marcotte, mRNA and protein levels are not exactly correlated and ~60% of variation in the protein concentration cannot be explained by mRNA expression [217]. As a next step, it was set as a goal to assess the *Adam10* protein level in Huh7 cells treated with **DA40** and **DA8** by using Western Blot method, since the cells, treated with **DA40** at a high concentration (20 µM), exhibited increased level of ADAM10 mRNA. Of note, it should be expected that the Huh7 cells are note highly abundant with the *Adam10* protein, according to the ADAM10 mRNA expression level ($c_{t\ untreated\ cells}$=28 cycle). As depicted in figure 36, the *Adam10* protein level was reduced after incubation with **DA40** (5-20 µM). A reduced *Adam10* protein level can point towards an unspecific cytotoxic effect, caused by **DA40**. In contrast to that the treatment with **DA8** at a 5 and 10 µM concentrations just slightly changed the *Adam10* protein level (0.86 and 1.15, respectively). However, the protein level was more dramatical decreased using a 20 µM concentration of **DA8**. Of note, the **antimiR-122** exposure caused a 1.5-fold increase of the *Adam10* protein at low 50 nM concentration, which is in agreement with published data[71].

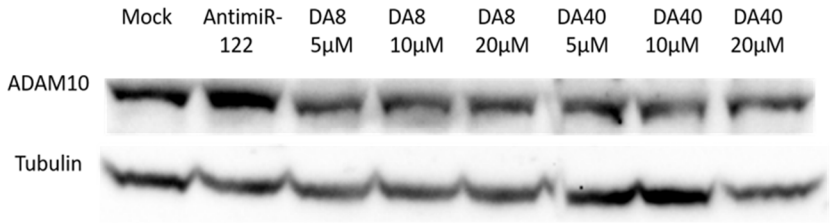

Samples	ADAM10 Intensity*
Mock	1,00
AntimiR-R122	1,51
DA8_5µM	0,86
DA8_10µM	1,15
DA8_20µM	0,66
DA40_5µM	0,70
DA40_10µM	0,45
DA40_20µM	0,75
*normalized on Tubulin	

Figure 36. Western blot analysis of the *Adam10* protein expression level in Huh7 cells treated with **DA8, DA40** or **antimiR-122** in comparison to untreated cells.

To conclude, although the **antimiR-122** treated Huh7 cells have not demonstrated any change in the ADAM10 gene expression, the *Adam10* protein level increased in 1.5 times. In contrast to that the ADAM10 gene expression, as well as *Adam10* protein level, were slightly decreased in Huh7 cells treated by **DA40**. Only cells, incubated with **DA40** using a concentration of 20 µM, showed an increase of the ADAM10 gene expression. The *Adam10* protein level did not critical change after **DA8** treatment at a concentration range of 5-10 µM, but 1.5-times decreased using a high 20 µM concentration. Conclusively, **DA8** and **DA40** did not cause the increase of the *Adam10* protein expression as **antimiR-122** did. It might be possible that in addition to the miR-122 inhibition, **DA8** and **DA40** bind to multiple off-targets and cause cytotoxic effect. For example, it was reported that antibiotics of the aminoglycoside family interact with the bacterial ribosomal RNA[133-134] and, therefore, can change the translation level of numerous proteins. The compounds **DA8** and **DA40** contain the two 2-desoxystreptamine for interaction with the secondary structures of pre-miRs, which is also present in the aminoglycoside antibiotic Neamine. [1] If **DA8** and **DA40** would bind unspecifically to ribosomal RNA in human Huh7 cells, this might lead to a common down-regulation of the protein translation in cells.

3.4.4 Cell Viability and Cell Cytotoxicity assays

As shown in the previous experiments, the evaluated SMIs **DA8** and **DA40** might be cytotoxic for cells. In order to investigate it, the cytotoxicity of **DA8** and **DA40** in Huh7 cells was assessed by performing an MTT cell viability assay (Thermo Fisher Scientific) and a Pierce LDH cell cytotoxicity assay (Thermo Fisher Scientific). The MTT colorimetric assay is a rapid and versatile method for the determination of the viable cell number. The MTT assay assesses the activity of the NAD(P)H-dependent cellular oxidoreductase enzymes, which converts the water soluble MTT (3-(4,5-dimethylthiazol-2-yl)-2,5-diphenyltetrazolium bromide) to an insoluble formazan. The concentration of the solubilized formazan is determined by the optical density at 570 nm. In contrast to the MTT assay, the Pierce LDH Cytotoxicity Assay defines the number of damaged cells by measuring the lactate dehydrogenase (LDH) level, which is released into the surrounding cell media upon cell damage or lysis.

For the experiment, the Huh7 cells were incubated with different concentrations (0 – 50 µM) of **DA8** and **DA40** for 48 h. The positive control for miR-122 inhibition, **antimir-122**, was transfected into cells using the lipofectamine 2000 transfection agent (Thermo Fisher Scientific) according to the manufacturer's protocol. After 48 h, the cell viability and cytotoxicity were assessed by performing the MTT assay and the LDH assay (Fig. 37). According to the results of the MTT assay, the **DA8** treated cells displayed a slightly decreased cell viability up to 20 µM (82 %). However, using a high 50 µM concentration of **DA8** resulted in a significant reduced cell viability (58%). Results from the LDH assay were in agreement to the results obtained by the MTT assay. Low cytotoxicity was shown for 10 and

20 µM concentrations of **DA8** (0.49 and 0.95 %, respectively) and increased cytotoxicity was observed at 50 µM (18%). As expected, the cell viability was more effected by the **DA40** treatment as judged by the data collected in the MTT assay (74%, 57% and 17% for 10, 20 and 50 µM concentrations, respectively). The LDH assay also showed an increased cytotoxicity for the cells incubated with **DA40** at 10, 20 and 50 µM (5%, 13% and 23%, respectively). The obtained data indicated a strong cytotoxic effect in a dose-dependent manner for **DA40**. The decreased cell viability (81%) of the positive control **antimiR-122** (Qiagen), transfected with lipofectamine was caused predominantly by the cytotoxic effect of the lipofectamine transfection agent, as can been seen by the control experiment, in which cells were incubated only with the lipofectamine (82% cell viability). Concluding the results, the selective miR-122 inhibition by **antimir-122** did not cause the cell death. **DA8** exhibited a significant cytotoxicity only at a high concentration of 50 µM, whereas **DA40** started to show the cytotoxic effect already at low 10 µM concentration. So pronounced cytotoxic effect for **DA40** can be explained by the presence of the multiply targets and, possibly, by cell susceptibility to its chemical hazard.

a) b)

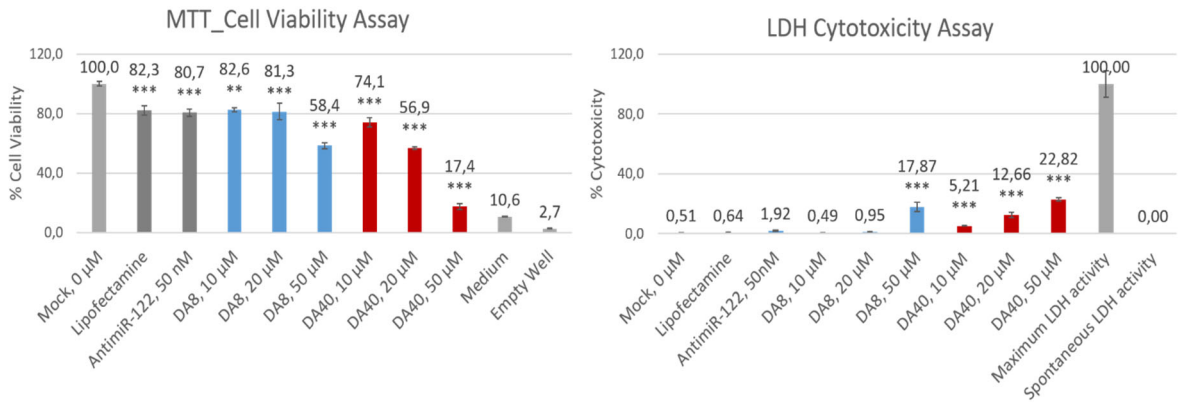

Figure 37. Determination of the cytotoxicity of **DA40** and **DA8** in Huh7 cells using the MTT cell viability assay (a) and LDH cytotoxicity assay (b). Huh7 cells were treated at different concentrations (0-50 µM) of **DA40** or **DA8** for 48 h. **AntimiR-122** have been used at a concentration of 50 nM. a) MTT cell viability assay. Bars represent the mean of absorbance at 580 nm ± SD in percentage terms and compared to untreated cells (n = 4). The cell viability of untreated cells is assigned as 100%. *** $p < 0.001$, ** $p < 0.01$, * $p < 0.05$ (Student's t test). b) LDH cytotoxicity assay. To determine LDH activity, the 680 nm absorbance value (background signal) was subtracted from the 490 nm absorbance. Bars represent the mean of absorbance at 490 nm (with subtracted background) ± SD in percentage terms and compared to untreated cells (n = 4). The controls Maximum LDH activity and Spontaneous LDH activity are provided by manufacture and their cytotoxicity is assigned as 100% and 0%, respectively. *** $p < 0.001$, ** $p < 0.01$, * $p < 0.05$ (Student's t test). Raw data is represented in supporting information, Fig. S15)

3.4.5 Summary and Conclusion

Here, the new developed SMIs, presumably targeting the miR-122 and miR-21 maturation, were investigated in cells. The miR-122 and miR-21-inhibiting SMIs (**DA8**, **DA40**, **D*A20**, **DA18** and **NA17**), identified in the BRCA assay, were validated in Huh7 cells by using the luciferase reporter assay. Two possible inhibitors of miR-122 maturation, **DA8** and **DA40**, were identified. None of the evaluated compounds exhibited the miR-21 inhibition. The miR-122 inhibitory activity of **DA40** and **DA8** was also assessed by RT-qPCR method. The decrease of relative miR-122 expression after treatment with **DA40** and **DA8** at a 5 µM concentration (2-3-fold) was lower compared to the commercial antisense miR-122 inhibitor, **antimir-122**, at a 100 nM concentration (5-fold). As a control, the expression of two additional miRNAs (miR-16 and miR-22) was tested in Huh7 cells after treatment with **DA40** and **DA8**

at a 10 µM concentration. In contrast to relative miR-122 expression, their expression remained unchanged. Therefore, the selectivity of **DA40** and **DA8** was demonstrated against two unspecific miRNAs.

To examine the miR-122 specific inhibition, the RT-qPCR quantification of miR-122 targets (ADAM10, AldoA and IGf1R) has been conducted in Huh7 cells incubated with **DA40**. Only ADAM10 level increased after treatment with a high concentration of **DA40** (20 µM), whereas the smaller **DA40** concentration (5 and 10 µM) did not affect the ADAM10 expression. Moreover, the expression of other two targets (AldoA and IGf1R) has even dropped after incubation with **DA40**. Surprisingly, the expression of all three miR-122 targets remained constant after incubation with the control miR-122 inhibitor, **antimiR-122** (Qiagen). However, it was already reported that the gene expression is often not correlated with the protein level due to, for example, the low rate of the mRNA transcription compared to protein translation or the differences in the mRNA and protein life-times[217].

Next, the *Adam10* protein level was assessed in Huh7 cells treated with **DA40** and **DA8** by using Western Blot method. The *Adam10* protein level was decreased after incubation with **DA40** (5-20 µM). The *Adam10* protein level was dramatically dropped after incubation with **DA8** at a 20 µM concentration, while the smaller **DA8** concentrations (5 and 10 µM) did not significantly affect the protein level. As expected, the treatment with validated **antimiR-122** inhibitor (50 nM) led to elevation of the *Adam10* protein level in 1.5-times. To summarize the results, the **DA8** and **DA40** did not increase the *Adam10* protein level, but even decreased it. These results can be explained by presence of multiple undesirable off-targets for **DA8** and **DA40**, the interaction with which causes the unspecific down-regulation of gene expression and protein translation and lead to the cytotoxic effect. The cytotoxicity of **DA8** and **DA40** in Huh7 cells was tested in a MTT cell viability assay and a Pierce LDH cell cytotoxicity assay. **DA8** exhibited a significant cytotoxicity only at a high concentration of 50 µM, whereas **DA40** demonstrated already cytotoxicity at low 10 µM concentration.

To draw a conclusion, the **DA8** and **DA40** can be used for inhibition of the miR-122 maturation, however, the phenotypic effect of miR-122 inhibition can be not obtained due to the presence of multiple additional off-targets. The interactions of these compounds with another intracellular targets are not investigated here. Despite the **DA40** showed a stronger miR-122 inhibition than **DA8**, the **DA40** displayed a concentration-dependant cytotoxicity starting from 10 µM.

4. Summary and Outlook

MiRNA play a crucial role in the regulation of cellular processes by modulating the gene expression. Altered miRNA expression has been associated with a variety of diseases. Understanding of the miRNA mechanisms in the normal and pathological states might lead to the development of novel therapeutic and diagnostical approaches. The work reported here is devoted to the development of tools for monitoring and inhibiting the dicer-mediated miRNA maturation in cells. The two alternative approaches, the antisense-oligonucleotides-based approach and small molecular inhibitors were chosen for this purpose. The miR-21 and miR-122 became the targets in this work, since they are highly promising diagnostic biomarkers and therapeutic drug-targets[65, 69]. MiR-21 is an oncogenic miRNA, which is implicated in the development of major cancer types and found to be overexpressed in cancer cells[60, 62, 218]. MiR-122 regulates the liver homeostasis, cholesterol and fatty acid metabolism. Abnormal expression of miR-122 is associated with liver disease, hepatocellular carcinoma and others[70, 219]. Moreover, miR-122 is an important antiviral (HCV and HBV) target.[74, 76]

Evaluation of inhibition of miR-21 maturation by PNA probes and TO PNA probe-mediated pre-miR21 detection in cells

In the first part of this work, six PNA probes (**Pre-21_1 – Pre-21_6)** were directed against the precursor miR-21 (pre-miR21). It was envisioned that the probes inhibit the dicer-mediated miR-21 maturation. In the cell-free BRCA assay all probes showed a similar inhibitory effect. This suggests that the probes inhibited the BRCA reaction rather than dicer-mediated cleavage. For further probe evaluation in cells the **Pre-21_1** and **Pre-21_5** probes, which are believed to be specific for pre-miR21 (only 3-nt overlap with the mature sequences), were selected. In this regard, two probes were resynthesized with a CPP ((RAhexR)$_4$) at the C-terminus to achieve an efficient cellular delivery. In contrast to the BRCA results, the qPCR-based miR-21 quantification data demonstrated that the treatment with the probes did not have an influence on the miR-21 level in cells. Even though the probes were delivered into cells, their accessibility for hybridization with the target is still questionable since they could be trapped in endosomes. It is also possible that the probes could not hybridize to the pre-miR21 by reason of dicer higher affinity or the probe hybridization does not affect dicer digestion. In order to verify the probe-target hybridization the FIT probes were used. These probes signal hybridization with a complementary target by affording enhancements of fluorescence. The TO-labeled **Pre-21_1*_2** and **Pre-21_5*_3** probes showed an increase (7.3- and 4.6-fold, respectively, 37°C) of TO fluorescence upon addition of pre-miR21. For the cell evaluation, the three cell lines were chosen: the high miR-21 abundant Hela cells, low miR-21 abundant A549 cells and control HEK293 cells (with the lowest miR21 level). To overcome the difference in cell uptake among cell lines, the probe fluorescence was normalised on the fluorescence of a mismatched control probe. As expected, the fluorescence ratio (**Pre-21_1*_2** probe vs. mismatched control) in the fluorescence microscopy and flow cytometry experiments (Figure 38) was higher in miR21-abundant Hela cells in comparison to control miR-21 abundant cells (HEK293). Unfortunately, the probe **Pre-21_1*_2** did not exhibit a predictable fluorescence ratio for low abundant A549 cells by means of fluorescence microscopy. The preliminary data shows that the developed TO PNA probe, **Pre-21_1*_2**, might distinguish between high miR-21 abundant and control cells. However, the statistical significance of this observation should be verified by additional experiments. Whether the probe hybridizes to its pre-miR21 target in live cells remains unshown.

According to the literature, the dicer recognizes the pre-miRNA substrate twicely[214]. Initially, the dicer anchors to the 5'-/3'-terminal ends of pre-miRs and adjusts the region to be cleaved into the catalytic center. Next, the dicer helicase domain recognizes a loop or bulge region of pre-miRNA and stabilizes the catalytic domains for precise cleavage [211, 214]. The first recognition is essential for the dicer cleavage, while the second would have more impact on enzyme preciseness. This fact can explain why after

treatment with the **Pre-21_1** and **Pre-21_5**, targeting the terminal loop of pre-miR21, the impaired level of miR-21 was not observed. After

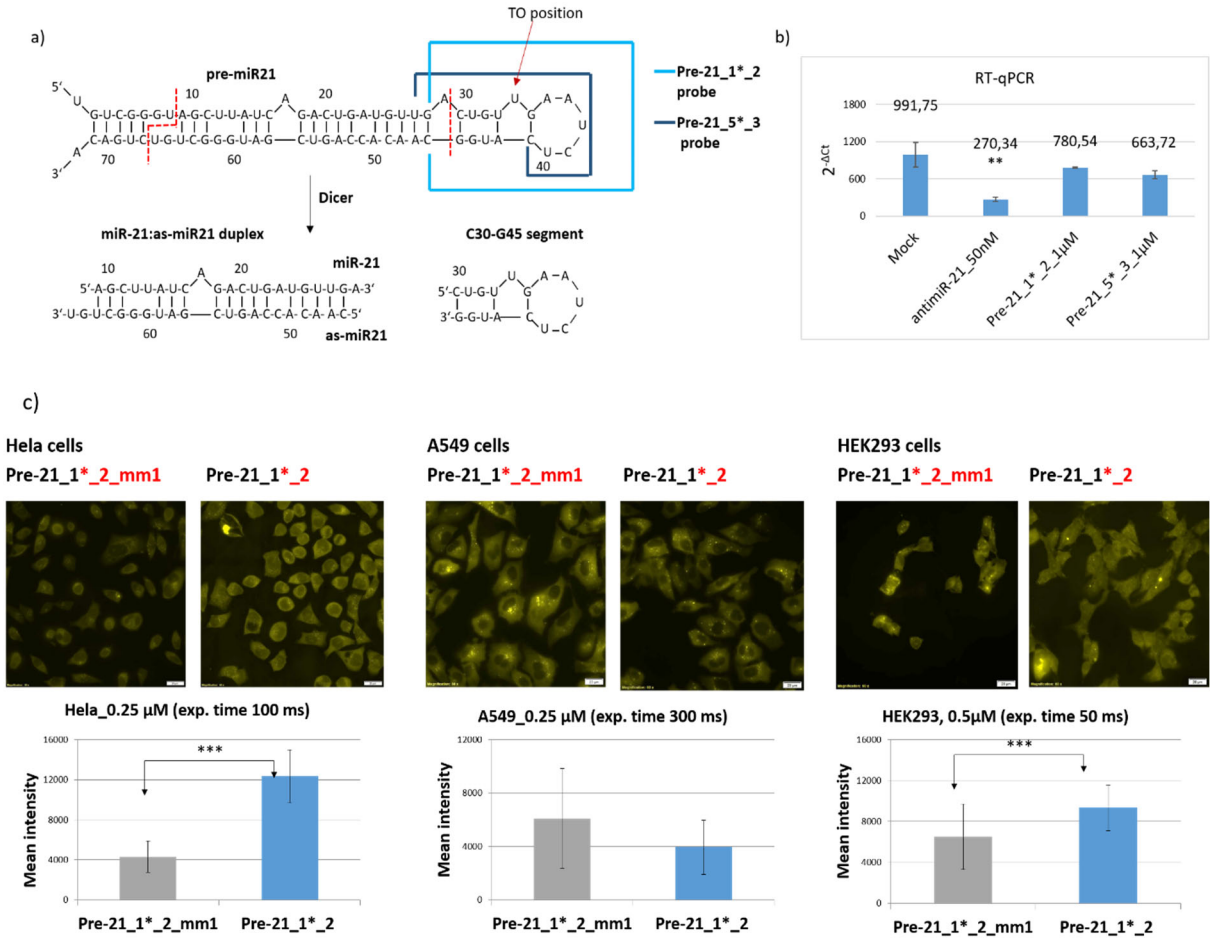

Figure 38. a) Dicer-mediated pre-miR21 cleavage. The binding sites for the **Pre-21_1*_2**, **Pre-21_5*_3** PNA probes are indicated by color. b) RT-qPCR quantification of the miR-21 expression (2-ΔCt, where $\Delta Ct=Ct_{miR21}-Ct_{U6}$, Ct-threshold cycle) of untreated cells (Mock), cells treated with **antimiR-21** (Qiagen) and with the **Pre-21_1*_2** /**Pre-21_5*_3** PNA probes. Data are mean (+SD) of 3-4 replicates (Student's *t* test significance: p-value, *p<0.05; **p<0.01; ***p<0,005). c) Fluorescence microscopy images of fixed Hela, A549 and HEK293 cells stained with the TO-labeled **Pre-21_1*_2** PNA probe and its mismatched control **Pre-21_1*_2_mm1**. The fluorescence of the PNA probes was recorded on the YFP channel (λex = 500 ± 24 nm, λem > 520 nm), using the same exposure time for measured samples within one cell line. The fluorescence intensity was calculated as a mean fluorescence of 50 cells from 5 pictures, using the region of interest (ROI) tool to surround the whole cells. (Student's *t* test significance: p-value, *p<0.05; **p<0,01; ***p<0,005).

the probe hybridization it would be more expected to detect the heterogeneous mature sequences as a result of unprecise dicer cleavage rather than the reduced level of miR-21, if the method of deep miRNA sequencing would be applied. In light of these findings and the data presented here, the probes directed against the 5'- and 3'-terminal ends of pre-miR21 in combination with the pre-miR21 loop specific **Pre-21_5** probe would presumably inhibit dicer cleavage.

The FIT probe concept is widely used for a variety of applications, including the signalling of RNA and DNA targets, detection of SNPs and point mutations, RNA imaging in fixed and life cells[165, 172, 177]. In this work, the application of TO-labelled PNA probes for pre-miR21 detection in fixed cells was evaluated. Although, the herein reported preliminary results indicate that this approach might be useful for the detection of pre-miR21, future work should be focused on improving the fluorescent properties of the FIT probes, such as higher brightness and responsiveness, in order to allow more sensitive detection.

To increase the brightness and the responsiveness the use of DNA-based FIT probes instead of the PNA-based probes should be tested in future studies [207]. However, the DNA-based probes have a lower affinity towards RNA than PNA and this might be crucial for targeting the stem-loop structured pre-miR21. The conjugation with CPPs can be applied for the delivery of DNA-FIT probe as well, since the responsiveness of DNA-based probes was proven not to be affected by CPP conjugation in the recent studies[207]. Nevertheless, the PNA- and DNA-based FIT probes are suggested to use with the pore-forming protein streptolysin-O (SLO) for uptake in living cells, which do not induce the probe aggregation in comparison to CPPs, as shown in the latest work of Seitz *et. al* [207]. As a future perspective, both strategies can be applied for development of the advanced pre-miR21 specific probe for imaging of pre-miR21 in fixed and, possibly, in living cells.

Monitoring dicer-mediated miR-21 maturation and Ago2-mediated miR-21 loading by a dual-colour FIT PNA probe set

In the second part of work, the FIT PNA probes were applied for monitoring the pre-miR21 cleavage reaction by dicer. Canonically, dicer cleaves the 72-nt long pre-miR21 and liberates a 22-nt long duplex, consisting of the mature miRNA-21 strand and the antisense mature miRNA-21 strand (as-miR21). The readout of pre-miR21 and as-miR21 in the homogeneous solution was achieved by using the two FIT PNA probes, bearing spectrally distinguishable QB and TO fluorophore (Fig. 39 a). The pre-miR21 specific **QB3** probe showed a high selectivity: in presence of pre-miR21 the **QB3** probe enhanced its fluorescence by 13.7-times, whereas no enhancement was detected in presence of the mature form. The as-miR21 specific **7nt_TO1*** PNA probe could successfully distinguish between pre-miR21 and as-miR21. The probe signaled the presence of as-miR21 by a fluorescence increase up to 10.3-fold, while in presence of pre-miR21 the probe fluorescence raised by 4.2-fold using an optimized $MgCl_2$-containing buffer. Nevertheless, the short **7nt_TO1*** probe had a difficulty to invade the miR21: as-miR21 duplex in order to detect the product of the dicer reaction. The affinity of the probe was improved by elongating its length from 7nt to 11nt, which resulted in a 3-fold discrimination rate between pre-miR21 and the miR-21: as-miR21 duplex.

To assess the feasibility for monitoring of Dicer cleavage, the **QB3** and the **11nt_TO1*** probes were incubated with a mix of synthetic RNA sequences comprising pre-miR21, miR-21, as-miR21 and the C30-G45 segment. As expected, the probe set provided convenient monitoring of the modelled dicer reaction by detecting a decrease in the QB fluorescence signal and an increase of the TO fluorescence (Fig. 39 b). In a next step, the probe combination was applied for the detection of the dicer enzyme reaction. In the experiments with rhDicer, the *in vitro* transcribed pre-miR21 (with additional three 5'-terminal guanine residues) was used, what supposedly caused an unspecific cleavage. In a time course study with rhDicer (10U rhDicer per 1 µg pre-miR21), surprisingly, the decrease in fluorescence was observed for both probes (fig. 39 c). To draw conclusions from collecting data, the gel electrophoresis data was analyzed: after 18 h of incubation no band for pre-miR21 was identified and a band for the cleavage product, detected by TO probe was shifted in comparison to the expected as-miR21. These results demonstrated the effective pre-miR21 cleavage and the loss of the binding site for the TO probe. For the robust dicer cleavage reaction,

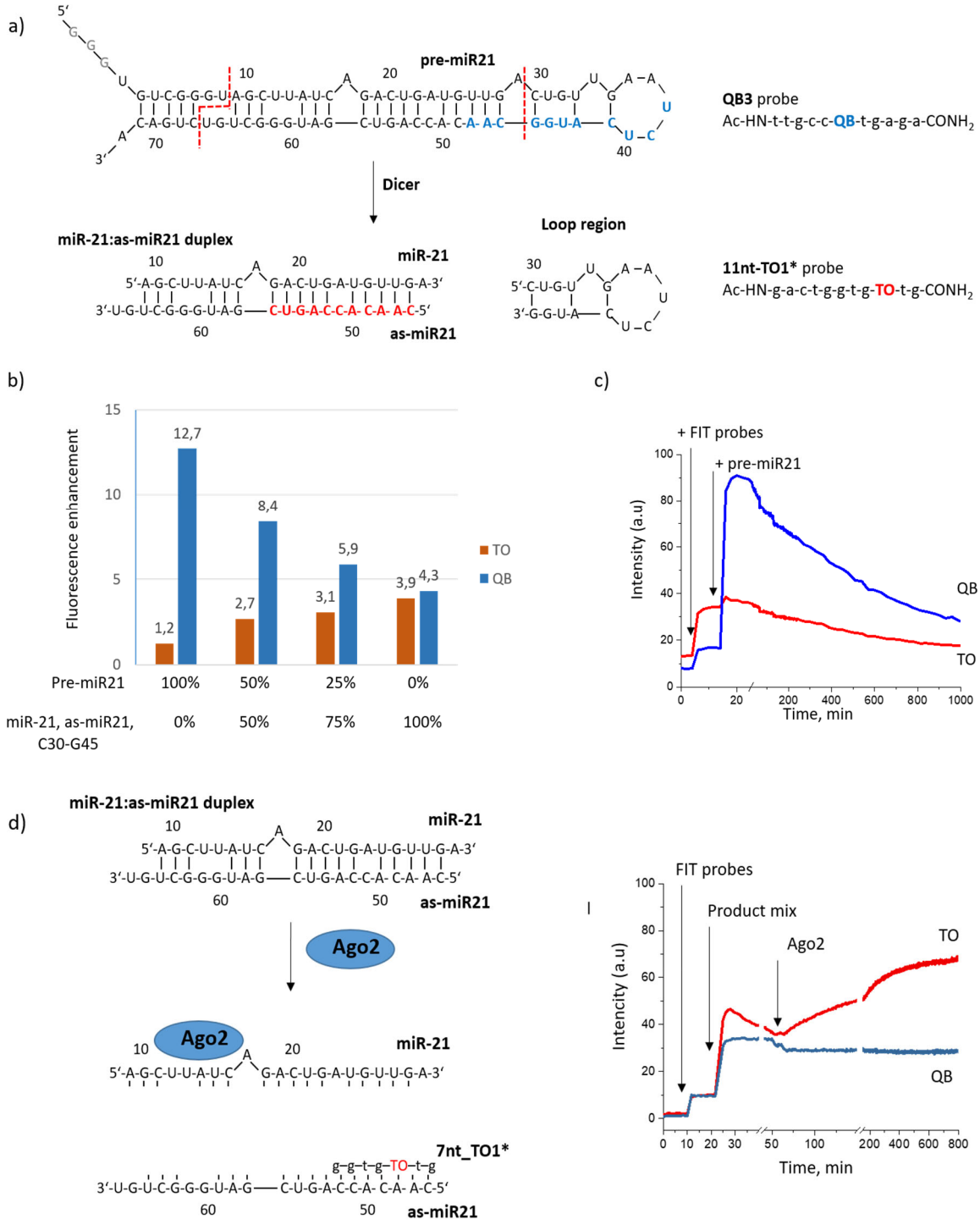

Figure 39. a) Concept of monitoring the dicer-mediated pre-miR21 cleavage by FIT probes. b) Fluorescence enhancements of **QB3** and **11nt_TO1*** in presence of the synthetic product mixes corresponding to 0%, 50%, 75% and 100% of dicer cleavage. c) Monitoring the pre-miR21 cleavage by **QB3** and **11nt_TO1*** probes using a 10-fold excess of rhDicer. d) Detection of the Ago-2-mediated miR-21 loading by using the as-miR21 specific **7nt_TO1*** PNA probe. Fluorescence spectra of **7nt_TO1*** and the control **QB3** PNA probe in presence of the Ago2 protein and product mix (the miR-21: as-miR21 duplex and the C30-G45 segment)

the shortened synthetic sequence of pre-miR21 can be used, which lacks the U1-G7 and C67-A72 segments of the predicted stem-loop obtained from miRNA registry, which has been proven to be digested in the canonical cleavage sites[212]. As a future application, the probe combination might provide a time-saving and effective *in vitro* screening of new Dicer inhibitors and pre-miR21 binders.

Although, the short **7nt_TO1*** probe was not able to monitor the dicer reaction product, this probe was successfully evaluated for the monitoring of the Ago-2-mediated miR-21 loading (Fig. 39 d). The Ago-2 protein loads the sense miRNA strand and forms the RNA-induced silencing complex (RISC) to mediate RNA silencing in cells. After the miR-21 loading into Ago-2, the released as-miR21 strand was accessible for probe hybridization and was signalled by a tenfold increased fluorescence of the **7nt_TO1*** probe. This probe would help to assess the Ago-2 functional activity and to screen the new Ago2 inhibitors without using a fluorogenic RNA substrate, as it is required for the state of the art[220-221]. This method can be compared with the BRCA-based Ago2-mediated cleavage assay, which was developed by Dr. Marlen Hesse and also does not require a fluorogenic RNA substrate[222]. The FIT PNA probe approach would also be transferable for other miRNA systems for monitoring of the dicer-mediated pre-miRNA cleavage and Ago2-mediated miRNA loading.

Small Molecular Inhibitors

Since the pre-miR21 specific PNA probes did not inhibit the dicer-mediated miR-21 maturation, the second approach, small molecular inhibitors (SMIs), came into focus. The SMIs, composed of the aminoglycoside neomycin, were reported to target the stem-loop miRNA precursors and affect their cleavage by the dicer enzyme[223]. Based on the results of Dr. Claudine Dojahn, the most potent SMIs inhibiting miR-122 (**DA8**, **DA40**, **D*A20**, and **DA18**) and miR-21 maturation (**DA8**, **DA40**, **D*A20**, **DA18** and **NA17**) were chosen for evaluation in cells.[224] **DA8** and **DA40** provided at a small 5 µM concentration a 6-9 % of miR-122 inhibition in the luciferase assay and a 2-3 fold decrease of the miR-122 expression in the RT-qPCR assay (Fig. 40 b). Moreover, the two SMIs did not affect the expression of two unspecific miRNAs (miR-16 and miR-22). Surprisingly, none of the validated SMIs caused the miR-21 inhibition in the luciferase reporter assay. Even though the treatment with **DA8** and **DA40** caused a drop in miR-122 expression, the level of *Adam10* protein, the direct miR-122 target, was not elevated, but even reduced (Fig. 40c). In contrast to **DA8** and **DA40**, the treatment with **antimir-122** led to a 1.5-fold increase of the *Adam10* protein level. With the aim to explain these contradictory findings, the cytotoxicity of **DA8** and **DA40** in Huh7 cells was examined using the MTT cell viability assay and the Pierce LDH cell cytotoxicity assay. **DA8** exhibited a significant cytotoxicity only at a high concentration of 50 µM, whereas **DA40** exhibited cytotoxicity already at 10 µM concentration.

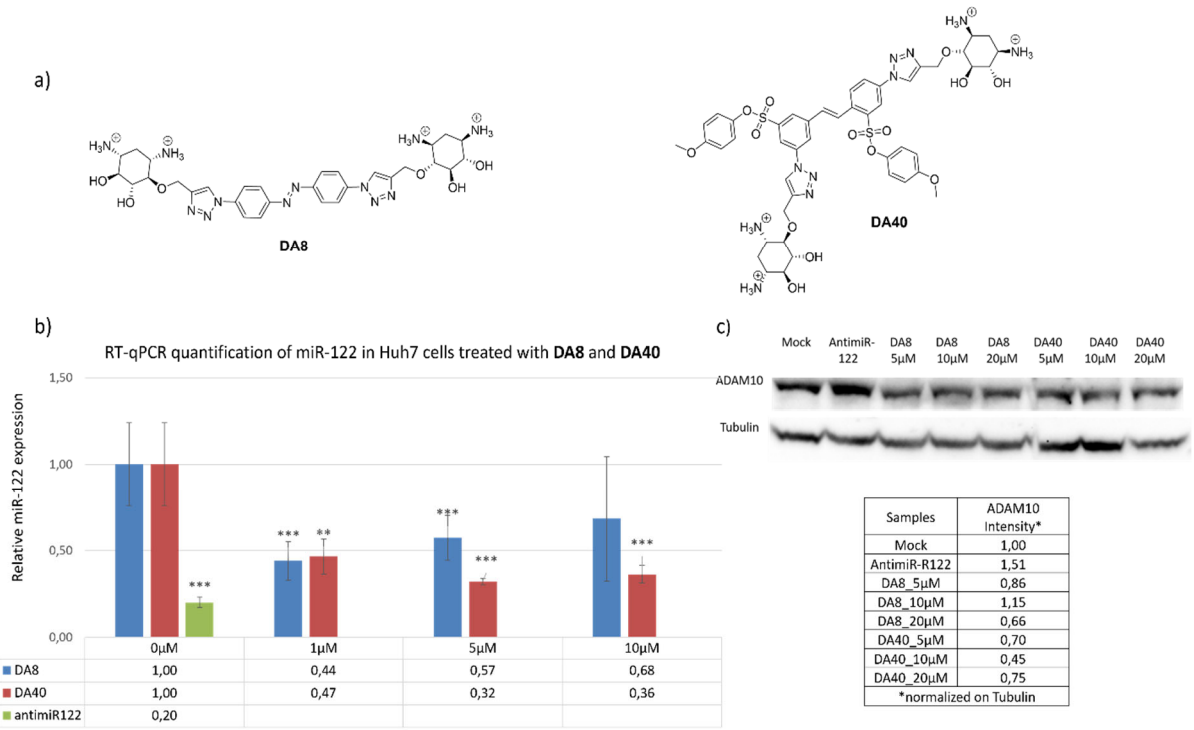

Figure 40. a) Chemical structures of the SMI compounds **DA8** and **DA40**, inhibiting the miR-122 maturation. b) RT-qPCR quantification of miR-122 in Huh7 cells after a 48 h treatment with **DA8**, **DA40** or **antimir-122**. **AntimiR-122** was transfected at a concentration of 100 nM. Bars represent the mean ± SD of miRNA expression normalized to the small nuclear RNA U6 and compared to untreated cells (n = 4). *p<0.05; **p<0.01; ***p<0.005 (Student's *t* test). d) Western blot analysis of the *Adam10* protein expression level in Huh7 cells treated with **DA8, DA40** or **antimiR-122** in comparison to untreated cells.

The cytotoxicity of SMIs might be caused by multiple off-target effects of **DA8** and **DA40**. The difficulty to achieve selective targeting by SMIs is described in the literature[137, 223, 225]. Here, the possibility of interaction with other pre-miRNAs and RNA molecules is not excluded. Moreover, the interaction with non-RNA molecules for cellular uptake is well-known for the aminoglycosides, such as transmembrane proteins, some phospholipases, Na^+/K^+ ATPase, etc [134]. This might be an additional reason of the **DA8** and **DA40** cytotoxicity. The specificity of **DA8** and **DA40** must be further assessed to evaluate the possible side effects. For identification of potential off-targets, the miRNA and RNA microarray might be useful, which provides the screening of thousand targets simultaneously. As a future prospect to improve the specificity, the SMIs could be conjugated to short specific PNA-sequences, which would address the SMI to their particular pre-miRNA target. This approach was already applied before by Schmidt *et. al.*, in which the authors designed the Ago2-inhibitors linked to short PNA, targeting the seed region of miRNA-122[220].

5. Experimental Section

5.1. Chemical Synthesis

General Procedures and Materials

Fmoc-protected PNA-monomers were purchased from Link technologies. RNA oligonucleotides were obtained from Biomers. Other chemicals were purchased from Novabiochem, Acros, Sigma-Aldrich, Lancaster or Merk. Water was purified with a Milli-Q Ultrapure Water Purification System (Millipore Corp.). Manual solid-phase synthesis was performed by using 5-mL polyethylene syringe reactors that are equipped with a fritted disc. Automated solid phase synthesis was performed on an Intavis ResPep parallel synthesizer equipped with 1 ml reactors. Fluorescence spectroscopy was performed with a Varian Cary Eclipse fluorescence spectrophotometer. For determination of concentration of PNA and RNA oligonucleotides the optical density was measured at 260 nm with Nanodrop2000 spectrophotometer. All column chromatography was performed with SDS 60 ACC silica gel and TLC with E. Merck Silica Gel 60 F_{254} plates.

UPLC-MS: Acquity System von Waters (Milford, USA) has been applied for UPLC and UPLC-MS analysis. For BEH130 C18 columns (2.1 x 50 mm, 1.7 µm) the mix of solutions A (0.1% TFA, 1% ACN, 98.9% H2O) and B (0.1% TFA, 1% H2O, 98.9% ACN) was used in a linear gradient with flow rate 0.5 mL/min. For CSH130 C18 columns (2.1 x 50 mm, 1.7 µm) the mix of solutions A (0.5% TFA, 1% ACN, 98.5% H2O) and B (0.5% TFA, 1% H2O, 98.5% ACN) was used in a linear gradient with flow rate 0.5 mL/min. Columns were heated to 50°C.

Analytical HPLC: Analytical HPLC measurements were performed with Agilent 1100 device (Santa Clara, USA) using Polaris C18-A (100 x 2 mm, 3 µm) column from Varian (Palo Alto, USA). Eluents A (0.1% Formic acid, 1% ACN, 98.9% H2O) and B (0.1% Formic acid, 1 % H2O, 98.9% ACN) were used in a linear gradient with a flow rate of 0.3 mL/min. Columns were heated till 55°C

Semi-preparative HPLC: Semi-preparative purification was performed with Agilent 1100 device (Santa Clara, USA) using Polaris C18-A (250 x 10 mm) column from Varian (Palo Alto, USA). The mix of solutions A (0.1% TFA, 1% ACN, 98.9% H2O) and B (0.1% TFA, 1% H2O, 98.9% ACN) has been used as a mobile phase for linear gradient (flow rate 6 mL/min)

NMR: ^{1}H- and ^{13}C NMR-spectra were recorded with Avance I 600 MHz- , Avance II 500 MHz- und Avance II 300 MHz-spectrometer von Bruker (Billerica, USA). The signals of the residual protonated solvent ($CDCl_3$ or [D_6] DMSO) were used as reference signals. Coupling constants are given in Hz. Signal multiplication is presented as s=singlet, d= doublet, t= triplet and m= multiplet.

Solid-phase synthesis of PNA probes

Intavis ResPep parallel synthesizer was applied for automated linear solid phase PNA synthesis. Before first coupling TentaGel R RAM resin (Rapp Polymere) 2µmol (with loading capacity ~0.18 µmol/mg) was allowed to swell for 10 min in DMF in micro scale columns.

Fmoc Cleavage: A solution of DMF/piperidine (4:1, 0.3 ml) was added to the resin for 2 min. This step was repeated. After Fmoc-deprotection resin was washed with DMF (6x 0.3 ml).

Coupling of Fmoc-protected PNA monomers: PNA monomers were dissolved in NMP solution to reach a concentration of 0.2M. Four eq. of PNA monomer, 4eq. HCTU, and 12eq. of NMM in DMF were mixed with resin. After 30 min incubation the solution was discarded, and the resin was washed with DMF (6x0.3 ml).

Coupling of Fmoc-Aeg(TO)-OH/ Fmoc-Aeg(QB)-OH: Labelled PNA monomers were dissolved in NMP (0.2M). Coupling of TO- and QB- PNA monomers was performed manually. Four eq. of TO- or QB-PNA monomer, 2 mg of PPTS (only for TO PNA monomer coupling), 4eq. PyBop, 12eq. NMM were added to resin for overnight incubation. Next day, coupling was repeated for 2h. After wash with DMF (5x 0.5 ml), DCM (5x 0.5ml) and DMF (5x 0.5ml) resin was loaded to synthesizer to continue automated synthesis.

Coupling of Fmoc-protected amino acids: Fmoc-protected amino acids were dissolved for coupling in DMF (0.3M). Six eq. of amino acid, 4eq. HCTU, and 12eq. of NMM in DMF were mixed with resin. After 30 min incubation the solution was discarded, and the resin was washed with DMF (6x0.3 ml).

Capping: 5% Acetic Anhydride, 6% 2, 6-*Lutidine solution* in DMF was added to the resin for 5min. The resin was washed by DMF (6x0.3ml)

Coupling of FAM: For evaluation of cellular uptake of the PNA probes, the fluorescein dye (FAM) was coupled to the side chain of lysine, which was attached to the N-terminus of the PNA probe. After completed automated solid-phase synthesis of PNA probes, the resin was transferred into a syringe and washed with DMF (5x times) and DCM (5x times). Then Mmt protection group of lysine was cleaved in a solution (2% TFA, 5% *triisopropylsilane*, 93% DCM) for 3min. The deprotection was repeated with the new solution once more for 3 min. Before dye coupling, resin was washed DCM (5x times), DMF (5x times), pyridine (2x times) and DMF (5x times). Six eq. of FAM, 4eq. Pybop, and 12eq. of NMM in DMF were mixed with resin. The resin was gently shaken at room temperature for 4h. The step of dye coupling was repeated. Afterwards, the resin was washed with DMF (5x times), DCM (5x times) and DMF (5x times) and proceeded for Fmoc cleavage as mentioned above. Before cleavage of PNA probe from resin, resin was washed in DMF (5x times) and DCM (10x times).

Cleavage of PNA probes from resin and their purification: High vacuum dried resin was suspended in 0.5ml cleavage mixture (95% TFA, 2% *triisopropylsilane*, 2% H_2O) for 1h (for PNA probes, containing cysteine, 5mg of cysteine methyl ester hydrochloride was added to the cleavage mixture). In 1h this step was repeated for 30 min. Cleavage mixture, containing PNA, was concentrated under air flow till 0.2 ml. After concentration, 2ml of ice cold diethyl ether was gently added to cleavage mixture and left for 15 min in dry ice. The precipitate was collected by centrifugation (20min, 4000 rpm, at 4°C). The residue was dissolved in water, analysed by analytical UPLC and purified by semi preparative HPLC using optimized gradient.

5.2 Fluorescence measurements

Fluorescence spectra were acquired by using a Varian Cary Eclipse spectrometer. Each fluorescence quartz cuvette contains 150 µl of the assay buffer (1 x PBS: 137 mM NaCl, 10 mM Phosphate, 2.7 mM KCl, and a pH of 7.4, with addition of $MgCl_2$ if it is mentioned, or special indicated buffer), 0.5 µM FIT PNA probe and 1 eq. of RNA target/ the reaction product. For the Ago2 experiments, 30pmol of the Ago2 recombinant protein (Sino Biological Inc., Beijing, China) was added as a last to assay cuvette. Other settings for spectra recording are TO: λ_{ex} = 516 nm, λ_{em} = 525 – 700 nm. QB: λ_{ex} = 588 nm, λ_{em} = 595 – 700 nm, $slit_{ex}$ = 5 nm, $slit_{em}$ = 10 nm, 37°C. For kinetic mode data were collected at 536 nm (for TO) and 606nm (for QB). For data analysis, buffer-only fluorescence was subtracted.

Dicer model reaction: for the modelling of the dicer reaction the synthetic RNA sequences were used corresponding to the sequences of as-miR21, miR21 and the C30-G45 segment. Pre-miR21 has been transcribed *in vitro*. The RNA sequences were purchased from Biomers: as-miR-21 5'-caacaccagucgaugggcugu-3', miR-21 5'-uagcuuaucagacugauguuga-3', the C30-G45 segment 5'-cuguugaaucucaugg-3'.

Recombinant dicer reaction: the dicer reaction was performed with Recombinant Dicer Enzyme Kit (Genlantis) according to the manufacturer's instructions with following modifications. The dicer buffer composition was changed (20mM tris HCl, pH 7.74, 2.5mM $MgCl_2$, 12mM NaCl, 1mM DTT)[210]. Recommended ratio of RNA template: Dicer enzyme as 1µg: 1U was optimized using 3- and 10-fold excess of the enzyme. The time of the reaction has been retained (18h) as given in the manufacturer's protocol. After the reactions with 1U and 3U of enzyme were completed, the products were added to the FIT probes and analysed by fluorescence spectrometer. For the kinetic analysis the dicer reaction (with the 10-fold excess of enzyme) was conducted directly in the spectrometer cuvette (35 pmol of pre-miR21, 1x dicer buffer, 10U dicer in 150µl of reaction) in the presence of the FIT probes (35 pmol of each probe).

5.3 Molecular and Cell Biology

In vitro transcription of pre-miRNA

Pre-mir21 has been prepared with TranscriptAid T7 High Yield Transcription Kit (Thermo Scientific Fermentas) according to the manufacturer's protocol. T7 Primer (5 µM) and pre-miR21 ssDNA template (2.6 µM) were used as starting materials and were incubated for 3min, 95°C and slowly cooled down to room temperature before transcription. After in vitro transcription reaction mix was treated by DNase I and followed by PCI extraction (Phenol/ chloroform/ isoamyl alcohol (25:24:1), Sigma Aldrich or Carl Roth) and ethanol precipitation. The results of the *in vitro* transcription were analysed by polyacrylamide gel electrophoresis (Fig. S16). In the reaction 1.9 nmol of pre-miR21 was obtained. Sequences of the pre-miR21 DNA template and T7 primer were purchased from Biomers:

Pre-miR21 short DNA template:

5'- $A_{OME}A_{OME}$ ggcccatcgactggtgttgccatgagattcaacagtcaacatcagtctgataagccctatagtgagtcgtatta-3'

Pre-miR21 DNA template:

5'-
tgtcagacaaaggcccatcgactggtgttgccatgagattcaacagtcaacatcagtctgataagctacccgacaccctatagtgagtcgtatta-3'

T7 primer: 5'-ggtaatacgactcactatag-3'

Polyacrylamide gel electrophoresis (PAGE): PAGE analysis has been done either with native or denaturating (8 M Urea) gels, containing 15-20% polyacrylamide gels (bis:acrylamide, 1:19). A Mini-PROTEAN® Tetra Handcast System von Bio-Rad (Hercules, CA, USA) was used. The gels were running under constant voltage (250V) in the 0.5xTBE buffer. For native gels 6x sucrose loading buffer (18mm EDTA, 0.05% bromphenol blue, 40% sucrose) was used. For denaturating gels 1x formamide loading buffer (90% formamide, 18mM EDTA and 0.05% bromphenol blue) was added to the samples at ratio 1:1 and incubated at 95°C for 5 min. and stored on ice before loading. Before visualization the gels were stained ~10 min. in the SYBR Gold solution (Invitrogen, 1:10,000 dilution in 1xTBE buffer). Gels were viewed under UV light by ChemiDoc Imaging System (Bio-RAD), Image Lab Software.

Dicer-mediated branched rolling-circular amplification assay (BRCA)

BRCA assay has been done as published before [156].

Dicer-cleavage reactions before BRCA assay: 50 nM renatured pre-miRNA21 (*in vitro* transcription from pre-miR-21 short DNA template) was incubated at first with the different concentrations of the PNA probes without Dicer for 1h, room temperature. Then, the recombinant Dicer enzyme (Genlantis) was added to the mixture at concentration 4 U/mL for 2 h at 37 °C in the dicer reaction buffer (20 mM

Tris-HCL (Tris = Tris(hydroxymethyl)aminomethan) pH 6.8, 12.5 mM NaCl, 2.5 mM MgCl2, 1 mM dithiothreitol).

BRCA assay: 5 µL of the dicer cleavage reaction was transferred to a BRCA reaction solution containing 1 × ThermoPol reaction buffer (NEB), 0.2 mM dNTPs, 0.2 µM secondary primer, 1:20000 dilution SYBR Gold, 2.5 nM circular ssDNA template, 5 % DMSO, 0.4 U/µL Bst Polymerase in the final volume of 20 µl. Amplification and detection were performed at 57 °C for 180 min with the iQ5 Real-Time PCR Detection System (Bio-Rad) in 96-well plates. The fluorescence was recorded every 2 min, and the slope of the initial linear range of the fluorescence increase was analysed.

The secondary primer and linear ssDNA template for circularization were purchased from Biotez (Berlin).

Secondary primer: 5'-ccaacgtagactcaaatgcc-3'

Linear ssDNA template: 5’-p-gcgttaagacaacagtcaacatcagtctgataagccaacgtagactcaaatgccaaatcgtaaa-3’

Circularization of the 5’-phosphorilated linear ssDNA template has been done by CircLigase ssDNA Ligase according to the manufacturer’s protocol with the following modifications in the reaction times: 4h at 60°C, followed by 12h at 16°C and the final heat-deactivation - 10min at 80°C. The reaction was then desalted with an Amicon 3K centrifuge filter.

Cell Culture and transfections

All cell lines were cultured in Dulbecco’ Modified Eagle Medium (DMEM) supplemented with 10% fetal bovine serum (FBS, GIBCO-Invitrogen) and 1% penicillin/ streptomycin and maintained at 37°C in a 5% CO_2 atmosphere. For the PNA probes and antimiRs transfections the Optimem® reduced serum medium (Thermo Fisher Scientific) was used. AntimiRs were delivered at a final concentration 50-100nM using Lipofectamine 2000 reagent (Invitrogen) according manufacturer’s protocol.

Quantitative RT-PCR

For miRNA quantification the specific cell lines were passaged in 6-well plates using standard DMEM supplemented with 10% FBS and 1% penicillin/ streptomycin. Next day, cells, reached 85-90% confluency, were transfected either with the PNA probes in the Optimem® reduced serum medium or with the small molecular inhibitors in the standard DMEM medium for 48h. After incubation the cells were used for RNA extraction by the miRNeasy Mini Kit (Qiagen) according to the manufacturer’s protocol.

For miRNA quantification Taqman® MicroRNA Reverse Transcription Kit, real-time RT-qPCR reagents, the primers and TaqMan probes were obtained from Applied Biosystem. Reverse transcription (RT) and real-time PCR were performed according to the manufacturer’s protocols using iQ5 Real-Time PCR Detection System (Bio-Rad, Hercules, CA, USA). Relative quantification is performed by the comparative C_T method (the alternative name is the $2^{-\Delta\Delta Ct}$ method), where the specific miRNA expression is calculated as a relative to the expression of a reference U6 snRNA according to formula:

$2^{-\Delta\Delta Ct} = [(C_{T\ \text{gene of interest}} - C_{T\ \text{reference gene}})]$ sample A - $[(C_{T\ \text{gene of interest}} - C_{T\ \text{reference gene}})]$ sample B,

where the $2^{-\Delta\Delta Ct}$ is a fold change in expression of specific miRNA between sample A and sample B.

For miR-122 targets (ADAM10, IGf1R and Aldo A) and LinN28B quantification, the SuperScript™ III First-Strand Synthesis System was used for reverse transcription (Thermo Fisher Scientific), and the Fast SYBR Green Master Mix (Thermo Fisher Scientific) was applied for real-time PCR according to manufacturer’s protocols. 1 µL of the reverse transcription reaction was transferred to the PCR mixture containing 1x Fast SYBR Green Master Mix and 4 pmol of each primer (forward and reverse).

Amplification was performed according to the manufacturer's protocol using iQ5 Real-Time PCR Detection System (Bio-Rad, Hercules, CA, USA). The comparative Ct method has been also used for the analysis of gene expression of the miR-122 targets using the housekeeping gene GAPDH as an internal control gene.

The PCR DNA primers were obtained from BioTeZ (Berlin Buch GmbH). The primer sequences are:

ADAM10_F: 5'- caa cct acg aat gaa gag gga cac -3'

ADAM10_R: 5'- cca cca cga gtc tgg atg aat c -3'

IGf1R_F: 5'- act tac tcg gac gtc tgg tcc ttc -3'

IGf1R_R: 5'- atc ttg ggg tta tac tgc cag cac -3'

AldoA_F: 5'- tca tcc tct tcc atg aga cac tct -3'

AldoA_R: 5'- att ctg ctg gca gat act ggc ata a -3'

Lin28B_F: 5'- cct cct cag cca aag aag tg -3'

Lin28B_R: 5'- gtg gtg atg tac agc cat gc -3'

GAPDH_F: 5'- gtc agt ggt gga cct gac ct -3'

GAPDH_R: 5'- tgc tgt agc caa att cgt tg -3'

Reporter Luciferase Assays

The assessment of the miR-122- and miR-21-mediated inhibition of translation was performed by the luciferase reporter plasmid psiCHECK-2 (Promega), which contains the perfectly matched antisense sequence to miR-122 or miR-21, respectively, downstream to the *Renilla* luciferase gene. On the day, previous to transfection, Huh7 cells were seeded into 96-well plates or 384-well plates. The next day cells, reached 80-90% confluency, were transfected with the 100ng of the plasmid, using Lipofectamine 2000 (Invitrogene), in the Optimem® reduced serum medium (Thermo Fisher Scientific). After 4h of incubation with the plasmid, the medium was exchanged for standard DMEM supplemented with 10% FBS, the indicated concentrations of the SMI were added to the cells, and the cells were maintained for 48h at 37°C in a 5% CO_2 atmosphere. Afterwards, the *Firefly* and *Renilla* luminescence were measured using the Dual Luciferase Assay (Promega) as indicated by the manufacturer on the plate reader VICTOR X (Perkin Elmer). For the analysis, the background of the only medium sample was subtracted, and *Renilla* luminescence was normalized on the *Firefly* luminescence for transfection efficiency.

Cell viability and cell cytotoxicity assays

Huh7 cells were plated in 96-well plated and treated with the SMI at the indicated concentrations. Cell proliferation and cytotoxicity were estimated by MTT cell viability assay (Thermo Fisher Scientific) the Pierce LDH cytotoxicity assay (Thermo Fisher Scientific) according to manufacturer's protocols.

Flow Cytometry and Fluorescence Microscopy.

For flow cytometry and fluorescence microscopy, the indicated cells were seeded and let grown overnight till they reach the 80-90% confluency. Afterwards, the cells were incubated with the PNA probes in the Optimem® reduced serum medium for 24h. The cells were then washed twice with PBS, detached by trypsinization and centrifuged (10min, 1000 x g).

For flow cytometry, after spinning down, the cells were resuspended in ice cold PBS buffer and centrifuged again (10min, 1000 x g). Then the supernatant was removed and the cells were gently

resuspended in 4% paraformaldehyde (PFA) solution in PBS for fixation and incubated 20 min at room temperature. The PFA solution was removed and the cells were washed in PBS buffer by centrifugation (the same conditions). Resuspended in PBS cells were stored at 4°C prior to analysis. The samples were analysed fresh (during 4h after preparation) by measuring 10000 non-gated events per sample in a FACSAria™ III analyser (Becton Dickinson, facility in the working group of Prof. Andreas Herrmann, Humboldt-Universität zu Berlin).

For fluorescence microscopy, the spin-down cells were seeded further on the polylysine coated glasses for overnight. Next day, the cells were fixed with 4% PFA solution in PBS for 10 min and, then, washed 3 times with the PBS buffer. The sample glasses were mounted on the microscopy slides and were analysed next day with an inverted *Olympus* IX83 microscope (Hamburg, Germany) with a 60×/1.35 UPLSAPO oil objective and an Orca Flash 4.0 V2 camera from Hamamatsu (Ammersee, Germany). A JC12V100W halogen lamp from Traydon (Frechen, Germany) for bright-field images and a light-emitting diode (LED) lamp (pE-4000) acquired from Cool LED (Andover, UK) with a λ=500/24 nm filter for the TO probes, from AHF (Pfrondorf, Germany) was applied, using the same exposure time for measured samples within the one cell line.The images were processed with the software CellSense Dimension von *Olympus* by using the region of interest (ROI) tool to surround the whole cells (at least 50 cells from 5 images were analyzed per every sample) .

Western Blot

Preparation of lysate from cell culture: Prior to western blot procedure, the Huh7 cells were treated with the indicated concentrations of DA8, DA40 and antimiR-122 (Qiagen) for 48h. Then, cells in 6-well plates were placed on ice and washed once with ice-cold PBS buffer, followed by lysis in 0.5 ml ice-cold lysis buffer (1x RIPA supplemented with 1x Protease inhibitor (Pierce protease inhibitor tablets, Thermo Fisher Scientific)) for 5 min. Lysates were transferred to pre-cooled microcentrifuge tubes and maintained constant agitation for 30 min at 4°C. The cell debris was pelleted by centrifugation for 20 min at 12,000 rpm, 4°C. The supernatant (lysate) was placed in a fresh tube kept on ice and stored at -20°C.

Determination of protein concentration was performed by using Pierce™ BCA Protein Assay Kit (Thermo Fisher Scientific) as indicated by manufacturer.

Gel electrophoresis and transfer: Before loading into gel the samples (60 µg) were mixed with gel loading buffer, 2x Laemmli buffer, in equal proportions, heated to 95°C for 5 min for denaturation and put on ice. Samples and reference PageRuler™ Prestained Protein Ladder (Thermo Fisher Scientific) were loaded on 10% SDS gel and run at 100V (0.3 mA) for 2.5h in the running buffer (1x Tris-Glycine buffer, pH 8.3) using Mini Trans-Blot Cell (Bio-Rad). The proteins were transferred onto Nitrocellulose membrane in transfer buffer (TS) at constant 100V (350mA) for 1h.

Blocking: After transfer, the nitrocellulose membrane was washed with 25ml of 1x TBS buffer for 5 min at RT (room temperature). The membrane was incubated in 25 ml of blocking buffer for 1h at RT. After incubation the membrane was washed 3 times for 5 min in 1x TBST buffer.

Primary Antibody: Primary rabbit ADAM-10 antibody (# 14194, Cell Signaling Technology) was used in dilution 1:1000 in 5% w/v BSA, 1xTBS, 0.1% Tween 20 and incubated with the membrane at 4°C with gentle shaking for overnight. Then the membrane was washed 3 times for 5min with 1x TBST.

Secondary Antibody: Secondary anti-rabbit IgG HRP-linked antibody (#7074, Cell Signaling Technology) was diluted 1:2,000 in blocking buffer and incubated with the membrane at RT for 1h prior to detection. The membrane was washed 6 times with 1x TBST.

Protein Detection:
The membrane was incubated for 1 min with the enhanced chemiluminescence ECL detection solution (SuperSignal™ West Femto Maximum Sensitivity Substrate, Thermo Fisher Scientific), which was mixed according to the manufacturer. The membrane was detected using ChemiDoc Imaging System (Bio-RAD), Image Lab Software.

Reference Antibody: After ADAM10 protein detection, the same membrane has been used for the analysis of the reference protein (Tubulin) following the same procedure with some modifications. After blocking the membrane was incubated with the reference rabbit β-Tubulin (9F3) antibody (#2128, Cell Signaling Technology) in dilution 1:1000 in 5% w/v BSA, 1xTBS, 0.1% Tween 20 at RT for 1h. The procedure with the secondary antibody remained unchanged. For the protein detection the less sensitive SuperSignal™ West Pico Chemiluminescent Substrate (Thermo Fisher Scientific) has been used as indicated by manufacturer.

Solutions:
1x RIPA: 150mM sodium chloride, 1% TritonX-100, 0.1 % SDS (sodium dodecyl sulfate), 50mM Tris, pH 8.0
2x Laemmli buffer: 4% SDS, 10% 2-mercaptoethanol, 20% glycerol, 0.004% bromphenol blue, 0.125 M Tris HCl, adjust pH to 6.8
Transfer buffer (TS): 47.9 mM Tris-base, 38.6mM Glycine, 0.0385% SDS, 20% Methanol (HPLC grade purity)
10x TBS buffer (for 1 liter): 24.2g Tris, 84g NaCl, adjust the pH to 7.6
TBST buffer: 1xTBS, 0.1% Tween 20
Blocking buffer: 1xTBST buffer, 5% nonfat dry milk

6 Supporting Information

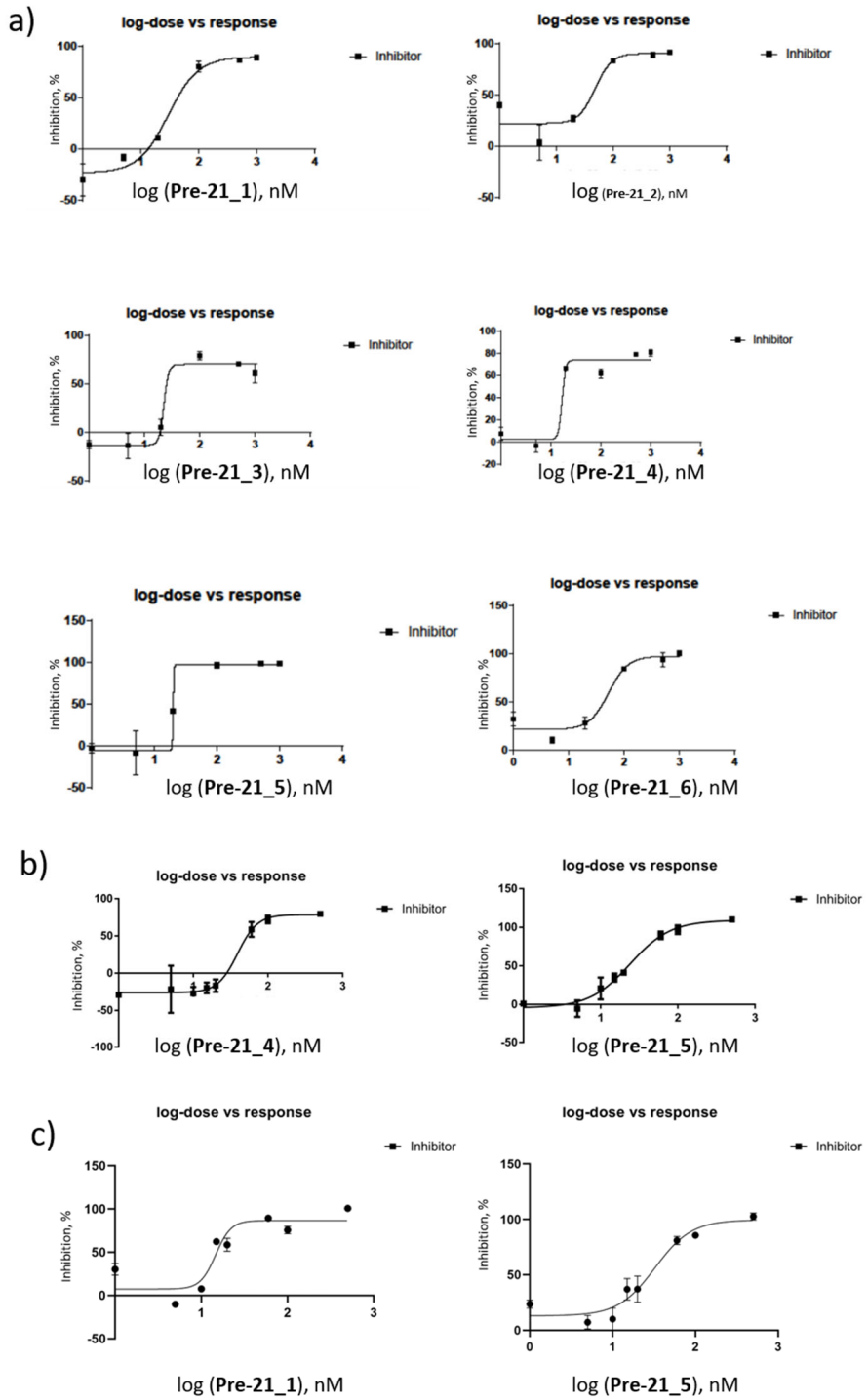

Figure S1. Graphical representation of the IC_{50} determination of inhibition of the miR-21 maturation by non-fluorogenic PNA probes (**Pre-21_1** – **Pre-21_6**) within concentration range of 1-1000 nM (a) and 1-500 nM (b, c) . Mean of independent triplicate BRCA experiments +/- SD.

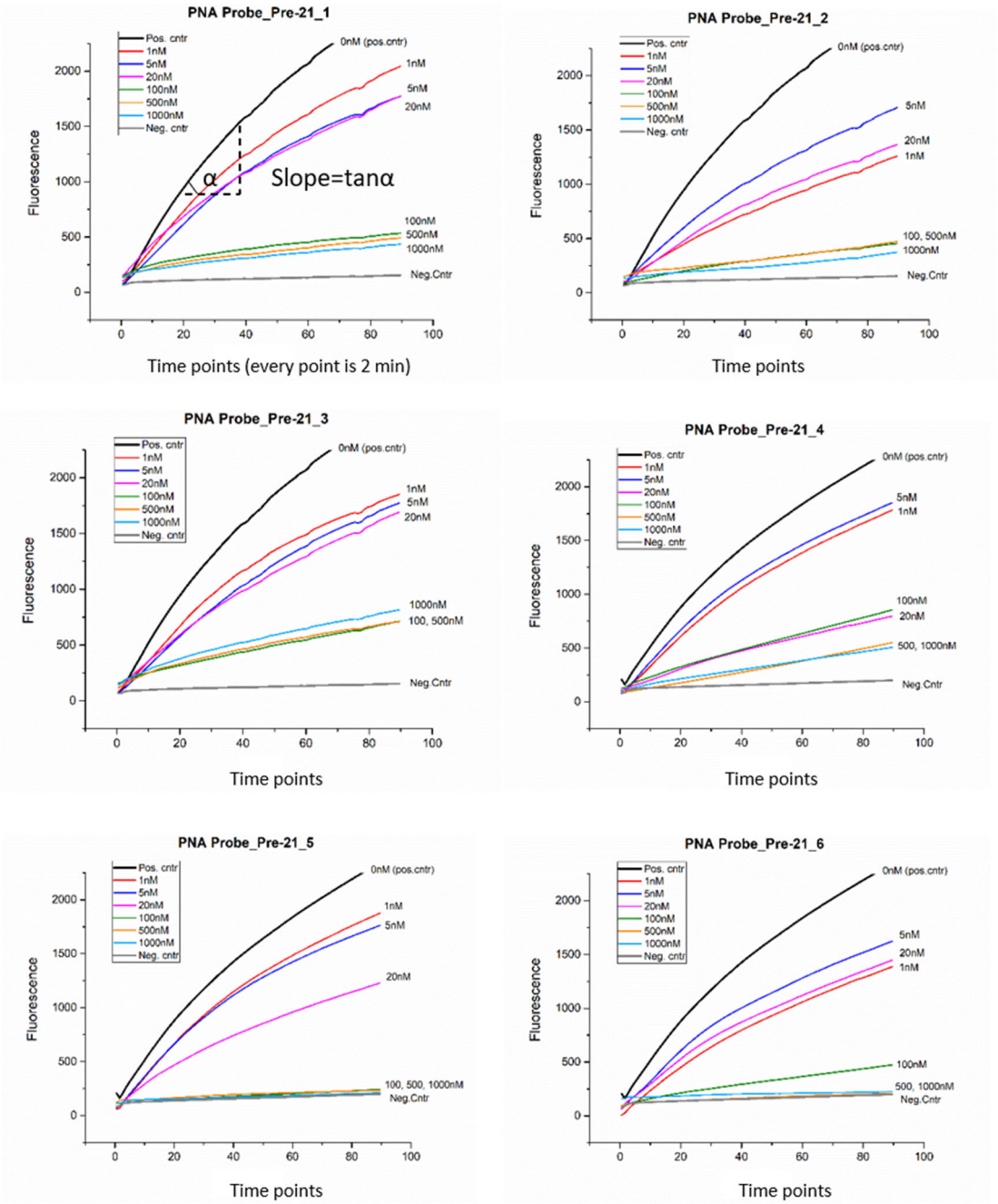

Figure S2. Time-course of fluorescence signal (the one of three independent experiments) of the dicer-mediated BRCA assay in the presence of the inhibitory PNA probes (**Pre-21_1** – **Pre-21_6**). Positive control (no PNA) and the negative control (no Dicer). The signal slope was determined within the linear range between 20 and 40 time points of the detection curve and was calculated as a tanα = $\Delta Y/\Delta X = (Y_{40}-Y_{20})/(X_{40}-X_{20})$ of linear approximation of fluorescence curve.

	Ct data						$\Delta Ct=Ct^{miR21}-Ct^{U6}$		
Name of PNA probe	U6_repeat 1	U6_repeat 2	U6_repeat 3	miR-21_repeat 1	miR-21_repeat 2	miR-21_repeat 3	repeat 1	repeat 2	repeat 3
cntr	20,55	20,11	20,33	28,34	28,10	28,26	-7,78	-7,99	-7,92
Pre-21_1_CPP_2µM	19,56	20,02		27,07	27,31		-7,51	-7,28	
Pre-21_5_CPP_2µM	19,61	19,80		29,14	28,16		-9,53	-8,36	
PNAmat21_CPP_0,5µM	26,34	25,58	24,76	26,99	27,26	27,66	-0,65	-1,67	-2,90

	$2^{-\Delta Ct}$			$2^{-\Delta Ct}$	$2^{-\Delta Ct}$	Fold Change due to treatment	Ttest
Name of PNA probe	repeat 1	repeat 2	repeat 3	Average	St. Deviation		
cntr	220,31	255,09	242,72	239,37	17,63		
Pre-21_1_CPP_2µM	181,67	155,61		168,64	18,43	-1,42	
Pre-21_5_CPP_2µM	736,94	329,05		533,00	288,42	-0,45	
PNAmat21_CPP_0,5µM	1,57	3,19	7,46	4,07	3,04	-58,76	0,01

Figure S3. RT-qPCR analysis of the inhibition of the dicer-mediated miR-21 maturation by the pre-miR21 specific PNA probes (**Pre-21_1** and **Pre-21_5**) in the Huh7 cells. Tables represent raw Ct data from two RT- qPCR and the calculation of the $2^{-\Delta Ct}$ and fold change due to treatment.

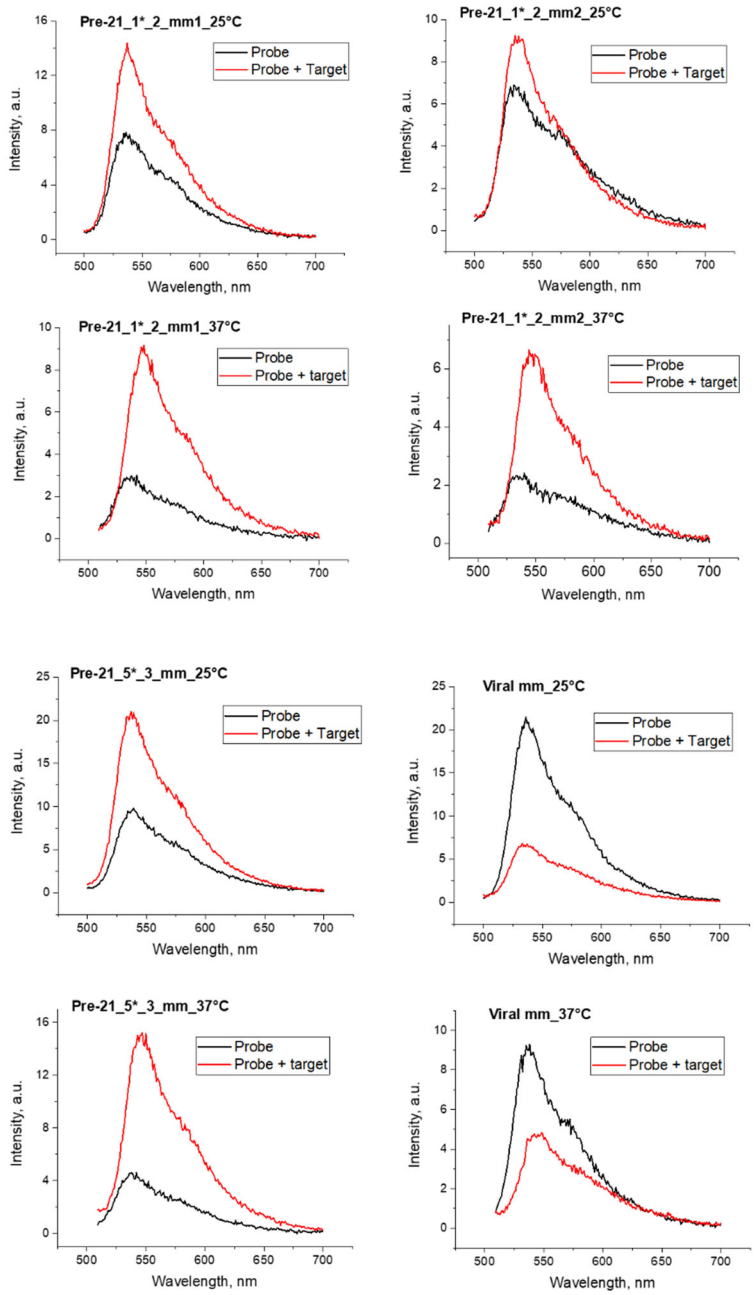

25°C				
Name	Sequence (N' → C')	I_0	I	I/I_0
Viral mm	C-K-cagtta(TO)tatgccgttg-CPP	21,3	4,5	0,2

37°C				
Name	Sequence (N' → C')	I_0	I	I/I_0
Viral mm	C-K-cagtta(TO)tatgccgttg-CPP	8,7	4,5	0,5

Figure S4. Fluorescence spectra of the control TO-labeled PNA probes (**Pre-21_1*_2_mm1** and **mm2, Pre-21_5*_3_mm, Viral mm)**. Conditions: in 150 µl of 1 x PBS, c(probe) = 0.5 µM, c (target) = 1.5 µM, TO: λ_{ex} = 485 nm, λ_{em}= 495-700 nm, emission maximum is detected at 536 nm, $slit_{ex}$= 5 nm, $slit_{em}$= 5 nm, at 25°C and 37°C. Before measurement at 25°C and 37°C, the mixture of the PNA probe and the pre-miR21 target was heated till 95°C and cooled down till 25°C or 37°C, respectively.

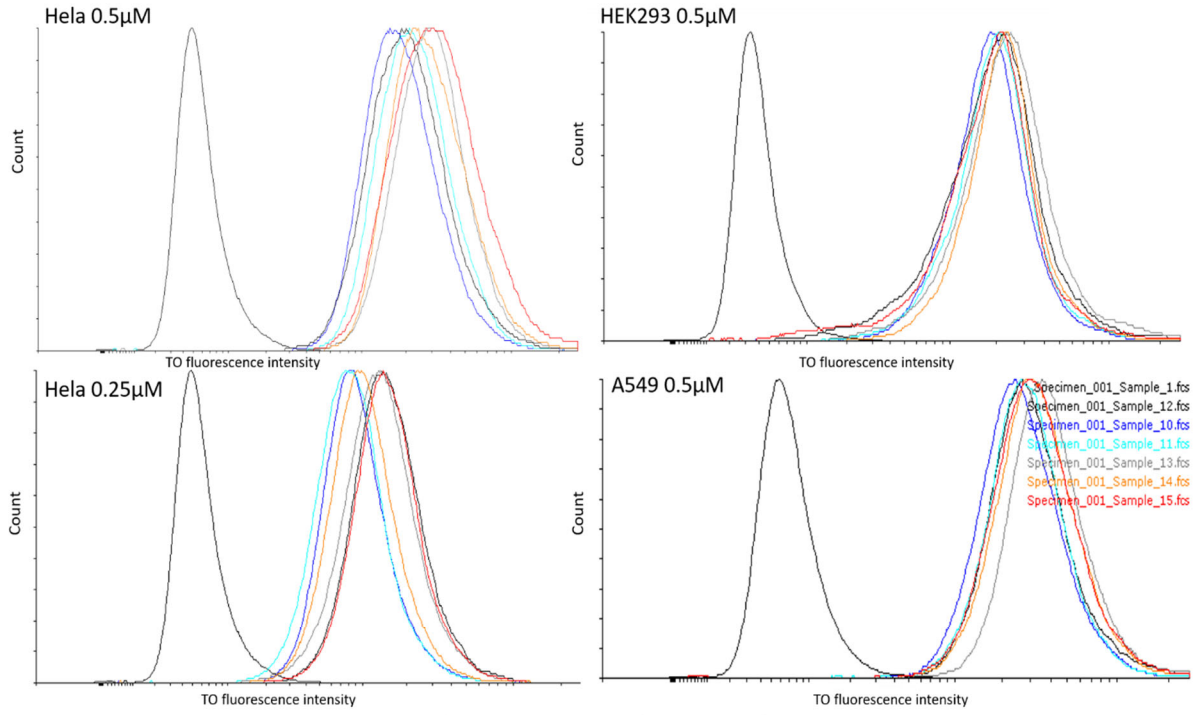

Mock	black
Pre-21_1*_2_mm1	blue
Pre-21_1*_2_mm2	bright blue
Pre-21_5*_3_mm	black
Viral mm	gray
Pre-21_1*_2	yellow
Pre-21_5*_3	red

Figure S5. Histogramm from flow cytometry analysis showing TO fluorescence in cells treated with pre-miR21 specific (**Pre-21_1*_2** and **Pre-21_5*_3**) or control probes (**Pre-21_1*_2_mm1** and **mm2**, **Pre-21_5*_3_mm)**.

Figure S6. Fluorescence spectroscopy conditions for measurements of rhDicer-mediated pre-mIR21 cleavage reaction (See Fig. 28). Conditions: **a)** Recommended ratio of pre-miR21 to rhDicer. Scan mode: in 150 µl of 1 x PBS, 3 mM $MgCl_2$, c(**11nt_TO1***) = c(**QB3**) = 0.5 µM PNA probe, 16 µl of the dicer reaction mixture (1 x dicer buffer, 75 pmol of pre-miR21, 2.5 U Dicer). The final concentration of the reaction mixture in the assay is 0.5 µM and equal to the probe concentration. TO: λ_{ex} = 516 nm, λ_{em} = 525 - 700 nm., $slit_{ex}$ = 5 nm, $slit_{em}$ = 10 nm, QB: λ_{ex} = 588 nm, λ_{em} = 598 -700 nm., $slit_{ex}$ = 5 nm, $slit_{em}$ = 10 nm, 37°C; **b)** Three-fold excess of rhDicer. Scan mode: in 150 µl of 1 x PBS, 3 mM $MgCl_2$, c(**11nt_TO1***) = c(**QB3**) = 0.25 µM and addition of 20 µl of the dicer reaction mixture (1 x dicer buffer, 35 pmol of pre-miR21, 3 U Dicer). The final concentration of the reaction mixture in the assay is 0.25 µM and equal to the probe concentration), TO: λ_{ex} = 516 nm, λ_{em} = 525 - 700 nm., $slit_{ex}$ = 5 nm, $slit_{em}$ = 10 nm, QB: λ_{ex}= 588 nm, λ_{em} = 598 -700 nm., $slit_{ex}$ = 5 nm, $slit_{em}$ = 10 nm, 37°C; **d, e)** Ten-fold excess of rhDicer. Kinetic mode: in 150 µl of 1 x dicer buffer, c(**11nt_TO1***) = c(**QB3**) = c(pre-miR21) = 0.25 µM, 10 U Dicer, TO: λ_{ex} = 516 nm, λ_{em} = 536 nm., $slit_{ex}$ = 5 nm, $slit_{em}$ = 10 nm, QB: λ_{ex} = 588 nm, λ_{em} = 606 nm., $slit_{ex}$ = 5 nm, $slit_{em}$ = 10 nm; 37°C. 1 x dicer buffer: 20 mM tris HCl, pH 7.74, 2.5 mM $MgCl_2$, 12 mM NaCl and 1 mM DTT.

Figure S7. Fluorescence spectroscopy conditions for **QB3** fluorescence measurements in presence of as-miR21/ pre-miR21 or the product mix (See Fig. 38b). Conditions: kinetic mode: in 150 µl of 1 x PBS, 3 mM $MgCl_2$, c(**QB3**) = c(target) = 0.5 µM, target: as-miR21, pre-miR21 or the product mix; product mix = miR-21, as-miR21 and the loop region, , TO: λ_{ex} = 516 nm, λ_{em} = 536 nm., $slit_{ex}$ = 5 nm, $slit_{em}$ = 10 nm, QB: λ_{ex} = 588 nm, λ_{em} = 606 nm., $slit_{ex}$ = 5 nm, $slit_{em}$ = 10 nm; 37°C.

	Background	Reporter without miR-binding site	Reporter with miR-122-binding site	antimiR-122	DA8				DA40			
					1μM	5μM	10μM	25μM	1μM	5μM	10μM	25μM
Firefly luminiscence	2064	109812	240302	235623	304115	170078	199871	59785	261499	261333	207665	48697
	2412	116409	253021	222747	292810	162353	211411	66157	255295	233347	211351	47027
	3880	89105	228709	224124	298113	157235	215265	63718	240783	195428	207402	45176
Renilla luminiscence	2054	246942	83136	353178	117132	77455	95137	48259	102252	130262	115418	53624
	2294	256701	87474	342937	114040	76783	97593	51321	101355	120640	118251	53930
	2300	195376	80606	343420	116543	74829	98880	48227	97357	106408	118155	53816

	DA18				D*A20			
	1μM	5μM	10μM	25μM	1μM	5μM	10μM	25μM
Firefly luminiscence	195124	30620	5690	6396	250581	324624	220751	163339
	203611	30992	3698	5202	265489	328986	235893	170497
	201081	30586	3166	5370	255907	315741	220915	163102
Renilla luminiscence	90076	23908	3240	2208	108376	137258	96690	76523
	91952	23010	2494	1840	113049	142651	101115	78412
	91573	24130	2366	1562	108448	141015	98050	76811

Figure S8. *Renilla* and *Firefly* luciferase luminiscence in Huh7 cells treated with the miR-122 reporter psiCHECK-2 and SMIs (**DA8, DA40, DA18** or **D*A20**).

	Background	Reporter without miR-binding site	Reporter with miR-21-binding site	DA8, 10μM	DA40, 10μM	D*A20, 10μM	NA17, 10μM	DA18				
								0.1μM	0.5μM	1μM	5μM	10μM
Firefly luminiscence	376	19867	66241	47875	49104	59209	42851	67560	63167	54955	9892	2164
	344	19347	64710	46991	48045	58875	42549	66614	62107	54336	9778	2212
	338	19365	64310	46870	47381	57722	42096	65275	61458	53482	9566	2236
Renilla luminiscence	644	47619	1516	1174	1218	1322	1168	1706	1530	1786	442	144
	658	51723	1524	1118	1222	1360	1142	1730	1590	1744	448	154
	714	54732	1662	1150	1238	1340	1220	1714	1620	1828	450	162

	Background	Reporter without miR-binding site	Reporter with miR-21-binding site	antimiR-21
Firefly luminiscence	2064	109812	506101	224249
	2412	116409	524242	217610
	3880	89105	499548	214277
Renilla luminiscence	2054	246942	17647	34950
	2294	256701	18425	34441
	2300	195376	17909	33877

Figure S9. *Renilla and Firefly* luciferase luminiscence inHuh7 cellls treated with the miR-21 reporter psiCHECK-2 and SMIs (**DA8, DA40, DA18, DA*20** or **NA17**)

	Ct data								ΔCt=Ct$_{miR122}$-Ct$_{U6}$			
Name of Sample	U6_repeat 1	U6_repeat 2	U6_repeat 3	U6_repeat 4	miR-122_repeat 1	miR-122_repeat 2	miR-122_repeat 3	miR-122_repeat 4	repeat 1	repeat 2	repeat 3	repeat 4
Mock (0μM)	32,21	31,71	31,32	31,22	22,59	22,57	22,37	22,33	-9,61	-9,14	-8,95	-8,89
antimiR-122	31,48	31,31	31,19	30,75	24,48	24,37	24,23	24,26	-7,00	-6,94	-6,96	-6,49
DA8, 1μM	30,88	30,53	29,95	30,37	22,61	22,30	22,53	22,46	-8,27	-8,23	-7,42	-7,91
DA8, 5μM	31,20	30,52	30,27	30,34	22,40	22,30	22,18	22,07	-8,80	-8,23	-8,09	-8,27
DA8, 10μM	30,67	30,29	30,04	31,52	22,08	22,29	22,08	22,08	-8,59	-7,99	-7,96	-9,44
DA40, 1μM	30,79	30,83	30,49	30,15	22,62	22,41	22,56	22,49	-8,17	-8,42	-7,93	-7,66
DA40, 5μM	30,64	30,48	30,24	30,31	23,00	23,00	22,78	22,73	-7,64	-7,48	-7,46	-7,58
DA40, 10μM	30,56	30,55	30,03	30,22	22,68	22,71	22,58	22,57	-7,87	-7,84	-7,46	-7,65

	$2^{-\Delta Ct}$				$2^{-\Delta Ct}$	$2^{-\Delta Ct}$	$2^{-\Delta Ct\ treated}$ / $2^{-\Delta Ct\ untreated}$	Fold Change due to treatment	Ttest	
Name of Sample	repeat 1	repeat 2	repeat 3	repeat 4	Average	St. Deviation			Significance	
Mock (0μM)	782,39	563,34	494,51	474,66	578,73	141,00	1,00	-1,00		
antimiR-122	128,39	122,90	124,87	90,00	116,54	17,84	0,20	-4,97	0,00042725	***
DA8, 1μM	307,82	299,77	171,27	240,81	254,92	63,26	0,44	-2,27	0,0039986	***
DA8, 5μM	445,53	299,88	273,19	308,42	331,75	77,32	0,57	-1,74	0,00103335	***
DA8, 10μM	384,76	254,97	248,37	694,55	395,66	208,92	0,68	-1,46	0,20280031	
DA40, 1μM	288,03	341,82	244,22	202,83	269,23	59,60	0,47	-2,15	0,00558901	**
DA40, 5μM	199,16	178,60	176,00	191,09	186,22	10,86	0,32	-3,11	0,00143506	***
DA40, 10μM	234,36	229,10	175,81	200,70	209,99	27,17	0,36	-2,76	0,00102026	***

Figure S10. RT-qPCR data and calculation of miR-122 expression in Huh7 cells treated with DA8 and DA40 at a 1, 5 and 10 μM concentrations. AntimiR-122 was transfected at a 100 nM concentration. MiR-122 expression fold ($2^{-\Delta Ct}$, where $\Delta Ct=Ct_{miR122}-Ct_{U6}$, Ct-threshold cycle) of treated cells was compared to untreated cells (Mock). MiR-122 expression was normalized to endogenous control small nuclear RNA U6 (concentration control). Data are mean (+SD) of 4 replicates, *p<0.05; **p<0.01; ***p<0.005 (Student's t test).

	Ct data						ΔCt=Ct$_{miR16}$-Ct$_{U6}$		
Name of Sample	U6_repeat 1	U6_repeat 2	U6_repeat 3	miR-16_repeat 1	miR-16_repeat 2	miR-16_repeat 3	repeat 1	repeat 2	repeat 3
Mock (0μM)	28,47	27,87	28,40	21,55	21,10	21,10	-6,92	-6,77	-7,30
DA8, 10μM	27,82	28,15	27,55	20,71	20,77	20,53	-7,11	-7,38	-7,02
DA40, 10μM	28,02	27,90	27,91	20,88	20,73	20,60	-7,13	-7,17	-7,31

	Ct data						ΔCt=Ct$_{miR22}$-Ct$_{U6}$		
Name of Sample	U6_repeat 1	U6_repeat 2	U6_repeat 3	miR-22_repeat 1	miR-22_repeat 2	miR-22_repeat 3	repeat 1	repeat 2	repeat 3
Mock (0μM)	28,47	27,87	28,40	25,77	26,07	25,71	-2,70	-1,80	-2,69
DA8, 10μM	27,82	28,15	27,55	25,57	25,57	25,39	-2,25	-2,58	-2,16
DA40, 10μM	28,02	27,90	27,91	25,83	25,88	25,58	-2,19	-2,01	-2,34

$2^{-\Delta Ct}$			$2^{-\Delta Ct}$	$2^{-\Delta Ct}$	$2^{-\Delta Ct\ treated}$ / $2^{-\Delta Ct\ untreated}$	Fold Change due to treatment
repeat 1	repeat 2	repeat 3	Average	St. Deviation		
120,92	109,51	157,23	129,22	24,92	1,00	-1,00
138,57	166,23	129,50	144,77	19,13	1,12	-0,89
140,16	143,98	158,70	147,61	9,79	1,14	-0,88

$2^{-\Delta Ct}$			$2^{-\Delta Ct}$	$2^{-\Delta Ct}$	$2^{-\Delta Ct\ treated}$ / $2^{-\Delta Ct\ untreated}$	Fold Change due to treatment
repeat 1	repeat 2	repeat 3	Average	St. Deviation		
6,50	3,49	6,44	5,48	1,72	1,00	-1,00
4,76	6,00	4,47	5,08	0,81	0,93	-1,08
4,56	4,03	5,06	4,55	0,51	0,83	-1,20

Figure S11. RT-qPCR quantification of unspecific miRNAs (miR-16 and miR-22) in Huh7 cells treated with **DA8** and **DA40**. The expression of control miRNAs was normalized to the small nuclear RNA U6. Data are mean (+SD) of 3 replicates, *p<0.05; **p<0.01; ***p<0.005 (Student's *t* test).

	Ct data						ΔCt=Ct$_{miR122}$-Ct$_{U6}$		
Name of Sample	U6_repeat 1	U6_repeat 2	U6_repeat 3	miR-122_repeat 1	miR-122_repeat 2	miR-122_repeat 3	repeat 1	repeat 2	repeat 3
Mock (0μM)	35,32	32,76	32,62	24,49	24,03	23,97	-10,83	-8,73	-8,65
DA8, 5μM	30,66	30,69	30,19	23,25	23,04	23,12	-7,41	-7,65	-7,07
DA8, 10μM	30,90	29,98	29,11	23,73	23,77	23,44	-7,17	-6,21	-5,67
DA8, 20μM	29,47	29,67	28,92	23,35	23,11	22,84	-6,11	-6,56	-6,08
DA40, 5μM	32,39	30,63	30,20	23,60	23,50	23,26	-8,79	-7,13	-6,93
DA40, 10μM	29,94	30,10	29,57	23,96	23,57	22,51	-5,98	-6,53	-7,05
DA40, 20μM	30,36	30,39	30,10	26,81	26,57	25,88	-3,55	-3,83	-4,21

	$2^{-\Delta Ct}$			$2^{-\Delta Ct}$	$2^{-\Delta Ct}$	$2^{-\Delta Ct\ treated} / 2^{-\Delta Ct\ untreated}$	Fold Change due to treatment	Ttest				
								ΔCt			Significance	
Name of Sample	repeat 1	repeat 2	repeat 3	Average	St. Deviation							
Mock (0μM)	1819,75	424,63	400,87	881,75	812,42	1,00	-1,00	-10,83	-8,73	-8,65		
DA8, 5μM	169,84	200,26	133,90	168,00	33,22	0,19	-5,25	-7,41	-7,65	-7,07	0,10391303	no
DA8, 10μM	144,32	73,82	50,93	89,69	48,68	0,10	-9,83	-7,17	-6,21	-5,67	0,0114211	*
DA8, 20μM	69,22	94,34	67,88	77,15	14,90	0,09	-11,43	-6,11	-6,56	-6,08	0,05774149	no
DA40, 5μM	441,64	139,93	122,31	234,63	179,49	0,27	-3,76	-8,79	-7,13	-6,93	0,00546405	**
DA40, 10μM	63,01	92,41	132,83	96,08	35,05	0,11	-9,18	-5,98	-6,53	-7,05	0,10235774	no
DA40, 20μM	11,69	14,17	18,56	14,81	3,48	0,02	-59,54	-3,55	-3,83	-4,21	0,02441354	*

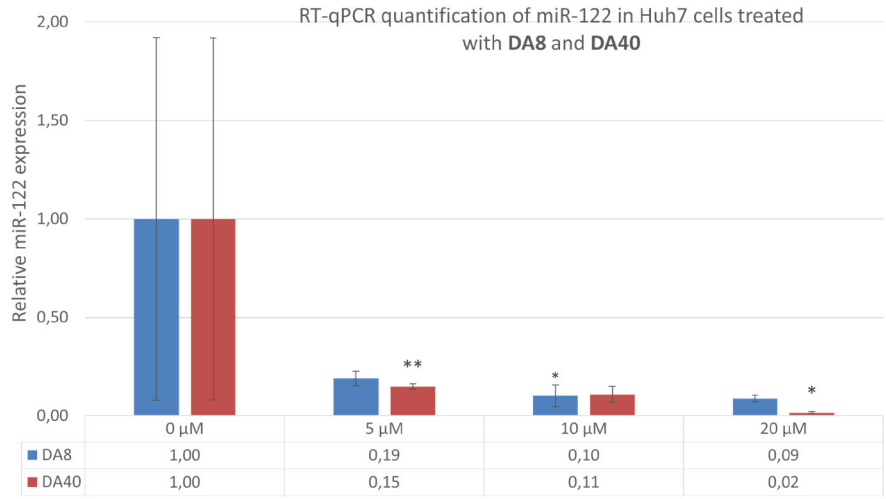

Figure S12. RT-qPCR quantification of miR-122 in Huh7 cells after incubation with **DA8** or **DA40** at a 5, 10 and 20 μM concentration. MiR-122 expression fold ($2^{-\Delta Ct}$, where $\Delta Ct=Ct_{miR122}-Ct_{U6}$, Ct-threshold cycle) of treated cells was compared to untreated cells (Mock). MiR-122 expression was normalized to endogenous control small nuclear RNA U6 (concentration control). Data are mean (+SD) of 3 replicates (T test significance: p-value, *p<0.05; **p<0.01; ***p<0,005).

		Ct data			$\Delta Ct=Ct_{Gene}-Ct_{GAPDH}$			$2^{-\Delta Ct}$		
Name of Sample		repeat 1	repeat 2	repeat 3	repeat 1	repeat 2	repeat 3	repeat 1	repeat 2	repeat 3
Mock (0μM)	ADAM10	28,58	28,66	28,94	7,85	8,25	8,56	0,00435	0,00328	0,00266
	IGf1R	29,82	29,64	29,16	9,08	9,23	8,77	0,00184	0,00167	0,00229
	AldoA	24,29	24,12	24,08	3,56	3,71	3,69	0,08505	0,07642	0,07747
	GAPDH	20,74	20,41	20,39	0,00	0,00	0,00	1,00000	1,00000	1,00000
DA40, 5μM	ADAM10	28,99	27,51	27,84	9,41	8,87	8,30	0,00147	0,00214	0,00317
	IGf1R	29,71	29,88	29,55	10,13	11,24	10,01	0,00089	0,00041	0,00097
	AldoA	23,45	23,51	23,17	3,87	4,87	3,63	0,06848	0,03413	0,08077
	GAPDH	19,58	18,64	19,54	0,00	0,00	0,00	1,00000	1,00000	1,00000
DA40, 10μM	ADAM10	27,31	26,92	26,67	9,18	8,99	8,80	0,00173	0,00196	0,00224
	IGf1R	29,88	29,34	29,27	11,74	11,41	11,40	0,00029	0,00037	0,00037
	AldoA	22,69	22,66	22,88	4,56	4,73	5,01	0,04252	0,03765	0,03108
	GAPDH	18,14	17,93	17,87	0,00	0,00	0,00	1,00000	1,00000	1,00000
DA40, 20μM	ADAM10	24,88	24,70	24,64	7,11	7,30	7,11	0,00724	0,00633	0,00722
	IGf1R	27,76	27,89	27,68	10,00	10,49	10,15	0,00098	0,00070	0,00088
	AldoA	22,61	22,70	22,69	4,84	5,31	5,16	0,03484	0,02529	0,02797
	GAPDH	17,77	17,40	17,53	0,00	0,00	0,00	1,00000	1,00000	1,00000

$2^{-\Delta Ct}$		$2^{-\Delta Ct\ treated}$ / $2^{-\Delta Ct\ untreated}$	Fold Change due to treatment	Ttest		Name of Sample	
Average	St. Deviation			Significance			
0,00343	0,00085					Mock (0μM)	ADAM10
0,00194	0,00032						IGf1R
0,07965	0,00471						AldoA
1,00000	0,00000						GAPDH
0,00226	0,00086	0,66	-1,52	0,346		DA40, 5μM	ADAM10
0,00076	0,00030	0,39	-2,55	0,040	*		IGf1R
0,06113	0,02417	0,77	-1,30	0,322			AldoA
1,00000	0,00000						GAPDH
0,00198	0,00026	0,58	-1,73	0,133		DA40, 10μM	ADAM10
0,00034	0,00004	0,18	-5,64	0,004	***		IGf1R
0,03708	0,00574	0,47	-2,15	0,008	**		AldoA
1,00000	0,00000						GAPDH
0,00693	0,00052	2,02	-0,49	0,038	*	DA40, 20μM	ADAM10
0,00085	0,00014	0,44	-2,27	0,014	*		IGf1R
0,02937	0,00493	0,37	-2,71	0,004	***		AldoA
1,00000	0,00000						GAPDH

Figure S13. RT-qPCR quantification of ADAM 10, IGF1R and AldoA expression ($2^{-\Delta Ct}$, where $\Delta Ct=Ct_{miR122\text{-}target\ gene} - Ct_{reference\ gene\ GAPDH}$, Ct-threshold cycle) in **DA40** treated cells.

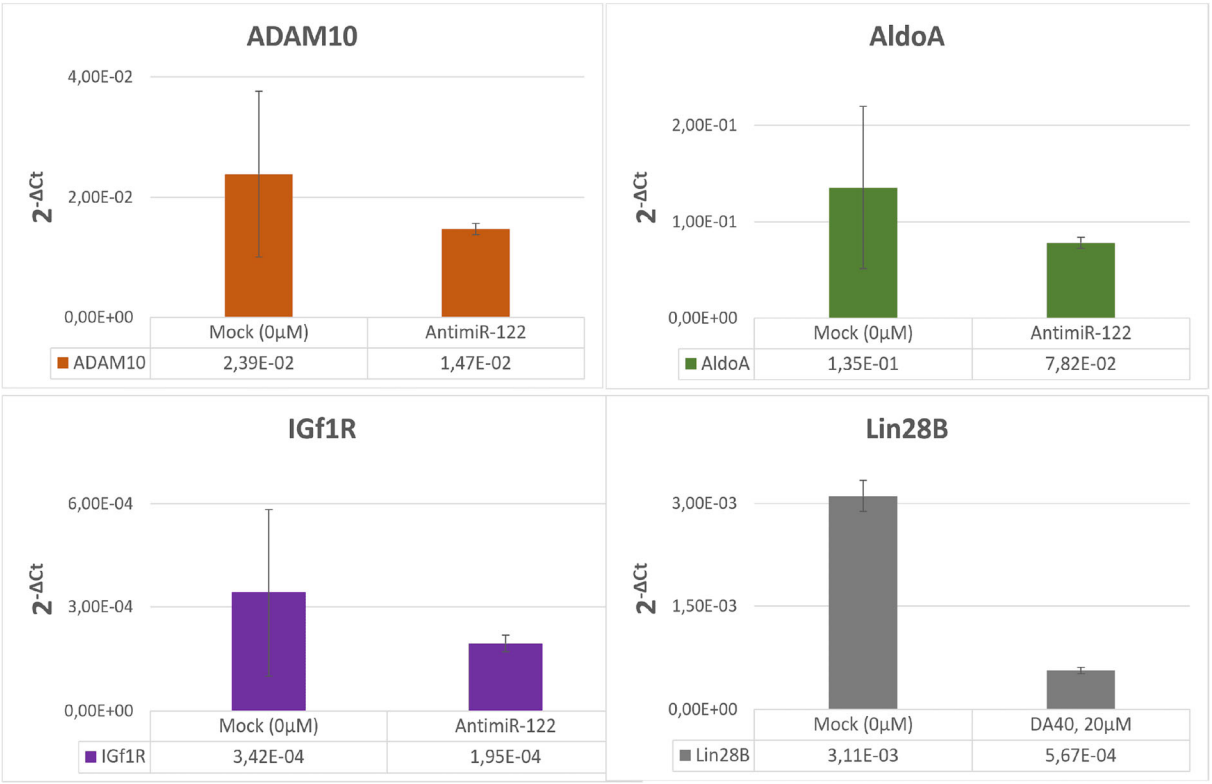

		Ct data			ΔCt=Ct$_{Gene}$-Ct$_{GAPDH}$			$2^{-\Delta Ct}$		
Name of Sample		repeat 1	repeat 2	repeat 3	repeat 1	repeat 2	repeat 3	repeat 1	repeat 2	repeat 3
Mock (0μM)	ADAM10	21,39	21,44	21,40	6,02	5,93	4,65	0,01540	0,01646	0,03976
	IGf1R	27,63	27,78	27,40	12,27	12,27	10,65	0,00020	0,00020	0,00062
	AldoA	19,07	18,86	18,86	3,71	3,35	2,11	0,07651	0,09798	0,23190
	GAPDH	15,36	15,51	16,75	0,00	0,00	0,00	1,00000	1,00000	1,00000
AntimiR-122	ADAM10	21,22	21,01	21,16	6,08	6,00	6,18	0,01482	0,01560	0,01376
	IGf1R	27,29	27,41	27,44	12,14	12,41	12,46	0,00022	0,00018	0,00018
	AldoA	18,94	18,64	18,58	3,80	3,64	3,60	0,07195	0,08025	0,08245
	GAPDH	15,15	15,00	14,98	0,00	0,00	0,00	1,00000	1,00000	1,00000
Mock (0μM)	Lin28B	24,99	24,86	24,75	8,44	8,33	8,23	0,00288	0,00312	0,00333
	GAPDH	16,56	16,53	16,52	0,00	0,00	0,00	1,00000	1,00000	1,00000
DA40, 20μM	Lin28B	27,18	27,08	26,88	10,92	10,76	10,69	0,00052	0,00058	0,00061
	GAPDH	16,26	16,32	16,20	0,00	0,00	0,00	1,00000	1,00000	1,00000

$2^{-\Delta Ct}$		$2^{-(\Delta Ct\ treated\ -\Delta Ct\ untreated)}$	Fold Change due to treatment	Ttest		Name of Sample	
Average	St. Deviation			Significance			
0,02387	0,01377					Mock (0μM)	ADAM10
0,00034	0,00024						IGf1R
0,13546	0,08421						AldoA
1,00000	0,00000						GAPDH
0,01472	0,00093	0,62	-1,62	0,374		AntimiR-122	ADAM10
0,00019	0,00002	0,57	-1,76	0,423			IGf1R
0,07822	0,00554	0,58	-1,73	0,291			AldoA
1,00000	0,00000						GAPDH
0,00311	0,00023					Mock (0μM)	Lin28B
1,00000	0,00000						GAPDH
0,00057	0,00005	0,18	-5,48	0,00003	***	DA40, 20μM	Lin28B
1,00000	0,00000						GAPDH

Figure S14. RT-qPCR quantification of the ADAM 10, IGF1R and AldoA expression ($2^{-\Delta Ct}$, where $\Delta Ct=Ct_{miR122\text{-}target\ gene}-Ct_{reference\ gene\ GAPDH}$, Ct-threshold cycle) in Huh7 cells treated with antimiR-122 (Qiagen) and RT-qPCR quantification of the non-miR-122 target, Lin28B, in Huh7 cells treated with DA40 (20μM). Data are mean (+SD) of 3 replicates (T test significance: p-value, *p<0.05; **p<0.01; ***p<0,005).

a)

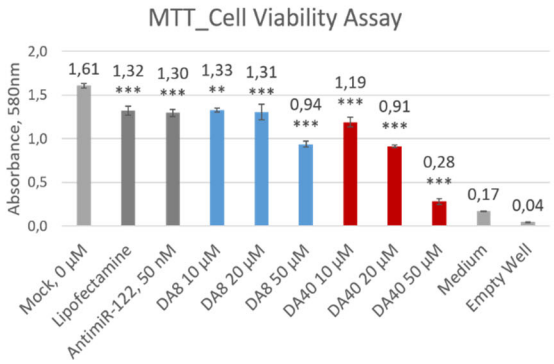

b)

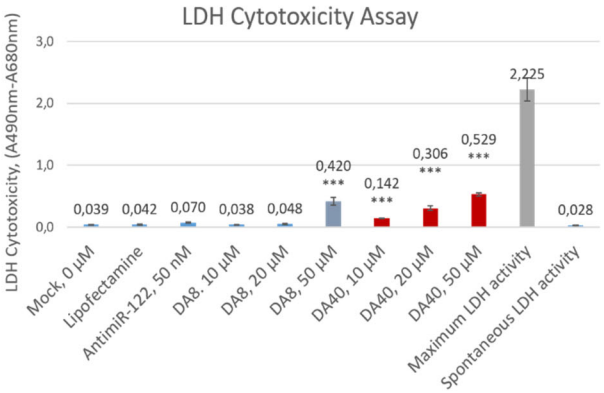

Figure S15. Determination of DA40 or DA8 cytotoxicity in Huh7 cells using MTT cell viability assay (a) and LDH cytotoxicity assay (b). Huh7 cells were treated with the different concentrations (0-50 µM) of DA40 or DA8 for 48 h. AntimiR-122 have been used at a concentration of 50 nM. a) MTT cell viability assay. Bars represent the mean of absorbance at 580 nm ± SD and compared to untreated cells (n = 4). *** $p < 0.001$, ** $p < 0.01$, * $p < 0.05$ (Student's t test). b) LDH cytotoxicity assay. To determine LDH activity, the 680 nm absorbance value (background signal) was subtracted from the 490 nm absorbance. Bars represent the mean of absorbance at 490 nm (with subtracted 680 nm absorbance) ± SD and compared to untreated cells (n = 4). The controls Maximum LDH activity and Spontaneous LDH activity are provided by manufacture. *** $p < 0.001$, ** $p < 0.01$, * $p < 0.05$ (Student's t test).

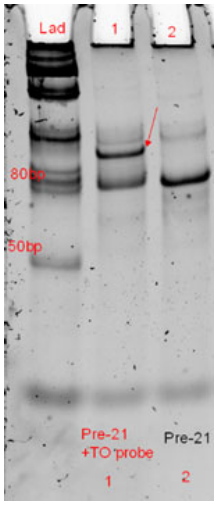

Figure S16. In vitro transcribed pre-miR21 integrity assessment by the polyacrylamide (PAAG) gel electrophoresis. As a Ladder (Lad), the low molecular weight ssRNA ladder (NEB) was used. The band in the row №2 corresponds to pre-miR21 (75 nt). The shift of the band of pre-miR21 is shown on the row №1, when pre-miR21 is in the complex with the probe. Conditions: Native PAAG gel (20%), UV transillumination.

7 Appendix

UPLC spectra

To the chapter 3.1.:

Pre-21_1: gagattcaacagtca-G

HPLC-MS: HPLC spectrum ($UV_{\lambda=260\,nm}$), ESI-MS – m/z = 1384.8 ($(M+3H)^{3+}$, calc.: 1384.2), 1038.9 ($(M+4H)^{4+}$, calc.: 1038.4), 831.4 ($(M+5H)^{5+}$, calc.: 830.9), 693.0 ($(M+6H)^{6+}$, calc.: 692.6) Formula: $C_{164}\,H_{204}\,N_{92}\,O_{43}$, MW_{exp}= 4151.93 g*mol^{-1} (MW_{calc} = 4151.9647g*mol^{-1}), Exact $Mass_{calc}$= 4149.6598g*mol^{-1};

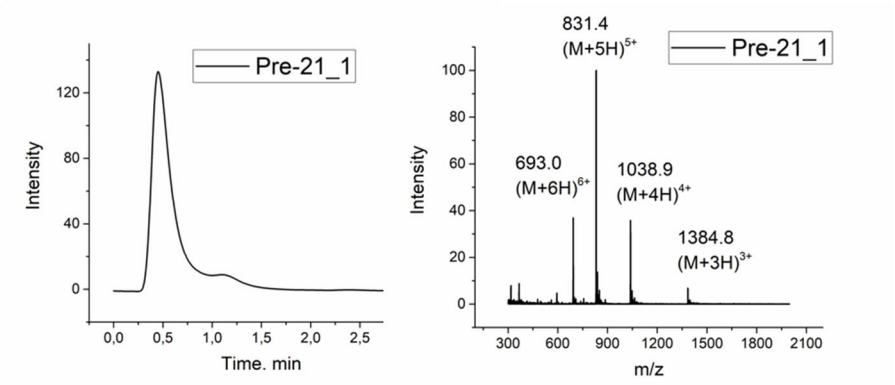

Pre-21_2: gattcaacagtcaacatc-G

HPLC-MS: HPLC spectrum ($UV_{\lambda=260\,nm}$), ESI-MS – m/z = 1227.1 ($(M+4H)^{4+}$, calc.: 1226.5), 981.9 ($(M+5H)^{5+}$, calc.: 981.4), 818.5 ($(M+6H)^{6+}$, calc.: 818.0), 701.7 ($(M+7H)^{7+}$, calc.: 701.3), Formula: $C_{195}\,H_{244}\,N_{106}\,O_{52}$, MW_{exp}= 4904.71 g*mol^{-1} (MW_{calc} = 4904.7023 g*mol^{-1}), Exact $Mass_{calc}$= 4901.9699g*mol^{-1};

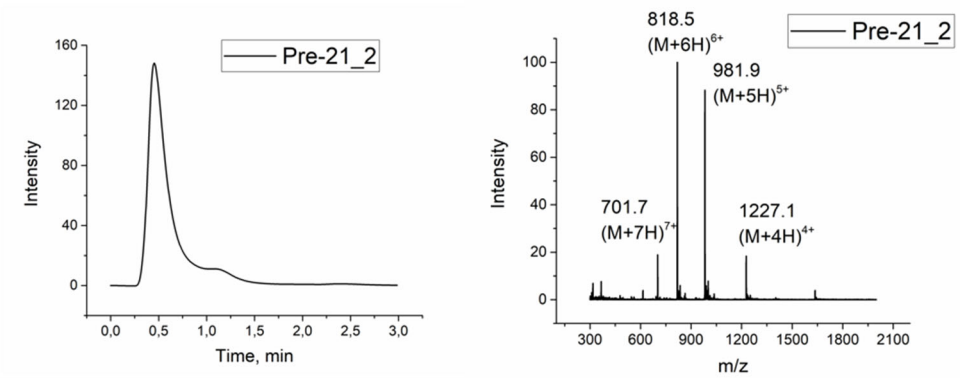

Pre-21_3: gtgttgccatgag-G

HPLC-MS: HPLC spectrum ($UV_{\lambda=260\,nm}$), ESI-MS – m/z =1216.8 ($(M+3H)^{3+}$, calc.: 1216.5), 913.0 ($(M+4H)^{4+}$, calc.: 912.6), 730.7 ($(M+5H)^{5+}$, calc.: 730.3), 609.1 ($(M+6H)^{6+}$, calc.: 608.7), Formula: $C_{143}\,H_{179}\,N_{77}\,O_{42}$, MW_{exp}=3648.48 g*mol^{-1} (MW_{calc} = 3648.4416 g*mol^{-1}), Exact $Mass_{calc}$= 3646.4235 g*mol^{-1};

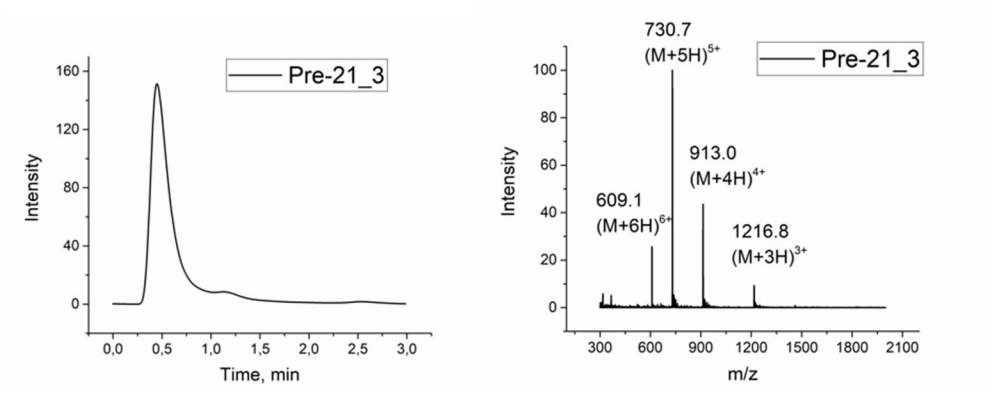

Pre-21_4: cgactggtgttgccatgag-G

HPLC-MS: HPLC spectrum ($UV_{\lambda=260\,nm}$), ESI-MS – m/z = 1319.6 ($(M+4H)^{4+}$, calc.: 1319.0), 1055.8 ($(M+5H)^{5+}$, calc.: 1055.4), 880.0 ($(M+6H)^{6+}$, calc.: 879.7), 754.6 ($(M+7H)^{7+}$, calc.: 754.2), Formula: $C_{207}\,H_{258}\,N_{112}\,O_{60}$, MW_{exp}= 5274.18 g*mol^{-1} (MW_{calc} = 5274.9772 g*mol^{-1}), Exact $Mass_{calc}$= 5272.0576 g*mol^{-1};

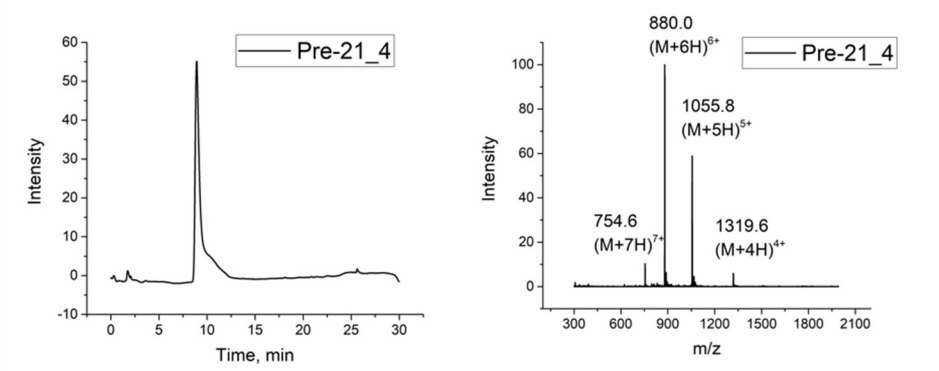

Pre-21_5: gccatgagattcaacagtc-G

HPLC-MS: HPLC spectrum ($UV_{\lambda=260\,nm}$), ESI-MS – m/z = 1303.8 ($(M+4H)^{4+}$, calc.: 1303.3), 1043.3 ($(M+5H)^{5+}$, calc.: 1042.8), 869.7 ($(M+6H)^{6+}$, calc.: 869.2), 745.6 ($(M+7H)^{7+}$, calc.: 745.2), Formula: $C_{206}\,H_{257}\,N_{113}\,O_{56}$, MW_{exp}= 5211.94 g*mol^{-1} (MW_{calc} = 5211.9677 g*mol^{-1}), Exact $Mass_{calc}$= 5209.0729 g*mol^{-1};

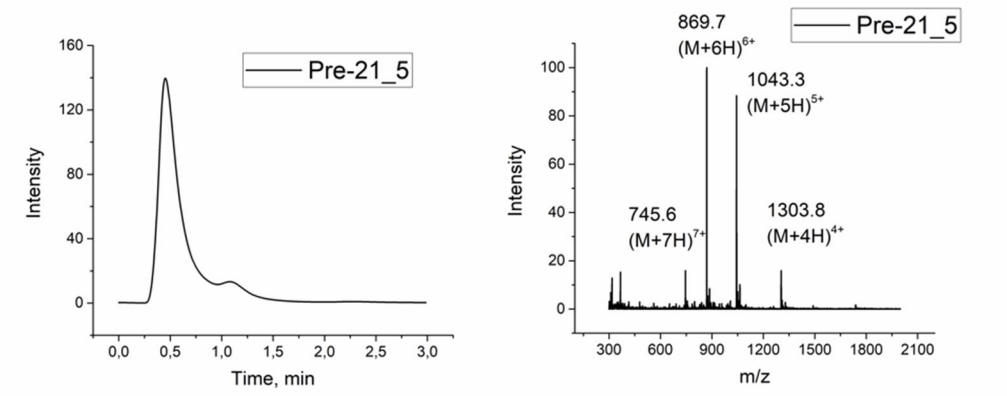

Pre-21_6: gattcaacagtcaacatcagtc-G

HPLC-MS: HPLC spectrum ($UV_{\lambda=260\,nm}$), ESI-MS – m/z = 1198.4 ($(M+5H)^{5+}$, calc.: 1198.1), 999.0 ($(M+6H)^{6+}$, calc.: 998.6), 856.4 ($(M+7H)^{7+}$, calc.: 856.1), Formula: $C_{238}\,H_{297}\,N_{129}\,O_{64}$, MW_{exp}= 5987.64 g*mol^{-1} (MW_{calc} = 5988.73 g*mol^{-1}), Exact $Mass_{calc}$= 5985.3942 g*mol^{-1};

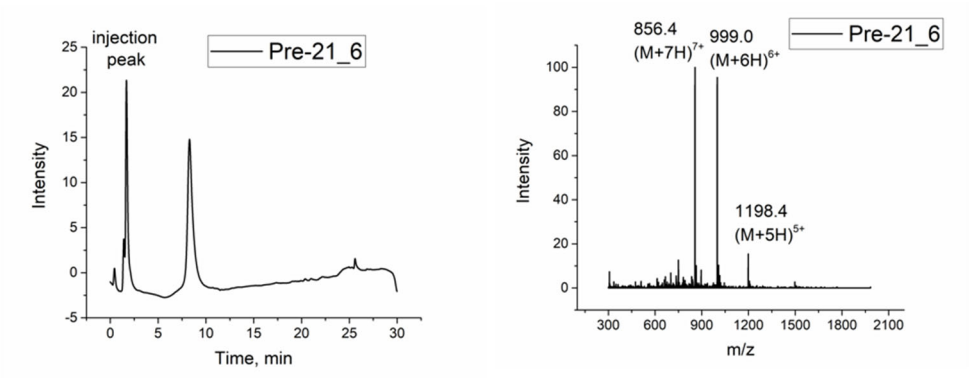

K3: C-K(FAM)-(Pre-21_1)-KKK

HPLC-MS: HPLC spectrum ($UV_{\lambda=260\ nm}$), ESI-MS – m/z =1690.5 $((M+3H)^{3+}$, calc.: 1689.7), 1268.1 $((M+4H)^{4+}$, calc.: 1267.5), 1014.7 $((M+5H)^{5+}$, calc.: 1014.2), 845.8 $((M+6H)^{6+}$, calc.: 845.4), 725.1 $((M+7H)^{7+}$, calc.: 724.7), 634.6 $((M+8H)^{8+}$, calc.: 634.3), 564.3 $((M+9H)^{9+}$, calc.: 563.9), 508.0 $((M+10H)^{10+}$, calc.: 507.6), Formula: $C_{210}\ H_{264}\ N_{100}\ O_{53}\ S_1$, MW_{exp}= 5068.92 g*mol^{-1} (MW_{calc} = 5069.046 g*mol^{-1}), Exact $Mass_{calc}$= 5066.0748 g*mol^{-1};

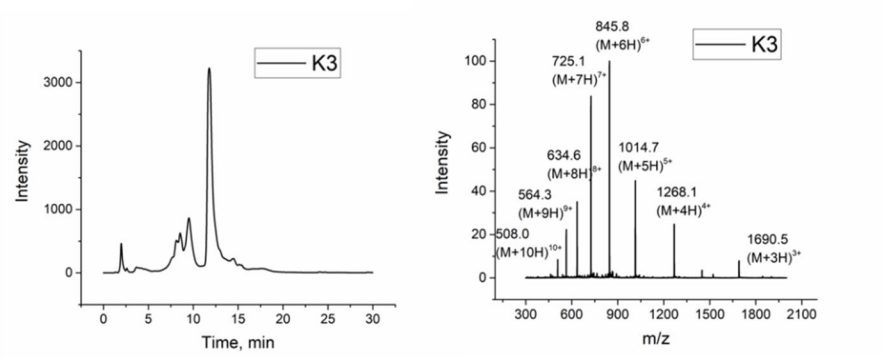

(RAhexR)$_4$: C-K(FAM)- (Pre-21_1)-GG-(RAhexR)$_4$ Ahex β

HPLC-MS: HPLC spectrum ($UV_{\lambda=260\ nm}$), ESI-MS – m/z =1115.0 $((M+6H)^{6+}$, calc.: 1114.5), 956.0 $((M+7H)^{7+}$, calc.: 955.5), 836.6 $((M+8H)^{8+}$, calc.: 836.1), 743.8 $((M+9H)^{9+}$, calc.: 743.4), 669.5 $((M+10H)^{10+}$, calc.: 669.1), 608.8 $((M+11H)^{11+}$, calc.: 608.4), 558.1 $((M+12H)^{12+}$, calc.: 557.8), 515.3 $((M+13H)^{13+}$, calc.: 514.9), 478.5 $((M+14H)^{14+}$, calc.: 478.2), Formula: $C_{277}\ H_{390}\ N_{134}\ O_{66}\ S_1$, MW_{exp}= 6684.97 (MW_{calc} = 6684.9832 g*mol^{-1}), MW_{exp} +1TFA = 6798.63 g*mol^{-1} (MW_{calc}+1TFA = 6799.00 g*mol^{-1}), MW_{exp} +2TFA = 6912.46 g*mol^{-1} (MW_{calc}+2TFA = 6913.02 g*mol^{-1}), MW_{exp} +3TFA = 7026.29 g*mol^{-1} (MW_{calc}+3TFA = 7027.02 g*mol^{-1}), Exact $Mass_{calc}$= 6681.0988g*mol^{-1}; On the MS-spectra the peaks are corresponded to the mass of compound and mass of compound with 1*TFA/ 2*TFA/ 3*TFA.

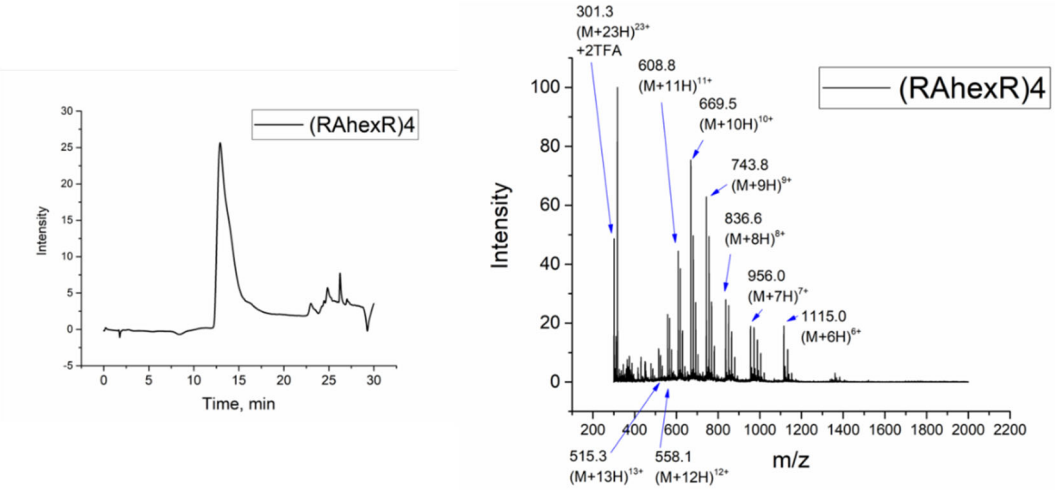

TAT: C-K(FAM)- (Pre-21_1)-GG-RRRQRRKKR

HPLC-MS: HPLC spectrum ($UV_{\lambda=260\ nm}$), ESI-MS – m/z = 1530.6 ($(M+4H)^{4+}$, calc.: 1530.2), 1224.9 ($(M+5H)^{5+}$, calc.: 1224.3), 1021.0 ($(M+6H)^{6+}$, calc.: 1020.5), Formula: $C_{249}\ H_{338}\ N_{126}\ O_{62}\ S_1$, MW_{exp}= 6119.72 g*mol^{-1} (MW_{calc} = 6120.2197 g*mol^{-1}), Exact $Mass_{calc}$= 6116.6878 g*mol^{-1}; On the MS-spectra the desired compound contains ~20% of non-FAM-labelled impurity (ESI-MS – m/z = 1559.3 ($(M+2H)^{2+}$, calc.: 1559.4), 1040.0 ($(M+3H)^{3+}$, calc.: 1039.9), $MW_{truncated\ sequence}$ = 3116.78 g*mol^{-1}).

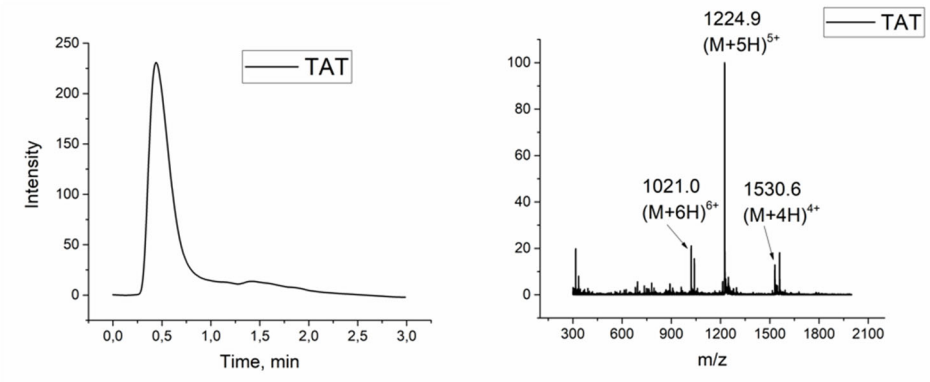

Pre-21_5_CPP: C-K- gccatgagattcaacagtc -GG-$(RAhexR)_4$ Ahex β

UPLC-MS: HPLC spectrum ($UV_{\lambda=260\ nm}$), on the MS-spectra the peaks are corresponded to the mass of compound and mass of compound with 1*TFA/ 2*TFA/ 3*TFA/ 4*TFA. ESI-MS – m/z = 1056.1/ 1071.9/ 1088.8/ 1105.1/ 1121.0 ($(M+7H)^{7+}$, calc.: 1055.6/ 1071.9 (1*TFA)/ 1088.2 (2*TFA)/ 1104.5 (3*TFA), 1120.8 (4*TFA)); 938.6/ 952.8/ 967.1/ 981.4 ($(M+8H)^{8+}$, calc.: 938.1 (1*TFA)/ 952.3 (2*TFA)/ 966.6 (3*TFA)/ 980.8 (4*TFA)); 821.8/ 834.4/ 846.9/ 859.5 ($(M+9H)^{9+}$, calc.: 821.3/ 834.0 (1*TFA)/ 846.6 (2*TFA)/ 859.3 (3*TFA)); 739.8/ 751.1/ 762.7/ 773.2 ($(M+10H)^{10+}$, calc.: 739.3/ 750.7 (1*TFA)/ 762.1 (2*TFA)/ 773.5(3*TFA)); 672.7/ 682.9 ($(M+11H)^{11+}$, calc.: 672.1/ 682.5 (1*TFA)); 616.85 ($(M+12H)^{12+}$, calc.: 616.2); Formula: $C_{298}\ H_{433}\ N_{155}\ O_{73}\ S_1$, MW_{calc} = 7386.6857 g*mol^{-1}, Exact $Mass_{calc}$= 7382.4642 g*mol^{-1}, 7496.4842 g*mol^{-1} (1*TFA), 7610.5042 g*mol^{-1} (2*TFA), 7724.5242 g*mol^{-1} (3*TFA), 7838.5442 g*mol^{-1} (4*TFA); multiple peaks are due to multiple TFA adducts.

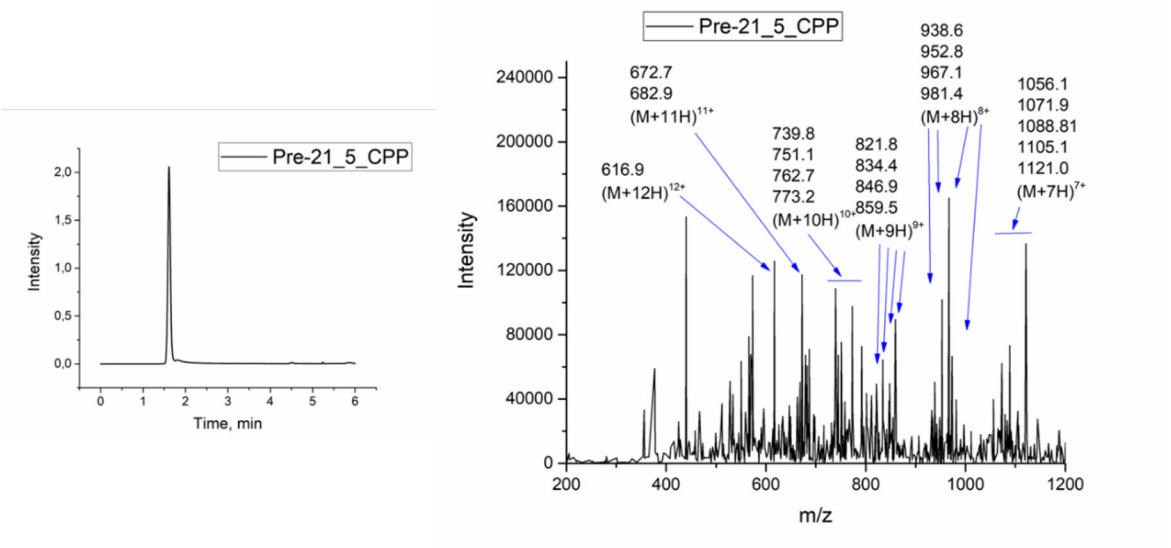

PNAmat21_CPP: C-K- tcaacatcagtctgataagcta- GG-$(RAhexR)_4$ Ahex β

UPLC-MS: HPLC spectrum ($UV_{\lambda=260\ nm}$), on the MS-spectra the peaks are corresponded to the mass of compound and mass of compound with 1*TFA/ 2*TFA/ 3*TFA/ 4*TFA. ESI-MS – m/z = 1234.2 $((M+7H)^{7+}$, calc.: 1233.8 (4*TFA)); 1080.5 $((M+8H)^{8+}$, calc.: 1079.7 (4*TFA)); 947.7 $((M+9H)^{9+}$, calc.: 947.2 (3*TFA); 819.0 $((M+10H)^{10+}$, calc.: 818.4), 744.7 $((M+11H)^{11+}$, calc.: 744.1); 682.7/ 692.5 $((M+12H)^{12+}$, calc.: 682.2/ 691.7 (1*TFA)); Formula: $C_{331}\ H_{474}\ N_{170}\ O_{82}\ S_1$, MW_{calc} = 8178.4593 g*mol^{-1}, Exact $Mass_{calc}$= 8173.7852 g*mol^{-1}, 8287.805 g*mol^{-1} (1*TFA), 8401.825 g*mol^{-1} (2*TFA), 8515.845 g*mol^{-1} (3*TFA), 8629.865 g*mol^{-1} (4*TFA); multiple peaks are due to multiple TFA adducts, compound contains some part of truncated sequences.

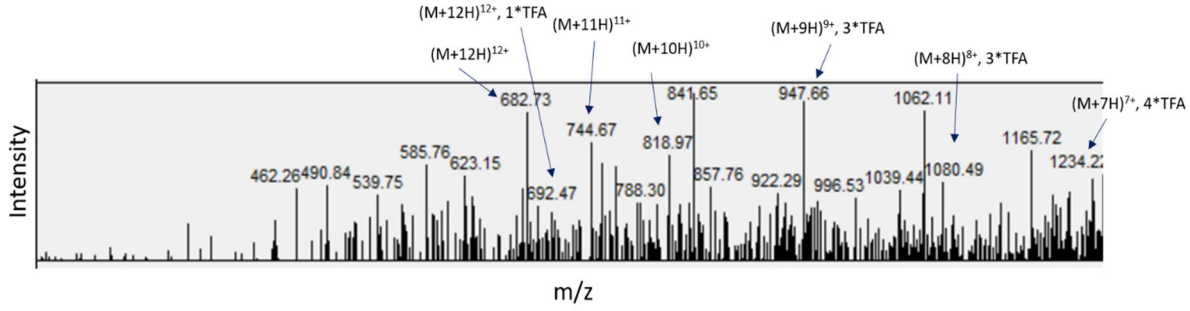

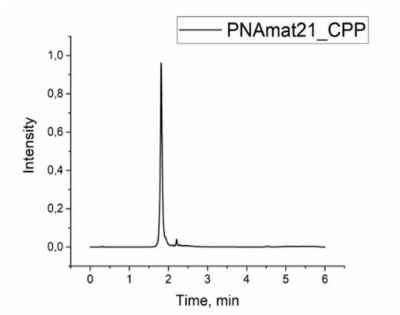

To the chapter 3.2:

Pre-21_1*_1: C-K- gagattcaa(TO)agtca - GG-(RAhexR)$_4$ Ahex β

UPLC-MS: HPLC spectrum (UV$_{\lambda=260\ nm}$), on the MS-spectra the peaks are corresponded to the mass of compound and mass of compound with 1*TFA/ 2*TFA/ 3*TFA/ 4*TFA. ESI-MS – m/z = 1085.3/ 1104.4/ 1123.6/ 1141.76 ((M+6H)$^{6+}$, calc.: 1084.9/ 1103.9 (1*TFA)/ 1122.9 (2*TFA)/ 1141.9 (3*TFA), 1160.9 (4*TFA)); 930.8/ 946.1/ 962.4/ 979.6 ((M+7H)$^{7+}$, calc.: 930.0/ 946.3 (1*TFA)/ 962.6 (2*TFA)/ 978.9 (3*TFA)); 814.3/ 828.9/ 843.0 ((M+8H)$^{8+}$, calc.: 813.9/ 828.1 (1*TFA)/ 842.4 (2*TFA))); 726.2/ 736.7 ((M+9H)$^{9+}$, calc.: 726.6/ 736.2 (1*TFA)); 651.5 ((M+10H)$^{10+}$, calc.: 651.3); Formula: C_{270} H_{390} N_{133} O_{59} S_2, MW_{calc} = 6506.9908 g*mol^{-1}, Exact $Mass_{calc}$= 6503.1093 g*mol^{-1}, 6617.1293 g*mol^{-1} (1*TFA), 6731.1493 g*mol^{-1} (2*TFA), 6845.1693 g*mol^{-1} (3*TFA), 6959.1893 g*mol^{-1} (4*TFA); multiple peaks are due to multiple TFA adducts.

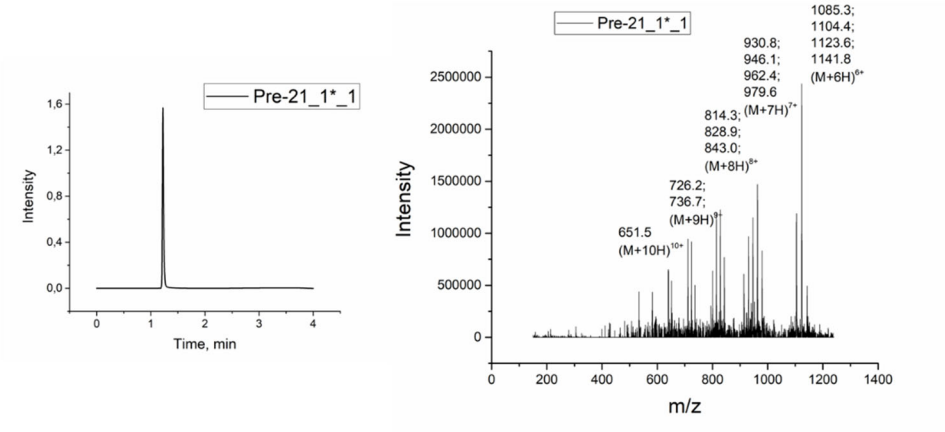

Pre-21_1*_2: C-K- gagattc(TO)acagtca - GG-(RAhexR)$_4$ Ahex β

UPLC-MS: HPLC spectrum (UV$_{\lambda=260\ nm}$), on the MS-spectra the peaks are corresponded to the mass of compound and mass of compound with 1*TFA/ 2*TFA/ 3*TFA/ 4*TFA. ESI-MS – m/z = 1080.5/ 1100.5/ 1118.8/ 1138.5 ((M+6H)$^{6+}$, calc.: 1080.9/ 1099.9 (1*TFA)/ 1118.9 (2*TFA)/ 1137.9 (3*TFA), 1156.9 (4*TFA)); 926.6/ 943.2/ 959.8/ 975.8 ((M+7H)$^{7+}$, calc.: 926.6/ 942.9 (1*TFA)/ 959.2 (2*TFA)/ 975.5 (3*TFA)); 811.1/ 825.7/ 839.2 ((M+8H)$^{8+}$, calc.: 810.9/ 825.1 (1*TFA)/ 839.4 (2*TFA))); 721.0/ 733.5 ((M+9H)$^{9+}$, calc.: 720.9/ 733.6 (1*TFA)); 641.9 ((M+11H)$^{11+}$, calc.: 641.8 (5*TFA)), 579.6 ((M+12H)$^{12+}$, calc.: 578.9 (4*TFA)); Formula: C_{269} H_{390} N_{131} O_{60} S_2, MW_{calc} = 6482.9661 g*mol^{-1}, Exact $Mass_{calc}$= 6479.0981 g*mol^{-1}, 6593.1181 g*mol^{-1} (1*TFA), 6707.1381 g*mol^{-1} (2*TFA), 6821.1581 g*mol^{-1} (3*TFA), 6935.1781 g*mol^{-1} (4*TFA), 7049.1781 g*mol^{-1} (5*TFA); multiple peaks are due to multiple TFA adducts.

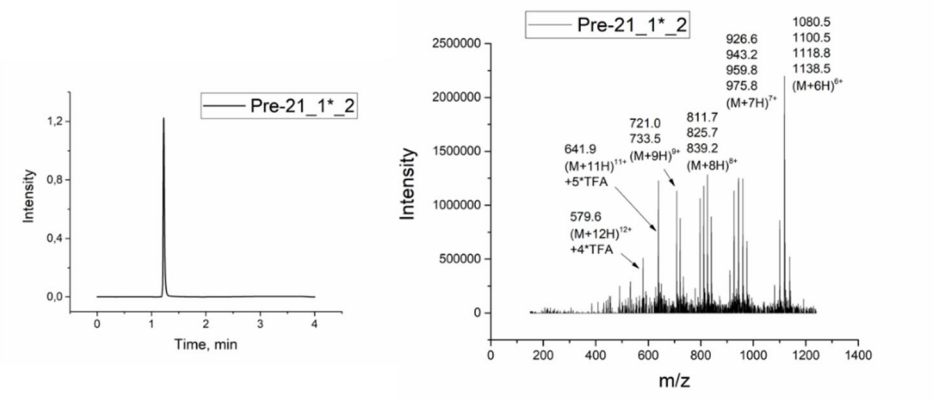

Pre-21_5*_1: C-K- gccatga(TO)attcaacagtc- GG-(RAhexR)$_4$ Ahex β

UPLC-MS: HPLC spectrum (UV$_{\lambda=260\ nm}$), on the MS-spectra the peaks are corresponded to the mass of compound and mass of compound with 1*TFA/ 2*TFA/ 3*TFA/ 4*TFA. ESI-MS – m/z = 1076.0/ 1092.0/ 1108.3/ 1124.2 ((M+7H)$^{7+}$, calc.: 1075.7/ 1091.9 (1*TFA)/ 1108.2 (2*TFA)/ 1124.5 (3*TFA)); 941.3/ 956.0/ 971.0/ 984.7 ((M+8H)$^{8+}$, calc.: 941.3/ 955.6 (1*TFA)/ 969.8 (2*TFA)/ 984.1 (3*TFA)); 836.6/ 851.0/ 862.8 ((M+9H)$^{9+}$, calc.: 836.8/ 849.5 (1*TFA)/ 862.2 (2*TFA))); 753.9/ 764.8 ((M+10H)$^{10+}$, calc.: 753.3/ 764.7 (1*TFA)); 685.0/ 695.8 ((M+11H)$^{11+}$, calc.: 684.9/ 695.2 (1*TFA)), 628.2 ((M+12H)$^{12+}$, calc.: 627.9); Formula: $C_{311}H_{443}N_{152}O_{72}S_2$, MW$_{calc}$ = 7526.9697 g*mol^{-1}, Exact Mass$_{calc}$= 7522.5162 g*mol^{-1}, 7636.5362 g*mol^{-1} (1*TFA), 7750.5562 g*mol^{-1} (2*TFA), 7864.5762 g*mol^{-1} (3*TFA), 7978.5962 g*mol^{-1} (4*TFA), 8092.6162 g*mol^{-1} (5*TFA); multiple peaks are due to multiple TFA adducts.

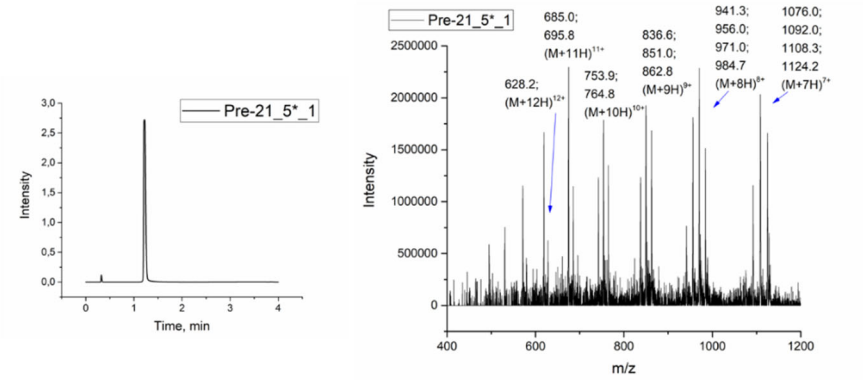

Pre-21_5*_3: C-K- gccatgagattc(TO)acagtc- GG-(RAhexR)$_4$ Ahex β

UPLC-MS: HPLC spectrum (UV$_{\lambda=260\ nm}$), on the MS-spectra the peaks are corresponded to the mass of compound and mass of compound with 1*TFA/ 2*TFA/ 3*TFA/ 4*TFA. ESI-MS – m/z = 1078.3/ 1094.2/ 1110.8/ 1126.7 ((M+7H)$^{7+}$, calc.: 1077.9/ 1094.2 (1*TFA)/ 1110.5 (2*TFA)/ 1126.8 (3*TFA)); 943.9/ 958.2/ 971.6/ 986.6 ((M+8H)$^{8+}$, calc.: 943.3/ 957.6 (1*TFA)/ 971.8 (2*TFA)/ 986.6 (3*TFA)); 838.9/ 851.6/ 864.1 ((M+9H)$^{9+}$, calc.: 838.6/ 851.3 (1*TFA)/ 864.0 (2*TFA))); 755.2/ 766.1 ((M+10H)$^{10+}$, calc.: 754.9/ 766.3 (1*TFA)); 686.3/ 697.4 ((M+11H)$^{11+}$, calc.: 686.3/ 696.7 (1*TFA)), 630.4 ((M+12H)$^{12+}$, calc.: 629.2); 677.0 ((M+12H)$^{12+}$, calc.: 676.7 (5*TFA)); 580.6 ((M+13H)$^{13+}$, calc.: 580.9); 572.6 ((M+14H)$^{14+}$, calc.: 572.1 (4*TFA)); Formula: $C_{311}H_{443}N_{152}O_{73}S_2$, MW$_{calc}$ = 7542.9691 g*mol^{-1}, Exact Mass$_{calc}$= 7538.5112 g*mol^{-1}, 7652.5312 g*mol^{-1} (1*TFA), 7766.5512 g*mol^{-1} (2*TFA), 7880.5712 g*mol^{-1} (3*TFA), 7994.5912 g*mol^{-1} (4*TFA), 8108.6112 g*mol^{-1} (5*TFA); multiple peaks are due to multiple TFA adducts.

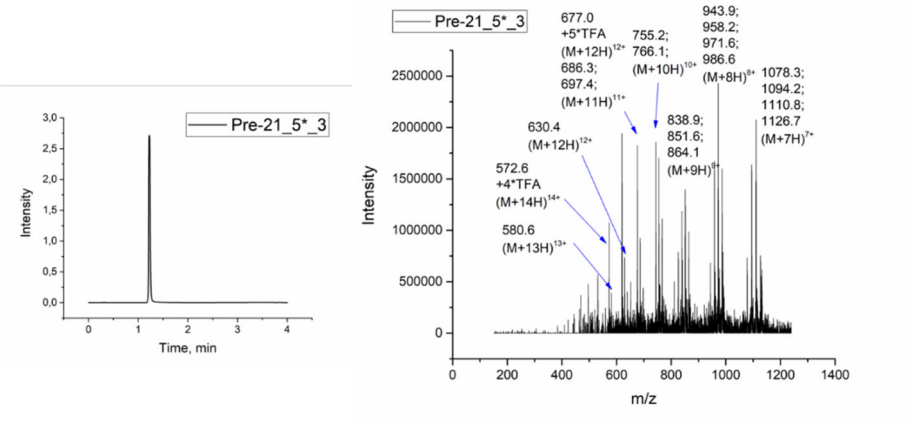

Pre-21_1*_2_mm1: C-K- gagatta(TO)ccagtca- GG-$(RAhexR)_4$ Ahex β

UPLC-MS: HPLC spectrum ($UV_{\lambda=260\ nm}$), on the MS-spectra the peaks are corresponded to the mass of compound and mass of compound with 1*TFA/ 2*TFA/ 3*TFA/ 4*TFA. ESI-MS – m/z = 1100.3/ 1119.4/ 1138.5/ 1156.8 $((M+6H)^{6+}$, calc.: 1099.9 (1*TFA)/ 1118.9 (2*TFA)/ 1137.9 (3*TFA), 1156.9 (4*TFA)); 943.9/ 959.8/ 976.1/992.0 $((M+7H)^{7+}$, calc.: 926.6/ 942.9 (1*TFA)/ 959.2 (2*TFA)/ 975.5 (3*TFA)/ 991.7 (4*TFA)); 810.1/ 825.1/ 838.9/ 853.9/ 867.9 $((M+8H)^{8+}$, calc.: 810.9/ 825.1 (1*TFA)/ 839.4 (2*TFA)/ 853.7 (3*TFA)/ 867.9 (4*TFA)); 721.1/ 734.2/ 746.6/ 759.4 $((M+9H)^{9+}$, calc.: 720.9/ 733.6 (1*TFA)/ 746.2 (2*TFA)/ 758.9 (3*TFA)); 649.2/ 660.4 $((M+10H)^{10+}$, calc.: 648.9/ 660.3 (1*TFA)), 590.8/ 601.0 $((M+11H)^{11+}$, calc.: 590.0/ 600.4 (1*TFA)); 541.0 $((M+12H)^{10+}$, calc.: 540.9); Formula: $C_{269}\ H_{390}\ N_{131}\ O_{60}\ S_2$, MW_{calc} = 6482.9661 g*mol^{-1}, Exact $Mass_{calc}$= 6479.0981 g*mol^{-1}, 6593.1181 g*mol^{-1} (1*TFA), 6707.1381 g*mol^{-1} (2*TFA), 6821.1581 g*mol^{-1} (3*TFA), 6935.1781 g*mol^{-1} (4*TFA), 7049.1781 g*mol^{-1} (5*TFA); multiple peaks are due to multiple TFA adducts.

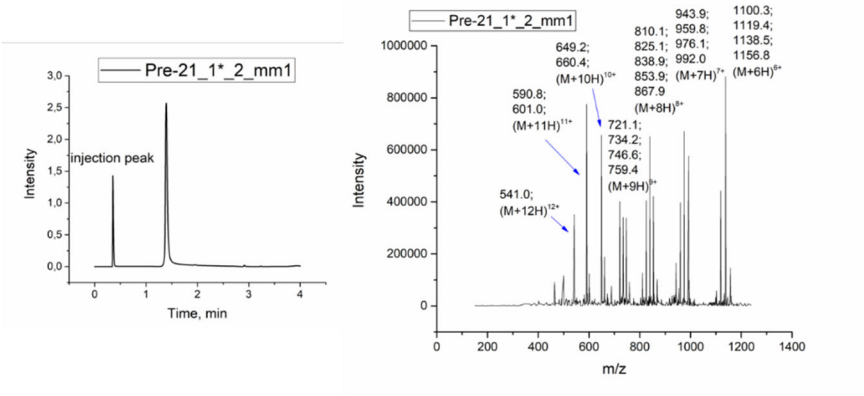

Pre-21_1*_2_mm2: C-K- gaggttc(TO)acaatca- GG-$(RAhexR)_4$ Ahex β

UPLC-MS: HPLC spectrum ($UV_{\lambda=260\ nm}$), on the MS-spectra the peaks are corresponded to the mass of compound and mass of compound with 1*TFA/ 2*TFA/ 3*TFA/ 4*TFA. ESI-MS – m/z = 1081.1/ 1100.0/ 1119.1/ 1138.6 $((M+6H)^{6+}$, calc.: 1080.9/ 1099.9 (1*TFA)/ 1118.9 (2*TFA)/ 1137.9 (3*TFA)); 926.9/ 943.2/ 959.1/ 975.8 $((M+7H)^{7+}$, calc.: 926.6/ 942.9 (1*TFA)/ 959.2 (2*TFA)/ 975.5 (3*TFA)); 811.4/ 825.8 $((M+8H)^{8+}$, calc.: 810.9/ 825.1 (1*TFA)); 720.4/ 733.8/ 797.4 $((M+9H)^{9+}$, calc.: 720.9/ 733.6 (1*TFA)/ 796.9 (6*TFA)); Formula: $C_{269}\ H_{390}\ N_{131}\ O_{60}\ S_2$, MW_{calc} = 6482.9661 g*mol^{-1}, Exact $Mass_{calc}$= 6479.0981 g*mol^{-1}, 6593.1181 g*mol^{-1} (1*TFA), 6707.1381 g*mol^{-1} (2*TFA), 6821.1581 g*mol^{-1} (3*TFA), 6935.1781 g*mol^{-1} (4*TFA), 7049.1781 g*mol^{-1} (5*TFA); 7163.1981 g*mol^{-1} (6*TFA); multiple peaks are due to multiple TFA adducts.

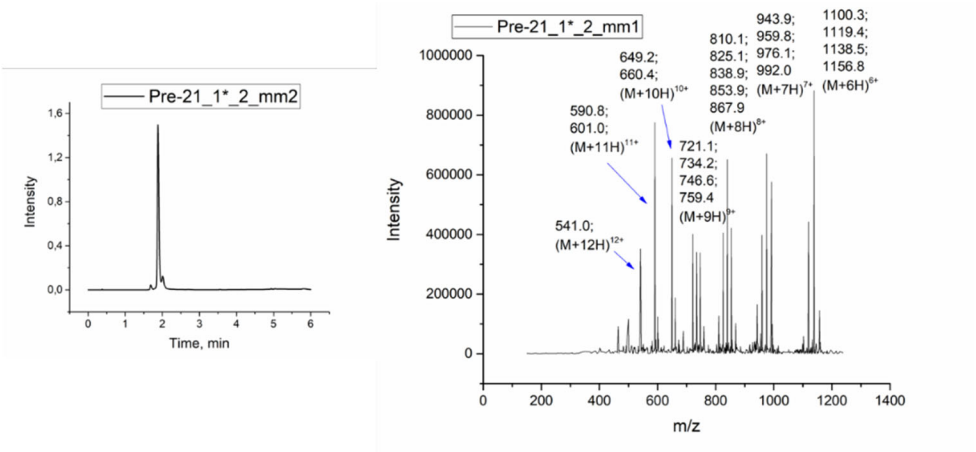

Pre-21_5*_3_mm: C-K- gccatgagatta(TO)ccagtc- GG-$(RAhexR)_4$ Ahex β

UPLC-MS: HPLC spectrum ($UV_{\lambda=260\ nm}$), on the MS-spectra the peaks are corresponded to the mass of compound and mass of compound with 1*TFA/ 2*TFA/ 3*TFA/ 4*TFA. ESI-MS – m/z = 1094.5/ 1110.2/ 1126.1/ 1143.4 $((M+7H)^{7+}$, calc.: 1094.2 (1*TFA)/ 1110.5 (2*TFA)/ 1126.8 (3*TFA)/ 1143.1(4*TFA)); 956.9/ 972.0/ 986.3/ 1001.0 $((M+8H)^{8+}$, calc.: 957.6 (1*TFA)/ 971.8 (2*TFA)/ 986.6 (3*TFA)/ 1000.3 (4*TFA)); 838.9/ 851.6/ 864.4/ 876.8 $((M+9H)^{9+}$, calc.: 838.6/ 851.3 (1*TFA)/ 864.0 (2*TFA)/ 876.6(3*TFA)); 754.9/ 766.6/ 778.2 $((M+10H)^{10+}$, calc.: 754.9/ 766.3 (1*TFA)/ 777.7 (2*TFA)); 686.9/ 697.4 $((M+11H)^{11+}$, calc.: 686.3/ 696.7 (1*TFA)), 639.0 $((M+12H)^{12+}$, calc.: 629.2); Formula: $C_{311}H_{443}N_{152}O_{73}S_2$, MW_{calc} = 7542.9691 g*mol^{-1}, Exact $Mass_{calc}$= 7538.5112 g*mol^{-1}, 7652.5312 g*mol^{-1} (1*TFA), 7766.5512 g*mol^{-1} (2*TFA), 7880.5712 g*mol^{-1} (3*TFA), 7994.5912 g*mol^{-1} (4*TFA); multiple peaks are due to multiple TFA adducts.

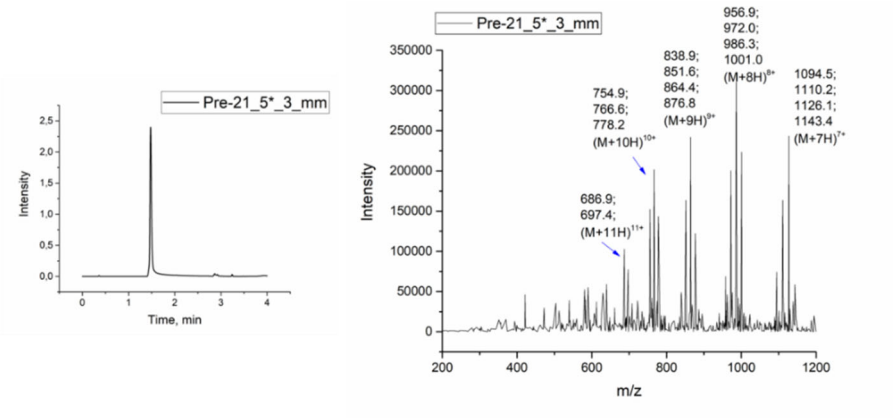

Viral mm: C-K- cagtta(TO)tatgccgttg- GG-$(RAhexR)_4$ Ahex β

UPLC-MS: HPLC spectrum ($UV_{\lambda=260\ nm}$), on the MS-spectra the peaks are corresponded to the mass of compound and mass of compound with 1*TFA/ 2*TFA/ 3*TFA/ 4*TFA. ESI-MS – m/z = 1189.9/ 1209.4/ 1227.8 $((M+6H)^{6+}$, calc.: 1189.7 (1*TFA)/ 1208.7 (2*TFA)/ 1227.7 (3*TFA)); 1020.1/ 1036.4/ 1052.7/ 1069.3 $((M+7H)^{7+}$, calc.: 1019.9 (1*TFA)/ 1036.2 (2*TFA)/ 1052.5 (3*TFA)/ 1068.8(4*TFA)); 878.7/ 892.4/ 906.7/ 920.8 $((M+8H)^{8+}$, calc.: 878.3/ 892.5 (1*TFA)/ 906.8 (2*TFA)/ 921.1 (3*TFA)); 780.8/ 793.9/ 806.1 $((M+9H)^{9+}$, calc.: 780.8/ 793.5 (1*TFA)/ 806.2 (2*TFA)); 703.3/ 714.9/ 726.2 $((M+10H)^{10+}$, calc.: 702.8/ 714.2 (1*TFA)/ 725.6 (2*TFA)); 639.2 $((M+11H)^{11+}$, calc.: 639.0), 586.4 $((M+12H)^{12+}$, calc.: 585.9); Formula: $C_{291}H_{419}N_{136}O_{71}S_2$, MW_{calc} = 7022.4585 g*mol^{-1}, Exact $Mass_{calc}$= 7018.2846 g*mol^{-1}, 7132.3046 g*mol^{-1} (1*TFA), 7246.3246 g*mol^{-1} (2*TFA), 7360.3446 g*mol^{-1} (3*TFA), 7474.3646 g*mol^{-1} (4*TFA); multiple peaks are due to multiple TFA adducts.

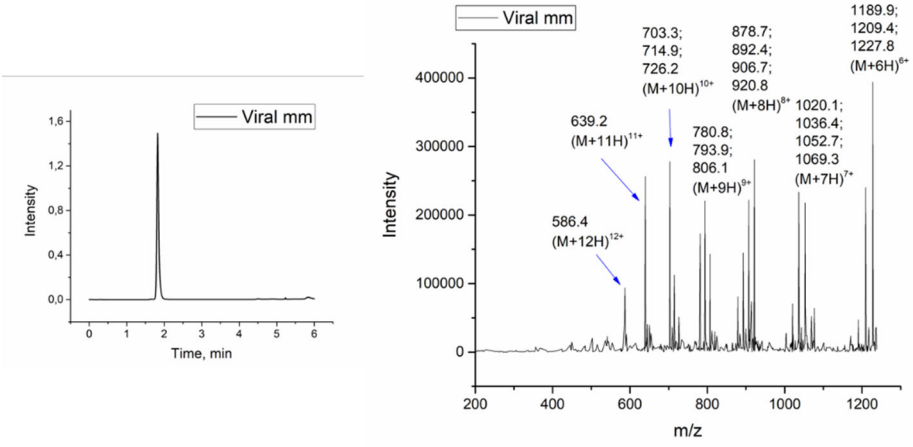

To the chapter 3.3:

TO1: ttg(TO)catgaga

UPLC-MS: UPLC spectrum ($UV_{\lambda=260\ nm}$), ESI-MS – m/z = 1066.19 ($(M+3H)^{3+}$, calc.: 1066.4), 800.29 ($(M+4H)^{4+}$, calc.: 800.1), Formula: $C_{133}H_{159}N_{64}O_{32}S_1$, MW_{calc} = 3198.1798 g*mol^{-1}, Exact $Mass_{calc}$=3196.2558 g*mol^{-1};

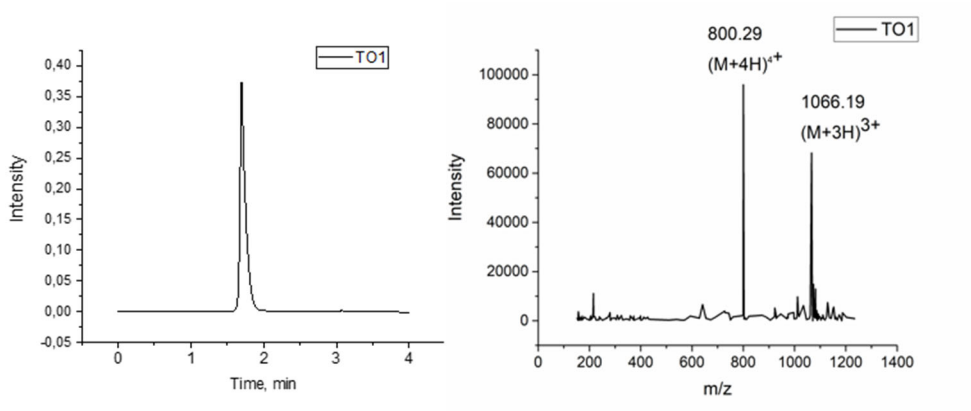

TO2: ttgc(TO)atgaga

UPLC-MS: UPLC spectrum ($UV_{\lambda=260\ nm}$), ESI-MS – m/z = 1066.8 ($(M+3H)^{3+}$, calc.: 1066.4), 800.3 ($(M+4H)^{4+}$, calc.: 800.1), Formula: $C_{133}H_{159}N_{64}O_{32}S_1$, MW_{calc} = 3198.1798 g*mol^{-1}, Exact $Mass_{calc}$=3196.2558 g*mol^{-1};

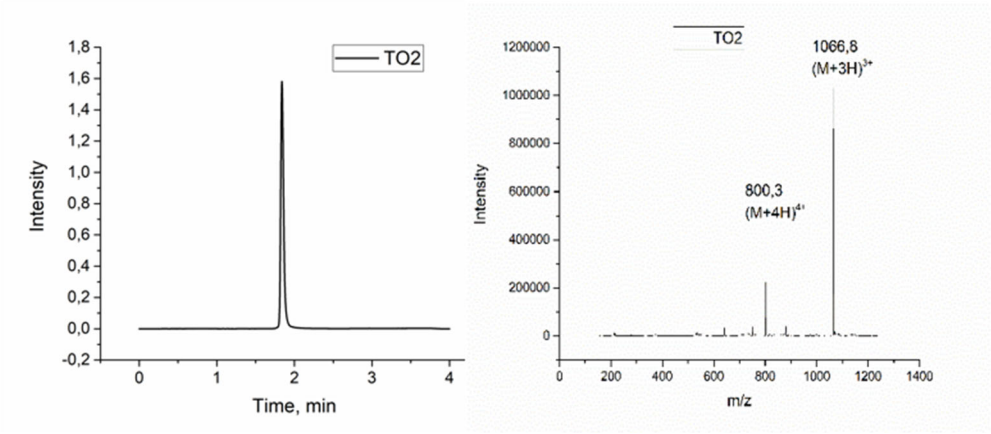

TO3: ttgcc(TO)tgaga

UPLC-MS: UPLC spectrum ($UV_{\lambda=260\ nm}$), ESI-MS – m/z = 1059.1 ($(M+3H)^{3+}$, calc.: 1058.4), 794.4 ($(M+4H)^{4+}$, calc.: 794.1), Formula: $C_{132}H_{159}N_{62}O_{33}S_1$, MW_{calc} = 3174.1551 g*mol^{-1}, Exact $Mass_{calc}$=3172.2446 g*mol^{-1};

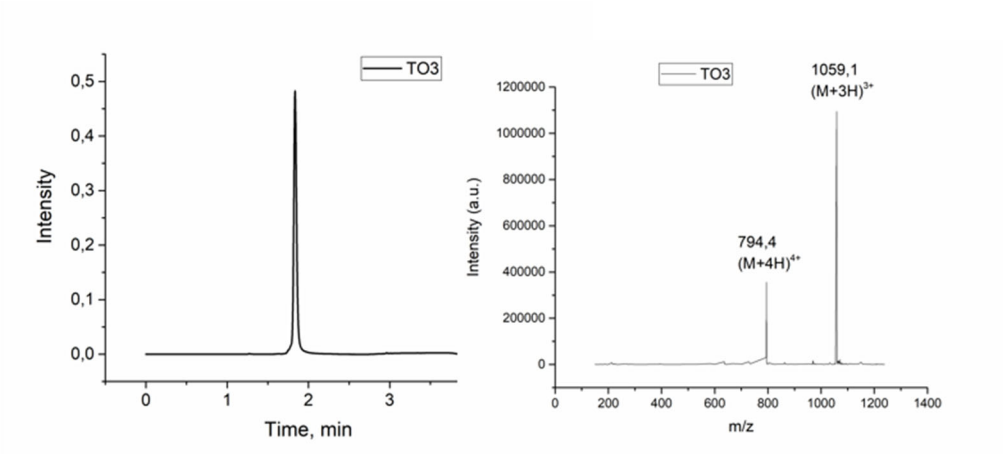

TO4: ttgcca(TO)gaga

UPLC-MS: UPLC spectrum ($UV_{\lambda=260\ nm}$), ESI-MS – m/z = 1061.5 ($(M+3H)^{3+}$, calc.: 1061.4), 796.7 ($(M+4H)^{4+}$, calc.: 796.3), Formula: $C_{132}H_{158}N_{65}O_{31}S_1$, MW_{calc} = 3183.1685 g*mol^{-1}, Exact $Mass_{calc}$=3181.2561 g*mol^{-1};

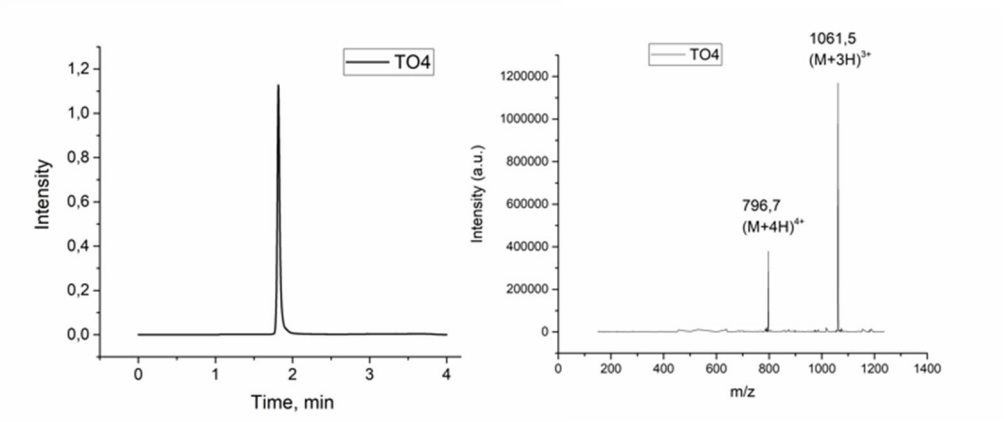

TO6: ttgccatg(TO)ga

UPLC-MS: UPLC spectrum ($UV_{\lambda=260\ nm}$), ESI-MS – m/z = 1058.4 ($(M+3H)^{3+}$, calc.: 1058.4), 794.3 ($(M+4H)^{4+}$, calc.: 794.1), Formula: $C_{132}H_{159}N_{62}O_{33}S_1$, MW_{calc} = 3174.1551 g*mol^{-1}, Exact $Mass_{calc}$=3172.2446 g*mol^{-1};

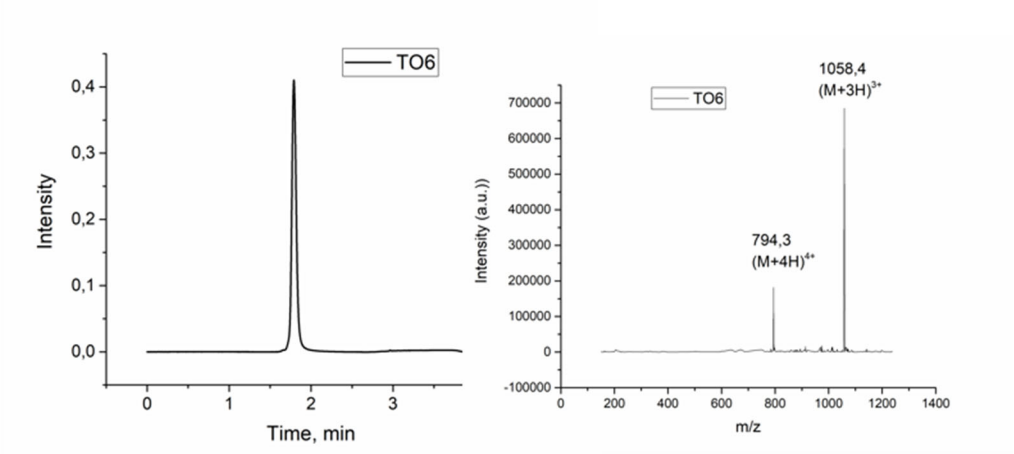

QB1: ttg(QB)catgaga

UPLC-MS: UPLC spectrum ($UV_{\lambda=260\ nm}$), ESI-MS – m/z = 1064.6 ($(M+3H)^{3+}$, calc.: 1064.4), 798.9 ($(M+4H)^{4+}$, calc.: 798.6), Formula: $C_{135}H_{161}N_{64}O_{32}$, MW_{calc} = 3192.1598 g*mol^{-1}, Exact $Mass_{calc}$=3190.3058 g*mol^{-1};

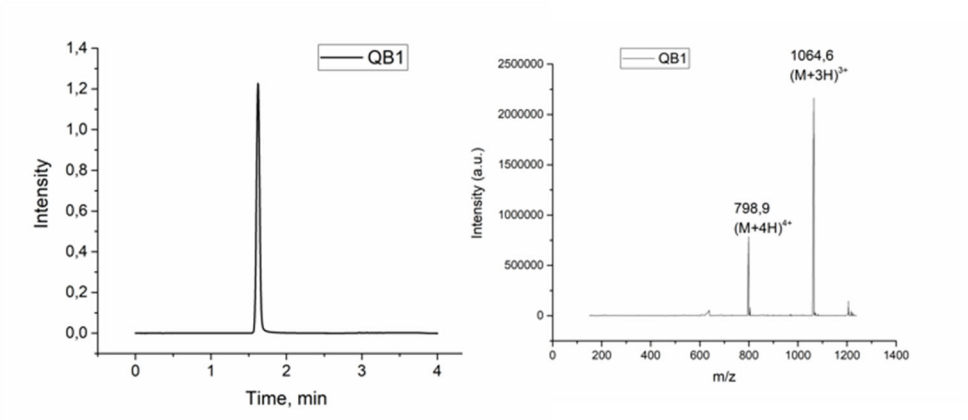

QB2: ttgc(QB)atgaga

UPLC-MS: UPLC spectrum ($UV_{\lambda=260\ nm}$), ESI-MS – m/z = 1064.6 ($(M+3H)^{3+}$, calc.: 1064.4), 798.8 ($(M+4H)^{4+}$, calc.: 798.6), Formula: $C_{135}H_{161}N_{64}O_{32}$, MW_{calc} = 3192.1598 g*mol^{-1}, Exact $Mass_{calc}$=3190.3058 g*mol^{-1};

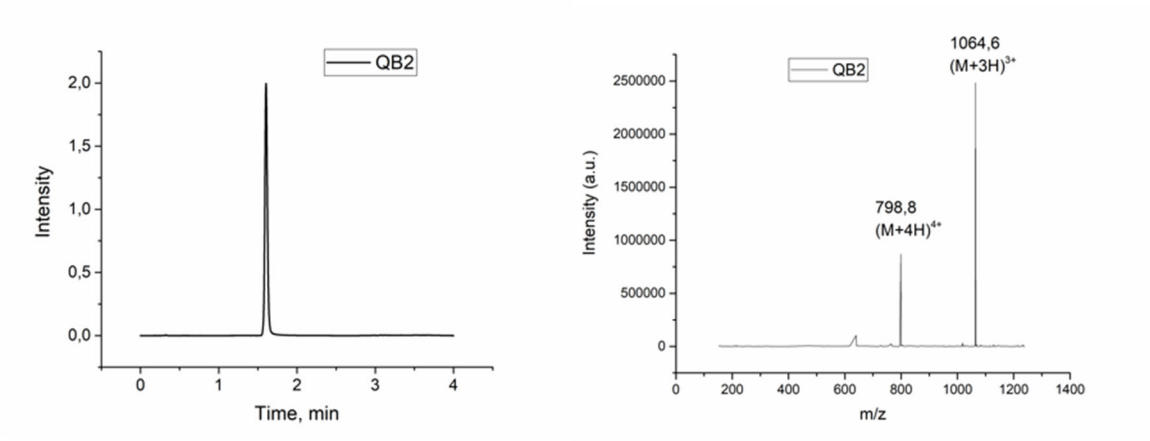

QB3: ttgcc(QB)tgaga

UPLC-MS: UPLC spectrum ($UV_{\lambda=260\ nm}$), ESI-MS – m/z = 1056.5 ($(M+3H)^{3+}$, calc.: 1056.4), 792.8 ($(M+4H)^{4+}$, calc.: 792.6), Formula: $C_{134}H_{161}N_{62}O_{33}$, MW_{calc} = 3168.1351 g*mol^{-1}, Exact $Mass_{calc}$=3166.2946 g*mol^{-1};

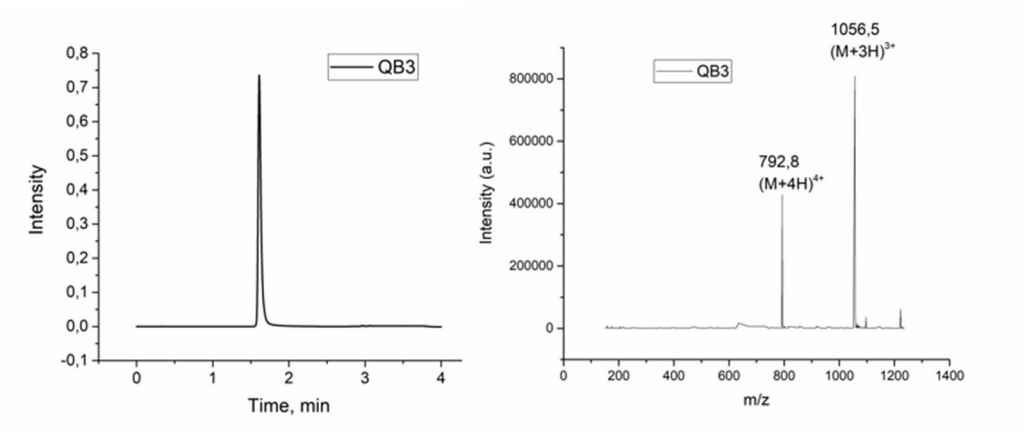

QB4: ttgcca(QB)gaga

UPLC-MS: UPLC spectrum ($UV_{\lambda=260\ nm}$), ESI-MS – m/z = 1059.6 $((M+3H)^{3+}$, calc.: 1059.4), 795.1 $((M+4H)^{4+}$, calc.: 794.8), Formula: $C_{134}H_{160}N_{65}O_{31}$, MW_{calc} = 3177.1485 g*mol^{-1}, Exact $Mass_{calc}$=3175.3061 g*mol^{-1};

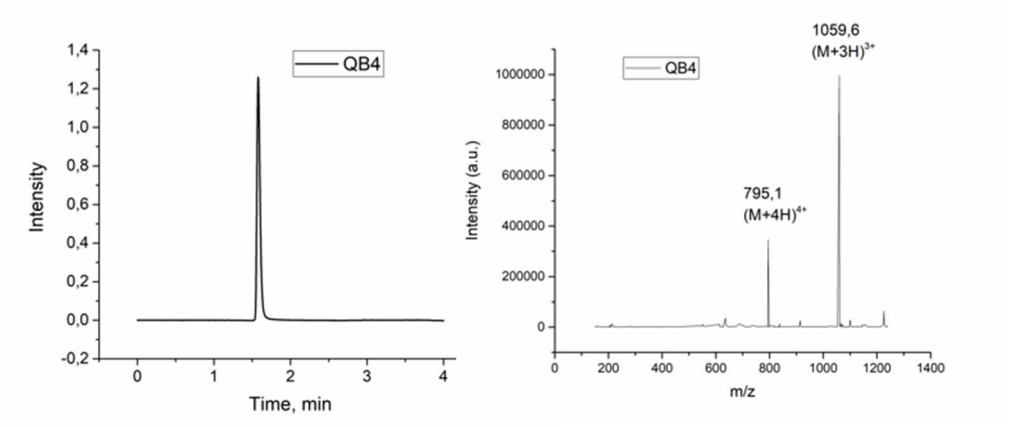

QB6: ttgccatg(QB)ga

UPLC-MS: UPLC spectrum ($UV_{\lambda=260\ nm}$), ESI-MS – m/z = 1056.6 $((M+3H)^{3+}$, calc.: 1056.4), 792.9 $((M+4H)^{4+}$, calc.: 792.6), 634.6 $((M+5H)^{5+}$, calc.: 634,3), Formula: $C_{134}H_{161}N_{62}O_{33}$, MW_{calc} = 3168.1351 g*mol^{-1}, Exact $Mass_{calc}$=3166.2946 g*mol^{-1};

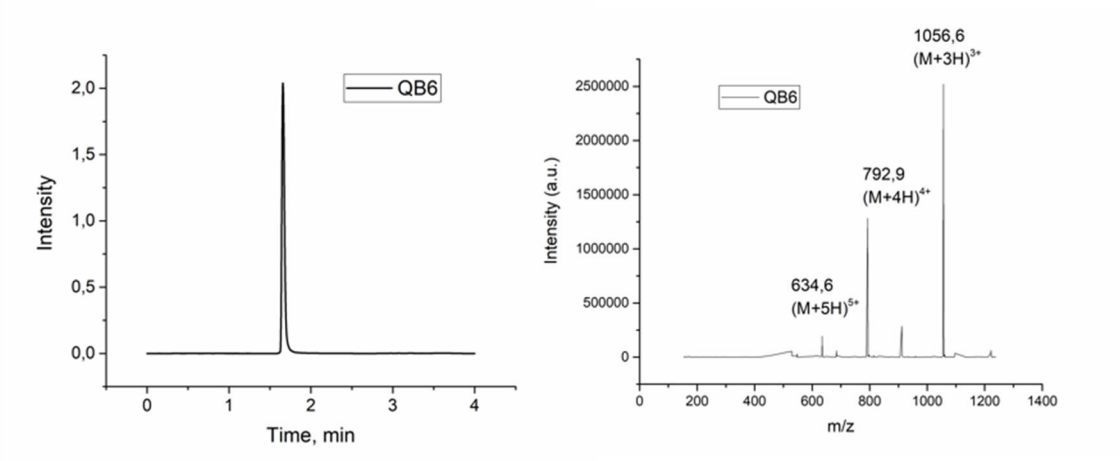

QB7: ttgccatga(QB)a

UPLC-MS: UPLC spectrum ($UV_{\lambda=260\ nm}$), ESI-MS – m/z = 1051.2 ($(M+3H)^{3+}$, calc.: 1051.1), 788.9 ($(M+4H)^{4+}$, calc.: 788.6), Formula: $C_{134}H_{161}N_{62}O_{32}$, MW_{calc} = 3152.1357 g*mol^{-1}, Exact $Mass_{calc}$=3150.2996 g*mol^{-1};

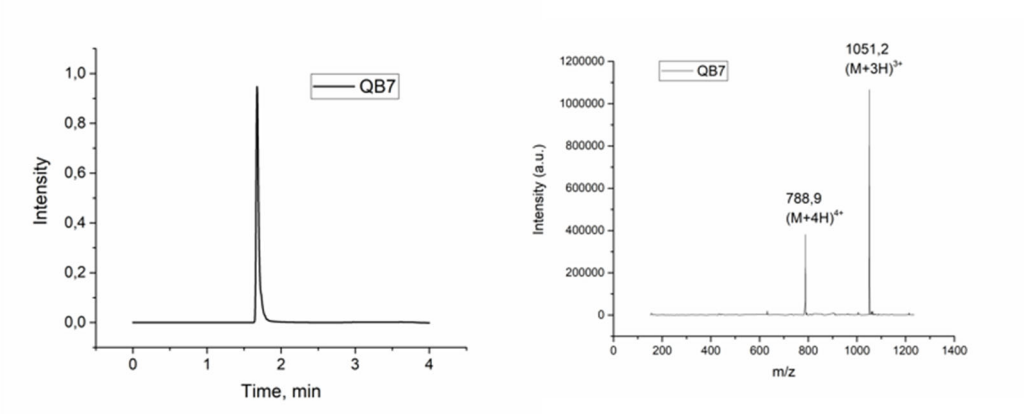

TO1*: ggtg(TO)tg

UPLC-MS: UPLC spectrum ($UV_{\lambda=260\ nm}$), ESI-MS – m/z = 1073.4 ($(M+2H)^{2+}$, calc.: 1073.4), 716.1 ($(M+3H)^{3+}$, calc.: 715.9), Formula: $C_{90}H_{106}N_{41}O_{22}S_1$, MW_{calc} = 2146.1509 g*mol^{-1}, Exact $Mass_{calc}$=2144.8215 g*mol^{-1};

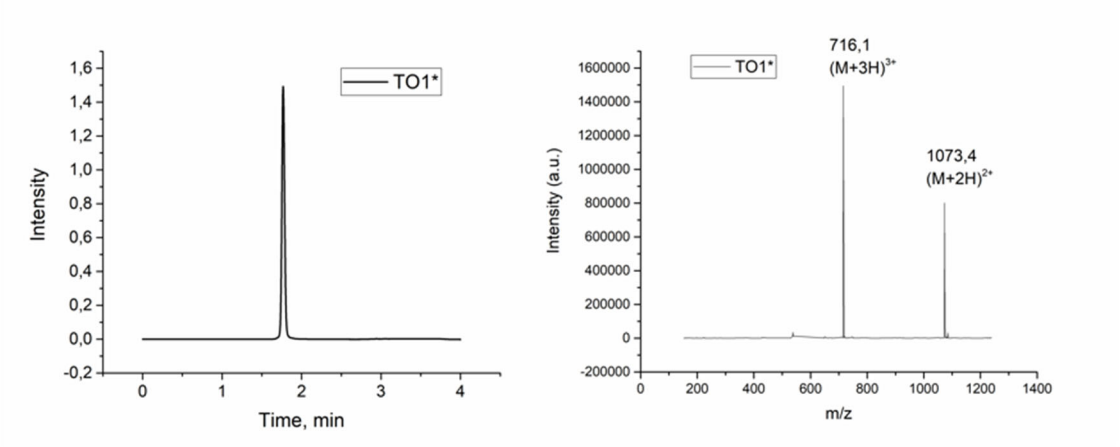

TO2*: ggt(TO)ttg

UPLC-MS: UPLC spectrum ($UV_{\lambda=260\ nm}$), ESI-MS – m/z = 1060.9 ($(M+2H)^{2+}$, calc.: 1060.9), 707.7 ($(M+3H)^{3+}$, calc.: 707.6), 531.0 ($(M+4H)^{4+}$, calc.: 531.0), Formula: $C_{90}H_{107}N_{32}O_{23}S_1$, MW_{calc} = 2121.1381 g*mol^{-1}, Exact $Mass_{calc}$=2119.815 g*mol^{-1};

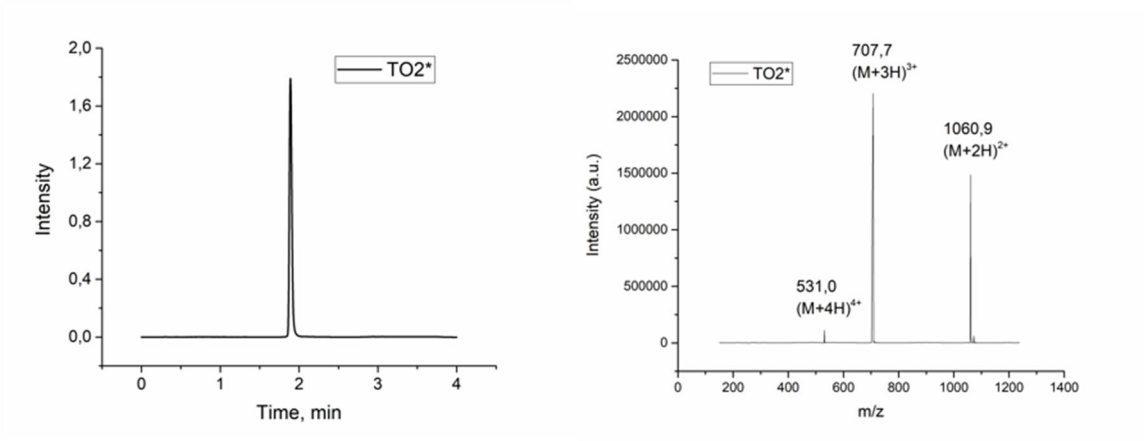

TO3*: gg(TO)gttg

UPLC-MS: UPLC spectrum ($UV_{\lambda=260\ nm}$), ESI-MS – m/z = 1073.3 ($(M+2H)^{2+}$, calc.: 1073.4), 715.8 ($(M+3H)^{3+}$, calc.: 715.9), Formula: $C_{90}H_{106}N_{41}O_{22}S_1$, MW_{calc} = 2146.1509 g*mol^{-1}, Exact $Mass_{calc}$=2144.8215 g*mol^{-1};

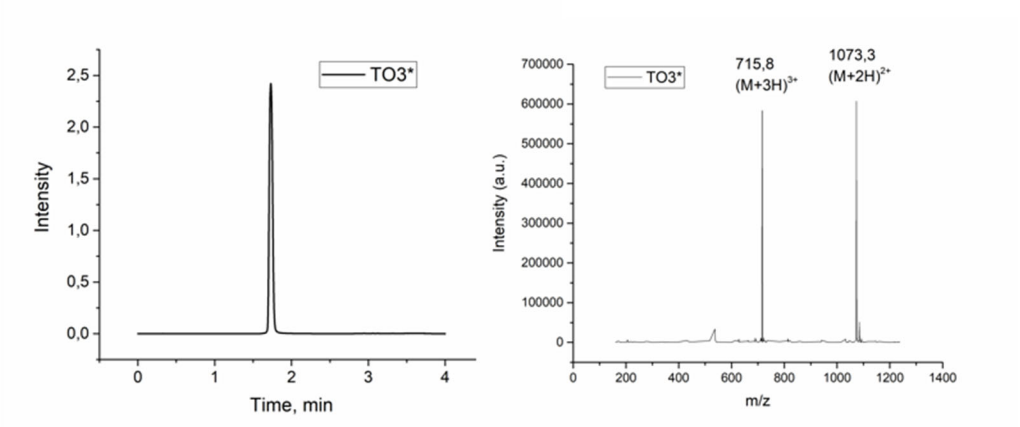

TO4*: g(TO)tgttg

UPLC-MS: UPLC spectrum ($UV_{\lambda=260\ nm}$), ESI-MS – m/z = 1061.0 ($(M+2H)^{2+}$, calc.: 1060.9), 707.8 ($(M+3H)^{3+}$, calc.: 707.6), Formula: $C_{90}H_{107}N_{32}O_{23}S_1$, MW_{calc} = 2121.1381 g*mol^{-1}, Exact $Mass_{calc}$=2119.815 g*mol^{-1};

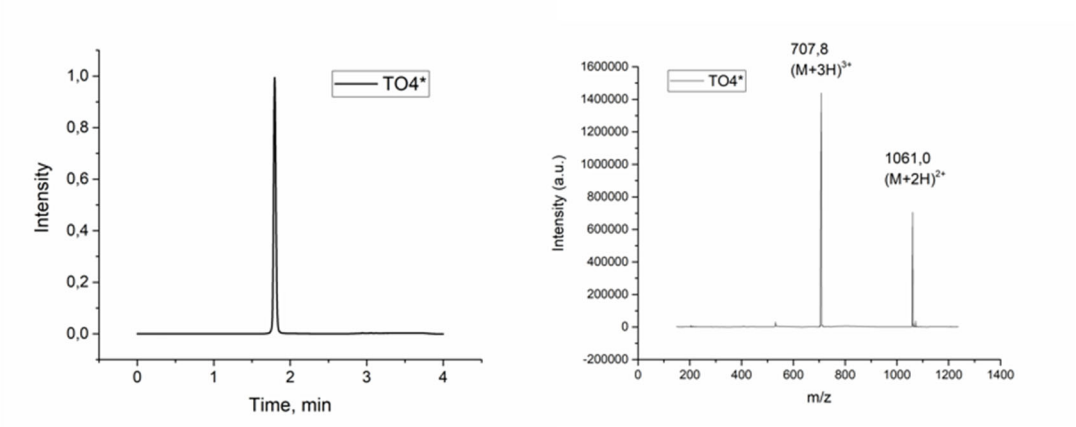

TO1*_8nt: tggtg(TO)tg

UPLC-MS: UPLC spectrum ($UV_{\lambda=260\ nm}$), ESI-MS – m/z = 1206.6 ($(M+2H)^{2+}$, calc.: 1206.5), 804.7 ($(M+3H)^{3+}$, calc.: 804.6), 603.8 ($(M+4H)^{4+}$, calc.: 603.7), Formula: $C_{101}H_{120}N_{45}O_{26}S_1$, MW_{calc} = 2412.4041 g*mol^{-1}, Exact $Mass_{calc}$=2410.923 g*mol^{-1};

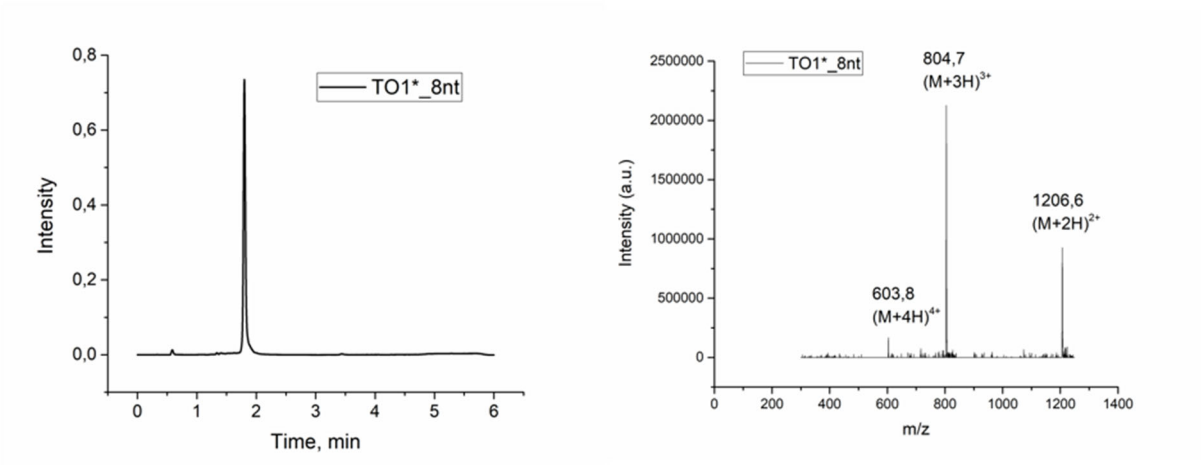

TO1*_9nt: ctggtg(TO)tg

UPLC-MS: UPLC spectrum ($UV_{\lambda=260\ nm}$), ESI-MS – m/z = 888.7 ($(M+3H)^{3+}$, calc.: 888.3), 667.1 ($(M+4H)^{4+}$, calc.: 666.5), Formula: $C_{111}H_{133}N_{50}O_{29}S_1$, MW_{calc} = 2663.646 g*mol^{-1}, Exact $Mass_{calc}$=2662.0248 g*mol^{-1};

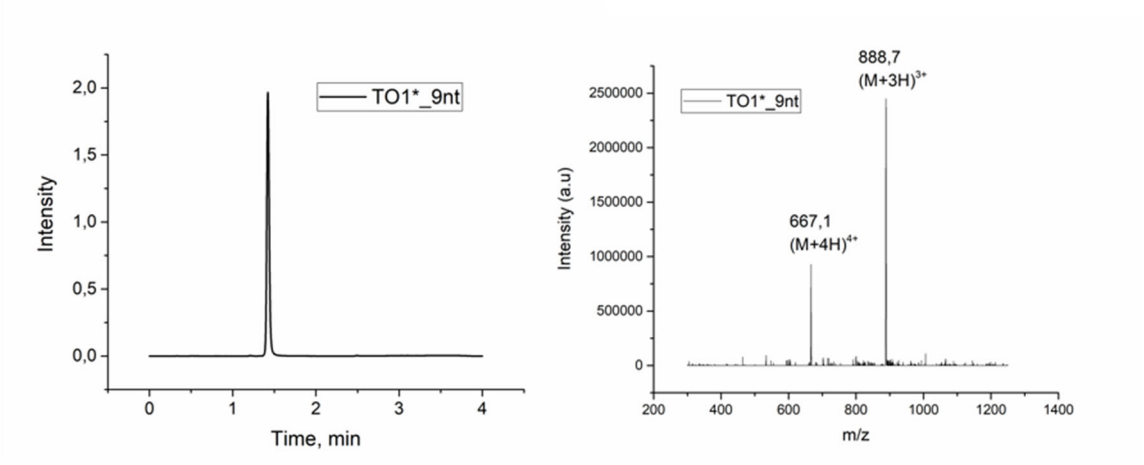

TO1*_10nt: actggtg(TO)tg

UPLC-MS: UPLC spectrum ($UV_{\lambda=260\ nm}$), ESI-MS – m/z = 980.2 ($(M+3H)^{3+}$, calc.: 980.1), 735.4 ($(M+4H)^{4+}$, calc.: 735.3), 588.6 ($(M+5H)^{5+}$, calc.: 588.4) Formula: $C_{122}H_{146}N_{57}O_{31}S_1$, MW_{calc} = 2938.9126 g*mol^{-1}, Exact $Mass_{calc}$=2937.1378 g*mol^{-1};

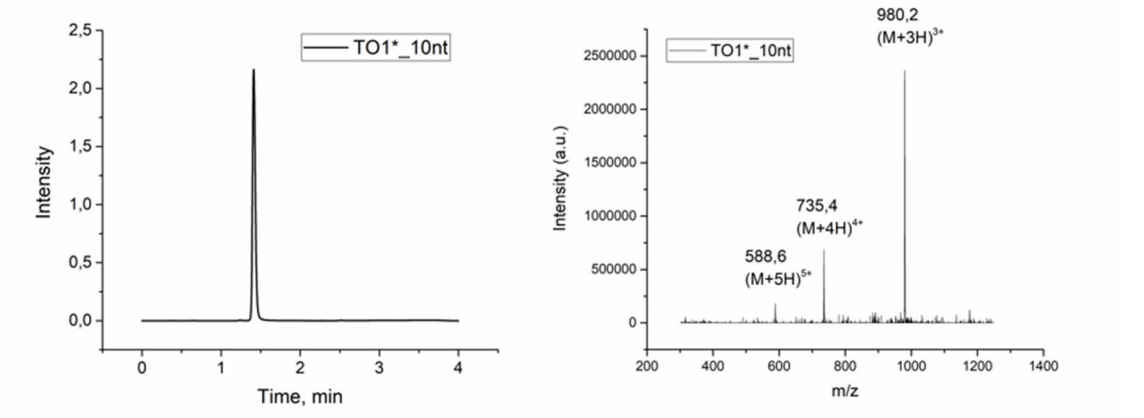

TO1*_11nt: gactggtg(TO)tg

UPLC-MS: UPLC spectrum ($UV_{\lambda=260\ nm}$), ESI-MS – m/z = 1077.4 ($(M+3H)^{3+}$, calc.: 1077.1), 808.2 ($(M+4H)^{4+}$, calc.: 808.1), 646.2 ($(M+5H)^{5+}$, calc.: 646.7) Formula: $C_{133}H_{159}N_{64}O_{34}S_1$, MW_{calc} = 3230.1786 g*mol^{-1}, Exact $Mass_{calc}$=3228.2458 g*mol^{-1};

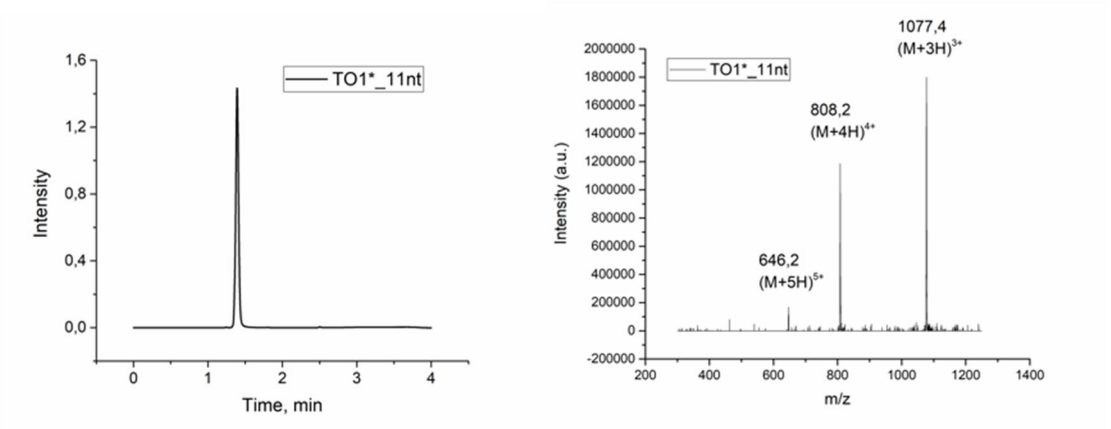

8 Literature

1. Dojahn, C. M., Synthese und Screening von Inhibitoren der mikroRNA-Reifung. *Dissertation* **2013**.
2. Rajewsky, N., microRNA target predictions in animals. *Nature genetics* **2006,** *38 Suppl*, S8-13.
3. Friedman, R. C.; Farh, K. K.; Burge, C. B.; Bartel, D. P., Most mammalian mRNAs are conserved targets of microRNAs. *Genome research* **2009,** *19* (1), 92-105.
4. Macfarlane, L. A.; Murphy, P. R., MicroRNA: Biogenesis, Function and Role in Cancer. *Current genomics* **2010,** *11* (7), 537-61.
5. Katti, P.; Thimmaya, D.; Madan, A.; Nongthomba, U., Overexpression of miRNA-9 Generates Muscle Hypercontraction Through Translational Repression of Troponin-T in Drosophila melanogaster Indirect Flight Muscles. *G3 (Bethesda, Md.)* **2017,** *7* (10), 3521-3531.
6. Li, Y.; Huo, C.; Pan, T.; Li, L.; Jin, X.; Lin, X.; Chen, J.; Zhang, J.; Guo, Z.; Xu, J.; Li, X., Systematic review regulatory principles of non-coding RNAs in cardiovascular diseases. *Briefings in bioinformatics* **2017**.
7. Kumarswamy, R.; Volkmann, I.; Thum, T., Regulation and function of miRNA-21 in health and disease. *RNA biology* **2011,** *8* (5), 706-13.
8. Han, J.; Lee, Y.; Yeom, K. H.; Kim, Y. K.; Jin, H.; Kim, V. N., The Drosha-DGCR8 complex in primary microRNA processing. *Genes Dev* **2004,** *18* (24), 3016-27.
9. Ha, M.; Kim, V. N., Regulation of microRNA biogenesis. *Nature reviews. Molecular cell biology* **2014,** *15* (8), 509-24.
10. Lee, Y.; Jeon, K.; Lee, J. T.; Kim, S.; Kim, V. N., MicroRNA maturation: stepwise processing and subcellular localization. *The EMBO journal* **2002,** *21* (17), 4663-70.
11. Lee, Y.; Ahn, C.; Han, J.; Choi, H.; Kim, J.; Yim, J.; Lee, J.; Provost, P.; Radmark, O.; Kim, S.; Kim, V. N., The nuclear RNase III Drosha initiates microRNA processing. *Nature* **2003,** *425* (6956), 415-9.
12. Zeng, Y.; Cullen, B. R., Sequence requirements for micro RNA processing and function in human cells. *RNA (New York, N.Y.)* **2003,** *9* (1), 112-23.
13. Du, T.; Zamore, P. D., microPrimer: the biogenesis and function of microRNA. *Development (Cambridge, England)* **2005,** *132* (21), 4645-52.
14. Gregory, R. I.; Shiekhattar, R., MicroRNA biogenesis and cancer. *Cancer research* **2005,** *65* (9), 3509-12.
15. Han, J.; Lee, Y.; Yeom, K. H.; Nam, J. W.; Heo, I.; Rhee, J. K.; Sohn, S. Y.; Cho, Y.; Zhang, B. T.; Kim, V. N., Molecular basis for the recognition of primary microRNAs by the Drosha-DGCR8 complex. *Cell* **2006,** *125* (5), 887-901.
16. Yi, R.; Qin, Y.; Macara, I. G.; Cullen, B. R., Exportin-5 mediates the nuclear export of pre-microRNAs and short hairpin RNAs. *Genes Dev* **2003,** *17* (24), 3011-6.
17. Bohnsack, M. T.; Czaplinski, K.; Gorlich, D., Exportin 5 is a RanGTP-dependent dsRNA-binding protein that mediates nuclear export of pre-miRNAs. *RNA (New York, N.Y.)* **2004,** *10* (2), 185-91.
18. Okada, C.; Yamashita, E.; Lee, S. J.; Shibata, S.; Katahira, J.; Nakagawa, A.; Yoneda, Y.; Tsukihara, T., A high-resolution structure of the pre-microRNA nuclear export machinery. *Science (New York, N.Y.)* **2009,** *326* (5957), 1275-9.
19. Zeng, Y.; Cullen, B. R., Structural requirements for pre-microRNA binding and nuclear export by Exportin 5. *Nucleic acids research* **2004,** *32* (16), 4776-85.
20. Lund, E.; Dahlberg, J. E., Substrate selectivity of exportin 5 and Dicer in the biogenesis of microRNAs. *Cold Spring Harbor symposia on quantitative biology* **2006,** *71*, 59-66.
21. Lau, P. W.; Guiley, K. Z.; De, N.; Potter, C. S.; Carragher, B.; MacRae, I. J., The molecular architecture of human Dicer. *Nature structural & molecular biology* **2012,** *19* (4), 436-40.
22. Sawh, A. N.; Duchaine, T. F., Turning Dicer on its head. *Nature structural & molecular biology* **2012,** *19* (4), 365-6.
23. Bernstein, E.; Caudy, A. A.; Hammond, S. M.; Hannon, G. J., Role for a bidentate ribonuclease in the initiation step of RNA interference. *Nature* **2001,** *409* (6818), 363-6.

24. Hutvagner, G.; McLachlan, J.; Pasquinelli, A. E.; Balint, E.; Tuschl, T.; Zamore, P. D., A cellular function for the RNA-interference enzyme Dicer in the maturation of the let-7 small temporal RNA. *Science (New York, N.Y.)* **2001,** *293* (5531), 834-8.
25. Filippov, V.; Solovyev, V.; Filippova, M.; Gill, S. S., A novel type of RNase III family proteins in eukaryotes. *Gene* **2000,** *245* (1), 213-21.
26. Chakravarthy, S.; Sternberg, S. H.; Kellenberger, C. A.; Doudna, J. A., Substrate-specific kinetics of Dicer-catalyzed RNA processing. *Journal of molecular biology* **2010,** *404* (3), 392-402.
27. Lee, H. Y.; Zhou, K.; Smith, A. M.; Noland, C. L.; Doudna, J. A., Differential roles of human Dicer-binding proteins TRBP and PACT in small RNA processing. *Nucleic acids research* **2013,** *41* (13), 6568-76.
28. Zhang, H.; Kolb, F. A.; Brondani, V.; Billy, E.; Filipowicz, W., Human Dicer preferentially cleaves dsRNAs at their termini without a requirement for ATP. *The EMBO journal* **2002,** *21* (21), 5875-85.
29. Murphy, D.; Dancis, B.; Brown, J. R., The evolution of core proteins involved in microRNA biogenesis. *BMC evolutionary biology* **2008,** *8*, 92.
30. Elbashir, S. M.; Lendeckel, W.; Tuschl, T., RNA interference is mediated by 21- and 22-nucleotide RNAs. *Genes Dev* **2001,** *15* (2), 188-200.
31. Filipowicz, W.; Jaskiewicz, L.; Kolb, F. A.; Pillai, R. S., Post-transcriptional gene silencing by siRNAs and miRNAs. *Current opinion in structural biology* **2005,** *15* (3), 331-41.
32. Haase, A. D.; Jaskiewicz, L.; Zhang, H.; Laine, S.; Sack, R.; Gatignol, A.; Filipowicz, W., TRBP, a regulator of cellular PKR and HIV-1 virus expression, interacts with Dicer and functions in RNA silencing. *EMBO reports* **2005,** *6* (10), 961-7.
33. Zamore, P. D.; Tuschl, T.; Sharp, P. A.; Bartel, D. P., RNAi: double-stranded RNA directs the ATP-dependent cleavage of mRNA at 21 to 23 nucleotide intervals. *Cell* **2000,** *101* (1), 25-33.
34. Lee, Y. S.; Nakahara, K.; Pham, J. W.; Kim, K.; He, Z.; Sontheimer, E. J.; Carthew, R. W., Distinct roles for Drosophila Dicer-1 and Dicer-2 in the siRNA/miRNA silencing pathways. *Cell* **2004,** *117* (1), 69-81.
35. Jiang, F.; Ye, X.; Liu, X.; Fincher, L.; McKearin, D.; Liu, Q., Dicer-1 and R3D1-L catalyze microRNA maturation in Drosophila. *Genes Dev* **2005,** *19* (14), 1674-9.
36. Tian, Y.; Simanshu, D. K.; Ma, J. B.; Park, J. E.; Heo, I.; Kim, V. N.; Patel, D. J., A phosphate-binding pocket within the platform-PAZ-connector helix cassette of human Dicer. *Molecular cell* **2014,** *53* (4), 606-16.
37. Park, J. E.; Heo, I.; Tian, Y.; Simanshu, D. K.; Chang, H.; Jee, D.; Patel, D. J.; Kim, V. N., Dicer recognizes the 5' end of RNA for efficient and accurate processing. *Nature* **2011,** *475* (7355), 201-5.
38. Macrae, I. J.; Zhou, K.; Li, F.; Repic, A.; Brooks, A. N.; Cande, W. Z.; Adams, P. D.; Doudna, J. A., Structural basis for double-stranded RNA processing by Dicer. *Science (New York, N.Y.)* **2006,** *311* (5758), 195-8.
39. MacRae, I. J.; Zhou, K.; Doudna, J. A., Structural determinants of RNA recognition and cleavage by Dicer. *Nature structural & molecular biology* **2007,** *14* (10), 934-40.
40. Macrae, I. J.; Li, F.; Zhou, K.; Cande, W. Z.; Doudna, J. A., Structure of Dicer and mechanistic implications for RNAi. *Cold Spring Harbor symposia on quantitative biology* **2006,** *71*, 73-80.
41. Zhang, H.; Kolb, F. A.; Jaskiewicz, L.; Westhof, E.; Filipowicz, W., Single processing center models for human Dicer and bacterial RNase III. *Cell* **2004,** *118* (1), 57-68.
42. Bartel, D. P., MicroRNAs: target recognition and regulatory functions. *Cell* **2009,** *136* (2), 215-33.
43. Bartel, D. P., MicroRNAs: genomics, biogenesis, mechanism, and function. *Cell* **2004,** *116* (2), 281-97.
44. Winter, J.; Jung, S.; Keller, S.; Gregory, R. I.; Diederichs, S., Many roads to maturity: microRNA biogenesis pathways and their regulation. *Nature cell biology* **2009,** *11* (3), 228-34.
45. Starega-Roslan, J.; Koscianska, E.; Kozlowski, P.; Krzyzosiak, W. J., The role of the precursor structure in the biogenesis of microRNA. *Cellular and molecular life sciences : CMLS* **2011,** *68* (17), 2859-71.

46. Herrera-Carrillo, E.; Berkhout, B., Dicer-independent processing of small RNA duplexes: mechanistic insights and applications. *Nucleic acids research* **2017,** *45* (18), 10369-10379.
47. Mourelatos, Z.; Dostie, J.; Paushkin, S.; Sharma, A.; Charroux, B.; Abel, L.; Rappsilber, J.; Mann, M.; Dreyfuss, G., miRNPs: a novel class of ribonucleoproteins containing numerous microRNAs. *Genes Dev* **2002,** *16* (6), 720-8.
48. Kawamata, T.; Tomari, Y., Making RISC. *Trends in biochemical sciences* **2010,** *35* (7), 368-76.
49. Chendrimada, T. P.; Gregory, R. I.; Kumaraswamy, E.; Norman, J.; Cooch, N.; Nishikura, K.; Shiekhattar, R., TRBP recruits the Dicer complex to Ago2 for microRNA processing and gene silencing. *Nature* **2005,** *436* (7051), 740-4.
50. Yang, X.; Du, W. W.; Li, H.; Liu, F.; Khorshidi, A.; Rutnam, Z. J.; Yang, B. B., Both mature miR-17-5p and passenger strand miR-17-3p target TIMP3 and induce prostate tumor growth and invasion. *Nucleic acids research* **2013,** *41* (21), 9688-704.
51. Tseng, H. H.; Tseng, Y. K.; You, J. J.; Kang, B. H.; Wang, T. H.; Yang, C. M.; Chen, H. C.; Liou, H. H.; Liu, P. F.; Ger, L. P.; Tsai, K. W., Next-generation Sequencing for microRNA Profiling: MicroRNA-21-3p Promotes Oral Cancer Metastasis. *Anticancer research* **2017,** *37* (3), 1059-1066.
52. Simerzin, A.; Zorde-Khvalevsky, E.; Rivkin, M.; Adar, R.; Zucman-Rossi, J.; Couchy, G.; Roskams, T.; Govaere, O.; Oren, M.; Giladi, H.; Galun, E., The liver-specific microRNA-122*, the complementary strand of microRNA-122, acts as a tumor suppressor by modulating the p53/mouse double minute 2 homolog circuitry. *Hepatology (Baltimore, Md.)* **2016,** *64* (5), 1623-1636.
53. Shi, J.; Bei, Y.; Kong, X.; Liu, X.; Lei, Z.; Xu, T.; Wang, H.; Xuan, Q.; Chen, P.; Xu, J.; Che, L.; Liu, H.; Zhong, J.; Sluijter, J. P.; Li, X.; Rosenzweig, A.; Xiao, J., miR-17-3p Contributes to Exercise-Induced Cardiac Growth and Protects against Myocardial Ischemia-Reperfusion Injury. *Theranostics* **2017,** *7* (3), 664-676.
54. Shan, S. W.; Fang, L.; Shatseva, T.; Rutnam, Z. J.; Yang, X.; Du, W.; Lu, W. Y.; Xuan, J. W.; Deng, Z.; Yang, B. B., Mature miR-17-5p and passenger miR-17-3p induce hepatocellular carcinoma by targeting PTEN, GalNT7 and vimentin in different signal pathways. *Journal of cell science* **2013,** *126* (Pt 6), 1517-30.
55. Bang, C.; Batkai, S.; Dangwal, S.; Gupta, S. K.; Foinquinos, A.; Holzmann, A.; Just, A.; Remke, J.; Zimmer, K.; Zeug, A.; Ponimaskin, E.; Schmiedl, A.; Yin, X.; Mayr, M.; Halder, R.; Fischer, A.; Engelhardt, S.; Wei, Y.; Schober, A.; Fiedler, J.; Thum, T., Cardiac fibroblast-derived microRNA passenger strand-enriched exosomes mediate cardiomyocyte hypertrophy. *The Journal of clinical investigation* **2014,** *124* (5), 2136-46.
56. Almeida, M. I.; Reis, R. M.; Calin, G. A., MicroRNA history: discovery, recent applications, and next frontiers. *Mutation research* **2011,** *717* (1-2), 1-8.
57. Cimmino, A.; Calin, G. A.; Fabbri, M.; Iorio, M. V.; Ferracin, M.; Shimizu, M.; Wojcik, S. E.; Aqeilan, R. I.; Zupo, S.; Dono, M.; Rassenti, L.; Alder, H.; Volinia, S.; Liu, C. G.; Kipps, T. J.; Negrini, M.; Croce, C. M., miR-15 and miR-16 induce apoptosis by targeting BCL2. *Proceedings of the National Academy of Sciences of the United States of America* **2005,** *102* (39), 13944-9.
58. Johnson, S. M.; Grosshans, H.; Shingara, J.; Byrom, M.; Jarvis, R.; Cheng, A.; Labourier, E.; Reinert, K. L.; Brown, D.; Slack, F. J., RAS is regulated by the let-7 microRNA family. *Cell* **2005,** *120* (5), 635-47.
59. Medina, P. P.; Nolde, M.; Slack, F. J., OncomiR addiction in an in vivo model of microRNA-21-induced pre-B-cell lymphoma. *Nature* **2010,** *467* (7311), 86-90.
60. Si, M. L.; Zhu, S.; Wu, H.; Lu, Z.; Wu, F.; Mo, Y. Y., miR-21-mediated tumor growth. *Oncogene* **2007,** *26* (19), 2799-803.
61. Zhu, S.; Wu, H.; Wu, F.; Nie, D.; Sheng, S.; Mo, Y.-Y., MicroRNA-21 targets tumor suppressor genes in invasion and metastasis. *Cell Research* **2008,** *18*, 350.
62. Markou, A.; Zavridou, M.; Lianidou, E. S., miRNA-21 as a novel therapeutic target in lung cancer. *Lung Cancer (Auckland, N.Z.)* **2016,** *7*, 19-27.
63. Meng, F.; Henson, R.; Wehbe-Janek, H.; Ghoshal, K.; Jacob, S. T.; Patel, T., MicroRNA-21 regulates expression of the PTEN tumor suppressor gene in human hepatocellular cancer. *Gastroenterology* **2007,** *133* (2), 647-58.

64. Asangani, I. A.; Rasheed, S. A.; Nikolova, D. A.; Leupold, J. H.; Colburn, N. H.; Post, S.; Allgayer, H., MicroRNA-21 (miR-21) post-transcriptionally downregulates tumor suppressor Pdcd4 and stimulates invasion, intravasation and metastasis in colorectal cancer. *Oncogene* **2008,** *27* (15), 2128-36.
65. Jazbutyte, V.; Thum, T., MicroRNA-21: from cancer to cardiovascular disease. *Current drug targets* **2010,** *11* (8), 926-35.
66. Girard, M.; Jacquemin, E.; Munnich, A.; Lyonnet, S.; Henrion-Caude, A., miR-122, a paradigm for the role of microRNAs in the liver. *Journal of hepatology* **2008,** *48* (4), 648-56.
67. Bandiera, S.; Pfeffer, S.; Baumert, T. F.; Zeisel, M. B., miR-122--a key factor and therapeutic target in liver disease. *Journal of hepatology* **2015,** *62* (2), 448-57.
68. Hsu, S. H.; Wang, B.; Kota, J.; Yu, J.; Costinean, S.; Kutay, H.; Yu, L.; Bai, S.; La Perle, K.; Chivukula, R. R.; Mao, H.; Wei, M.; Clark, K. R.; Mendell, J. R.; Caligiuri, M. A.; Jacob, S. T.; Mendell, J. T.; Ghoshal, K., Essential metabolic, anti-inflammatory, and anti-tumorigenic functions of miR-122 in liver. *The Journal of clinical investigation* **2012,** *122* (8), 2871-83.
69. Tsai, W. C.; Hsu, S. D.; Hsu, C. S.; Lai, T. C.; Chen, S. J.; Shen, R.; Huang, Y.; Chen, H. C.; Lee, C. H.; Tsai, T. F.; Hsu, M. T.; Wu, J. C.; Huang, H. D.; Shiao, M. S.; Hsiao, M.; Tsou, A. P., MicroRNA-122 plays a critical role in liver homeostasis and hepatocarcinogenesis. *The Journal of clinical investigation* **2012,** *122* (8), 2884-97.
70. Zeisel, M. B.; Pfeffer, S.; Baumert, T. F., miR-122 acts as a tumor suppressor in hepatocarcinogenesis in vivo. *Journal of hepatology* **2013,** *58* (4), 821-3.
71. Bai, S.; Nasser, M. W.; Wang, B.; Hsu, S. H.; Datta, J.; Kutay, H.; Yadav, A.; Nuovo, G.; Kumar, P.; Ghoshal, K., MicroRNA-122 inhibits tumorigenic properties of hepatocellular carcinoma cells and sensitizes these cells to sorafenib. *The Journal of biological chemistry* **2009,** *284* (46), 32015-27.
72. Fornari, F.; Gramantieri, L.; Giovannini, C.; Veronese, A.; Ferracin, M.; Sabbioni, S.; Calin, G. A.; Grazi, G. L.; Croce, C. M.; Tavolari, S.; Chieco, P.; Negrini, M.; Bolondi, L., MiR-122/cyclin G1 interaction modulates p53 activity and affects doxorubicin sensitivity of human hepatocarcinoma cells. *Cancer research* **2009,** *69* (14), 5761-7.
73. Xu, Y.; Xia, F.; Ma, L.; Shan, J.; Shen, J.; Yang, Z.; Liu, J.; Cui, Y.; Bian, X.; Bie, P.; Qian, C., MicroRNA-122 sensitizes HCC cancer cells to adriamycin and vincristine through modulating expression of MDR and inducing cell cycle arrest. *Cancer letters* **2011,** *310* (2), 160-9.
74. Jopling, C. L.; Yi, M.; Lancaster, A. M.; Lemon, S. M.; Sarnow, P., Modulation of hepatitis C virus RNA abundance by a liver-specific MicroRNA. *Science (New York, N.Y.)* **2005,** *309* (5740), 1577-81.
75. Chen, Y.; Shen, A.; Rider, P. J.; Yu, Y.; Wu, K.; Mu, Y.; Hao, Q.; Liu, Y.; Gong, H.; Zhu, Y.; Liu, F.; Wu, J., A liver-specific microRNA binds to a highly conserved RNA sequence of hepatitis B virus and negatively regulates viral gene expression and replication. *FASEB journal : official publication of the Federation of American Societies for Experimental Biology* **2011,** *25* (12), 4511-21.
76. Wang, S.; Qiu, L.; Yan, X.; Jin, W.; Wang, Y.; Chen, L.; Wu, E.; Ye, X.; Gao, G. F.; Wang, F.; Chen, Y.; Duan, Z.; Meng, S., Loss of microRNA 122 expression in patients with hepatitis B enhances hepatitis B virus replication through cyclin G(1) -modulated P53 activity. *Hepatology (Baltimore, Md.)* **2012,** *55* (3), 730-41.
77. Bader, A. G.; Brown, D.; Winkler, M., The promise of microRNA replacement therapy. *Cancer research* **2010,** *70* (18), 7027-30.
78. Broderick, J. A.; Zamore, P. D., MicroRNA therapeutics. *Gene therapy* **2011,** *18* (12), 1104-10.
79. van Rooij, E.; Kauppinen, S., Development of microRNA therapeutics is coming of age. *EMBO molecular medicine* **2014,** *6* (7), 851-64.
80. Chorn, G.; Klein-McDowell, M.; Zhao, L.; Saunders, M. A.; Flanagan, W. M.; Willingham, A. T.; Lim, L. P., Single-stranded microRNA mimics. *RNA (New York, N.Y.)* **2012,** *18* (10), 1796-804.
81. Li, J.; Tan, S.; Kooger, R.; Zhang, C.; Zhang, Y., MicroRNAs as novel biological targets for detection and regulation. *Chemical Society reviews* **2014,** *43* (2), 506-17.
82. Thorsen, S. B.; Obad, S.; Jensen, N. F.; Stenvang, J.; Kauppinen, S., The therapeutic potential of microRNAs in cancer. *Cancer journal (Sudbury, Mass.)* **2012,** *18* (3), 275-84.

83. Ling, H.; Fabbri, M.; Calin, G. A., MicroRNAs and other non-coding RNAs as targets for anticancer drug development. *Nature reviews. Drug discovery* **2013,** *12* (11), 847-65.
84. Bader, A. G., miR-34 - a microRNA replacement therapy is headed to the clinic. *Frontiers in genetics* **2012,** *3*, 120.
85. Trang, P.; Wiggins, J. F.; Daige, C. L.; Cho, C.; Omotola, M.; Brown, D.; Weidhaas, J. B.; Bader, A. G.; Slack, F. J., Systemic delivery of tumor suppressor microRNA mimics using a neutral lipid emulsion inhibits lung tumors in mice. *Molecular therapy : the journal of the American Society of Gene Therapy* **2011,** *19* (6), 1116-22.
86. Tazawa, H.; Tsuchiya, N.; Izumiya, M.; Nakagama, H., Tumor-suppressive miR-34a induces senescence-like growth arrest through modulation of the E2F pathway in human colon cancer cells. *Proceedings of the National Academy of Sciences of the United States of America* **2007,** *104* (39), 15472-7.
87. Tivnan, A.; Orr, W. S.; Gubala, V.; Nooney, R.; Williams, D. E.; McDonagh, C.; Prenter, S.; Harvey, H.; Domingo-Fernandez, R.; Bray, I. M.; Piskareva, O.; Ng, C. Y.; Lode, H. N.; Davidoff, A. M.; Stallings, R. L., Inhibition of neuroblastoma tumor growth by targeted delivery of microRNA-34a using anti-disialoganglioside GD2 coated nanoparticles. *PloS one* **2012,** *7* (5), e38129.
88. Hong, D. S.; Kang, Y. K.; Borad, M.; Sachdev, J.; Ejadi, S.; Lim, H. Y.; Brenner, A. J.; Park, K.; Lee, J. L.; Kim, T. Y.; Shin, S.; Becerra, C. R.; Falchook, G.; Stoudemire, J.; Martin, D.; Kelnar, K.; Peltier, H.; Bonato, V.; Bader, A. G.; Smith, S.; Kim, S.; O'Neill, V.; Beg, M. S., Phase 1 study of MRX34, a liposomal miR-34a mimic, in patients with advanced solid tumours. *British journal of cancer* **2020,** *122* (11), 1630-1637.
89. Simoes-Wust, A. P.; Hopkins-Donaldson, S.; Sigrist, B.; Belyanskaya, L.; Stahel, R. A.; Zangemeister-Wittke, U., A functionally improved locked nucleic acid antisense oligonucleotide inhibits Bcl-2 and Bcl-xL expression and facilitates tumor cell apoptosis. *Oligonucleotides* **2004,** *14* (3), 199-209.
90. Stenvang, J.; Kauppinen, S., MicroRNAs as targets for antisense-based therapeutics. *Expert opinion on biological therapy* **2008,** *8* (1), 59-81.
91. Baek, J.; Kang, S.; Min, H., MicroRNA-targeting therapeutics for hepatitis C. *Archives of pharmacal research* **2014,** *37* (3), 299-305.
92. Nielsen, P. E.; Egholm, M., An introduction to peptide nucleic acid. *Current issues in molecular biology* **1999,** *1* (1-2), 89-104.
93. Egholm, M.; Buchardt, O.; Christensen, L.; Behrens, C.; Freier, S. M.; Driver, D. A.; Berg, R. H.; Kim, S. K.; Norden, B.; Nielsen, P. E., PNA hybridizes to complementary oligonucleotides obeying the Watson-Crick hydrogen-bonding rules. *Nature* **1993,** *365* (6446), 566-8.
94. Giesen, U.; Kleider, W.; Berding, C.; Geiger, A.; Orum, H.; Nielsen, P. E., A formula for thermal stability (Tm) prediction of PNA/DNA duplexes. *Nucleic acids research* **1998,** *26* (21), 5004-6.
95. Sebastian Tomac, M. S., Tommi Ratilainen, Pernilla Wittung, Peter E. Nielsen, Bengt Norden, and Astrid Graslund, Ionic effects on the stability and conformation of peptide nucleic acid (PNA) complexes. *J. Am. Chem. Soc. 1996, 118, 5544-5552* **1996**.
96. Jensen, K. K.; Orum, H.; Nielsen, P. E.; Norden, B., Kinetics for hybridization of peptide nucleic acids (PNA) with DNA and RNA studied with the BIAcore technique. *Biochemistry* **1997,** *36* (16), 5072-7.
97. D'Agata, R.; Giuffrida, M. C.; Spoto, G., Peptide Nucleic Acid-Based Biosensors for Cancer Diagnosis. *Molecules (Basel, Switzerland)* **2017,** *22* (11).
98. Larsen, H. J.; Bentin, T.; Nielsen, P. E., Antisense properties of peptide nucleic acid. *Biochimica et biophysica acta* **1999,** *1489* (1), 159-66.
99. Betts, L.; Josey, J. A.; Veal, J. M.; Jordan, S. R., A nucleic acid triple helix formed by a peptide nucleic acid-DNA complex. *Science (New York, N.Y.)* **1995,** *270* (5243), 1838-41.
100. Brown, S. C.; Thomson, S. A.; Veal, J. M.; Davis, D. G., NMR solution structure of a peptide nucleic acid complexed with RNA. *Science (New York, N.Y.)* **1994,** *265* (5173), 777-80.

101. Egholm, M.; Christensen, L.; Dueholm, K. L.; Buchardt, O.; Coull, J.; Nielsen, P. E., Efficient pH-independent sequence-specific DNA binding by pseudoisocytosine-containing bis-PNA. *Nucleic acids research* **1995,** *23* (2), 217-22.
102. Wittung, P.; Nielsen, P. E.; Buchardt, O.; Egholm, M.; Norden, B., DNA-like double helix formed by peptide nucleic acid. *Nature* **1994,** *368* (6471), 561-3.
103. Spizzo, R.; Rushworth, D.; Guerrero, M.; Calin, G. A., RNA inhibition, microRNAs, and new therapeutic agents for cancer treatment. *Clinical lymphoma & myeloma* **2009,** *9 Suppl 3*, S313-8.
104. Gildea, B. D.; Casey, S.; MacNeill, J.; Perry-O'Keefe, H.; Sørensen, D.; Coull, J. M., PNA solubility enhancers. *Tetrahedron Letters* **1998,** *39* (40), 7255-7258.
105. Nielsen, P. E.; Haaima, G.; Lohse, A.; Buchardt, O., Peptide Nucleic Acids (PNAs) Containing Thymine Monomers Derived from Chiral Amino Acids: Hybridization and Solubility Properties of D-Lysine PNA. *Angewandte Chemie International Edition in English* **1996,** *35* (17), 1939-1942.
106. Christensen, L.; Fitzpatrick, R.; Gildea, B.; Petersen, K. H.; Hansen, H. F.; Koch, T.; Egholm, M.; Buchardt, O.; Nielsen, P. E.; Coull, J.; Berg, R. H., Solid-Phase synthesis of peptide nucleic acids. *Journal of Peptide Science* **1995,** *1* (3), 175-183.
107. Thomson, S. A.; Josey, J. A.; Cadilla, R.; Gaul, M. D.; Fred Hassman, C.; Luzzio, M. J.; Pipe, A. J.; Reed, K. L.; Ricca, D. J.; Wiethe, R. W.; Noble, S. A., Fmoc mediated synthesis of Peptide Nucleic Acids. *Tetrahedron* **1995,** *51* (22), 6179-6194.
108. Sharma, C.; Awasthi, S. K., Versatility of peptide nucleic acids (PNAs): role in chemical biology, drug discovery, and origins of life. *Chemical biology & drug design* **2017,** *89* (1), 16-37.
109. Koppelhus, U.; Nielsen, P. E., Cellular delivery of peptide nucleic acid (PNA). *Advanced drug delivery reviews* **2003,** *55* (2), 267-80.
110. Jarver, P.; Coursindel, T.; Andaloussi, S. E.; Godfrey, C.; Wood, M. J.; Gait, M. J., Peptide-mediated Cell and In Vivo Delivery of Antisense Oligonucleotides and siRNA. *Molecular therapy. Nucleic acids* **2012,** *1*, e27.
111. Joliot, A. H.; Triller, A.; Volovitch, M.; Pernelle, C.; Prochiantz, A., alpha-2,8-Polysialic acid is the neuronal surface receptor of antennapedia homeobox peptide. *The New biologist* **1991,** *3* (11), 1121-34.
112. Frankel, A. D.; Pabo, C. O., Cellular uptake of the tat protein from human immunodeficiency virus. *Cell* **1988,** *55* (6), 1189-93.
113. Derossi, D.; Joliot, A. H.; Chassaing, G.; Prochiantz, A., The third helix of the Antennapedia homeodomain translocates through biological membranes. *The Journal of biological chemistry* **1994,** *269* (14), 10444-50.
114. Vives, E.; Brodin, P.; Lebleu, B., A truncated HIV-1 Tat protein basic domain rapidly translocates through the plasma membrane and accumulates in the cell nucleus. *The Journal of biological chemistry* **1997,** *272* (25), 16010-7.
115. Said Hassane, F.; Saleh, A. F.; Abes, R.; Gait, M. J.; Lebleu, B., Cell penetrating peptides: overview and applications to the delivery of oligonucleotides. *Cellular and molecular life sciences : CMLS* **2010,** *67* (5), 715-26.
116. Rothbard, J. B.; Kreider, E.; VanDeusen, C. L.; Wright, L.; Wylie, B. L.; Wender, P. A., Arginine-rich molecular transporters for drug delivery: role of backbone spacing in cellular uptake. *Journal of medicinal chemistry* **2002,** *45* (17), 3612-8.
117. Morris, M. C.; Vidal, P.; Chaloin, L.; Heitz, F.; Divita, G., A new peptide vector for efficient delivery of oligonucleotides into mammalian cells. *Nucleic acids research* **1997,** *25* (14), 2730-6.
118. Pooga, M.; Hallbrink, M.; Zorko, M.; Langel, U., Cell penetration by transportan. *FASEB journal : official publication of the Federation of American Societies for Experimental Biology* **1998,** *12* (1), 67-77.
119. Richard, J. P.; Melikov, K.; Vives, E.; Ramos, C.; Verbeure, B.; Gait, M. J.; Chernomordik, L. V.; Lebleu, B., Cell-penetrating peptides. A reevaluation of the mechanism of cellular uptake. *The Journal of biological chemistry* **2003,** *278* (1), 585-90.

120. Lundberg, M.; Johansson, M., Positively charged DNA-binding proteins cause apparent cell membrane translocation. *Biochemical and biophysical research communications* **2002,** *291* (2), 367-71.
121. Drin, G.; Mazel, M.; Clair, P.; Mathieu, D.; Kaczorek, M.; Temsamani, J., Physico-chemical requirements for cellular uptake of pAntp peptide. Role of lipid-binding affinity. *European journal of biochemistry* **2001,** *268* (5), 1304-14.
122. Richard, J. P.; Melikov, K.; Brooks, H.; Prevot, P.; Lebleu, B.; Chernomordik, L. V., Cellular uptake of unconjugated TAT peptide involves clathrin-dependent endocytosis and heparan sulfate receptors. *The Journal of biological chemistry* **2005,** *280* (15), 15300-6.
123. Almeida, C.; Sousa, J. M.; Rocha, R.; Cerqueira, L.; Fanning, S.; Azevedo, N. F.; Vieira, M. J., Detection of Escherichia coli O157 by peptide nucleic acid fluorescence in situ hybridization (PNA-FISH) and comparison to a standard culture method. *Applied and environmental microbiology* **2013,** *79* (20), 6293-300.
124. Machnik, G.; Labuzek, K.; Skudrzyk, E.; Rekowski, P.; Ruczynski, J.; Wojciechowska, M.; Mucha, P.; Giri, S.; Okopien, B., A peptide nucleic acid (PNA)-mediated polymerase chain reaction clamping allows the selective inhibition of the ERVWE1 gene amplification. *Molecular and cellular probes* **2014,** *28* (5-6), 237-41.
125. Miyano, S.; Hanazawa, K.; Kitabatake, T.; Fujisawa, M.; Kojima, K., Detecting KRAS mutations in peripheral blood of colorectal cancer patients by peptide nucleic acid clamp PCR. *Experimental and therapeutic medicine* **2012,** *4* (5), 790-794.
126. Shi, H.; Yang, F.; Li, W.; Zhao, W.; Nie, K.; Dong, B.; Liu, Z., A review: fabrications, detections and applications of peptide nucleic acids (PNAs) microarray. *Biosensors & bioelectronics* **2015,** *66*, 481-9.
127. Nguyen, D. D.; Chang, S., Development of Novel Therapeutic Agents by Inhibition of Oncogenic MicroRNAs. *International journal of molecular sciences* **2017,** *19* (1).
128. Pecot, C. V.; Calin, G. A.; Coleman, R. L.; Lopez-Berestein, G.; Sood, A. K., RNA interference in the clinic: challenges and future directions. *Nature reviews. Cancer* **2011,** *11* (1), 59-67.
129. Garzon, R.; Marcucci, G.; Croce, C. M., Targeting microRNAs in cancer: rationale, strategies and challenges. *Nature reviews. Drug discovery* **2010,** *9* (10), 775-89.
130. Thomas, J. R.; Hergenrother, P. J., Targeting RNA with Small Molecules. *Chemical Reviews* **2008,** *108* (4), 1171-1224.
131. Hermann, T.; Patel, D. J., Stitching together RNA tertiary architectures. *Journal of molecular biology* **1999,** *294* (4), 829-49.
132. Weeks, K. M.; Crothers, D. M., Major groove accessibility of RNA. *Science (New York, N.Y.)* **1993,** *261* (5128), 1574-7.
133. Foloppe, N.; Matassova, N.; Aboul-Ela, F., Towards the discovery of drug-like RNA ligands? *Drug discovery today* **2006,** *11* (21-22), 1019-27.
134. Vicens, Q.; Westhof, E., RNA as a drug target: the case of aminoglycosides. *Chembiochem* **2003,** *4* (10), 1018-23.
135. Tor, Y., Targeting RNA with small molecules. *Chembiochem* **2003,** *4* (10), 998-1007.
136. Zapp, M. L.; Stern, S.; Green, M. R., Small molecules that selectively block RNA binding of HIV-1 Rev protein inhibit Rev function and viral production. *Cell* **1993,** *74* (6), 969-78.
137. Monroig Pdel, C.; Chen, L.; Zhang, S.; Calin, G. A., Small molecule compounds targeting miRNAs for cancer therapy. *Advanced drug delivery reviews* **2015,** *81*, 104-16.
138. Chen, L.; Calin, G. A.; Zhang, S., Novel insights of structure-based modeling for RNA-targeted drug discovery. *Journal of chemical information and modeling* **2012,** *52* (10), 2741-53.
139. Gumireddy, K.; Young, D. D.; Xiong, X.; Hogenesch, J. B.; Huang, Q.; Deiters, A., Small-molecule inhibitors of microrna miR-21 function. *Angewandte Chemie (International ed. in English)* **2008,** *47* (39), 7482-4.
140. Young, D. D.; Connelly, C. M.; Grohmann, C.; Deiters, A., Small molecule modifiers of microRNA miR-122 function for the treatment of hepatitis C virus infection and hepatocellular carcinoma. *Journal of the American Chemical Society* **2010,** *132* (23), 7976-81.

141. Velagapudi, S. P.; Gallo, S. M.; Disney, M. D., Sequence-based design of bioactive small molecules that target precursor microRNAs. *Nature chemical biology* **2014,** *10* (4), 291-7.
142. Costales, M. G.; Haga, C. L.; Velagapudi, S. P.; Childs-Disney, J. L.; Phinney, D. G.; Disney, M. D., Small Molecule Inhibition of microRNA-210 Reprograms an Oncogenic Hypoxic Circuit. *Journal of the American Chemical Society* **2017,** *139* (9), 3446-3455.
143. Xing, Z.; Wang, X.; Liu, J.; Liu, G.; Zhang, M.; Feng, K.; Wang, X., Effect of MiR-210 on the Chemosensitivity of Breast Cancer by Regulating JAK-STAT Signaling Pathway. *BioMed research international* **2021,** *2021*, 7703159.
144. Costales, M. G.; Hoch, D. G.; Abegg, D.; Childs-Disney, J. L.; Velagapudi, S. P.; Adibekian, A.; Disney, M. D., A Designed Small Molecule Inhibitor of a Non-Coding RNA Sensitizes HER2 Negative Cancers to Herceptin. *Journal of the American Chemical Society* **2019,** *141* (7), 2960-2974.
145. Neubacher, S.; Dojahn, C. M.; Arenz, C., A rapid assay for miRNA maturation by using unmodified pre-miRNA. *Chembiochem* **2011,** *12* (15), 2302-5.
146. Davies, B. P.; Arenz, C., A fluorescence probe for assaying micro RNA maturation. *Bioorganic & medicinal chemistry* **2008,** *16* (1), 49-55.
147. Davies, B. P.; Arenz, C., A homogenous assay for micro RNA maturation. *Angewandte Chemie (International ed. in English)* **2006,** *45* (33), 5550-2.
148. Bose, D.; Jayaraj, G. G.; Kumar, S.; Maiti, S., A molecular-beacon-based screen for small molecule inhibitors of miRNA maturation. *ACS chemical biology* **2013,** *8* (5), 930-8.
149. F., P., Polarization of light of fluorescence, average life of molecules. *J Phys Radium.* **1926,** *7:390–401.*
150. Jameson, D. M.; Croney, J. C., Fluorescence polarization: past, present and future. *Combinatorial chemistry & high throughput screening* **2003,** *6* (3), 167-73.
151. Lea, W. A.; Simeonov, A., Fluorescence polarization assays in small molecule screening. *Expert Opinion on Drug Discovery* **2011,** *6* (1), 17-32.
152. Tan, G. S.; Chiu, C. H.; Garchow, B. G.; Metzler, D.; Diamond, S. L.; Kiriakidou, M., Small molecule inhibition of RISC loading. *ACS chemical biology* **2012,** *7* (2), 403-10.
153. Bose, D.; Jayaraj, G.; Suryawanshi, H.; Agarwala, P.; Pore, S. K.; Banerjee, R.; Maiti, S., The tuberculosis drug streptomycin as a potential cancer therapeutic: inhibition of miR-21 function by directly targeting its precursor. *Angewandte Chemie (International ed. in English)* **2012,** *51* (4), 1019-23.
154. Cheng, Y.; Zhang, X.; Li, Z.; Jiao, X.; Wang, Y.; Zhang, Y., Highly Sensitive Determination of microRNA Using Target-Primed and Branched Rolling-Circle Amplification. *Angewandte Chemie International Edition* **2009,** *48* (18), 3268-3272.
155. Jonstrup, S. P.; Koch, J.; Kjems, J., A microRNA detection system based on padlock probes and rolling circle amplification. *RNA (New York, N.Y.)* **2006,** *12* (9), 1747-52.
156. Neubacher, S.; Arenz, C., Rolling-Circle Amplification: Unshared Advantages in miRNA Detection. *ChemBioChem* **2009,** *10* (8), 1289-1291.
157. Cherkasov, A.; Muratov, E. N.; Fourches, D.; Varnek, A.; Baskin, II; Cronin, M.; Dearden, J.; Gramatica, P.; Martin, Y. C.; Todeschini, R.; Consonni, V.; Kuz'min, V. E.; Cramer, R.; Benigni, R.; Yang, C.; Rathman, J.; Terfloth, L.; Gasteiger, J.; Richard, A.; Tropsha, A., QSAR modeling: where have you been? Where are you going to? *Journal of medicinal chemistry* **2014,** *57* (12), 4977-5010.
158. Jamal, S.; Periwal, V.; Scaria, V., Computational analysis and predictive modeling of small molecule modulators of microRNA. *Journal of cheminformatics* **2012,** *4* (1), 16.
159. Shi, Z.; Zhang, J.; Qian, X.; Han, L.; Zhang, K.; Chen, L.; Liu, J.; Ren, Y.; Yang, M.; Zhang, A.; Pu, P.; Kang, C., AC1MMYR2, an inhibitor of dicer-mediated biogenesis of Oncomir miR-21, reverses epithelial-mesenchymal transition and suppresses tumor growth and progression. *Cancer research* **2013,** *73* (17), 5519-31.
160. Kummer, S.; Knoll, A.; Herrmann, A.; Seitz, O., Sequence-specific imaging of influenza A mRNA in living infected cells using fluorescent FIT-PNA. *Methods in molecular biology (Clifton, N.J.)* **2013,** *1039*, 291-301.

161. Socher, E.; Knoll, A.; Seitz, O., Dual fluorophore PNA FIT-probes--extremely responsive and bright hybridization probes for the sensitive detection of DNA and RNA. *Organic & biomolecular chemistry* **2012,** *10* (36), 7363-71.
162. Kummer, S.; Knoll, A.; Socher, E.; Bethge, L.; Herrmann, A.; Seitz, O., PNA FIT-probes for the dual color imaging of two viral mRNA targets in influenza H1N1 infected live cells. *Bioconjugate chemistry* **2012,** *23* (10), 2051-60.
163. Kohler, O.; Jarikote, D. V.; Seitz, O., Forced intercalation probes (FIT Probes): thiazole orange as a fluorescent base in peptide nucleic acids for homogeneous single-nucleotide-polymorphism detection. *Chembiochem* **2005,** *6* (1), 69-77.
164. Karunakaran, V.; Perez Lustres, J. L.; Zhao, L.; Ernsting, N. P.; Seitz, O., Large dynamic Stokes shift of DNA intercalation dye Thiazole Orange has contribution from a high-frequency mode. *Journal of the American Chemical Society* **2006,** *128* (9), 2954-62.
165. Kolevzon, N.; Hashoul, D.; Naik, S.; Rubinstein, A.; Yavin, E., Single point mutation detection in living cancer cells by far-red emitting PNA-FIT probes. *Chemical communications (Cambridge, England)* **2016,** *52* (11), 2405-7.
166. Hovelmann, F.; Gaspar, I.; Chamiolo, J.; Kasper, M.; Steffen, J.; Ephrussi, A.; Seitz, O., LNA-enhanced DNA FIT-probes for multicolour RNA imaging. *Chemical Science* **2016,** *7* (1), 128-135.
167. Sonar, M. V.; Wampole, M. E.; Jin, Y. Y.; Chen, C. P.; Thakur, M. L.; Wickstrom, E., Fluorescence detection of KRAS2 mRNA hybridization in lung cancer cells with PNA-peptides containing an internal thiazole orange. *Bioconjugate chemistry* **2014,** *25* (9), 1697-708.
168. Kam, Y.; Rubinstein, A.; Nissan, A.; Halle, D.; Yavin, E., Detection of endogenous K-ras mRNA in living cells at a single base resolution by a PNA molecular beacon. *Molecular pharmaceutics* **2012,** *9* (3), 685-93.
169. Pellegata, N. S.; Sessa, F.; Renault, B.; Bonato, M.; Leone, B. E.; Solcia, E.; Ranzani, G. N., K-ras and p53 gene mutations in pancreatic cancer: ductal and nonductal tumors progress through different genetic lesions. *Cancer research* **1994,** *54* (6), 1556-60.
170. Socher, E.; Jarikote, D. V.; Knoll, A.; Roglin, L.; Burmeister, J.; Seitz, O., FIT probes: peptide nucleic acid probes with a fluorescent base surrogate enable real-time DNA quantification and single nucleotide polymorphism discovery. *Analytical biochemistry* **2008,** *375* (2), 318-30.
171. Kummer, S.; Knoll, A.; Socher, E.; Bethge, L.; Herrmann, A.; Seitz, O., Fluorescence imaging of influenza H1N1 mRNA in living infected cells using single-chromophore FIT-PNA. *Angewandte Chemie (International ed. in English)* **2011,** *50* (8), 1931-4.
172. Ge-min Fang, J. C., Svenja Kankowski, Felix Hovelmann, Dhana Friedrich, Alexander Lower, Jochen C. Meier and Oliver Seitz, A bright FIT-PNA hybridization probe for the hybridization state specific analysis of a C/U RNA edit via FRET in a binary system. *Chemical Science* **2018**.
173. Svanvik, N.; Westman, G.; Wang, D.; Kubista, M., Light-up probes: thiazole orange-conjugated peptide nucleic acid for detection of target nucleic acid in homogeneous solution. *Analytical biochemistry* **2000,** *281* (1), 26-35.
174. Hayashi, G.; Yanase, M.; Takeda, K.; Sakakibara, D.; Sakamoto, R.; Wang, D. O.; Okamoto, A., Hybridization-sensitive fluorescent oligonucleotide probe conjugated with a bulky module for compartment-specific mRNA monitoring in a living cell. *Bioconjugate chemistry* **2015,** *26* (3), 412-7.
175. Gaspar, I.; Hovelmann, F.; Chamiolo, J.; Ephrussi, A.; Seitz, O., Quantitative mRNA Imaging with Dual Channel qFIT Probes to Monitor Distribution and Degree of Hybridization. *ACS chemical biology* **2018**.
176. Hovelmann, F.; Seitz, O., DNA Stains as Surrogate Nucleobases in Fluorogenic Hybridization Probes. *Accounts of chemical research* **2016,** *49* (4), 714-23.
177. Hovelmann, F.; Gaspar, I.; Ephrussi, A.; Seitz, O., Brightness enhanced DNA FIT-probes for wash-free RNA imaging in tissue. *Journal of the American Chemical Society* **2013,** *135* (50), 19025-32.
178. Ikeda, S.; Kubota, T.; Yuki, M.; Okamoto, A., Exciton-controlled hybridization-sensitive fluorescent probes: multicolor detection of nucleic acids. *Angewandte Chemie (International ed. in English)* **2009,** *48* (35), 6480-4.

179. Ikeda, S.; Kubota, T.; Yanagisawa, H.; Yuki, M.; Okamoto, A., Synthesis of exciton-controlled fluorescent probes for RNA imaging. *Nucleic acids symposium series (2004)* **2009,** (53), 155-6.
180. Oomoto, I.; Suzuki-Hirano, A.; Umeshima, H.; Han, Y. W.; Yanagisawa, H.; Carlton, P.; Harada, Y.; Kengaku, M.; Okamoto, A.; Shimogori, T.; Wang, D. O., ECHO-liveFISH: in vivo RNA labeling reveals dynamic regulation of nuclear RNA foci in living tissues. *Nucleic acids research* **2015,** *43* (19), e126.
181. Holzhauser, C.; Wagenknecht, H. A., In-stem-labeled molecular beacons for distinct fluorescent color readout. *Angewandte Chemie (International ed. in English)* **2011,** *50* (32), 7268-72.
182. Menacher, F.; Rubner, M.; Berndl, S.; Wagenknecht, H. A., Thiazole orange and Cy3: improvement of fluorescent DNA probes with use of short range electron transfer. *The Journal of organic chemistry* **2008,** *73* (11), 4263-6.
183. Holzhauser, C.; Liebl, R.; Goepferich, A.; Wagenknecht, H. A.; Breunig, M., RNA "traffic lights": an analytical tool to monitor siRNA integrity. *ACS chemical biology* **2013,** *8* (5), 890-4.
184. Hunt, E. A.; Broyles, D.; Head, T.; Deo, S. K., MicroRNA Detection: Current Technology and Research Strategies. *Annual review of analytical chemistry (Palo Alto, Calif.)* **2015,** *8*, 217-37.
185. Qavi, A. J.; Kindt, J. T.; Bailey, R. C., Sizing up the future of microRNA analysis. *Analytical and bioanalytical chemistry* **2010,** *398* (6), 2535-49.
186. Chen, C.; Ridzon, D. A.; Broomer, A. J.; Zhou, Z.; Lee, D. H.; Nguyen, J. T.; Barbisin, M.; Xu, N. L.; Mahuvakar, V. R.; Andersen, M. R.; Lao, K. Q.; Livak, K. J.; Guegler, K. J., Real-time quantification of microRNAs by stem-loop RT-PCR. *Nucleic acids research* **2005,** *33* (20), e179.
187. Raymond, C. K.; Roberts, B. S.; Garrett-Engele, P.; Lim, L. P.; Johnson, J. M., Simple, quantitative primer-extension PCR assay for direct monitoring of microRNAs and short-interfering RNAs. *RNA (New York, N.Y.)* **2005,** *11* (11), 1737-44.
188. Shi, R.; Chiang, V. L., Facile means for quantifying microRNA expression by real-time PCR. *BioTechniques* **2005,** *39* (4), 519-25.
189. Andreasen, D.; Fog, J. U.; Biggs, W.; Salomon, J.; Dahslveen, I. K.; Baker, A.; Mouritzen, P., Improved microRNA quantification in total RNA from clinical samples. *Methods (San Diego, Calif.)* **2010,** *50* (4), S6-9.
190. Li, J.; Yao, B.; Huang, H.; Wang, Z.; Sun, C.; Fan, Y.; Chang, Q.; Li, S.; Wang, X.; Xi, J., Real-time polymerase chain reaction microRNA detection based on enzymatic stem-loop probes ligation. *Analytical chemistry* **2009,** *81* (13), 5446-51.
191. Schmittgen, T. D.; Livak, K. J., Analyzing real-time PCR data by the comparative C(T) method. *Nature protocols* **2008,** *3* (6), 1101-8.
192. Torres, A. G.; Fabani, M. M.; Vigorito, E.; Williams, D.; Al-Obaidi, N.; Wojciechowski, F.; Hudson, R. H.; Seitz, O.; Gait, M. J., Chemical structure requirements and cellular targeting of microRNA-122 by peptide nucleic acids anti-miRs. *Nucleic acids research* **2012,** *40* (5), 2152-67.
193. Yan, L. X.; Wu, Q. N.; Zhang, Y.; Li, Y. Y.; Liao, D. Z.; Hou, J. H.; Fu, J.; Zeng, M. S.; Yun, J. P.; Wu, Q. L.; Zeng, Y. X.; Shao, J. Y., Knockdown of miR-21 in human breast cancer cell lines inhibits proliferation, in vitro migration and in vivo tumor growth. *Breast cancer research : BCR* **2011,** *13* (1), R2.
194. Oh, S. Y.; Ju, Y.; Park, H., A highly effective and long-lasting inhibition of miRNAs with PNA-based antisense oligonucleotides. *Molecules and cells* **2009,** *28* (4), 341-5.
195. Gan, L.; Denecke, B., Profiling Pre-MicroRNA and Mature MicroRNA Expressions Using a Single Microarray and Avoiding Separate Sample Preparation. *Microarrays (Basel, Switzerland)* **2013,** *2* (1), 24-33.
196. Avitabile, C.; Saviano, M.; D'Andrea, L.; Bianchi, N.; Fabbri, E.; Brognara, E.; Gambari, R.; Romanelli, A., Targeting pre-miRNA by peptide nucleic acids: a new strategy to interfere in the miRNA maturation. *Artificial DNA, PNA & XNA* **2012,** *3* (2), 88-96.
197. Chen, Y.; Yang, F.; Zubovic, L.; Pavelitz, T.; Yang, W.; Godin, K.; Walker, M.; Zheng, S.; Macchi, P.; Varani, G., Targeted inhibition of oncogenic miR-21 maturation with designed RNA-binding proteins. *Nature chemical biology* **2016,** *12* (9), 717-23.

198. Kurzynska-Kokorniak, A.; Koralewska, N.; Tyczewska, A.; Twardowski, T.; Figlerowicz, M., A new short oligonucleotide-based strategy for the precursor-specific regulation of microRNA processing by dicer. *PloS one* **2013,** *8* (10), e77703.
199. Kuhn, H.; Demidov, V. V.; Frank-Kamenetskii, M. D., Rolling-circle amplification under topological constraints. *Nucleic acids research* **2002,** *30* (2), 574-80.
200. Perelson, A. S.; Deeks, S. G., Drug effectiveness explained: the mathematics of antiviral agents for HIV. *Science translational medicine* **2011,** *3* (91), 91ps30.
201. Ferrari, A.; Pellegrini, V.; Arcangeli, C.; Fittipaldi, A.; Giacca, M.; Beltram, F., Caveolae-mediated internalization of extracellular HIV-1 tat fusion proteins visualized in real time. *Molecular therapy : the journal of the American Society of Gene Therapy* **2003,** *8* (2), 284-94.
202. Fittipaldi, A.; Ferrari, A.; Zoppé, M.; Arcangeli, C.; Pellegrini, V.; Beltram, F.; Giacca, M., Cell membrane lipid rafts mediate caveolar endocytosis of HIV-1 Tat fusion proteins. *The Journal of biological chemistry* **2003,** *278* (36), 34141-9.
203. Wadia, J. S.; Stan, R. V.; Dowdy, S. F., Transducible TAT-HA fusogenic peptide enhances escape of TAT-fusion proteins after lipid raft macropinocytosis. *Nature medicine* **2004,** *10* (3), 310-5.
204. Duchardt, F.; Fotin-Mleczek, M.; Schwarz, H.; Fischer, R.; Brock, R., A comprehensive model for the cellular uptake of cationic cell-penetrating peptides. *Traffic (Copenhagen, Denmark)* **2007,** *8* (7), 848-66.
205. Lennox, K. A.; Behlke, M. A., Chemical modification and design of anti-miRNA oligonucleotides. *Gene therapy* **2011,** *18* (12), 1111-1120.
206. Jarikote, D. V.; Köhler, O.; Socher, E.; Seitz, O., Divergent and Linear Solid-Phase Synthesis of PNA Containing Thiazole Orange as Artificial Base. *European Journal of Organic Chemistry* **2005,** *2005* (15), 3187-3195.
207. Chamiolo, J.; Fang, G. M.; Hovelmann, F.; Friedrich, D.; Knoll, A.; Loewer, A.; Seitz, O., Comparing Agent-Based Delivery of DNA and PNA Forced Intercalation (FIT) Probes for Multicolor mRNA Imaging. *Chembiochem* **2018**.
208. Abes, R.; Arzumanov, A. A.; Moulton, H. M.; Abes, S.; Ivanova, G. D.; Iversen, P. L.; Gait, M. J.; Lebleu, B., Cell-penetrating-peptide-based delivery of oligonucleotides: an overview. *Biochemical Society transactions* **2007,** *35* (Pt 4), 775-9.
209. Hashoul, D.; Shapira, R.; Falchenko, M.; Tepper, O.; Paviov, V.; Nissan, A.; Yavin, E., Red-emitting FIT-PNAs: "On site" detection of RNA biomarkers in fresh human cancer tissues. *Biosensors & bioelectronics* **2019,** *137*, 271-278.
210. Davies, B. P., A Homogenous Fluorescence Assay of micro RNA Maturation. **2008**.
211. Feng, Y.; Zhang, X.; Graves, P.; Zeng, Y., A comprehensive analysis of precursor microRNA cleavage by human Dicer. *RNA (New York, N.Y.)* **2012,** *18* (11), 2083-2092.
212. Ando, Y.; Maida, Y.; Morinaga, A.; Burroughs, A. M.; Kimura, R.; Chiba, J.; Suzuki, H.; Masutomi, K.; Hayashizaki, Y., Two-step cleavage of hairpin RNA with 5' overhangs by human DICER. *BMC molecular biology* **2011,** *12*, 6.
213. Flores-Jasso, C. F.; Arenas-Huertero, C.; Reyes, J. L.; Contreras-Cubas, C.; Covarrubias, A.; Vaca, L., First step in pre-miRNAs processing by human Dicer. *Acta pharmacologica Sinica* **2009,** *30* (8), 1177-85.
214. Gu, S.; Jin, L.; Zhang, Y.; Huang, Y.; Zhang, F.; Valdmanis, P. N.; Kay, M. A., The loop position of shRNAs and pre-miRNAs is critical for the accuracy of dicer processing in vivo. *Cell* **2012,** *151* (4), 900-911.
215. Vermeulen, A.; Behlen, L.; Reynolds, A.; Wolfson, A.; Marshall, W. S.; Karpilow, J.; Khvorova, A., The contributions of dsRNA structure to Dicer specificity and efficiency. *RNA (New York, N.Y.)* **2005,** *11* (5), 674-82.
216. Shea, C. M.; Tzertzinis, G., Controlled expression of functional miR-122 with a ligand inducible expression system. *BMC biotechnology* **2010,** *10*, 76.
217. Vogel, C.; Marcotte, E. M., Insights into the regulation of protein abundance from proteomic and transcriptomic analyses. *Nature reviews. Genetics* **2012,** *13* (4), 227-32.

218. Peng, Q.; Zhang, X.; Min, M.; Zou, L.; Shen, P.; Zhu, Y., The clinical role of microRNA-21 as a promising biomarker in the diagnosis and prognosis of colorectal cancer: a systematic review and meta-analysis. *Oncotarget* **2017,** *8* (27), 44893-44909.
219. Thakral, S.; Ghoshal, K., miR-122 is a unique molecule with great potential in diagnosis, prognosis of liver disease, and therapy both as miRNA mimic and antimir. *Current gene therapy* **2015,** *15* (2), 142-50.
220. Schmidt, M. F.; Korb, O.; Abell, C., MicroRNA-Specific Argonaute 2 Protein Inhibitors. *ACS chemical biology* **2013,** *8* (10), 2122-2126.
221. Tan, G. S.; Chiu, C.-H.; Garchow, B. G.; Metzler, D.; Diamond, S. L.; Kiriakidou, M., Small molecule inhibition of RISC loading. *ACS chemical biology* **2012,** *7* (2), 403-410.
222. Hesse, M.; Arenz, C., *A rapid and versatile assay of Ago2-mediated cleavage using branched rolling circle amplification*. 2015; Vol. 17.
223. Vo, D. D.; Staedel, C.; Zehnacker, L.; Benhida, R.; Darfeuille, F.; Duca, M., Targeting the production of oncogenic microRNAs with multimodal synthetic small molecules. *ACS chemical biology* **2014,** *9* (3), 711-21.
224. Dojahn, C. M., Synthese und Screening von Inhibitoren der mikroRNA-Reifung. *Dissertation*.
225. Vo, D. D.; Tran, T. P.; Staedel, C.; Benhida, R.; Darfeuille, F.; Di Giorgio, A.; Duca, M., Oncogenic MicroRNAs Biogenesis as a Drug Target: Structure-Activity Relationship Studies on New Aminoglycoside Conjugates. *Chemistry (Weinheim an der Bergstrasse, Germany)* **2016,** *22* (15), 5350-62.

Acknowledgements

First of all, I would like to heartily thank my both supervisors Prof. Christoph Arenz und Prof. Oliver Seitz for giving me a chance to do my PhD in their groups, for being honest and delicate with me, for their great support, professional advising, interesting discussions and for sharing their knowledge.

I would like also to thank Simon Loibl, Margherita Di Pisa and Christina Kuznia for reading and corrections for my thesis; and Gunnar Bachem for reading the PNA synthesis part of introduction.

Huge thanks to the members of the "biolab": Marlen Hesse, Stephanie Diederich, Christina Klotz, Christina Kuznia, Marcel Geufke, for helping me with the various devices, for supporting in the learning process of new methods and for lovely atmosphere in the lab.

My special thanks to the colleagues, who was helping me with the learning the chemical synthesis and with the device using: Andrea Knoll, Olalla Vázquez, Simon Loibl, and Katharina Gröger.

I am grateful to Dr. Claudine M. Dojahn for generous use of her synthesized small molecular inhibitors and to the members of the group of Prof. Andreas Herrmann for the use and their help with the flow cytometry.

I am also thankful to Sabine Heinz for helping me in all administrative issues and for creating a good mood in the group.

I wish to sincere thank all my colleagues from the groups of Prof. Arenz and Prof. Seitz for sharing knowledge, ideas and inspiration, collective work and great time together!

Last, but not least I would like to thank my mother Natalia Ogorodnikova and my father Andrej Ogorodnikov, who passed away, my parents-in-law Marion and Georg Loibl and my small family - my husband Simon Loibl and our children Maja and Maria Loibl - for giving me so much support, love, knowledge, and motivation.

I declare that I have completed the thesis independently using only the aids and tools specified. I have not applied for a doctor's degree in the doctoral subject elsewhere and do not hold a corresponding doctor's degree. I have taken due note of the Faculty of Mathematics and Natural Sciences PhD Regulations, published in the Official Gazette of Humboldt-Universität zu Berlin no. 42/2018 on 11/07/2018.